STUDIES OF THE HIGH TEMPERATURE TRIBOLOGICAL BEHAVIOUR OF SOME SUPERALLOYS

Simon Robert Rose

A thesis submitted in partial fulfilment
of the requirements of the
University of Northumbria at Newcastle
for the degree of Doctor of Philosophy

June 2000

"... a ring is worn thin next to the finger with continual rubbing. Dripping water hollows a stone, a curved ploughshare, iron though it is, dwindles imperceptibly in the furrow. We see the cobble stones of the highway worn by feet of many wayfarers. The bronze statures by the city gates show there right hands worn thin by the touch of all travellers who have greeted them in passing. We see that all these are being diminished since they are worn away. But to perceive what particles drip off at any particular time is a power grudged to us by our ungenerous sense of sight."

The Nature of the Universe

Lucretius

55 BC

Contents

List of Tables

List of Figures

Acknowledgements

I would like to thank Prof. Santu Datta and Dr. Jim Burnell-Gray, my supervisors, for their help, advice and encouragement with this thesis. I also wish to take the opportunity to thank the other staff and research students within the Advanced Materials Research Institute and the School Engineering for all the help and assistance given.

In particular I wish to thank Bob Best for assistance and help with electron microscopy and Ray Bradly and Clive Hartis for help in the day-to-day running of this project. I also wish to acknowledge Dr Mari Gellue formally of the University of Exeter for collaboration with hot hardness testing.

Finally I wish to thank EPSRC, for their funding of this project.

Declaration

I hereby declare that:

During the period I have been registered for the degree of PhD, for which the thesis is submitted, I have not been a registered candidate for any other award of a University.

Furthermore, that I have attended relevant seminars within the University of Northumbria, annual symposia of the Institute of Corrosion, and presented papers at several conferences and relevant meetings on the subject of high temperature wear.

Studies of the High Temperature Tribological Behaviour of some Superalloys

By Simon Robert Rose

Abstract

High temperature wear is a serious problem in many applications in which relative motion and contact of components occur at elevated temperature. Under certain wearing conditions compacted debris layers known as 'glaze' layers which are highly resistant to further wear are formed. The principal aim of this project was to understand the mechanisms of such layer/glaze formation particularly during sliding of unlike materials against unlike materials. The influence of temperature, load and material compositions was of particular interest in this work.

This thesis examined the wear behaviour of four combinations of Superalloys worn using a block-on-cylinder type wear rig, developed in this laboratory which allows accelerated wear testing simulating the wear processes experienced in valve and valve seats in natural gas fuelled combined heat and power engines. The alloys studied included MA956 and Nimonic 80A predominately as samples and Stellite 6 and Incoloy 800 as predominantly counterfaces.

'Glazed' layers were found to form on three of the combinations tested: MA956 with Stellite 6 and Incoloy 800 counterfaces from 510°C and 690°C and with Nimonic 80A worn with Incoloy 800 from 630°C. In any system before the onset of 'glaze' formation, increasingly severe wear was encountered due to the loss in strength of the materials with increasing temperature, giving rise to high rates of material loss up to a certain maxima, dependent on the materials tested.

With MA956/Stellite 6 the maxima in the temperature/weight loss curve occurred at 0.13g at 510°C. The maxima was at 0.66g for MA956/Incoloy 800 at 630°C. A maximum of 0.49g was recorded at 630°C for Nimonic 80A worn with Stellite 6 counterfaces. However Nimonic 80A worn with Incoloy 800 counterfaces did not show such a maximum. The low wear of the sample was caused by the transfer of a metallic layer from the counterface providing protection below the minimum temperature of 'glaze' layer formation (630°C). However the counterfaces used suffered severe damage.

Testing over a range of loads (7 to 25N) revealed that the layers formed on MA956 with Stellite 6 and Incoloy 800 counterface demonstrated an increased rate of breakdown of the 'glaze' layers at higher loads (25N). For Nimonic 80A worn with Incoloy 800 no layers were formed above 10N; the wear mechanism became oxidational in nature.

Sliding combinations involving like-on-like and sample/counterfaces reversals demonstrated that dissimilar materials tend to undergo less adhesion and so promote layer formation and low wear.

Information on wear damage, debris characteristics, layer formation and subsurface deformation was obtained by optical microscopy, SEM, SEM/EDX and XRD analyses. These data were complemented by hardness and hot hardness measurements on worn and 'as-received' materials.

1. Introduction

Damage due to wear is a common occurrence in many systems whose components move against each other. Wear may occur by sliding, vibration or erosion by hard particles entrained in fluids, which lead to a wide range of mechanisms and rates of material loss [1].

Wear at elevated temperatures brings further complications due to faster kinetics of film formation, loss of mechanical strength of materials and alterations in the surface conditions leading to changes in adhesion between the surfaces. High temperature wear occurs in valve and valve seats in internal combustion engines, heat exchanger tubes and their supports in boilers, turbine blades in their fitting to the discs in gas turbines and areo engines or hot-rolling of metal sheets maybe also susceptible to high temperature wear.

High temperature wear processes are often associated with the presence of aggressive environments and this makes the traditional methods of controlling friction and wear inapplicable at high temperature. Lubricants and coating systems available at low temperature are often inapplicable to limit wear at high temperature and under aggressive environments. Materials selection is severely restricted by the exacting requirements of the applications, such as oxidation resistance, high strength and creep resistance.

To obtain greater thermal efficiency and longer lives of power generation and other high temperature systems, methods of improving high temperature wear resistance are required [2]. Coatings, preoxidation or other material preparations have been used in an attempt to improve the wear properties and prolong the lives of components in high temperature systems and reduce the highly damaging 'running-in' wear.

However one of the most elegant methods of generating surfaces resistant to high temperature wear is to take advantage of the process of oxidation that occurs at high temperature during wear. The production of oxidised debris together with the presence of high temperatures and moderate loads can lead to the formation of surface 'glaze'-type layers capable of minimising wear (see **Section 2.11**). However it is difficult to predict the temperatures, the kinetics of oxidation, the load and the mechanical properties of the materials in various combinations which will generate these wear resistant layers. These observations imply that the key to generating the wear resistant 'glaze' layers lies in the understanding of the mechanisms of their formation.

Much work (see **Section 2.11**) has been done on wear by fretting at elevated temperature of high alloy steels and Superalloys [3,4]. These alloys are based on the Group VIII A elements – iron, cobalt and nickel – with additions of other elements such as chromium and aluminium. Superalloys have been developed for their high strength, resistance to oxidation and high temperature corrosion in the hostile environments in which they are to be used.

Under fretting or low amplitude reciprocating sliding conditions, under low load and sliding speed at high temperature, the formation of surface layers resistant to wear has been found to occur. These layers associated with excellent wear and friction properties were originally thought to be 'glassy' and amorphous, although this has now been shown not to be the case, the term 'glaze' is still often used to describe the layers with distinctive morphology [5].

Debris produced in the initial stages of wear undergoes oxidation and fracture in the wearing interface until, after a given time, it forms a compacted 'third-body' layer of debris on the surface (**Section 2.11.8**) [4,6]. At elevated temperature sintering and further refinement lead to the formation of a solid, highly smooth layer. The presence of such layers is characterised by smooth running and low wear of the couple.

An investigation into the wear of valve and valve seats for natural gas fuelled combined heat and power engines was carried out by Wood *et al.* [7,8] within the Surface Engineering Research Group, University of Northumbria at Newcastle (see **Section 2.11.9**). A special wear rig was designed for the accelerated wear testing of valve and valve seats, which gave low debris retention in the wearing interfaces was used in this project. One of the principal characteristics of this type of wear rig is the low debris retention between the wearing surfaces. Here the formation of compacted oxide layers was reported at temperatures of 500 and 750°C.

Wood's work was particularly important because such studies of high temperature wear involved sliding of couples of unlike materials. Various high temperature materials were worn together in a variety of unlike combinations and complex patterns of wear behaviour were observed. Layer formation gave a wide range of wear rates. With some combinations, material was transferred from the counterface to the sample which at particular temperatures produced 'glaze'-type layers; other cases were characterised by no layer formation/transfer of particles between the surfaces.

Wood's work highlighted limitations that existed in the current understanding of the mechanism of high temperature wear under conditions in which unlike sliding combinations are employed and in particular for sliding systems in which the debris is not well retained within the interface, a consequence of the testing system used in this project.

The aim of the current study was to expand the investigation of high temperature wear of the sliding of unlike samples and counterfaces. This project was designed to examine effects of temperature, load and sample/counterface combinations on the processes of wear and to determine the controlling factors which govern the compacted layer formation under these conditions.

Additionally, the aims have been to study the processes of debris generation, the mode of particle transfer between the surfaces and the way these transferred particles lead to the formation of the compacted wear resistant layers.

This thesis is divided into eight chapters. Chapter 1 contains the Introduction. Chapter 2 gives a review of the relevant literature. Chapter 3 provides an introduction to the current study. Chapter 4 details the experimental methods and studies carried out. Chapter 5 reports the experimental findings. Chapter 6 discusses the results obtained from which the conclusions are drawn as reported in Chapter 7. In Chapter 8 some suggestions for further work are presented.

2. Literature review

2.1 Introduction

This chapter critically reviews the relevant literature related to unlubricated wear at elevated temperatures.

Section one deals with the main important aspects of the frictional force. Section two examines common theories of wear. Here the models for the contact of surfaces under load and under sliding conditions have been reviewed and aspects of oxidation and surface contamination have been considered. The processes of wear such as oxidational wear, adhesive wear and delamination wear have been described.

Section three examines the influence of wear debris within the wearing interface and its influence on the wear processes. The effect of debris retained in the interface and the establishment of so called 'third body' condition, and its role in the wear mechanisms have also been considered.

Section four reviews the work central to this thesis, the mechanism of wear for unlubricated systems at elevated temperature. The available work covering the theory of 'glaze' layer formation together with the experimental data obtained in previous work have been reviewed. The chapter concludes with a summary of the work carried out on elevated temperature wear.

2.2 Theories of friction

2.2.1 Types of friction

The frictional force is defined as the resistance to movement produced when one body moves over another. Friction can be either static friction (where the bodies do not move) or sliding friction where the bodies move relative to each other. Friction can also be defined as either rolling friction (**Figure 2.1 (a)**) or sliding friction (**Figure 2.1 (b)**). It should be noted however that in rolling friction there would almost certainly be an element of sliding.

However friction is more normally expressed as the coefficient of friction, which is denoted by the symbol μ:

$$\mu = F / W \qquad \{2.1\}$$

Where F is the frictional force and W is the normal load.

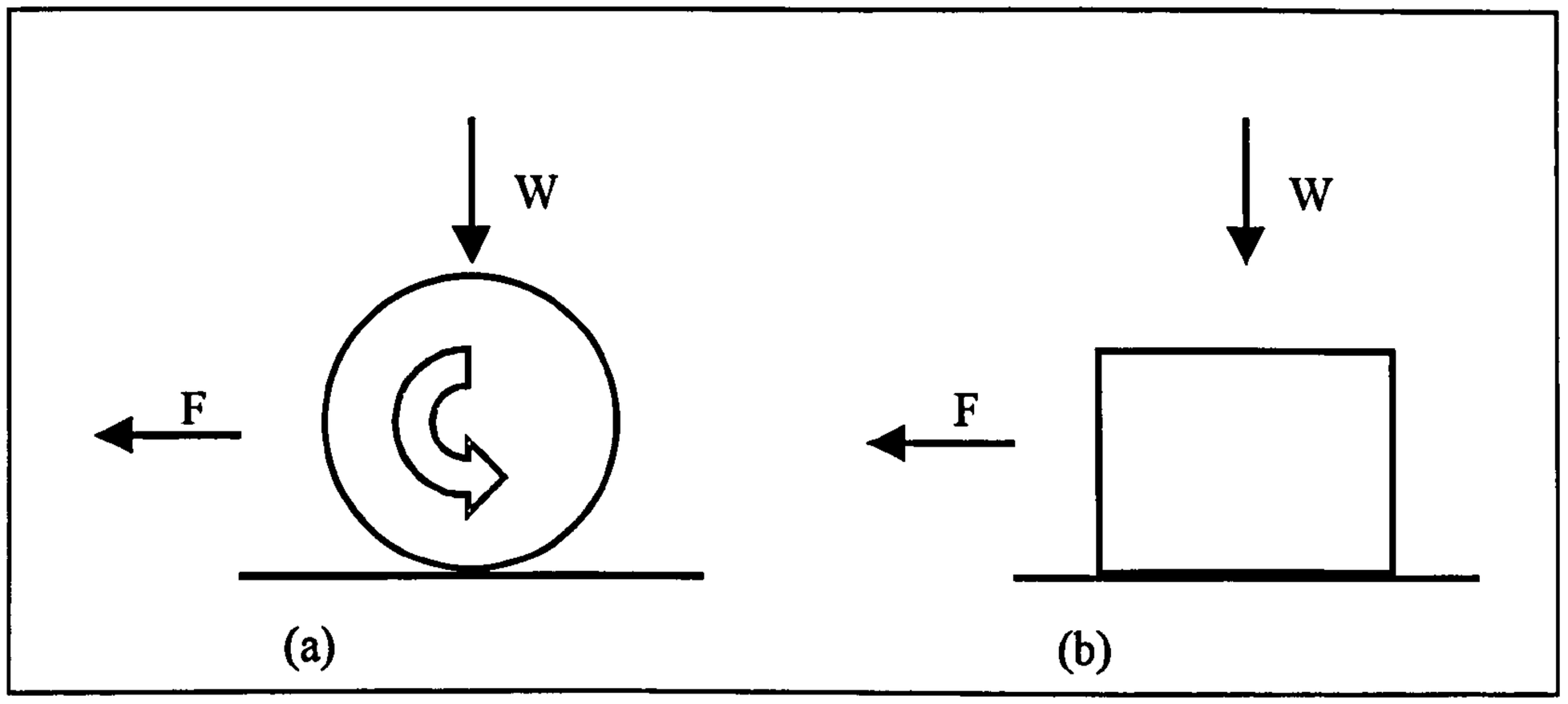

Figure 2.1 Two modes of relative motion: (a) rolling and (b) sliding [F is the frictional force and W is the applied load]

The coefficient of friction provides a useful measure of the frictional force. The coefficient of friction can vary from 0.001 for rolling friction to 10 for metals sliding under vacuum. However the normal range of coefficients of friction for sliding in air is 0.1 to 1.0.

2.2.2 Early work – the laws of friction

The first laws of friction are often attributed to Amontons, who rediscovered them some 200 years after they were first proposed by Leonardo da Vinci [9]. The three laws are stated as:

1) the frictional force is proportional to normal load;
2) the frictional force is independent of the apparent area of contact;
3) the frictional force is independent of the sliding velocity.

Although these laws are of limited use in wear science, they are often found to apply over a limited range of conditions for many systems. They also often fit well empirical observations. The first law of friction can be stated as:

$$F = \mu W \qquad \{2:2\}$$

Coulomb [1] proposed another early theory of friction, which is shown schematically in **Figure 2.2.** In this model wedge shaped asperities interlock, and as the surfaces move relative to each other the surfaces are moved apart as shown in **Figure 2.2 (b)** so work is done against the normal load, thus giving rise to the frictional force. This model accounts for the frictional force being

proportional to load and independent of area of contact. However this theory fails when the surfaces slide down the other side of the slopes (**Figure 2.2 (c)**), work is done by the system and so no net force is produced. In essence the theory contains no mechanism for the dissipation of energy and for this reason it must be rejected.

2.2.3 Development of current theory – contact of nominally smooth surfaces

When two nominally flat surfaces, which are in fact rough on a microscopic scale, are brought together, contact will be established only on a limited number of sites on each surface. At these points the surface will deform, either plastically or elasticity [10, 11], until a limit is reached by the load being supported. At these points intimate contact is achieved and bonding of the aspiratites may occur.

The work of Bowen and Tabor [1] related the frictional force to the interaction of these asperities as sliding proceeds. Two major components of friction were identified. These are adhesion of the surfaces and ploughing of the softer surface by the asperities of the harder surface. Hence the total friction μ is given by the sum of the friction arising from adhesion, μ_{adh} and ploughing, μ_{def} as shown in **Equation {2.3}**:

$$\mu_{total} = \mu_{adh} + \mu_{def} \qquad \{2.3\}$$

2.2.4 Adhesion

As a matter of common experience, metals pressed against each other do not adhere, however if they are clean and free from oxide films – this normally requires a vacuum – then strong adhesion is observed [1].

During the contact of surfaces rubbing with each other the surfaces will touch only at the asperities. The asperities will deform either by plastic or elastic deformation. It has been demonstrated that for all but the smoothest of surfaces this will be plastic deformation [10-13]. From this it can be seen that the true area of contact will be independent of the apparent area of contact but dependent upon the applied load and the deformation properties of the softer material, hence:

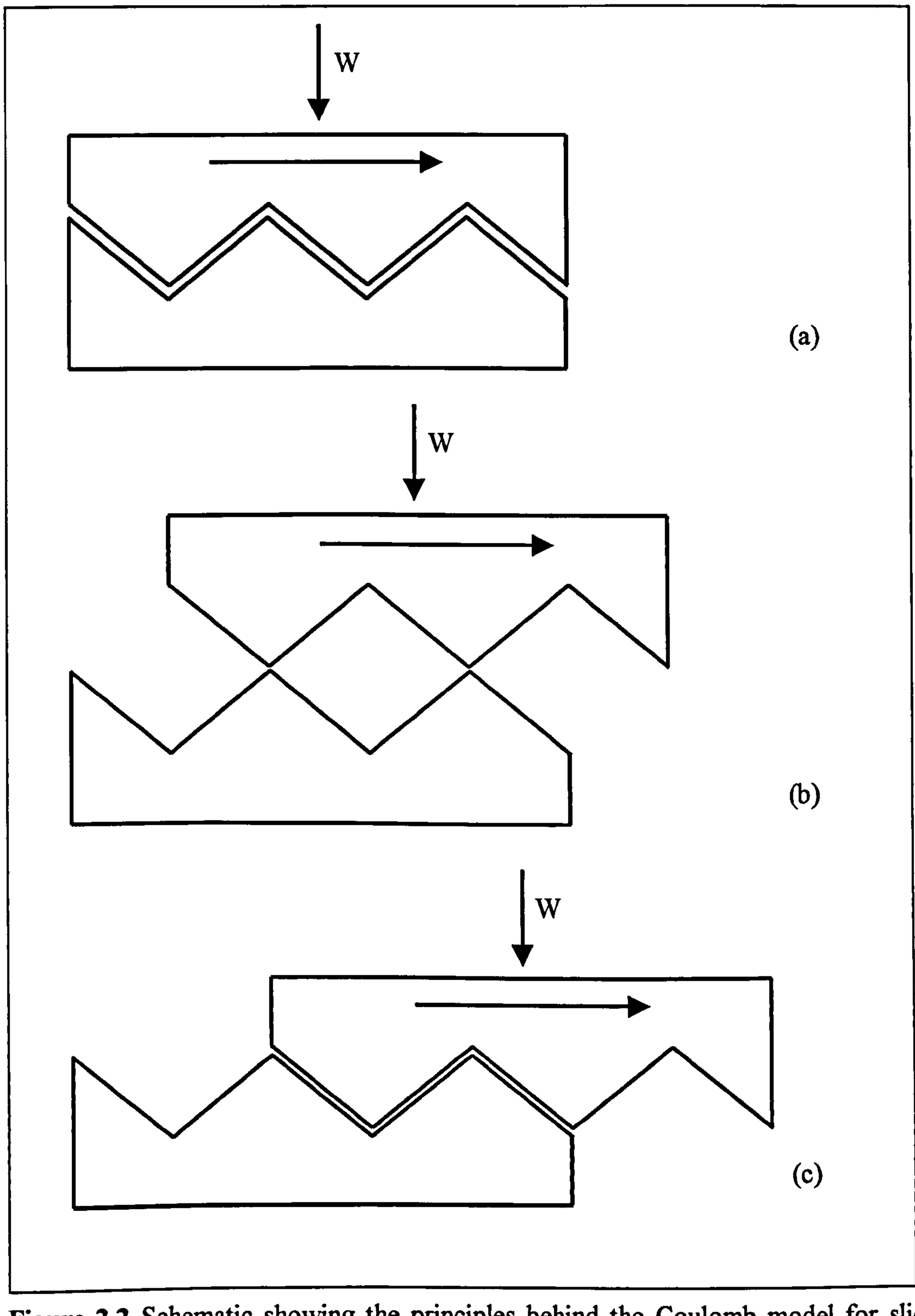

Figure 2.2 Schematic showing the principles behind the Coulomb model for sliding friction. Moving from (a) to (b) work is done against the normal load W, so giving rise to the frictional force. However, the normal load then does an equal amount of work on the system moving from (b) to (c) [1]

$$W \approx AH \qquad \{2.4\}$$

Where W is the applied load, A is the true area of contact and H is the indentation hardness of the softer material.

The frictional force produced by adhesion of these junctions will therefore be given by the shear strength of these junctions, hence:

$$F_{adh} = As \qquad \{2.5\}$$

Where F_{adh} is the frictional force due to adhesion and s is the shear strength of the junction. From this the contribution to the total friction given by adhesion will be:

$$\mu_{adh} = F_{adh} / W \approx s / H \qquad \{2.6\}$$

Since the junction will fail by the rupture of the weaker material, the shear strength of the junction can be taken to be that of the weaker material. For metals, the uniaxial yield stress can be taken to be approximately three time the hardness:

$$H \approx 3Y \qquad \{2.7\}$$

Y the yield stress will be 1.7 to 2.0 times the yield stress in pure shear, s, so :

$$H \approx 5s \qquad \{2.8\}$$

And so from this the frictional force due to adhesion can be given as:

$$\mu_{adh} \approx s / H \approx 0.2 \qquad \{2.9\}$$

So the contribution to the frictional coefficient produced by adhesion will be ~0.2. This leaves a considerable proportion of the frictional force commonly experienced in sliding to be accounted for, this can be attempted by estimating that produced by deformation.

2.2.5 Ploughing

The contribution to friction given by the deformation term is represented by ploughing of the softer surface by the harder one. This can be estimated by calculating the force required to drag a rigid conical asperity through a soft, deformable solid.

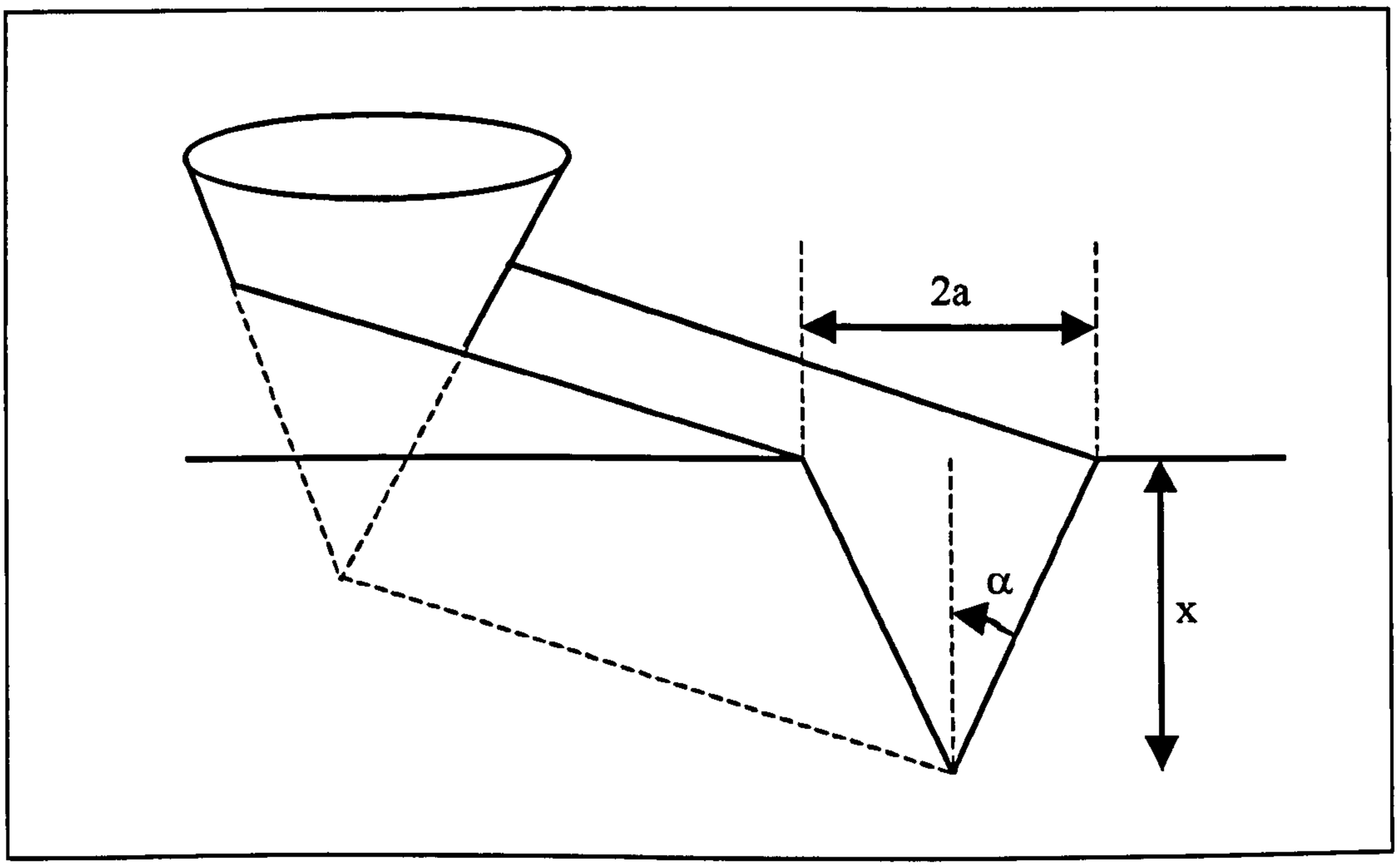

Figure 2.3 Ploughing of a deformable surface by a rigid asperity [11]

The ploughing action of a rigid cone of semi-angle α sliding over a plane surface is shown in **Figure 2.3**. The force required to displace the material will be the flow pressure, which is taken to be the indentation hardness, multiplied by the cross-section of the groove:

$$F_{def} = H\alpha x = Hx^2 \tan\alpha \qquad \{2.10\}$$

The load supported by the asperity is given by:

$$W = \frac{H\pi a^2}{2} = \tfrac{1}{2} Hx^2 \tan^2 \alpha \qquad \{2.11\}$$

And so the coefficient of friction due to the ploughing term will be:

$$\mu_{def} = F_{def} / W = (2/\pi)\cot\alpha \qquad \{2.12\}$$

From these models the coefficient of friction for metals can be calculated. Taking into account that the slopes of real asperities are almost always less that 10° then the coefficients of friction would always be less than 0.3 as μ_{adh} approaches 0.2 and μ_{def} approaches 0.1. For like-on-like sliding the deformation term would be negligible and so the coefficients of friction should be circa 0.2. This is clearly not the case, so other effects have to be taken into account to explain the levels of friction generally observed.

2.2.6 Junction growth

In the above models the area of contact is assumed to be proportional to the normal load and the inverse of the indentation hardness. For conditions of relative motion this is indeed an over simplification, the area of contact can also be affected by the tangential forces acting upon it causing further deformation of the asperity junction. This leads to growth of the junction, hence the term 'junction growth'.

This process can in theory continue indefinitely until the real area of contact approaches that of the apparent area of contact, although in practice junction growth is limited by the ductility of the materials. The effect of adsorbed gases and other surface contaminants also leads to weakening of the junction, so giving rise to the coefficients of friction which are commonly observed (0.1 to 1.0). For example, for an interface that is 10% weaker than the bulk material, a coefficient of friction of around unity is found.

2.3 Theories of wear

This section examines the commonly experienced wear mechanisms, and how they are related to the wear rates experienced. This section relates to dry wear – the absence of lubricants – of metals and alloys in a typical oxidising environment.

2.3.1 Classification of wear types

Wear can be classified in a number of ways [14-16]. As (a) fretting wear, in which the bodies move relative to each other via vibration. This is normally

defined as a displacement of less than 70μm, (b) if the displacement is greater than this then wear would be termed 'reciprocating sliding', and (c) where a sample moves only in one direction then wear would be defined as unidirectional sliding (such as pin-on-disc). These simple cases can of course occur in various, practical situations, such as the wear of valve and valve seats [14].

2.3.2 Classification of wear mechanisms

Wear can also be classified by considering the wear rates, the nature of the surface produced, the character of the wear debris and the coefficient of friction experienced by the couple. Rabinowicz [16] identified four types of wear mechanism:

1) ***Adhesive wear*** – in which material is removed from the contacting surfaces via adhesion, cold welding and plucking of material from the surfaces.
2) ***Abrasive wear*** – in which hard asperities on the opposing surfaces or particles within the interface ploughs and machines the surface, so leading to material loss.
3) ***Corrosive wear*** – corrosion products formed upon the contacting surface are removed by the action of sliding, so exposing a fresh surface on which new corrosion products may form.
4) ***Fatigue wear*** – damage is done to the surfaces by cyclic stressing. The surface undergoes loading and unloading as asperities of the opposing surface pass over it, so leading to fatigue, cracking and material loss.

Wear can also be defined, as it was by Archard and Hirst [17], as mild or severe. This classification is based upon the contact resistance between the sliding surface and the nature of the debris produced, so defining the state of the contacting surfaces produced. In mild wear oxidation of the surfaces plays an important role, severe wear proceeds when the surfaces are essentially oxide-free **(Section 2.5)**.

Many other definitions of wear mechanisms exist and are notoriously inconsistent from one author to another [18]. The following sections outline the main classes of wear mechanism which are used throughout this thesis.

2.4 Archard's theory of wear

Archard's theory of wear [17] was the first 'modern' theory and is analogous to Bowden and Tabor's theory of friction [1]. This assumes that the

surfaces only contact at a limited number of asperities. When these high points connect during relative motion of the surfaces, wear particles are created.

The number of asperity contacts is assumed to be proportional to the load and the indentation hardness of the material, hence:

$$W = {}^{KsP}/_{H} \qquad \{2.13\}$$

Where W is the worn volume, s the sliding distance, P the applied load, H the indentation hardness of the softer material, and K a constant related to the probability of an encounter leading to the generation of a wear particle. This can be simplified as:

$$W = K_1 Ps \qquad \{2.14\}$$

K_1 is often referred to as the *'K'* factor, and can be described as the wear coefficient (unit volume/unit load/). Changes in the K factor over a range of conditions (load and sliding speed) indicate transformations in the surface condition and so in the wear mechanism. This leads to the conclusion that the wear of a specific couple will be proportional to the sliding distance and the applied load. This was observed to be true over limited ranges of conditions, examples of which are shown in **Figures 2.4** and **2.5** [17].

It was found, however, that under certain conditions a transformation in the wear regime, characterised by a change in the surface conditions would lead to an increase or decrease in the wear rates and a different value of the *'K'* factor.

Archard's simple model of wear has never-the-less provided a very useful basis for understanding wear processes. Wear is still often assumed to be directly related to indentation hardness, despite the fact that this has often been shown not to be the case – see for instance oxidational or delamination wear models (see **Section 2.5**).

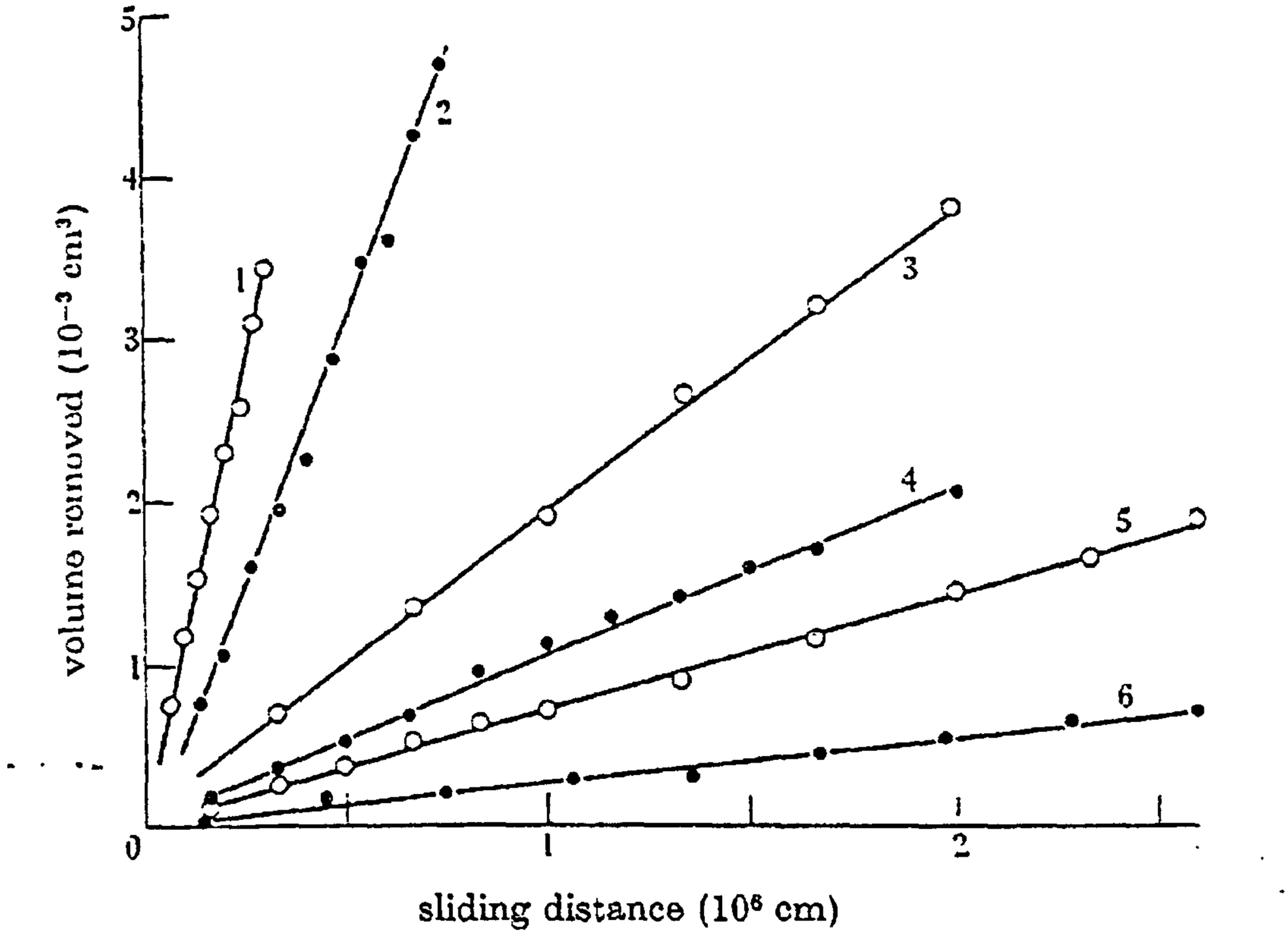

Figure 2.4 Like-on-like sliding at 180cm. s^{-1} (1) mild steel, 50g (2) ferritic stainless steel, 250g (3) 70/30 brass, 80g (4) Stellite, 2500g and (5) hardened tool steel, 300g [17]

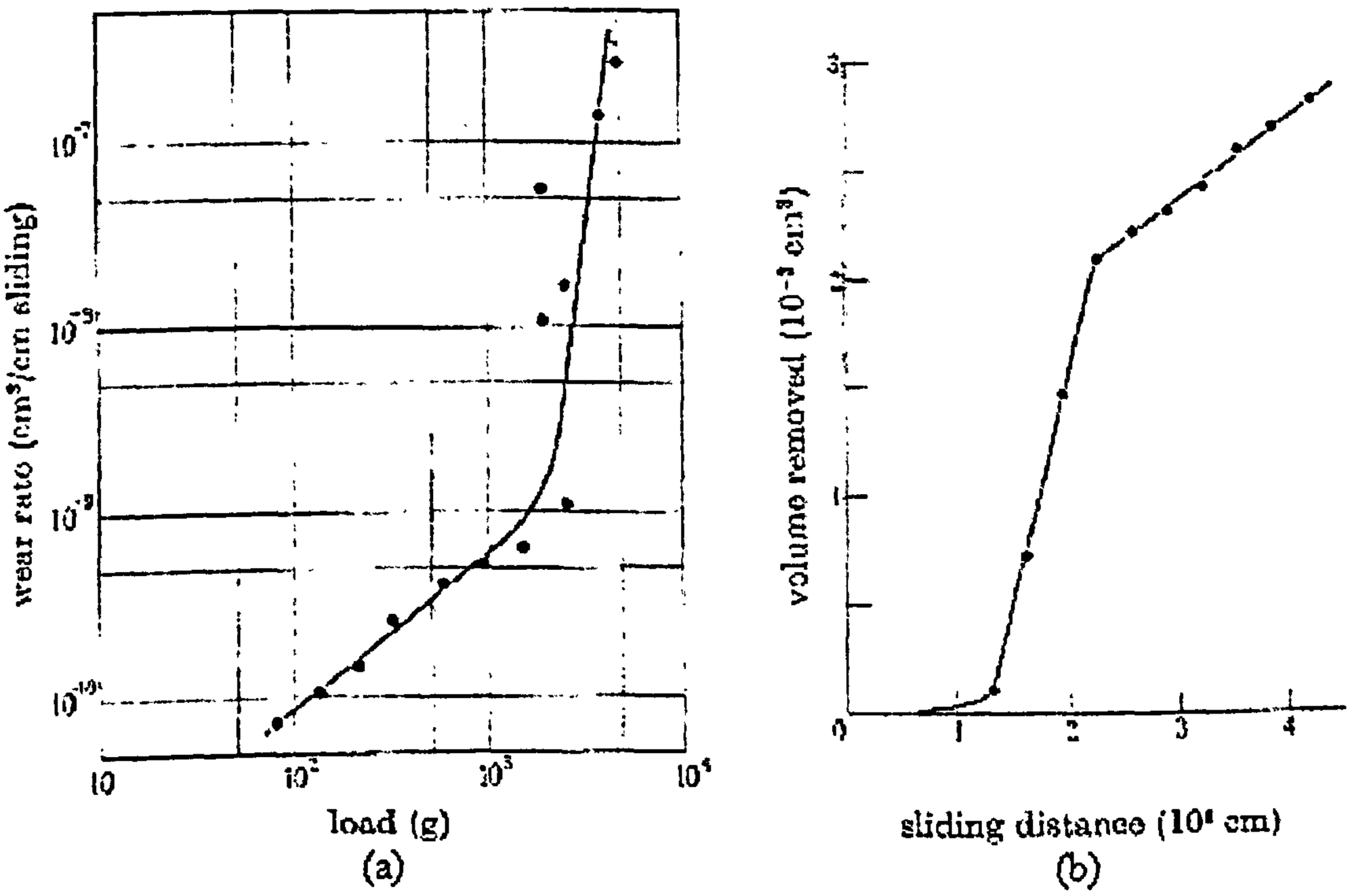

Figure 2.5 (a) wear rate against load for ferritic stainless steel (pin) worn with high-speed tool steel (ring) at 180cm. s^{-1} (b) wear rate against sliding distance for 70/30 brass (pin) worn with hardened tool steel (ring), load 1000g. Speed 180cm. s^{-1} [17]

2.5 Mild and severe wear

Wear of many materials has been shown to undergo marked changes in wear rate and coefficient of friction for relatively small changes in load or sliding speed [9, 19-21]. In an attempt to resolve these difficulties Archard and Hirst, proposed the theory of mild and severe wear [17].

According to this model wear can be defined as either mild or severe. These definitions refer to the state of the wearing surfaces. In severe wear the surfaces are in a metallic state and a low electrical contact resistance is observed between the contacting surfaces. Wear particles are generally large (~0.1 mm) and also in a metallic state. In mild wear the contacting surfaces are in an oxidised state and the electrical contact resistance is high. Wear rates are generally lower than those given by a severe wear mechanism, although this is not always the case.

Mild/severe wear transitions are affected by changes in load and temperature as well as availability of oxygen. **Figure 2.6** shows the effect of temperature as well as the partial pressure of oxygen on the extent of the severe wear regime [22].

2.6 Adhesive wear

Adhesive wear is one of the most severe wear mechanisms [23] leading to high wear rates, friction and surface damage. Adhesive wear takes place when the interfaces are effectively free from oxide layers or particles which separate the surfaces. At the asperity junctions, the surfaces adhere to each other and so to allow sliding to proceed, these junctions must shear.

For sliding of unlike materials, the adhesive strength of the bond between the surfaces is generally higher than the cohesive strength of the weaker (usually taken to be the softer) material. This leads to fracture occurring in the softer material so giving rise to 'plucking' and transfer.

The level of adhesion is determined by the material's ability to deform. This is shown by the relationship between hardness and wear rate, given by Archard's [22] wear equation ($W = K_1 Ps$ **Equation {2.14}**). However this cannot be taken as an absolute rule as this does not apply to wear in cases in which heat treatment has been used to harden an alloy. The effects of the frictional heating can also change the microstructure – and so hardness – of the surface layers.

The mutual solubility or compatibility of the alloys also affects adhesive

wear [23]. Subramanium [24-26] showed that for aluminium-silicon alloys worn with a variety of counterfaces the more soluble the counterface material was with respect to the sample the greater the adhesion – thus giving rise to higher wear rates.

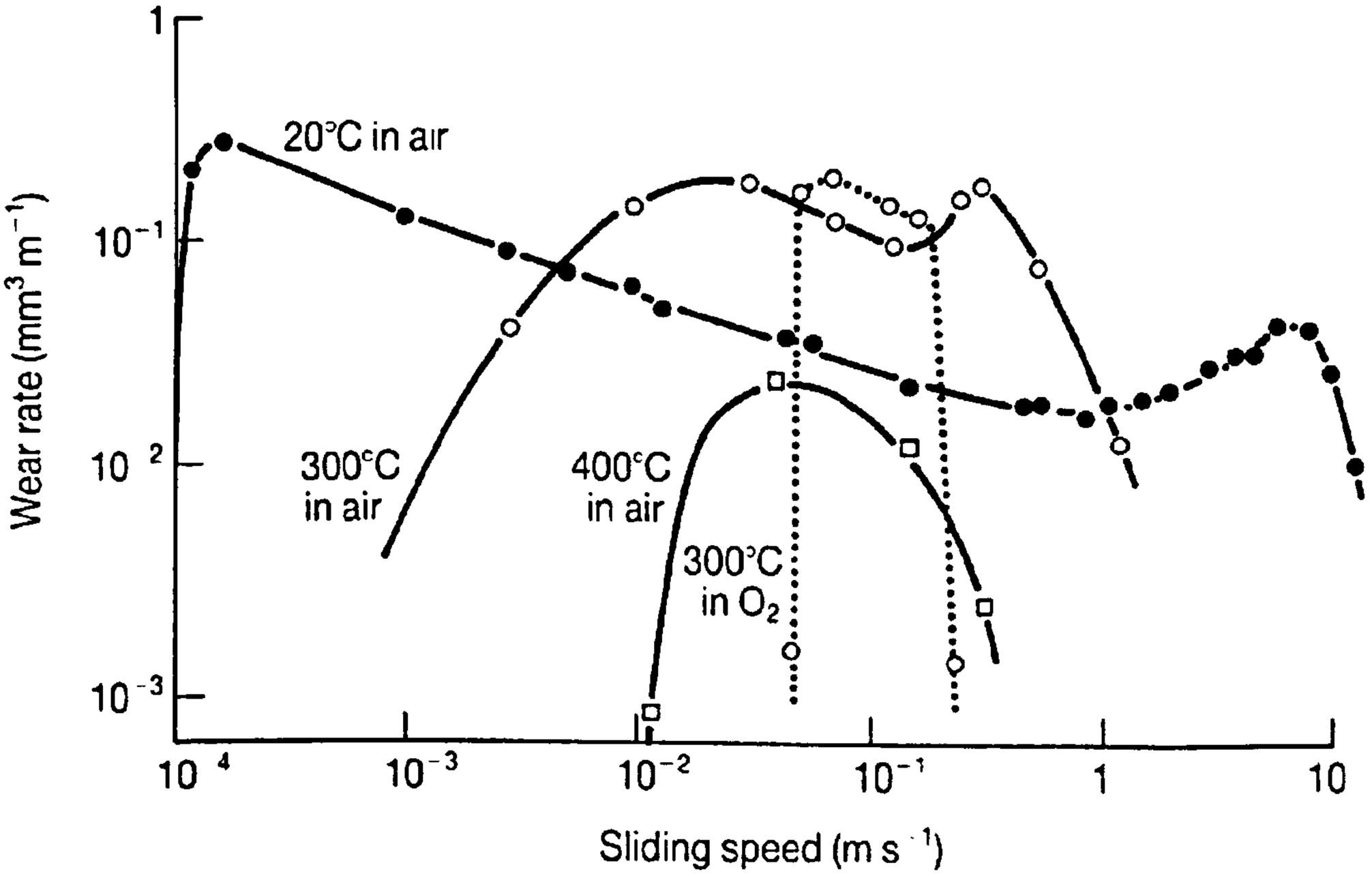

Figure 2.6 The variation in wear rate with sliding speed at various temperatures in air and pure oxygen for α/β brass sliding against steel [22]

2.7 Abrasive wear

Abrasive wear can be 'two body' or 'three body' depending upon whether wear takes place due to abrasions of a soft surface by a harder one – two body – or via hard particles between the wearing surfaces – three body. For abrasion to happen the abrasive medium must be 1.3 times the hardness of the surface undergoing abrasion and so able to scratch the softer surface – this coincides with to one unit on the Mohs' scale of mineral hardness [18].

Abrasive wear takes place via plastic deformation and brittle fracture. Both of these modes can occur together, although they are generally envisaged as tacking place independently.

There are three common models for abrasive wear via plastic deformation, these are; cutting, wedge-forming and ploughing (**Figure 2.7**) [1]. Cutting wear is characterised by the formation of long strip-like debris particles and deep

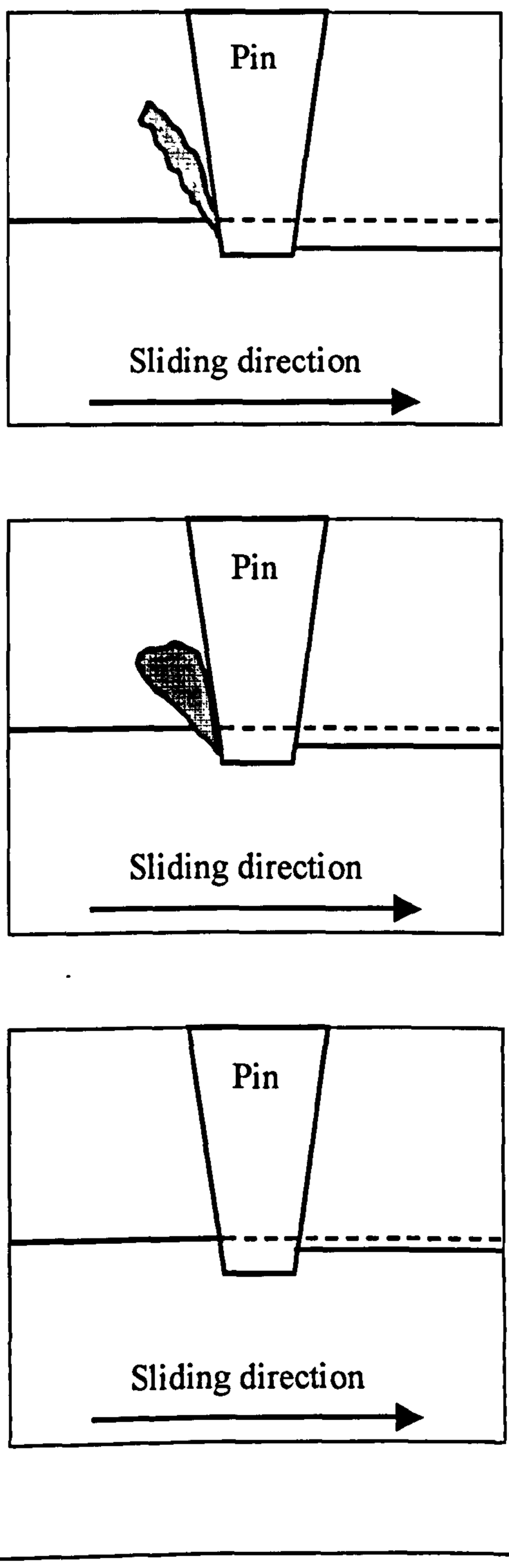

(a) cutting mode

(b) wedge-forming mode

(c) ploughing mode

Figure 2.7 Schematic showing the three modes of abrasive wear [1]

grooves upon the sample surface.

In wedge-forming, material builds-up ahead of the counterface asperities. Wedge-forming gives notably lower wear rates than those experienced in the cutting mode. The wear scar produced is grooved with characteristic transverse cracks. This mode of wear occurs when adhesion is strong.

In the ploughing mode, the formation of a wear particle cannot be clearly seen at the point of contact. The asperity produces only a shallow groove in the surface. Ploughing occurs where adhesion at the interface is weak and penetration of the asperity is relatively small.

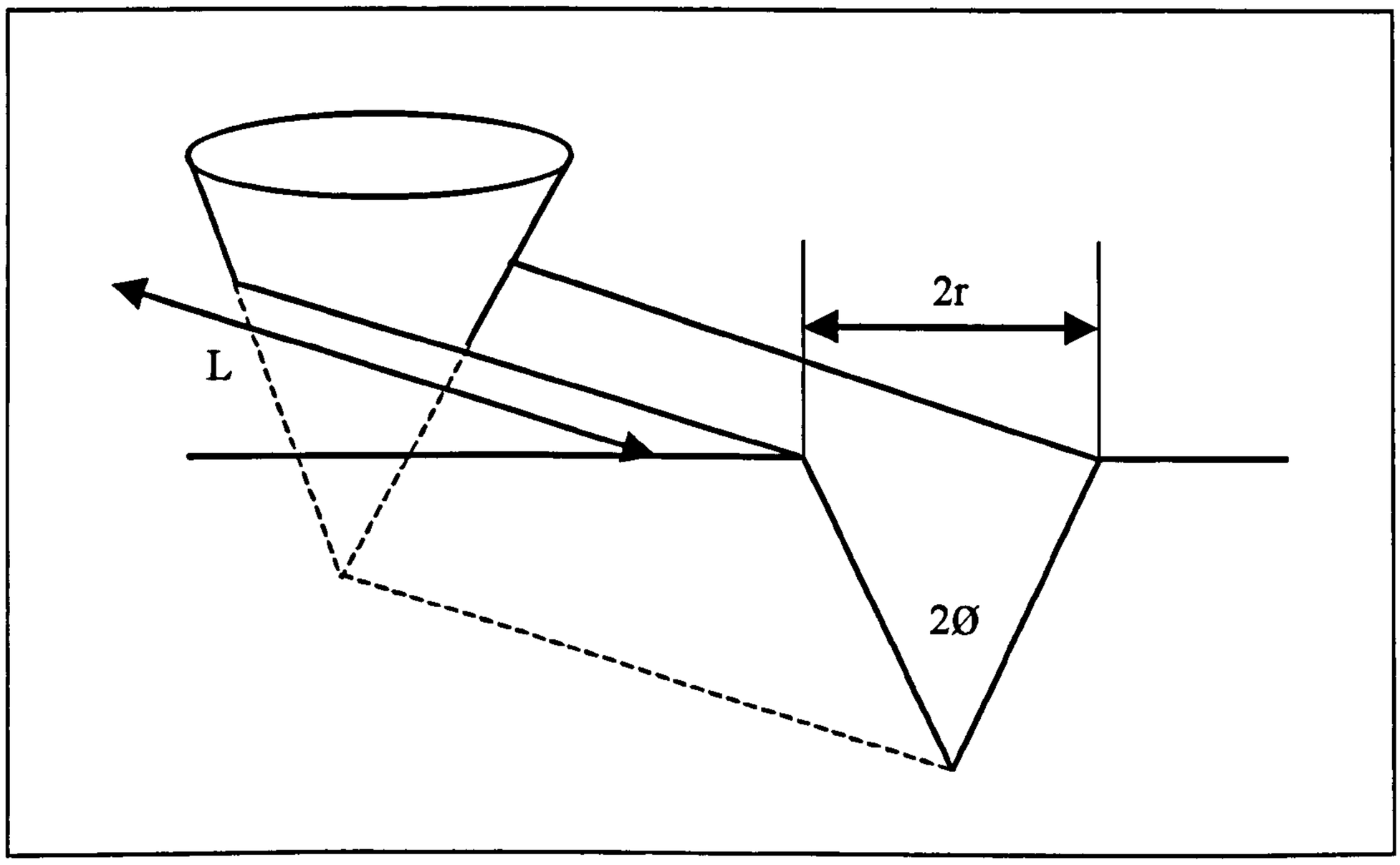

Figure 2.8 Abrasive wear due to an idealised conical asperity and a flat surface [27] (c.f. **Figure 2.3**)

In the plastic flow model, the abrasive element is idealised as a cone of semi-angle θ travelling through a surface of plastically deformable material, shown in **Figure 2.8** [27]. The volume of material removed from the surface after the cone has travelled a distance L is:

$$V = Lr^2 \cot\theta \qquad \{2.15\}$$

Where L is the distance travelled by the asperity, $2r$ is the width of the groove produced in the substrate and 2θ is the angle of the idealised asperity.

Now assuming that the softer material has yielded under normal load, each asperity supports a pressure of $\pi r2P/2$ where P is the yield pressure of the softer material. Hence the load, W, carried by the particle is given by:

$$W = P\frac{n\pi r^2}{2} \qquad \{2.16\}$$

Combining **Equations {2.15}** and **{2.16}** for n asperities:

$$V = \frac{2\cot\theta WL}{\pi P} \qquad \{2.17\}$$

This can be simplified as the indentation hardness can be substituted for flow pressure as $P \approx 1/3\ H$ where H is the hardness of the softer material:

$$V = \frac{6\cot\theta WL}{\pi H} \qquad \{2.18\}$$

So, by substituting K_a the Archard wear coefficient, for $6cot\theta/\pi$ then V is given by:

$$V = K_a \frac{W}{H} L \qquad \{2.19\}$$

Equation {2.18} is similar to the Archard wear equation – **Equation {2.14}** – only derived via a different route, and the wear coefficient relates to the geometry of the wear particles or asperities by the angle of the idealised wearing element. The model, however, ignores brittle fracture of the surface, which is commonly experienced with abrasive wear.

2.8 Fatigue wear or delamination wear

Wear mechanisms also exist that propose the removal of material from the sliding surfaces by cyclic stressing of the contact areas during relative motion. The delamination wear mechanism was proposed by Suh [28]. The theory is based upon the behaviour of dislocations within the material immediately below the wearing surface. This was proposed as an alternative mechanism for the wear type normally classified as 'adhesive wear'.

Surface layers which undergo deformation and plastic flow during the wearing process rapidly become worked and dislocations build-up. Close to the surface these dislocations are released to the surface via the image force (able to

move and be released to the surface). However further from the surface they are unable to move so a highly deformed layer of material builds-up beneath the wear scar/track. This leads to the formation of cracks and voids within the subsurface layer. After a given time the layer is no longer stable and a sheet of material is removed as plate-like wear debris. The process is then repeated for the next layer of material. For this model the total wear V undergone by the system will be given by:

$$V = N_1\left(\frac{S}{So_1}\right)A_1h_1 + N_2\left(\frac{S}{So_2}\right)A_2h_2 \qquad \{2.20\}$$

Where A is the average area of the delaminated sheet, h the thickness of the sheet, S the total sliding distance, N the number of sheets removed, So the critical distance for removal of one layer of material. The subscripts *1* and *2* denote the two materials sliding with each other – the model assumes un-like sliding couples.

Later developments of the delimitation wear theory [29-31] led to a greater understanding of how a highly deformed layer forms beneath the very surface layer and the propagation of the subsurface cracks. The subsequent development of the theory proposed the formation of a cell structure in the very surface layer, which would allow the repeated deformation of the surface. Such a cell structure is shown in **Figure 2.9** [29].

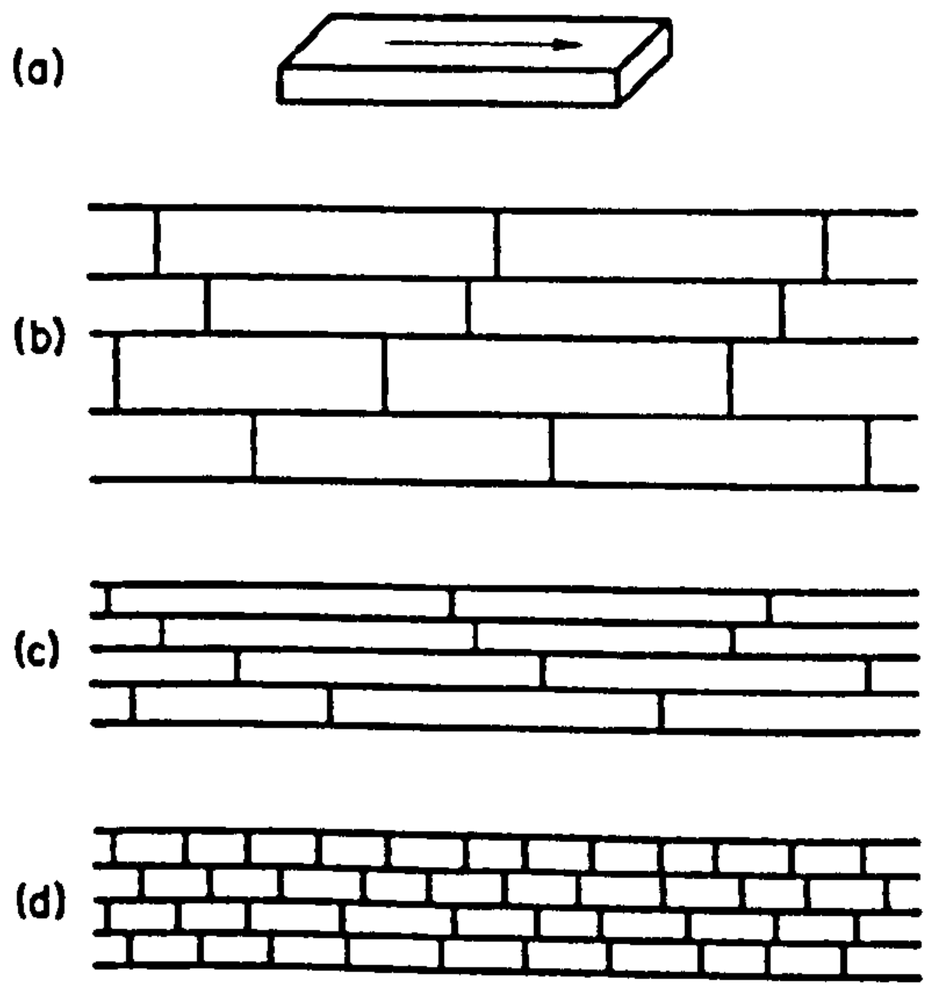

Figure 2.9 (a) Idealised cell showing relative dimensions, arrow indicating direction of sliding, (b), (c) and (d) showing plan, side and end structure of cells in the wear surface [29]

The great advantage of this theory is that it provides a mechanism which accounts for the production of wear debris as plate-like particles – such debris is often observed. The theory is based on the properties of materials and gives good agreement with the experimental observations.

2.9 Oxidational wear

The oxidational wear theory was first proposed to enable quantitative analysis of mild wear, to allow predictions of the wear rates from information about the materials and sliding conditions involved.

2.9.1 Quinn's theory of oxidational wear

Quinn proposed [32] a model which related the wear rate to the formation and removal of an oxide layer upon the contacting surfaces. As wear proceeds the hot-spots (high temperatures generated at asperity contact points) [24] generated upon the surfaces, oxidise to form an oxide layer. The layer is assumed to be mechanically stable until it reaches a critical thickness, where it is no longer able to withstand the tangential forces acting upon it. At this point the layer is assumed to fracture at the oxide/metal interface so allowing the process to repeat itself.

From Archard's wear equation – **Equation {2.14}** – where K is conceptualised as the probability of a wear particle being produced in a given encounter, $1/K$ can be seen to be the number of encounters required to produce a wear particle. In the case of oxidational wear, $1/K$ will be the number of encounters required to grow an oxide of the critical thickness ξ. If the time required to produce the critical oxide thickness at the contact temperature is t, and the time of each encounter will be τ, then:

$$t = \frac{\tau}{K} \qquad \{2.21\}$$

Since $\tau = (d/V)$, where d is the distance along which contact is maintained and V is the sliding speed, then:

$$t = \frac{d}{VK} \qquad \{2.22\}$$

Now assuming parabolic oxidation of the surface, where growth of oxide per unit area (Δm) in time t, then:

$$\Delta m^2 = k_p t \qquad \{2.23\}$$

Where K_p is the parabolic rate constant (other rate laws could be applied, but it was assumed to be parabolic when the model was derived). From this it can be stated that:

$$\Delta m = f \xi \rho \qquad \{2.24\}$$

Where f is the mass fraction of the oxide which is oxygen and ρ is the average density of the oxide. From this an expression for the K factor can be derived thus:

$$K = \frac{dk_p}{V \rho^2 \xi^2 f^2} \qquad \{2.25\}$$

Now assuming that the surfaces do oxidise under parabolic kinetics, the rate constant K_p can be obtained from the Arrhenius equation:

$$K = A_p e^{-Q_p/RT_o} \qquad \{2.26\}$$

Where A_p is the Arrhenius constant, Q_p is the activation energy for the reaction, R is the gas constant and T_o is the temperature at which the reaction occurs. Substituting this into **Equation {2.25}** gives a temperature-dependent expression for the K factor, thus:

$$K = \frac{dA_p e^{-(Q_p/RT_o)}}{\xi^2 \rho^2 V f^2} \qquad \{2.27\}$$

This can be put into Archard's equation – **Equation {2.14}** – to obtain an expression for the wear rate:

$$w = \frac{dAA_p e^{-(Q_p/RT_o)}}{\xi^2 \rho^2 V f^2} \qquad \{2.28\}$$

From **Equation {2.28}** an expression is obtained for wear in terms of the oxidation properties of the materials, the temperature produced at the interface at the time of contact and a critical thickness of oxide layer. Quinn [32] assumed

that the critical thickness of the oxide layer can be measured by microscopic observation, and knowing the static oxidation properties of the materials used, prediction of the wear rate should be easily achieved.

However the temperature of the rubbing surfaces is notoriously difficult to determine [33] especially where the surfaces are covered with an oxide layer whose thermal properties will be different to the alloys they are formed upon. In this model the approach was to obtain the temperature of oxidation from the oxides recovered in the wear debris. Oxides produced formed on dilute iron alloys are shown in **Table 2.1.**

Phase present	Temperature of formation
α-Fe_2O_3	Up to 200°C
Spinel (Fe_3O_4)	200° to 500°C
Wüstite (FeO)	Greater than 500°C

Table 2.1 Formation temperatures of oxides on dilute iron-based alloys [18]

The theory was further complicated when it was pointed out that oxidation during wear – tribo-oxidation – does not occur at the same rate as static oxidation [34, 35]. It was found that Q, the activation energy, does not change significantly from static to tribo-oxidation but, A_p the Arrhenius constant does. This is because the Arrhenius constant is strongly dependent upon the state of the surface and the presence of dislocations and voids within the material, which are in turn strongly affected by the wear process.

Subsequent developments of the oxidational wear theory found that the rates of oxidation calculated from wear rates were far higher than those measured in static oxidation studies. This was related to the wear surfaces becoming 'activated' by the wear process.

Such 'activation' in tribo-oxidation is believed to occur via the oxide formed upon a deformed surface having a large number of dislocations within its structure. These dislocations may act as sinks for voids, so preventing the formation of pores. Pore formation is observed in the static oxidation of these materials, but not in tribo-oxidation. The pores are believed to block the diffusion of ions through the oxide layer, thus slowing down the rate of oxidation [36].

Other modifications [37-39] have been made to the oxidational wear theory. It has been found that it is possible to have transfer of the oxide particles

in oxidational wear. Transfer occurs via the imbedding of debris in the oxide layers. The effects of cracks in the oxide layer, which further complicate the calculation of oxidation rate, have been shown to be significant in oxidational wear modelling, together with oxidation of the surfaces while out of contact [40] – the general theory of oxidational wear. The oxidational wear theory assumes that oxidation only takes place at the high temperatures generated during asperity interactions.

2.10 The role of wear debris in the wear mechanism and wear rate

All surfaces are covered with adsorbed gases, such as water, hydrocarbons and oxides except under exceptional circumstances (e.g. specially prepared samples in ultra-high vacuum). Although the presence of these films upon the surfaces are not normally considered to be 'third bodies' they do affect the wear processes [41, 42].

Wear debris produced in the wear of metals and alloys can be characterised as one of either two types [43]. These are (1) passive debris which is removed from the wear interface as soon as it is formed and (2) active debris which after its formation participates further in the wear processes. Passive debris generally consists of large particles, unmodified after formation so possibly containing features of the original surface. Active debris tends to be much finer, consisting of fine metallic and oxide material.

In most theories of wear, the debris produced is assumed to be removed from the area of contact as soon as it has been formed. However, many studies [44-47] show that wear particles retained within the wearing interface can play an important role in the wear mechanism.

Wear particles which are significantly harder than the wearing materials, either oxides or highly work hardened debris; may act as an abrasive, giving rise to an abrasive-type mechanism which is generally considered to increase the wear rate. For this to occur a debris hardness of 1.3 times that of the contacting materials is normally assumed to be required [18].

Conversely, wear particles may separate the surfaces so preventing adhesion and deformation. Such particles may be termed a 'third body', protecting the surfaces and so reducing wear. This effect is highly dependent upon the sliding conditions and the geometry of the wearing couple offering the ability to retain the debris. Such processes are most often seen in fretting wear as under these conditions removal of the debris is difficult. Although debris may

have no significant influence upon the wear mechanism/wear rate and its presence may be safely ignored.

2.10.1 Artificial supply and removal of wear debris

Iwabuchi [44, 46, 47] demonstrated the protective nature of 'third bodies' between wearing surfaces by the supply of artificial debris. Fretting wear tests of steels (0.45%C) in which artificial wear particles were supplied (1μm α-Fe_2O_3) showed a substantial reduction in the running-in wear rate so giving a marked reduction in the overall wear volume [46]. In the presence of artificial particles the increased surface roughness facilitated the retention of the particles thereby reducing the wear rate. With use of sufficient particles the running-in wear could be eliminated.

The optimum size of wear particles was found to be 0.3 μm with a surface roughness of 20μm R_{max} [44]. These particles were found to form a compacted layer of oxide material upon the wear scars' surface, so protecting the material from damage. This was not universal for all conditions, the artificially supplied debris had both positive and negative effects on wear rates depending upon the conditions of load and sliding speed employed, as displayed in **Figure 2.10** [44].

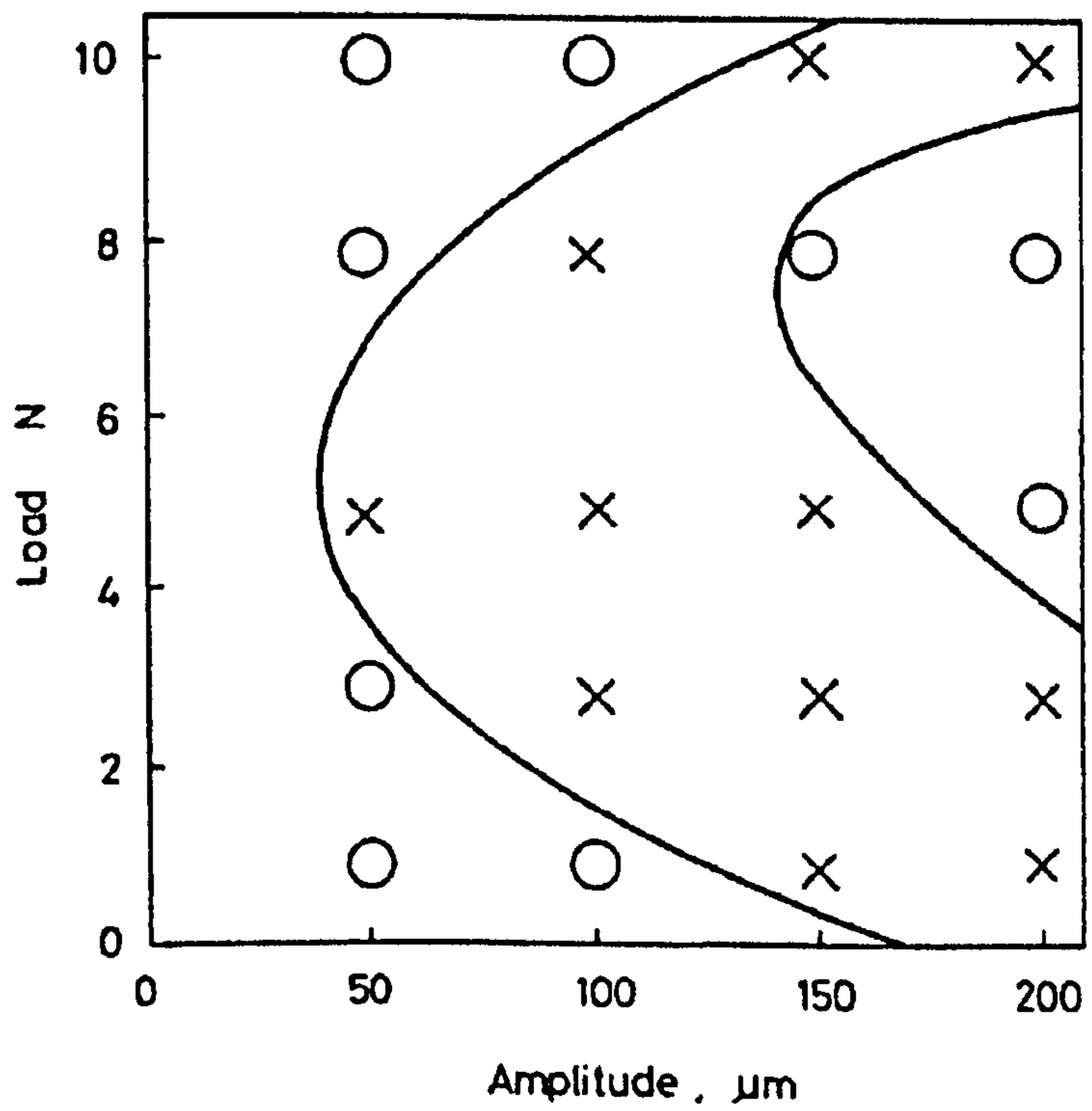

Figure 2.10 Map of the effectiveness of wear reduction by the supply of oxide particles: O beneficial effect; X hostile effect [44]

Wear tests which involved the use of interfacial air-flow through a cup-on-flat type wear rig of stainless steel (Fe-18%Cr, 9%Ni) [45] provided stronger evidence for the protective role of debris. Here, room temperature tests showed that an interfacial air-flow effectively removed the wear debris so maintaining the adhesive wear mechanism – resulting in higher wear rates. At higher temperatures (400°C and 500°C) the effect was less marked and the wear tests conducted with an interfacial air flow were still able to form compacted layers of particles upon their surfaces. This was attributed to the greater ability of the particles to become sintered and adhere to the surfaces at these higher temperatures. The effect of Van de Waals' forces acting upon the particles to prevent their removal in the air flow was also taken into account (see **Section 2.10.4**).

Similar results were observed where a magnetic field was imposed upon a wearing couple of a ferromagnetic material [48]. This work intended to investigate the effects of the magnetic field upon the tribo-oxidation. It was found that the wear rate decreased or increased depending upon whether the field direction allowed particle retention or particle elimination (via testing in oxidising and non-oxidising atmospheres).

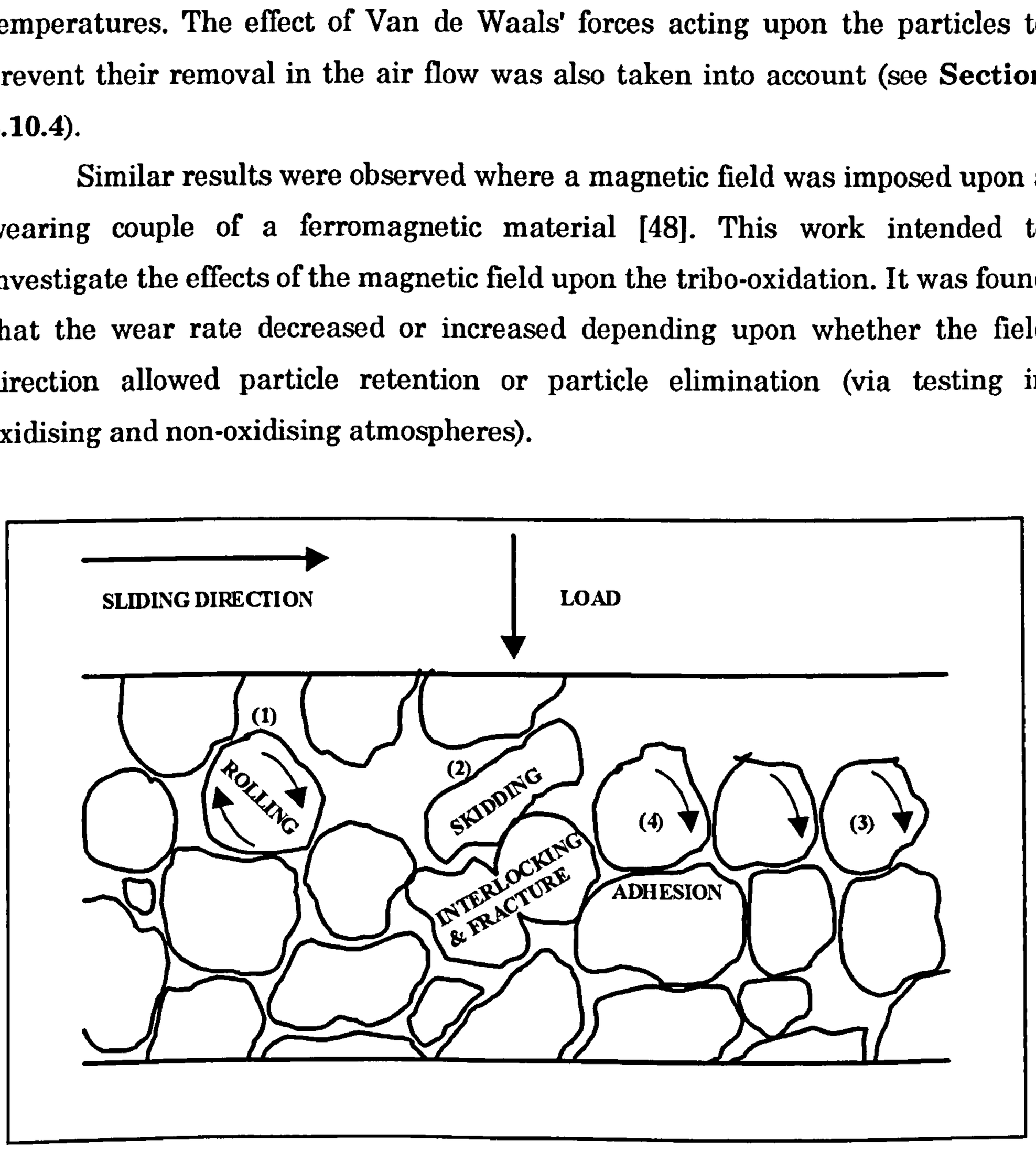

Figure 2.11 Possible motion of wear debris in a layer of particles between two first bodies [4]: (1) rolling, (2) skidding, (3) rolling and (4) adhesion

2.10.2 Behaviour of debris wearing the interface

The motion of wear particles caught in the sliding interface has been theorised by many authors. Jiang *et al.* [4, 49, 50] proposed a number of possible mechanisms for the movement of wear debris. Here the wear particles may skid over each other, act as rollers or become interlocked and undergo fracture. **Figure 2.11** [4] shows the possible behaviour of wear particles at the interface, viz:

1) If a particle is entrapped in front of a fixed object upon the surface then when it is in contact with the opposing surface it may be free to rotate around its own centre – leading to the **rotating** mechanism.
2) Where the particles are fixed to one surface and contacted by the opposing surface then they will skid across the opposing surface – hence the **skidding** mechanism.
3) Particles which are able to move freely will roll across the surface. A group of particles many undergo rolling between the surfaces – so giving the **rolling** mechanism.
4) Where strong adhesion develops between rolling particles, then rolling will become restricted. These particles will require a greater force to move. This is termed the **sintering/adhesion** affected rolling mechanism.

Fretting wear studies have shown that [51-53] the formation of a 'third body' is highly dependent upon the displacement and the applied load as to whether the particle 'beds' are established and maintained from the debris formed. If the conditions are not satisfied then the wear debris is removed from the system.

2.10.3 The effect of 'third bodies' on wear and coefficient of friction

Developments in the theory of 'third bodies' have led to many new models for friction and wear in terms of the behaviour of wear particles trapped within the wearing interface [54-55].

The effect of particles between the wearing surfaces upon the coefficient of friction is complex and may give rise to a higher or lower coefficient of friction. Halliday and Hirst [56] believed that the presence of debris at the interface in fretting wear may undergo a rolling motion, thus explaining the low coefficients of friction they observed.

It has also been shown [56] that the presence of the 'third body', by separating the two surfaces, removes the adhesion component of the frictional force, in a similar way to which wear is reduced.

Shu and Sin [57] have shown that the 'third body' particles in the interface can increase the coefficient of friction. This was attributed to the ploughing action of the particles. In tests the coefficients of friction increased with time as debris was generated. When the tests were paused and the debris removed, the friction returned to a lower value – only to rise again as new debris was generated. This equates to an abrasive wear mechanism.

The generation of wear debris, which is retained within the wearing interface, can be seen as part of the running-in process of wear. The generation and elimination of the wear particles will occur concurrently and equilibrium will eventually become established. After a certain volume of wear particles has become caught in the interface the particle layers will become 'load-bearing' and so will play in important role in the wear rate and the coefficient of friction. The volume of wear particles the surfaces are capable of holding will be determined by the surface roughness and the sizes of the particles [46].

Rice *et al.* [55] have shown that when a 'third body' particle layer exists between the contacting surfaces the coefficient of friction is determined primarily by the nature of the debris in the layer. The friction experienced by the system is determined not by the state of the 'first bodies' but by the size, quantity and mechanical properties of the debris.

2.10.4 Surface forces and the formation of third bodies

For the formation of a particle layer between the wearing surfaces attractive forces must exist between the particles and the tribo surfaces. It is most likely that particles are attached to the surface via Van der Waals' forces as electrostatic forces are only about 1% of the strength of Van der Waals' forces for non-conductive solids [54].

The force of attachment, F, is directly related to the size of the particle (assuming the particle is a sphere) by **Equation 2.29** [58]:

$$F = \frac{AR}{6r^2} \qquad \{2.29\}$$

Where A is the Hamaker constant, R the radius of the sphere, r the equilibrium separation. The Hamaker constant is related to the surface energy by **Equation {2.30}**

$$A = 9\pi \underline{r}^2 \gamma \qquad \{2.30\}$$

Where $\underline{r}$ is the distance affecting the mutual action of the Van der Waals' forces this can be estimated at 3 to 5 Å and γ is the surface energy (or adhesion energy). The surface energy is related to temperature by an Arrhenius-type dependence as shown in **Equation {2.31}**:

$$\gamma = \gamma_o \exp\left(-\frac{E}{RT}\right) \qquad \{2.31\}$$

Where R is the gas constant, E the activation energy for 'bonding' and T the absolute temperature. Van der Waals' forces are very short range forces produced by the induction of dipoles between the two bodies, which account for the attraction of fine wear particles to the wear scars' surface [59]. However very little work has be done on this in the context of wear.

The effect of sintering of particle layers also plays an important role. An investigation [60] into the sintering of ultra-fine iron, nickel and iron-25% nickel powders has shown that significant sintering can occur as soon as the powder is raised above room temperature. It can be seen that such conditions for sintering are readily available in the compacted particle layers in wearing interfaces.

The next section will examine the effect of sintering and thermal softening of debris, which gives rise to some radically different wear mechanisms at elevated temperatures.

2.11 Formation of compacted oxide 'glaze' layers

The formation of 'glaze'-type layers [61] upon the contacting surfaces at elevated temperature has been known for many years. These layers were originally thought to be 'glassy' amorphous oxide layers, hence the term 'glaze'. Such surfaces have now been shown to be crystalline [62]. They are comprised of oxides of elements from the sliding materials and their composition normally remains the same as that of the contacting materials in the case of like-on-like sliding.

The term 'glaze' has now come to be used to describe the highly smooth surfaces generated upon the top of the layer of oxide material which can be seen as a particular class of 'third body'. Such layers are most accurately termed 'compacted oxide layers' with a 'glaze'-type surface.

2.11.1 Friction and wear properties of compacted oxide layers – early models

Compacted oxide or 'glaze' layers are formed under conditions of wear at high temperature, low sliding speed and relatively low load. For situations in which the high temperature is generated by high sliding speed brought about by frictional heating, an oxidational wear mechanism is most lightly to prevail. The generation of 'glaze' layers has been shown to only occur above a minimum temperature dependent on the materials used and the sliding conditions, the formation time decreasing with increasing temperature. The establishment of such a wear mechanism has been shown to significantly reduce the levels of friction and the rates of wear often after an initial running-in period of relatively high wear rates.

Stott, Wood and Lin [62-67] investigated the fretting wear of a number of nickel-based alloys. Three mechanisms were proposed to account for the type of 'glaze' layers seen. The different mechanisms were thought applicable for different types of materials and temperatures relating to the oxidation properties and shear strengths of the materials. The mechanisms reported were:

1) Under some conditions the compacted oxide layer was believed to form from a build up of transient oxides [68] on the sample surface. Particles of transient oxides together with any pre-formed oxide are removed from the respective surfaces during the sliding process until sufficient material has built-up to form a layer of oxide, which undergoes thermal softening due to the high temperature and remains stable under the conditions of wear. Under the layer, formed in the very initial stage of wear, oxidation of the contacting elements still takes place by internal oxidation so thickening the layer.
2) At lower temperatures and for alloys of high strength, the oxide layers are thought to form by the grinding-down, compressing, smearing and sintering of oxide particles as a result of the sliding heat generated [63].
3) Finally a third mechanism was proposed in which the 'glaze' layer was continuously broken-down and reformed from the debris generated – although this mechanism was considered to be the least likely.

From this work it was proposed that properties of low wear and friction are associated with the physical state of the 'glaze' layers not with their chemical condition – because it was shown that the composition of these layers is generally similar to that of the alloys of which they were formed [62].

2.11.2 The effect of partial pressure of oxygen

An investigation of the effect of the partial pressure of oxygen was undertaken by Barnes *et al.* [69] employing a series of iron-chromium alloys (up to 40% chromium) in crossed-cylinder configuration at oxygen partial pressures of 10^{-4} to 10^{-6} Pa. The investigation found that coefficients of friction remained high at all test temperatures. Seizure was found to occur at 500 to 600°C, for Fe-40%Cr no seizure was apparent to temperatures up to 850°C.

Room temperature studies using reciprocating and unidirectional sliding of a pin-on-disc type rig [69-71] demonstrated that at pressures of $pO_2=10^{-6}$ Pa an adhesive wear mechanism dominated, although there was sufficient oxygen present to prevent seizure. At higher pressures ($p\ O_2=10^{-4}$ Pa) areas of compacted debris, termed 'islands' developed on the contacting surfaces – these were responsible for a transition to a mild wear mechanism. With further increases in partial pressure of oxygen ($pO_2=10^{-1}$Pa) these features were observed to develop far more rapidly.

It was noted that the shape of the stylus – conical and hemispherical – employed influenced the process of 'glaze' formation: hemispherical styli were able to trap more wear particles so giving more 'glazed' islands of compacted oxide material.

The compacted material was shown to be formed from oxide or oxide-covered debris. By changing the partial pressures of oxygen midway through the tests Barnes *et al.* demonstrated the debris to persist after oxygen had been removed for the wearing system. This established the stability of the compacted oxide layers once formed and their wear resistant nature.

This work showed clearly that the compacted oxide layers were formed from oxidised debris, compacted onto the wearing surface, so discounting some of the earlier proposed models for the formation of layers.

2.11.3 Wear of cobalt-based alloy Stellite 31

Investigation of the wear of cobalt-based alloy Stellite 31 (Co-0.5%C, 25.0%Cr, 10.0%Ni) was conducted by Stott, Stevenson and Wood [3]. Testing was

carried out under fretting conditions from room temperature to 800°C. It was found that Stellite 31 formed compacted oxide layers, in a similar way to those formed upon nickel- and iron-based alloys, containing all the elements of the alloy in approximately the same proportions. At room temperature it was revealed that Stellite 31 had a considerably lower wear rate compared to that obtained for nickel- and-iron based alloys (0.2 mm^3 for Stellite 31 compacted to 1.1 mm^3 for Nimonic 108 at 5 hours sliding at 20°C). This was attributed to the hexagonal-close packed structure of the alloy [72], which contains a lower number of available slip systems so leading to less deformation of the material.

At elevated temperatures, the formation of the compacted oxide layer was not accompanied by the marked reduction in the coefficient of friction seen with nickel-based alloys. This was also attributed to the hexagonal-close packed structure as the friction was already lower during metal-to-metal contact experienced before the compacted oxide layers was established.

2.11.4 Models for the generation of debris and compacted oxide layer formation

The work of Stott, Glascott and Wood [73-75] investigated the fretting wear of iron-based alloys in the temperature range of 200°C to 600°C. Here the formation of the compacted oxide layers was studied and three mechanisms were proposed for the generation of oxidised debris. Each is believed to operate under specific conditions of high temperature wear:

1) ***The oxidation-scrape-reoxidation mechanism*** – here the rate of oxidation is controlled by the 'flash' temperatures developed where metal-to-metal asperity contact takes place as well as by the 'bulk' material temperature. On subsequent traverses the oxides were removed. The oxides thus generated may either remain in the system to form oxide layers, and give rise to three-body abrasive wear, or be removed from the system. This process would then be repeated.
2) ***The total oxidation mechanism*** – if the oxide layers growing on the surface are not totally removed by the sliding action, and are coherent, then the film will continue to thicken and provide a protective layer.
3) ***The metal debris mechanism*** – here the oxides are generated from the metallic debris which is produced by abrasion of the surfaces. Once the debris is formed it is further broken-down within the wearing interface until it is small enough to become spontaneously oxidised.

These models were seen to represent the limiting cases for development of oxide debris within the sliding interface. Once formed these oxides build-up between the surfaces to form the compacted oxide layers.

2.11.5 Minimum temperature for compacted oxide layer formation

Wear testing in which the temperature of the test was altered during wear showed that the compacted oxide layers were not only unable to form below a certain critical temperature, dependent upon the materials and sliding conditions, but become unstable [76] below the critical temperature. When the temperature at which the layers formed was lower than the critical temperature, the layers were seen to break-down. Such a break-down of the layer demonstrates that the minimum temperature of formation is not related to the supply of debris but the influence of temperature upon the oxides. Sufficient temperature will allow suitable softening and sintering for the formation of 'glaze' layers. Below the transition temperature they are too brittle to form a coherent stable layer. Stopping the test and thermally cycling the compacted oxide layers had the effect of introducing stresses, which resulted in the break-down of the layers on the commencement of sliding.

Stott, Glascott and Woods [77, 78] explanation for the minimum temperature was that the frictional force decreased with increasing temperature for oxide/oxide sliding. When the temperature was suitably low, the mechanical forces acting upon the oxide layer were strong enough to cause its break-down. This corresponds to a coefficient of friction of ~0.8 for fretting wear studies, which in turn relates to a temperature of 200 to 300°C under these conditions. The differences in the minimum temperature seen for different materials were attributed to the relative ductility of the oxides generated – more ductile oxides being able to withstand higher stresses imposed during wear, thus giving a low transition temperature. Great care must be taken in comparing wear studies as it is known that small changes in the wear test conditions can have a marked affect on the wear rates experienced [71].

2.11.6 Wear in other environments

The presence of water vapour has been shown to also affect the formation and development of compacted oxide layers [36]. This is due to the hydration of the oxides, hydrated oxides are softer than their non-hydrated counterparts and so are more easily consolidated and sintered to form a compacted oxide layer [79].

Sullivan and Granville [80] carried out an investigation of Fe-9%Cr steel in a pin-on-disc-type rig in pure carbon dioxide atmospheres at temperatures from 200 to 550°C. The formation of compacted oxide layer was also seen to occur from the oxidation of the alloys by the carbon dioxide:

$$nCO_2 + M \rightarrow nCO + MO_n \qquad \{2.32\}$$

In this and other investigations [81] the wear mechanisms appeared to be very similar, if not identical to those examined in ordinary air. Wear in non-oxidising atmospheres will not result in the formation of compacted oxide layers although adsorbed gases will reduce adhesion and so reduce wear and friction [1].

2.11.7 Pre-oxidation, pre-sliding and oxygen-rich coatings

Pre-oxidation of wear samples [82, 83] has shown that an oxide-rich coating can supply oxide material in the initial stages of wear so reducing the time for the establishment of a compacted oxide layer. This in effect reduces the overall wear rate of the sample. It was seen that the oxide coating was broken-down to supply oxide debris, as opposed to the pre-oxidised layer directly forming the compacted oxide layer upon its surface. Ion implantation with oxygen [84] produces a similar result in reducing the running-in wear by increasing the supply of oxidised debris.

Conversely wear resistant coatings, such as titanium nitride [83], are gradually thinned during wear until they brake-down and a compacted oxide layer forms – if possible under the wearing conditions – via the normal route.

2.11.8 'Third-body' model for compacted oxide layer formation

Jiang *et al.* [4] took the approach of modelling the compacted oxide layer formation from the compaction and sintering of a 'third body'-type layer of debris on the contacting surfaces. From a study of the fretting wear of Nimonic 80A from room temperature to 250°C, the formation of the compacted layer was seen to take place from the loose debris present on the wearing surfaces. This loose compact of particles then underwent further compression and sintering, at elevated temperature, to form the compacted oxide layer. Further fracture and compaction led to the refining of the surface to give the 'glaze'-type finish. This model envisages the generation of the compacted particle layer and 'glaze'-type surface taking place via the sintering of a 'third body'-type layer of oxide debris,

when the temperature at the interface is above that required for 'glaze' formation.

A distinction was made between the compaction and sintering of an oxide particle layer, and the generating of the highly smooth surface – the 'glaze' layer. Ultrasonic cleaning of the wear scars revealed that beneath the loosely compacted layers of particles on the scar, sintering had often taken place to form more solid layers.

The compaction and sintering of the particle layers are considered to be temperature-dependent. Agglomerates of fine particles are generally stronger than those formed from larger particles, due to the greater number of points of contact that may adhere. The adhesion energy is also temperature-dependent, following the Arrhenius relationship, **Equation {2.26}**:

$$K_p = A_p e^{-Q_p/RT_o} \qquad \{2.26\}$$

In one test [49], a layer of loosely compacted particles formed during wear at 20°C was heated to 600°C for 90 minutes. Here it was seen that the particles in the layer sintered and contained some cracks derived from cooling which the sample had subsequently undergone.

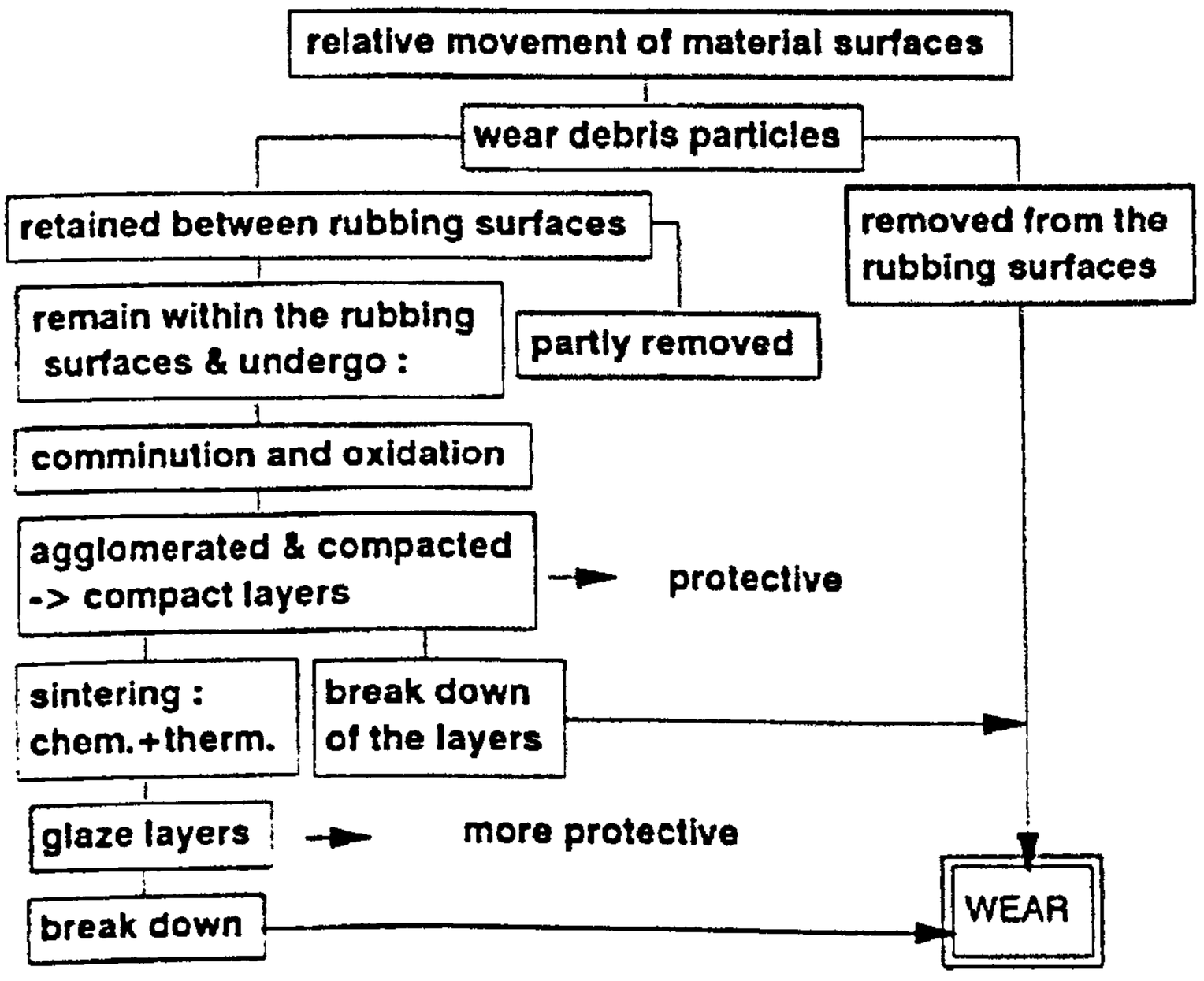

Figure 2.12 Scheme for wear protection offered by the formation of compacted oxide layers and 'glaze' layers [85]

The use of three-dimensional topographical [6] analysis capable of measuring contact resistance showed that the compacted oxide regions tended to form in the centre of the wear scars, further demonstrating the effect of debris retention. The coverage of the wear scar with high resistance, load-bearing layers was found to be 20 to 50%. Ultrasonic cleaning of the wear scar led to a slight reduction in the coverage of the surfaces with high resistance areas, as the loosely compacted particles were removed.

At 150°C, compacted oxide layers and loosely compacted particle layers were seen together. This model covers the formation of wear protective layers both above and below the critical temperature required for 'glaze' formation. The scheme for wear protection described by this model is shown in **Figure 2.12**

Although this model applies well to fretting wear systems and gave good agreement with experimental data, it would seem unlikely to be as appropriate to systems in which wear debris is not well retained within the interface. Under conditions where a 'third-body' of debris is not observed but compacted oxide layers are seen to form under conditions of elevated temperature [7, 45]

2.11.9 Unlike sliding combinations

Very little work is available on the formation of compacted oxide layer during the wear of unlike sliding couples, most of the available literature covers like-on-like fretting wear. It has been demonstrated that the nature of the sliding couple may strongly affect the retention of debris and the subsequent wear mechanism [71, 86].

Sample	Counterface	Wear rate
Iron-chromium (ODS)	Cobalt-chromium	Low ('glaze' layers)
Iron-chromium (ODS)	Iron-nickel-chromium	High (limited 'glaze' layers)
Nickel-chromium	Cobalt-chromium	High (No 'glaze' layers)
Nickel-chromium	Iron-nickel-chromium	Low ('glaze' layers)

Table 2.2 Results of unlike sliding wear tests carried out at 750°C [7]

Wood *et al.* [7, 8] carried out an investigation into the wear of a selection of high temperature materials at room temperature, 500 and 750°C. A reciprocating block-on-cylinder-type wear rig was used to simulate the wear of valve and valve seats for use in combined heat and power gas engines. In this work unlike sliding of four classes of alloys was considered: iron-chromium (ODS), nickel-chromium, iron-nickel-chromium and cobalt-chromium – a complex

pattern of wear behaviour was found, as shown in **Table 2.2**. Under these conditions, formation of compacted oxide layers was not initially expected, however several of the material combinations did exhibit the distinctive highly smooth surfaces formed upon a thick oxide layer. A complex pattern of transfer and non-transfer of counterface materials to the sample surface was seen to be taking place.

The results given were confirmed by a number of different alloys from each class, supplied by different manufacturers. It was postulated that the mechanisms were affected by either the nature of the oxides produced within the interface and their abilities to form debris layers or the materials ability to support the layers, without the layers being broken-up and removed from the opposing surface. However many of the underlying reasons for these effects were not clear, and further investigation was outside the remit of that project.

Summaries of the important steps towards the current understanding of this wear mechanism are given in **Table 2.3**. The latter developments gave a good understanding of the possesses involved in fretting wear and the models gave good agreement with experimental findings. However the work of Wood *et al.* [7, 8] shows that this wear mechanism operates under previously un-investigated conditions, in which the choice of materials appeared to be far more critical to the establishment of the compacted oxide layers. Understanding of the wear mechanisms under these conditions is clearly limited.

2.12 Summary of compacted oxide and 'glaze' studies

Authors	Test condition / rig	Conclusions
Stott, Wood and Lin and co-workers [62-67]	Fretting and unidirectional pin-on-disc type wear tests using iron- and nickel-based alloys in the temperature range room temperature to 800°C.	The effects on friction and wear of the compacted oxide layer were characterised. The effect of the minimum temperature of formation and changes in friction were established.
Barness *et al.* [69-71]	Crossed cylinder unidirectional sliding was used for an investigation of iron-chromium alloys in the temperature range room temperature to 800°C. Studies also carried out at room temperature to investigate the effect of lower partial pressure of oxygen by reciprocating and unidirectional pin-on-disc sliding.	The term 'island' was coined to describe the morphology of the regions of compacted oxide material. Oxide layers, once formed, were found to be relatively stable in non-oxidising conditions. This indicates that they undergo little wear once the layers are established.
Stott, Stevenson and Wood [3]	Fretting wear of cobalt-based alloy Stellite 31 from room temperature to 800°C under conditions of fretting wear.	Compacted oxide layers were found to form upon cobalt-based materials, although the changes in coefficient of friction associated with their formation with iron- and nickel-alloys were not seen. This was attributed to the HCP structure of the cobalt-based alloy.
Stott, Glascott and Wood [73-75, 77, 78]	Iron-based alloys were investigated in fretting wear type tests. These were conducted in the temperature range 200°C to 600°C.	Models were proposed for the generation of wear debris which subsequently forms the compacted oxide layers. Models were also proposed for the formation of the oxide layer, which took into account the changes in friction during their establishment.

Various authors [16, 36, 79-81]	Investigations into the effect of water vapour upon the formation of compacted oxide layers and wear in CO_2 environments under fretting conditions.	The effect of water vapour was to make formation of the layers easier. This was due to the hydration of the oxide debris. Formation of wear resistant oxide layers has been found to occur in other oxidising environments – such as CO_2.
Various authors [82-84]	Studies of pre-oxidation, wear resistant coating and ion implantation to reduce wear (various experimental conditions).	Oxide-rich coatings were shown to reduce the running in wear experienced by the system, so reducing the overall wear rate.
Jiang *et al.* [4, 6, 49, 50, 85]	Fretting wear studies of nickel-based alloy Nimonic 80A in the temperature range room temperature to 250°C. Topographical contact resistance used for characterisation of wear scars.	Here a more elaborate model was developed taking a 'third-body' approach to the formation of compacted oxide layers. In the model, the formation of oxide layer was akin to that for the formation of non-compacted layer of debris - which was seen as part of the formation process.
Wood *et al.* [7, 8]	A reciprocating block-on-cylinder configuration wear rig was used to investigate a variety of Superalloys and ceramics at room temperature, 500 and 750°C. Unlike sliding combinations were used.	Compacted oxide layers were shown to form preferentially from the oxide debris produced from either the sample or the counterface. The work demonstrated the importance of transfer processes in this type of wear and important differences in wear properties from one material to another.

Table 2.3 Summary of elevated temperature wear studies

3. Introduction to the current investigation

A significant amount of knowledge now exists relating to the formation of compacted oxide-type layers for wear under like-on-like fretting wear and low amplitude reciprocating sliding conditions. Mechanisms have been proposed for the generation of suitable debris [73], the formation of 'glaze' layers from the debris present upon the surfaces [4, 6] and for the processes by which these 'glaze' layers affect wear and friction. There exists a critical temperature below which the compaction and sintering of the debris do not occur. This temperature is dependent on the wearing system. The onset of layer formation is often associated with a decrease in friction coefficient.

Formation of compacted layers is highly dependent upon the sliding conditions employed. This is because the debris must be maintained within the interfaces to allow layer formation. Compared to the like-on-like systems, the high temperature wear involving unlike sliding has not been studied extensively.

A study conduced by Wood *et al.* [7, 8] in this laboratory using unlike sliding (**Section 2.11.9**) has shown that layers were formed under tests conducted using a block-on-cylinder-type rig at 500 and 750°C using a variety of Superalloys and intermetallics. The combinations of materials as samples and counterfaces gave some surprising results (**Table 2.2**), certain combinations of materials facilitated layer formation (MA956/Si_3N_4 counterface, PM2000/Stellite 6 counterface) and low wear, while others did not (Nimonic 80A/Stellite 6 counterface, TiAl/Si_3N_4 counterface). These behaviours were not easily explained, under certain conditions transfer of oxide material from the counterface led to the formation of compacted layers whilst in other cases layer formation did not take place.

The present research programme has been designed to achieve improved understanding of the generation of debris, the processes of transfer of material, the factors affecting such transfer and the mechanisms of layer formation involving unlike sliding. The influence of temperature and load were the key objective of this project.

In order to investigate the effect of the counterface under these conditions four alloy couples were chosen representative of those previously identified by Wood as giving the complex set of wear behaviour. These were MA956 and Nimonic 80A as samples and Stellite 6 and Incoloy 800 as counterfaces.

Often it is stated that the formation of compacted debris layers is a low-load phenomena [63], even though little work has been carried out into the effect

of load on the formation and maintenance of such layers. This project was planned to examine whether, at a certain load, the formation of such layers would no longer be favoured as the deformation of the alloys would cause breakdown of the layers. The fine debris required for the formation of layers would no longer be maintained within the interface, giving rise to a transition to an oxidational-type mechanism where oxide debris is expelled from the system resulting in a severe wear mechanism in which metal-to-metal contact dominates.

It is also unclear as to how wear rates are affected across the range of loads under which layers do form and how any such changes are effected by the choice of sample and counterface materials. To resolve these issues a study of the influence of load on the wear between the four alloy couples used throughout this project was conduced at 750°C.

It is known that, under given experimental conditions, the transition temperatures at which compacted oxide layers formed show good reproducibility. It is also known that layers are established faster and are more stable at higher temperatures. One of the principal aims of this project was to study the effect of temperature on various aspects of high temperature wear – debris formation, generation of surface layers and the affect of the mechanical properties of the materials across the range of temperatures investigated.

Many researchers have attempted to relate wear properties of materials to hardness [87] The great advantage of relating hardness to wear is the ease in which hardness data can be recorded, so allowing rapid assessment of candidate alloys. Hardness data provide a crude measurement of the material's resistance to deformation or yield strength which in turn affects the alloy's ability to resist wear. In the case of compacted layer formation it was thought that hot hardness data would be more appropriate to shed light on the ability of the materials to provide support for the compacted layers once formed. Hot hardness data would provide information on the influence of the changes in deformation characteristics of the materials on layer formation. To this purpose hardness/temperature profiles were determined for the four alloys used in this study. These data were to be used in the interpretation of the wear tests conducted from room temperature (~25) to 750°C.

It is known that the experimental set-up used for wear testing can have a marked result on the wear rates and mechanisms experienced. In order to assess the effect of the experimental arrangement employed on the processes of layer

formation in unlike sliding systems, each of the four couples were 'reversed' at 750°C, i.e. the sample materials were used as a counterface and vice versa.

Like-on-like sliding was also conducted for each of the materials at 750°C in order to examine the 'inherent' wear properties of the four alloys without the influence of an unlike counterface, allowing interpretation of data obtained at 750°C.

To examine the formation of layers, tests were conducted at the minimum temperature of layer formation (identified earlier in the programme) over a range of times covering the formation of the layers. The lowest temperature of formation was to be used as it is known that layers form at faster rates at higher temperatures. In summary the programme involved:

1) Investigation of wear at 750°C over a range of applied loads to ascertain any changes in mechanism over this load range and associated changes in wear rates.
2) Investigation of wear occurring between room temperature and 750°C to determine the minimum temperatures of formation of the compacted oxide layers and the associated changes in wear mechanisms and rates.
3) Determination of the hot hardness data for the four alloys from room temperature to as close to 750°C as possible to aid the interpretation of the wear data obtained between room temperature and 750°C.
4) Study of the system involving reversal of the sample and counterface and like-on-like sliding of the four alloys at 750°C in order to further characterise the effect of sample and counterface selection.
5) To carry out tests over a range of times around the minimum temperature of formation for selected alloy pairs to examine the formation mechanisms.

This programme was designed to characterise the generation of the compacted oxide layer under conditions of unlike sliding combinations via use of the block-on-cylinder-type rig.

4. Experimental

4.1 Materials used in the programme

The materials employed in this experimental programme were four commercially available Superalloys, from a variety of suppliers. Their compositions are shown in **Table 4.1** and brief descriptions of their properties are given in **Table 4.2.**

	C	Si	Mn	Co	Al	Fe	Ni	Cr	Ti	Other
MA956	0.05	-	-	-	4.5	bal.	-	20	0.5	Y 0.5
Nimonic 80A	0.08	0.1	-	-	1.4	0.7	bal.	19.4	2.5	-
Stellite 6	1.1	1.0	-	bal.	-	3.0	3.0	28.0	-	W 4.5
Incoloy 800	0.07	0.4	0.7	0.30	0.5	45.7	30.8	20.0	0.6	Cu 0.4

Table 4.1 Nominal composition of the alloys wt.%

Alloy	**Description**	**Vickers hardness (GPa)**	**Average grain size (μm)**
MA956	ODS alloy strengthened through a yttria dispersion in Fe-Cr-Al matrix	0.308	3000
Nimonic 80A	Precipitation hardened alloy through a $Ni_3(Al\text{-}Ti)$ phase	0.260	90
Stellite 6	Solid solution strengthened matrix in which carbides are distributed	0.363	50
Incoloy 800	Solid solution strengthened iron-based Superalloy containing an austenitic matrix	0.157	90

Table 4.2 Description of the materials used in the programme

4.2 Design and construction of the high temperature wear rig

The high temperature wear rig was constructed 'in-house' and based upon a block-on-cylinder design by Lancaster [88] and the subsequently modified high temperature design by Johnson *et al.* [89]. The rig was developed for the testing of valve and valve seat materials. In this later design, reciprocation of the sample was added. This was done to achieve stress cycling of the sample, to simulate the loading and unloading of the material in operation of valve/valve seats. Such a design also has the advantage of extending the wear scar along the sample's surface and maintaining the same apparent area of contact as material is progressively removed from the sample and counterface.

The design of the wear rig is shown in **Figure 4.1.** The rig consists of a variable speed electric motor which drives a rotating shaft. Upon the first section of the shaft is mounted a torque transducer. The shaft then runs through a furnace capable of operating from room temperature (~25) to 750°C. This second section of the shaft is of Nimonic 80A and upon which the counterface – a cylinder 50 mm in diameter – is mounted. The shaft rotates at a speed of 250rpm which equates to a sliding speed of 0.654 ms^{-1} and for a four hour experiment gives a total sliding distance of 9425 m

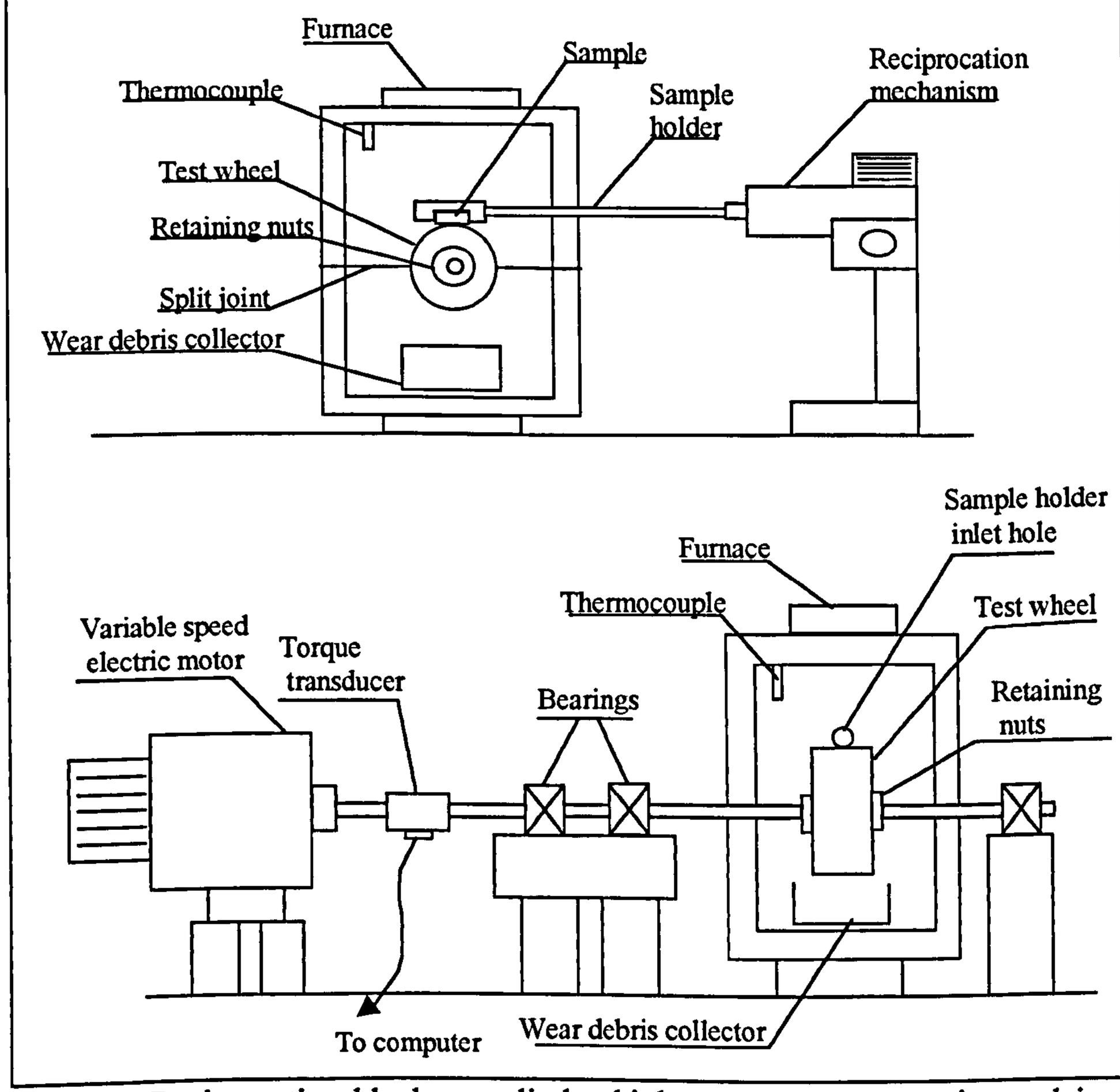

Figure 4.1 Reciprocating block-on-cylinder high temperature wear rig used in the experimental programme

The sample is held against the counterface by the sample holder, which fits through an opening in the side of the furnace. The sample – a pin of 5×5×45 mm – is loaded transversely against the counterface.

The sample arm can be reciprocated at a rate of three cycles per minute over a constant velocity stroke of 12mm. The sample holder fits into the reciprocating mechanism, which is then fastened by a locking grub screw. Great care must be taken when fitting the sample holder to ensure that the sample is mounted flat against the counterface.

A *Melbourne type TRP-50* torque transducer measures the coefficient of friction, the output from which is recorded by a *Thurlby multimeter/data logger type 1905a*. The recorded milli-volt readings were then converted to coefficients of friction values via a spread sheet.

The whole rig is built upon a large metal table to fix all the components firmly in place, reducing vibration and to earth the electrical components.

4.3 Test methods and sample preparation

4.3.1 Preparation of samples and counterfaces

Samples were prepared by grinding with successively finer grades of abrasive paper, followed by polishing to 1 μm diamond paste. Counterfaces were ground to 1200 grit grade abrasive paper. Samples and counterfaces were washed and degreased with alcohol (IMS) and distilled water before being fitted into the wear rig.

4.3.2 Wear test conditions

The wear tests in the programme fall into four main categories. (a) Tests at 750°C over a range of applied loads, (b) tests over a range of temperatures, (c) tests in which the counterface/sample materials were reversed and like-on-like testing used and (d) tests over a range of times for selected combinations of materials. The experimental conditions for each of these tests are shown in **Table 4.3**

For the study of wear with applied load, the alloys MA956 and Nimonic 80A were worn with the counterface materials Stellite 6 and Incoloy 800. The higher loads were achieved by attaching a dead weight to the sample arm, which made use of the reciprocation of the arm difficult. However the MA956 sample/ Stellite 6 counterface tests were repeated with reciprocation.

For the study of wear across a range of temperatures, temperatures were selected to cover the wear from room temperature (~25) to 750°C in approximately equal steps. When it was found that changes in wear rate

mechanism occurred more rapidly with changes in temperature, at the higher temperature, the extra tests at 450, 570 and 690°C were added.

For the test examining alternative combinations of samples and counterfaces, Stellite 6 and Incoloy 800 were used as sample materials and worn against MA956 and Nimonic 80A counterfaces. Like-on-like sliding of the four alloys was also carried out.

Test conditions for wear over a range of normal loads	
Variable	**Setting**
Time	4 hrs
Temperature	750°C
Load	7, 10, 15, 20 and 25 N
Reciprocation	Off
Test conditions for wear with temperature	
Variable	**Setting**
Time	4 hrs
Temperature	~25, 150, 270, 390, 450, 510, 570, 630, 690 and 750°C
Load	7 N
Reciprocation	On
Test conditions for alternative combinations of materials	
Variable	**Setting**
Time	4 hrs
Temperature	750°C
Load	7 N
Reciprocation	On
Test conditions for study of compacted oxide layer formation	
Variable	**Setting**
Time	10, 30, 60, 90, 120 and 240 minutes
Temperature	630°C and 690°C
Load	7 N
Reciprocation	On

Table 4.3 Test conditions for the studies carried out in the experimental programme

Wear experiments were conducted to investigate the formation of compacted oxide layers upon MA956 and Nimonic 80A worn with Incoloy 800. These tests were carried out at the lowest temperature at with the compacted oxide layers were seen to form at 690°C and 630°C respectively.

4.3.3 Wear test procedure

With the top half of the split furnace removed, the high temperature section of the shaft could be taken out and the counterface fitted in place with retaining nuts. The shaft could then be reattached to the rig. The counterface was then lined-up with the sample and the retaining nuts tightened ('copper slip'

was used to prevent seizure of the retaining nuts). The sample – first weighed on an analytical balance accurate to 0.0005g – was then fitted into the sample arm and its position checked to ensure that it would run flat against the counterface. A silica receptacle was placed beneath the counterface to collect any debris produced. The sample arm was then removed so that the top half of the furnace could be replaced.

To run the test the motor was started and the furnace, data logger and torque transducer switched on. Approximately 30 minutes were allowed for the temperature and 'background' torque (produced by the bearings) to stabilise. Then the datum reading of zero friction was taken, then the sample arm was inserted through the side of the furnace and positioned to run flat against the counterface, and the test commenced.

Readings from the torque transducer were automatically logged every 5 minutes (for normal four hour tests) and the rig was checked periodically to ensure the equipment was functioning correctly. At the end of the test the sample arm was removed from the furnace and the unloaded torque reading was again noted. The furnace was then switched off and the top half of the furnace removed.

After sufficient cooling time had been allowed the sample was re-weighed. The counterface was removed and its appearance noted. Any wear debris produced was collected and kept with the sample for analysis.

4.3.4 Accuracy of wear test data

The temperature of the furnace was calibrated by running with the sample arm removed, in its place a thermocouple was inserted through the side of the furnace. This was used to produce a plot of 'temperature set' against 'temperature achieved', with particular emphasis on the temperatures at which the wear tests were run. The furnace temperature was found to be +/- 3°C for all the test temperatures set, except 150°C, which was +/- 5°C, frictional heating was assumed to be negligible [90]. The room temperature test temperature was unrecorded.

Weight change data assume that the effect of oxidation of the unworn areas of the sample at the times and temperatures of testing are negligible. This assumption has been demonstrated to be correct for the materials employed in this study [7]. Generating reproducible wear data is well known to be a problem of high temperature wear studies [91]. However weight loss and coefficient of friction were generally good. Tests were all replicated once, where data were

dubious, further tests were undertaken. An indication of the error incurred is given with the results, where applicable.

4.3.5 Hardness testing from room temperature to 510°C

Hardness testing was carried out in collaboration with Dr. M.-O. Geillue at the University of Exeter. Coupons of MA956, Nimonic 80A, Stellite 6 and Incoloy 800 were prepared of approximately 15×15×5 mm, and were polished on one side to ¼ micron diamond paste and thoroughly cleaned with water and IMS.

Hardnesses were recorded using a *Leitz micro-hardness tester* with a Knoop indenter for each of the materials at room temperature. A rest mass of 50g and a dwell time of 12 seconds were used to make indentations. Five replicates were performed for each material.

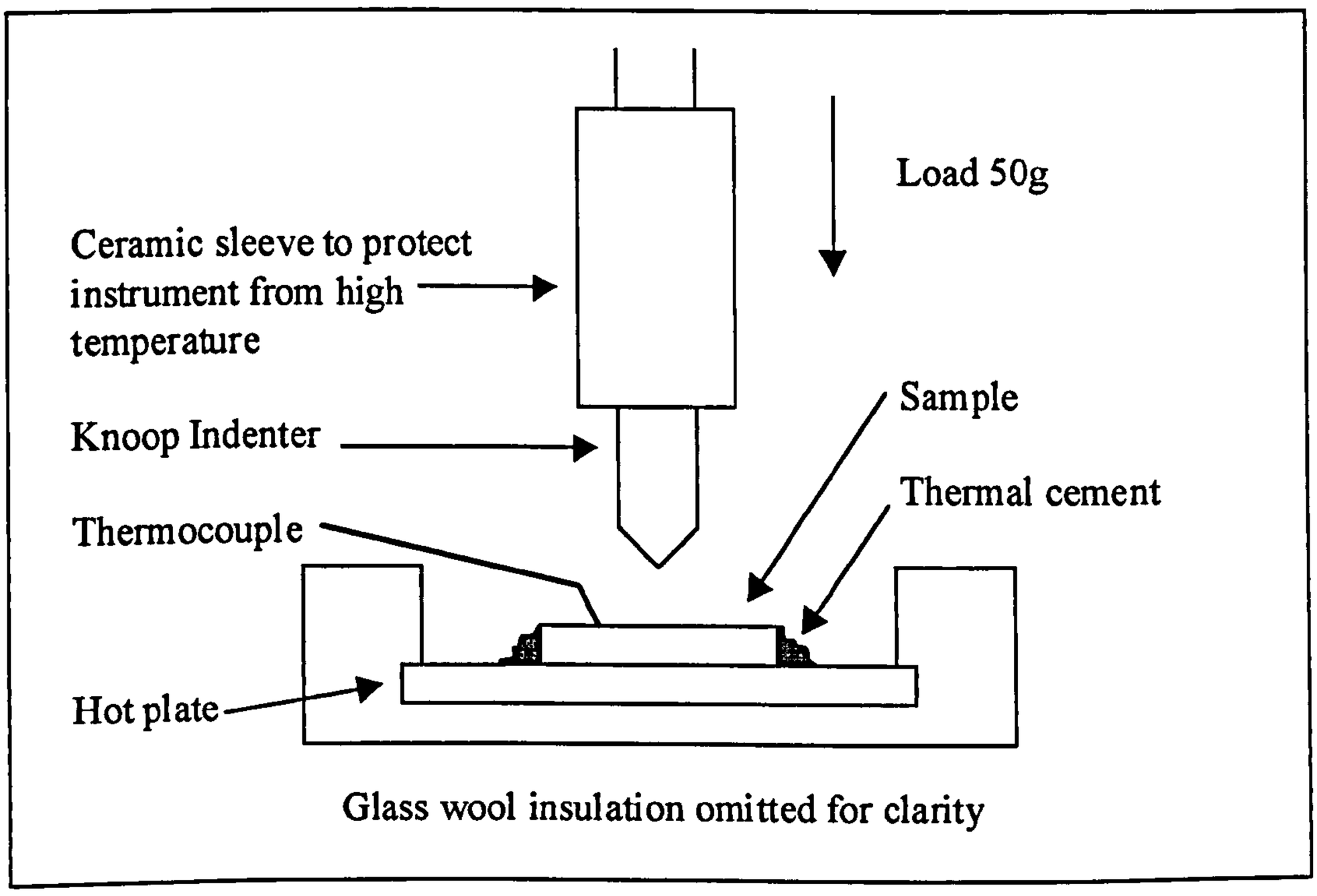

Figure 4.2 Modified indentation hardness test for determining Knoop indentation hardness from room temperature to 510°C

Hot-hardness data were obtained using a modified hardness tester as shown in **Figure 4.2**. This consisted of a hot stage of approximately 30mm in diameter mounted in the hardness tester. Samples were fixed in place on the hot plate using thermal cement, which was then thoroughly insulated with glass wool. The indenter arm was extended with a ceramic sleeve to prevent thermal conduction into the body of the instrument. This added to the rest mass of the indentor, which had to be taken into account in calculation of the hardness (weight of indentor extension 17.39 g +/- 0.01g).

To test each material, a sample was fitted to the hot stage and the temperature raised to the highest temperature to be tested. Using a thermocouple resting on the surfaces on the sample – as close the indentor as possible – the temperature was adjusted to +/- 5°C of the temperature of interest. The indentor was brought into contact with the surface for five minutes for the temperature to stabilise. The indentor was then raised and a series of indentations was made along the surface. The temperature was then adjusted to the next temperature and the procedure repeated.

Examination and measurement of the indentations were then made on a second hardness tester (due to the modifications made for operation at temperature, the microscope was no longer functional). Hot hardness profiles were then produced via the following equations: Knoop hardness is calculated from equation {4.1} [92]

$$H_K = 1.423\frac{L}{d^2} \qquad \{4.1\}$$

Where H_k is the Knoop hardness in Pascals (Pa), L is the applied load in kilograms kg) and d is the length of the indentation in metres (m). Similarly Vickers hardness can be calculated in the same units via Equation {4.2}

$$H_K = 1.854\frac{L}{d^2} \qquad \{4.2\}$$

Here d is an average of the two lengths between opposite corners of the indentation.

4.4 Analysis

4.4.1 Scanning Electron Microscopy with Energy Dispersive X-ray Analysis

Samples and debris morphologies were examined in the *Hitachi SM2400* scanning electron microscope (SEM). The instrument was also used for energy dispersive X-ray analysis (EDA) to determine the composition of samples and debris the data are most often displayed in the form of Digimaps.

4.4.2 X-ray Diffraction

As-received materials and wear scars were subjected to X-ray diffraction (XRD) analysis on a *Siemens Diffraktometer 5000* diffractometer. Diffractograms

were collected from 10 to 90° and phases were identified using the *DIFAC-DOS/ DIFAC+* software and database.

4.4.3 Weight changes and coefficients of friction

Weight changes for wear samples were calculated from their initial and final weights. Samples were weighed using a *Sartorius* analytical balance type MC210S, accurate to 0.0005 g.

Coefficients of friction were calculated from the torque transducer recorded by the data logger. A linear relationship was assumed between response of the transducer and applied torque with a torque of 50Nm giving a response of 10V. To calculate the coefficient of friction, first the 'background' torque was removed, this value was recorded while the sample was out of contact with the counterface. This was generally ~0.013V. With the background torque removed, the frictional force was calculated thus:

$$F = \frac{T}{r} \qquad \{4.3\}$$

Where F is friction force (N), T is the torque reading (Nm) and r is the radius of the counterface (m). From this the coefficient of friction was calculated thus:

$$\mu = \frac{F}{W} \qquad \{4.4\}$$

Where μ is the coefficient of friction and W is the applied load (N).

4.4.4 *Hardness testing of worn samples*

Although hardnesses of the wear scars cannot be directly measured due to the roughness of the surfaces, the hardness with depth of a cross-section can be evaluated. This results in a profile of hardness with depth for a wear scar, revealing the extent of hardening taking place in the wear process. This was carried out using a *Buehler Micromet II* Vickers micro-hardness tester using a 50g load and a dwell time of 12s. Wear samples were cut and mounted in conductive mounts so that the exposed surface ran parallel to the direction of sliding. Samples were polished to 0.25μm diamond paste. Indentations were made at 50μm intervals away from the surface to a depth of approximately 600μm. Further indentations were made around the first 100 to 150μm to ensure that any hardened layers had been detected. The distance of each indentation from the surface of the scar was measured using the micrometer on the hardness tester.

5. Results

5.1 Introduction

This chapter is divided into thirteen sections. In the first section the structure and hot hardness data from room temperature to 510°C are given for the alloys used in the programme.

Sections two and three report the wear testing of MA956 and Nimonic 80A with Stellite 6 and Incoloy 800 counterfaces over a range of normal loads (7 to 25N). Sections four and five detail the wear testing of MA956 and Nimonic 80A from room temperature to 750°C, MA956 and Nimonic 80A being worn with Stellite 6 and Incoloy 800 counterfaces.

Sections six, seven, eight and nine describe the wear of Nimonic 80A with Stellite 6, Nimonic 80A with Incoloy 800, MA956 with Stellite 6 and MA956 with Incoloy 800. Here the materials were used as both samples and counterfaces. Section ten reports the like-on-like wear of MA956, Nimonic 80A, Incoloy 800 and Stellite 6 at 750°C.

Sections eleven and twelve display the wear of MA956 and Incoloy 800 with Incoloy 800 counterfaces at 690 and 630°C at times of 10 to 240 minutes.

5.2 Testing of as-received materials

5.2.1 Hardness and hot hardness

Figure 5.1 shows the surface hardness with temperature profiles for the 'as-received' materials from room temperature (~25°) to 510°C (the limiting temperature before oxidation, and degradation of the indenter interferes with the testing). It can be seen that the harnesses of the alloys all decrease with temperature, MA956, Nimonic 80A and Incoloy 800 being of comparable hardness and have similar changes in hardness from room temperature to 510°C. Stellite 6 has considerably higher room temperature hardness but this falls rapidly with temperature to a value closer to the other materials at 510°C.

Above ~500°C some phase changes occur in these materials and hence extrapolation of hardness values to temperatures above ~500°C would not produce correct data [72].

5.2.2 XRD analysis

XRD analysis was carried out for all the materials used in the project. The phases identified for all the 'as-received' materials are given in **Table 5.1**.

Alloy	Phases identified
MA 956	Iron chromium stainless steel phase (Fe-Cr) (PCPDFWIN v. 2.01 number 34-0396)
Nimonic 80A	Iron chromium nickel stainless steel phases ($Cr_{0.19}$ $Fe_{0.7}$ $Ni_{0.11}$) (PCPDFWIN v. 2.01 number 33-0945)
Stellite 6	Cobalt chromium phase (PCPDFWIN v. 2.01 number 15-0806)
Incoloy 800	Iron chromium nickel stainless steel phase (Cr-Fe-Ni) (PCPDFWIN v. 2.01 number 33-0397)

Table 5.1 XRD analysis of the as-received materials

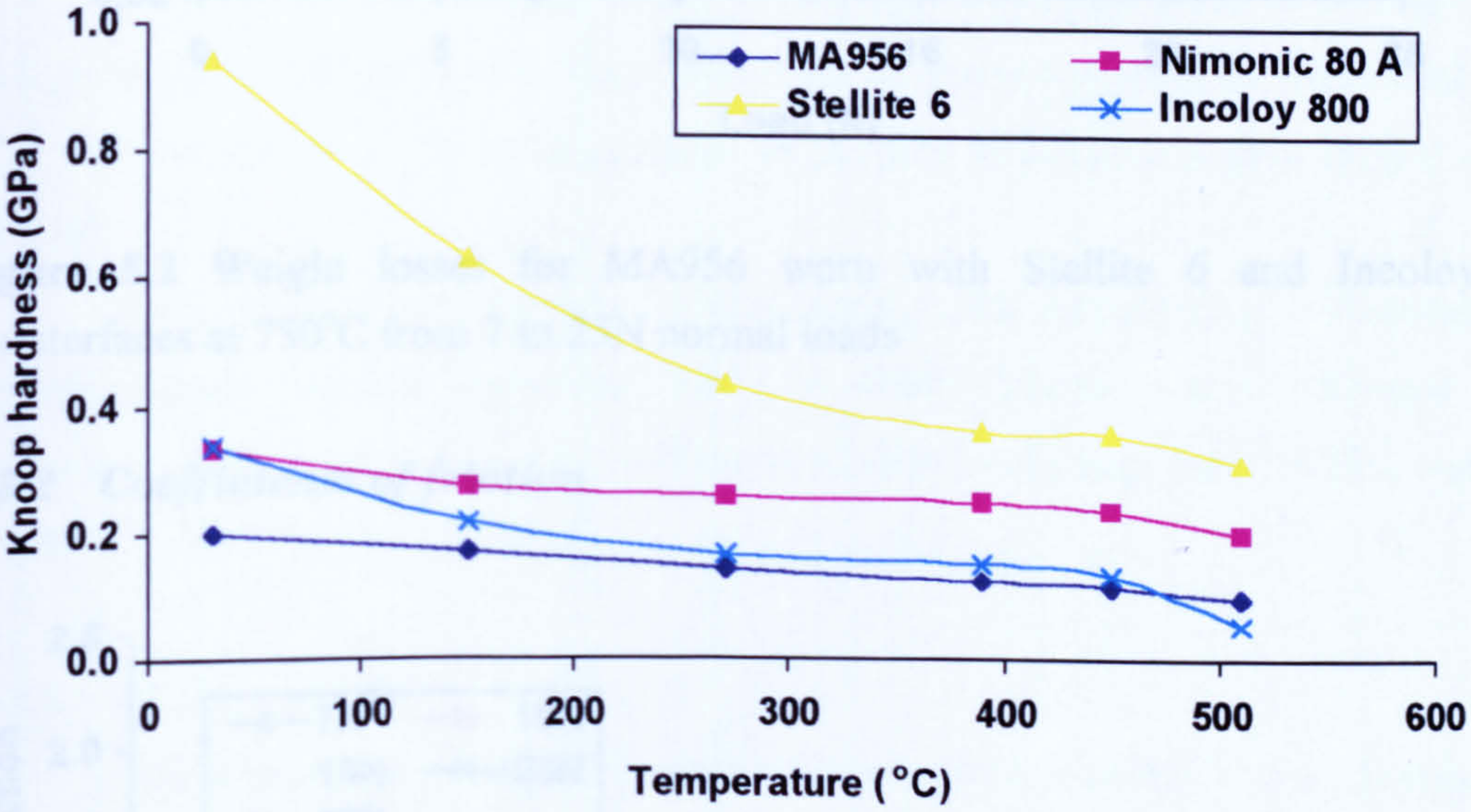

Figure 5.1 Hot-harnesses of the as-received materials recorded with a Knoop indenter measured with a 50g load and a 12s dwell time from ~25 to 510°C

5.3 Wear testing of MA956 with two counterfaces over a range of loads (7 to 25N) at 750°C

5.3.1 Weight changes

In **Figure 5.2** the weight loss data for MA956 worn with the two counterfaces – Stellite 6 and Incoloy 800 – from 7 to 25N are displayed. The Stellite 6 counterface produces lower weight losses compared to the Incoloy 800 counterface at all loads (7 to 25N) tested. The weight losses appeared to be

proportional to load from 7 to 20N. At 25N there is a marked increase in the weight losses for MA956 with both counterfaces.

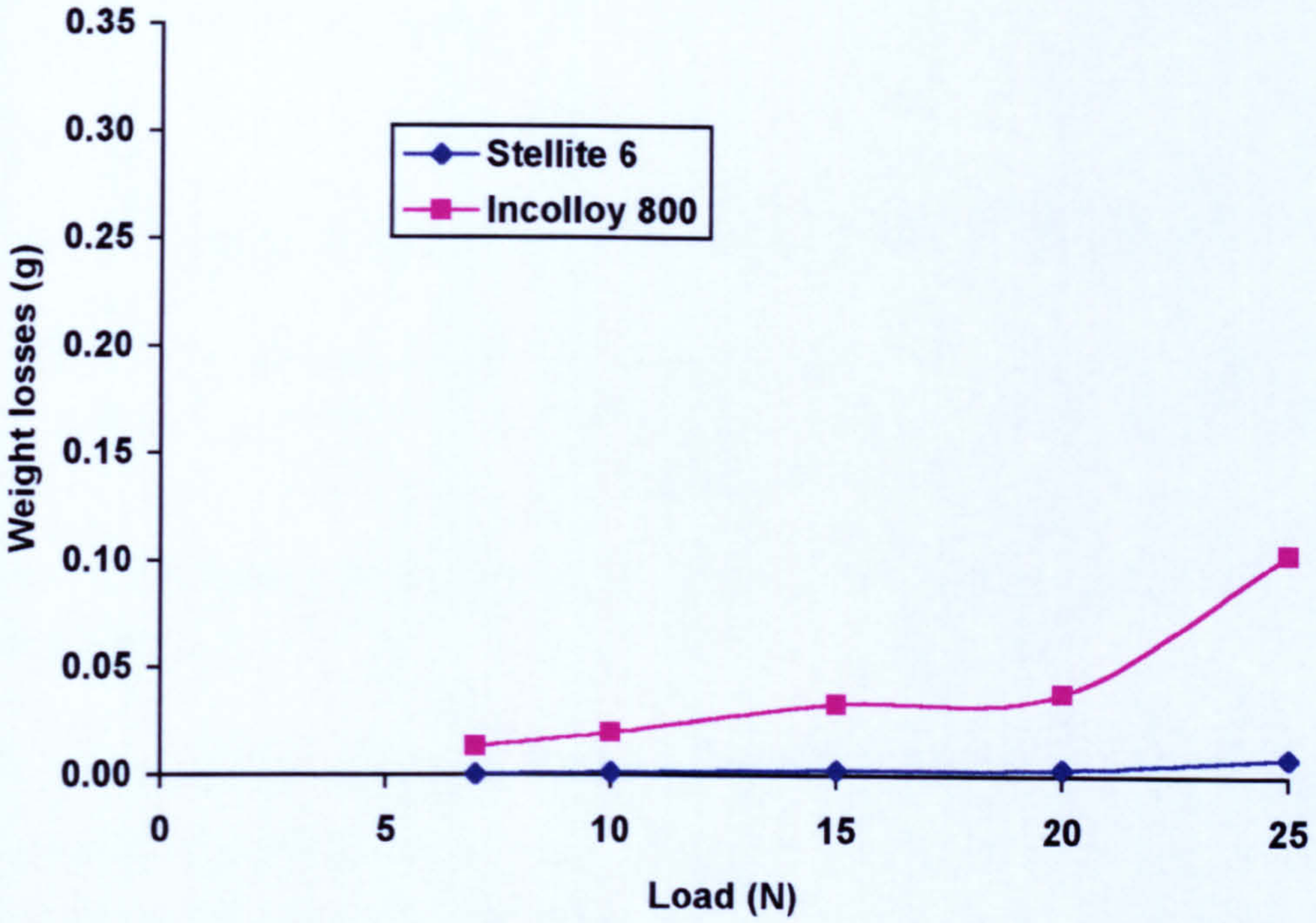

Figure 5.2 Weight losses for MA956 worn with Stellite 6 and Incoloy 800 counterfaces at 750°C from 7 to 25N normal loads

5.3.2 Coefficients of friction

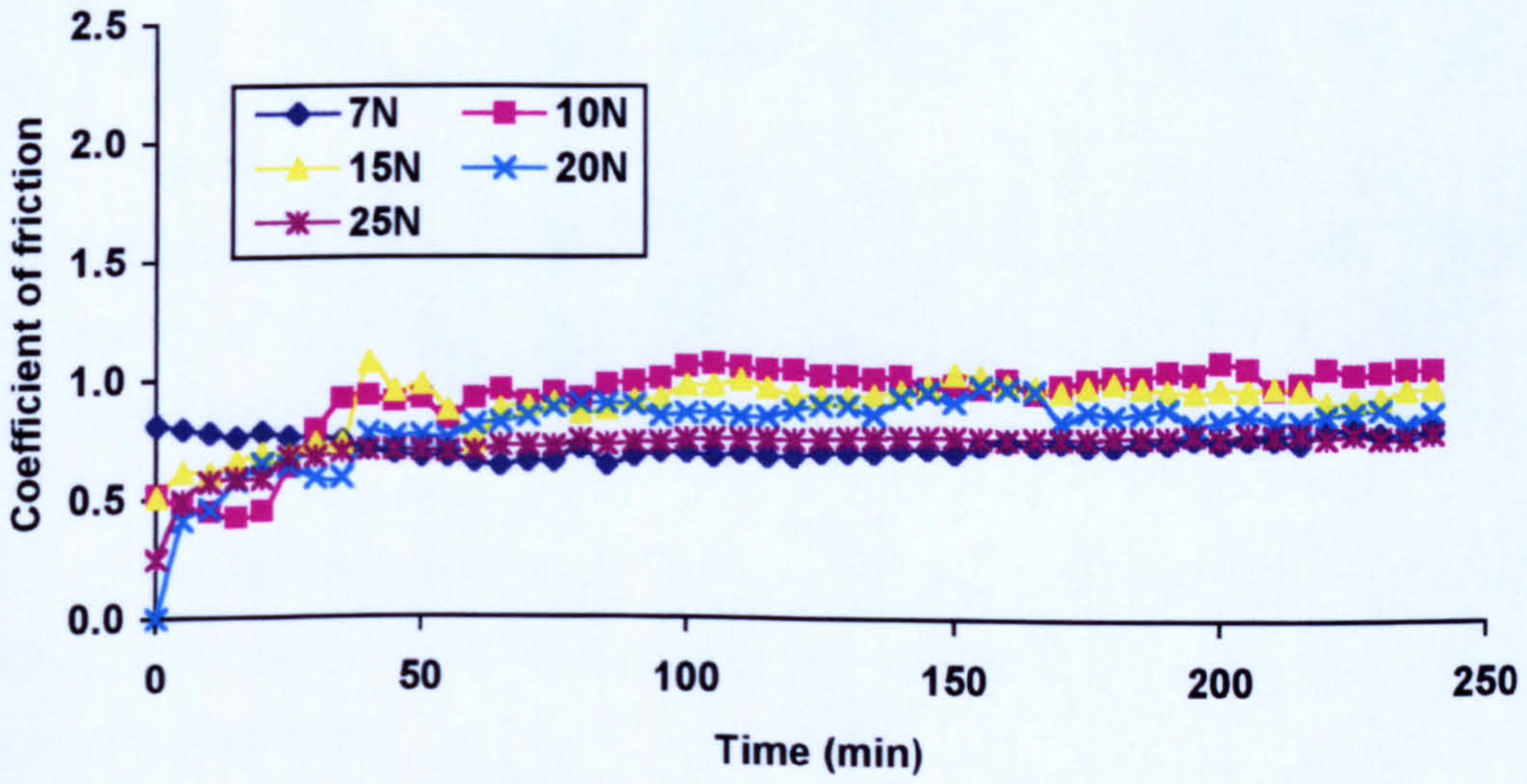

Figure 5.3 Coefficients of friction for MA956 worn with Stellite 6 at 750°C at normal loads from 7 to 25N

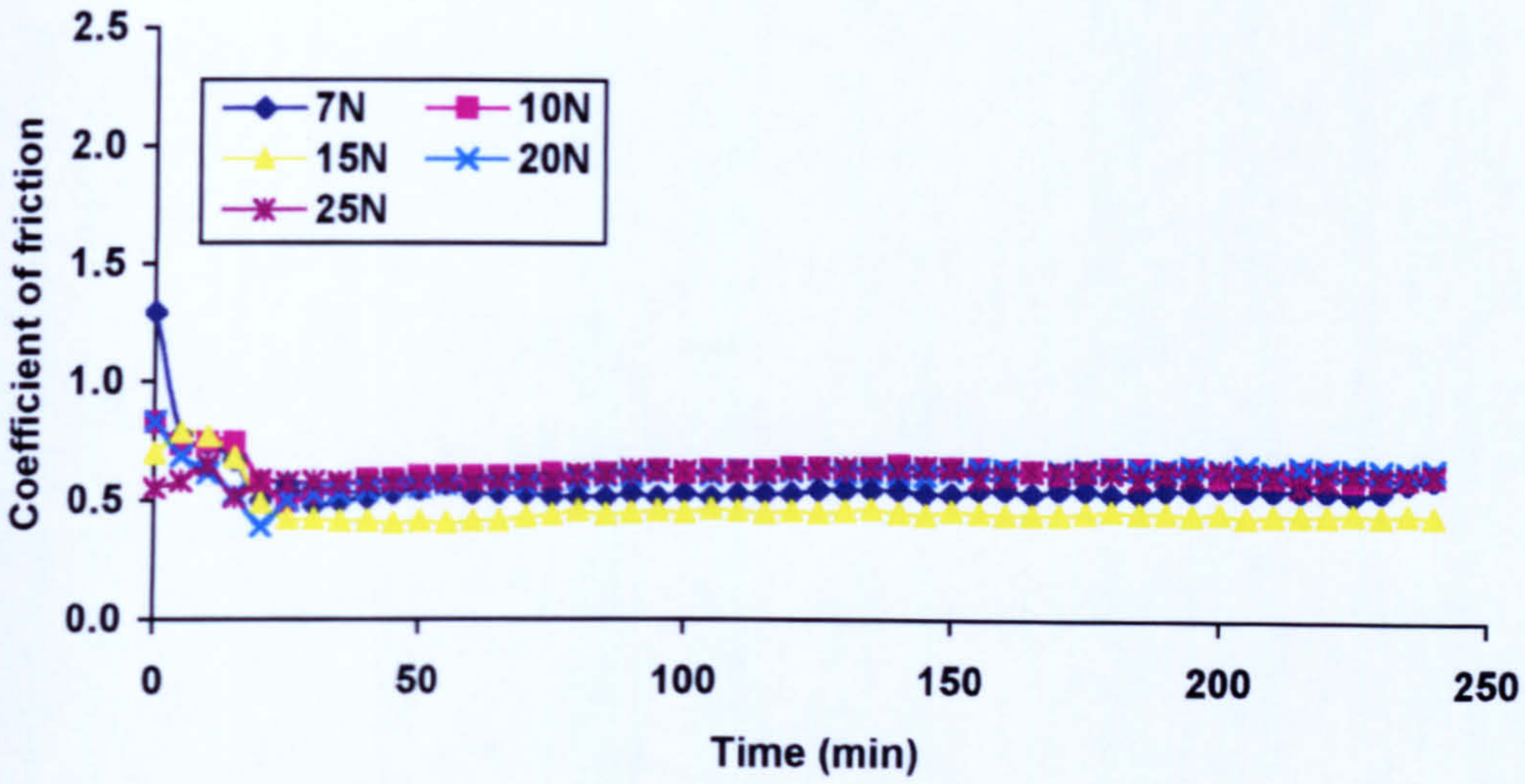

Figure 5.4 Coefficients of friction for MA956 worn with Incoloy 800 at 750°C at normal loads from 7 to 25N

The friction coefficient values for MA956 with the Stellite 6 counterface are presented in **Figure 5.3.** The coefficient of friction rose from an initial value of ~ 0.50 over the first 40 to 50 minutes of the test to achieve stable values of 0.60 to 1.20.

The coefficients of friction for the Incoloy 800 counterface – **Figure 5.4** – reveal steady values between 0.40 to 0.60. These were attained after approximately 30 minutes, the coefficient of friction falling from initial values of ~0.60 to 0.80.

5.3.3 XRD analysis

Diffractograms of MA956 samples worn with Stellite 6 and Incoloy 800 counterfaces are shown in **Figure 5.5** and **Figure 5.6** and the phases identified are shown in **Table 5.2**. For MA956 worn with Stellite 6, cobalt chromium oxide ($CoCr_2O_4$) and chromium iron oxide ($Cr_{1.3}Fe_{0.7}O_3$) phases were identified for MA956. These were detected at all the loads tested.

For MA956 worn with Incoloy 800, phases at all loads were identified which correspond to MA956 and chromium iron oxide ($Cr_{1.3}Fe_{0.7}O_3$) only, as shown in **Table 5.2**.

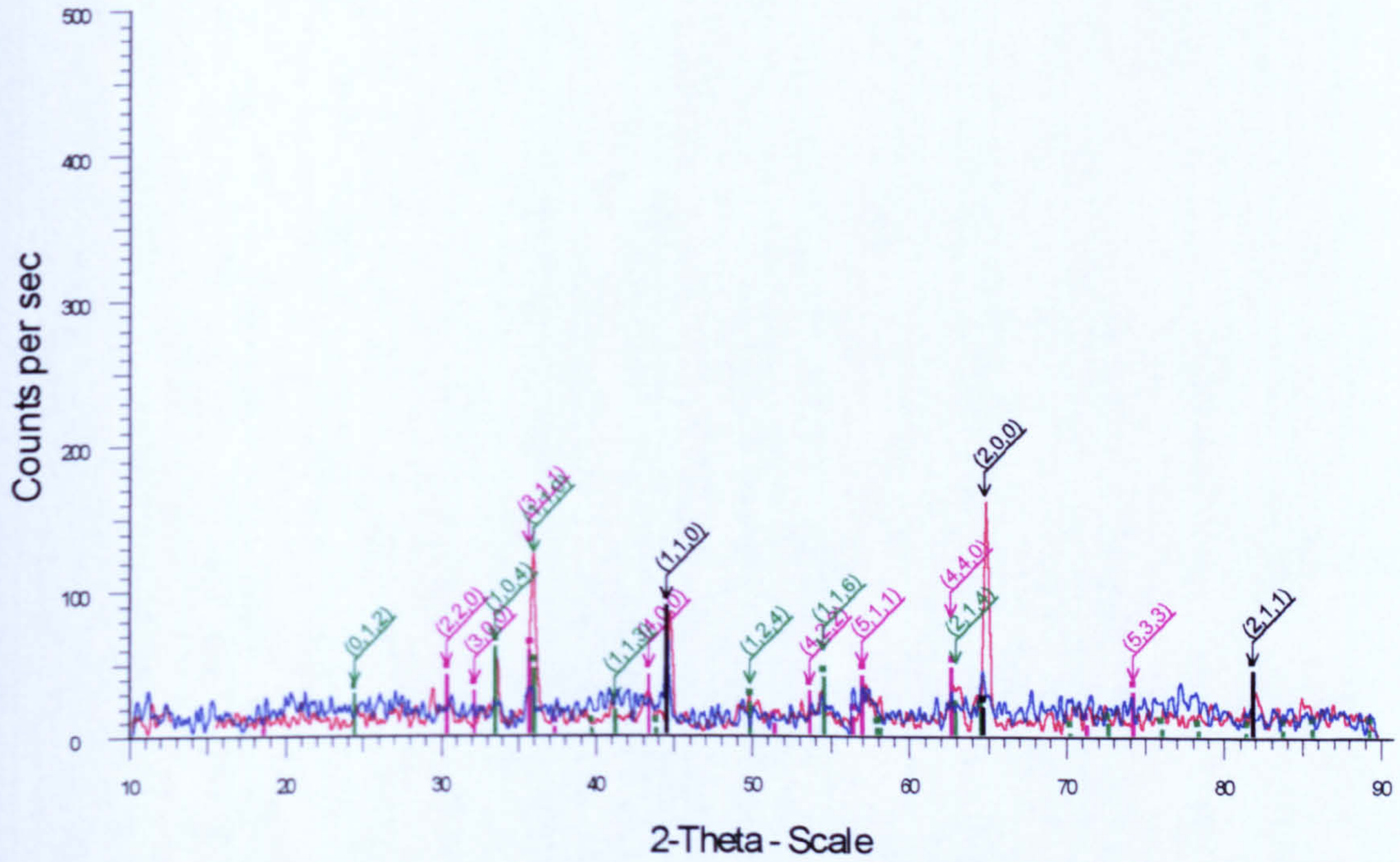

Figure 5.5 XRD data for MA956 worn with Stellite 6 at 750°C at loads of 7N and 25N. Phases identified iron-chromium phase (Fe-Cr) (MA956), cobalt chromium oxide ($CoCr_2O_4$) and chromium iron oxide ($Cr_{1.3}Fe_{0.7}O_3$)

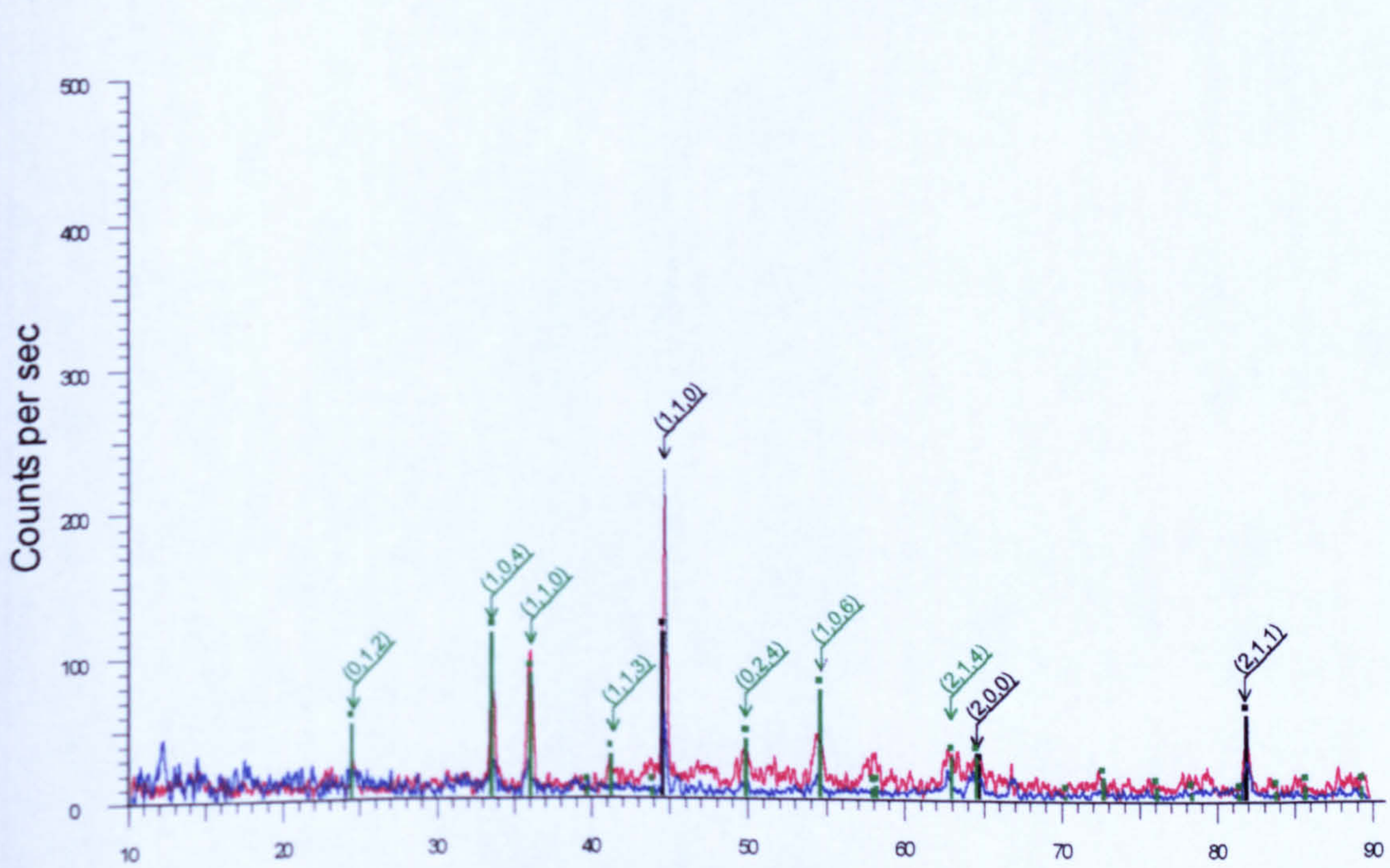

Figure 5.6 XRD data for MA956 worn with Incoloy 800 at 750°C at loads of 7N and 25N. Phases identified Iron-chromium phase (Fe-Cr) (MA956) and chromium iron oxide ($Cr_{1.3}Fe_{0.7}O_3$)

MA956 worn with Stellite 6 counterfaces	
Phase identified	**Conditions identified / interpretation**
Iron-chromium stainless steel phase (Fe-Cr)	MA956 substrate, all loads tested
Cobalt chromium oxide ($CoCr_2O_4$)	All loads tested
Chromium iron oxide ($Cr_{1.3}Fe_{0.7}O_3$)	All loads tested
MA956 worn with Incoloy 800 counterfaces	
Phase identified	**Conditions identified / interpretation**
Iron-chromium stainless steel phase (Fe-Cr)	MA956 substrate, all loads tested
Chromium iron oxide ($Cr_{1.3}Fe_{0.7}O_3$)	All loads tested

Table 5.2 XRD analysis of MA956 samples worn with Incoloy 800 and Stellite 6 at 750°C from 7 to 25N

5.3.4 SEM morphological analysis

SEM micrographs of surfaces worn at 7 and 25N load are shown in **Figure 5.7** for MA956 worn with Stellite 6 and Incoloy 800 counterfaces. For MA956 worn with a Stellite 6 counterface, the wear scars were covered with a highly smooth compacted oxide layer at all loads examined. At 25N load there appeared to be some cracking and break-up of the layer, this being accompanied by fine wear particles being caught in the remaining hollows and depressions.

For MA956 worn with an Incoloy 800 counterface, again the scars were covered with a compacted oxide layer. The layer was of similar appearance to that formed with a Stellite 6 counterface, although there were more areas of loosely compacted particles present at all loads test. At 25N, there again appeared to be more cracking and break-up on the layer.

5.3.5 SEM/EDX cross-section analysis

Cross-sectional SEM/EDX element maps of the wear scars display the composition of the oxide layers formed. Maps of the scars formed upon MA956 worn with Stellite 6 and Incoloy 800 counterfaces are given in **Figure 5.8** and **Figure 5.9** respectively. The presence of cobalt in the surface layer on MA956 worn with Stellite 6 indicates transfer of material from the counterface, while chromium may have originated from either the counterface or the sample. The samples worn with an Incoloy 800 counterface gave iron and chromium oxides and a small amount of nickel in the surface layers. Iron and chromium were detected in both the sample and the counterface, although the nickel was only present in the counterface and therefore was transferred.

The structures of the oxide layer also appear to be quite different for the two counterfaces. With the Incoloy 800 counterface there appears to be a second layer consisting of iron, chromium and aluminium beneath the compacted oxide layer. This is probably a partially oxidised and highly deformed layer. Such a layer does not appear to have formed with the Stellite 6 counterfaces.

5.3.6 Analysis of wear debris

Wear debris collected from MA956 worn with Stellite 6 and Incoloy 800 counterfaces are presented in **Figure 5.10**. Debris collected where the Stellite 6 counterface was employed consisted of large flakes of material, 50 to 250μm in size, many of which appear to be delaminated fragments of the compacted oxide layer. There are also finer particles of material, which are often observed to be attached to the larger particles.

For an Incoloy 800 counterface the debris also shows large particles in the range 50 to 250μm. The particle shown in **Figure 5.10 (d)** strongly resembles the compacted oxide layer seen on the wear scars. The debris collected with the Incoloy 800 counterface appears to have finer particles (1 to 5μm) associated with the larger fragments, again these are often attached to the larger particles.

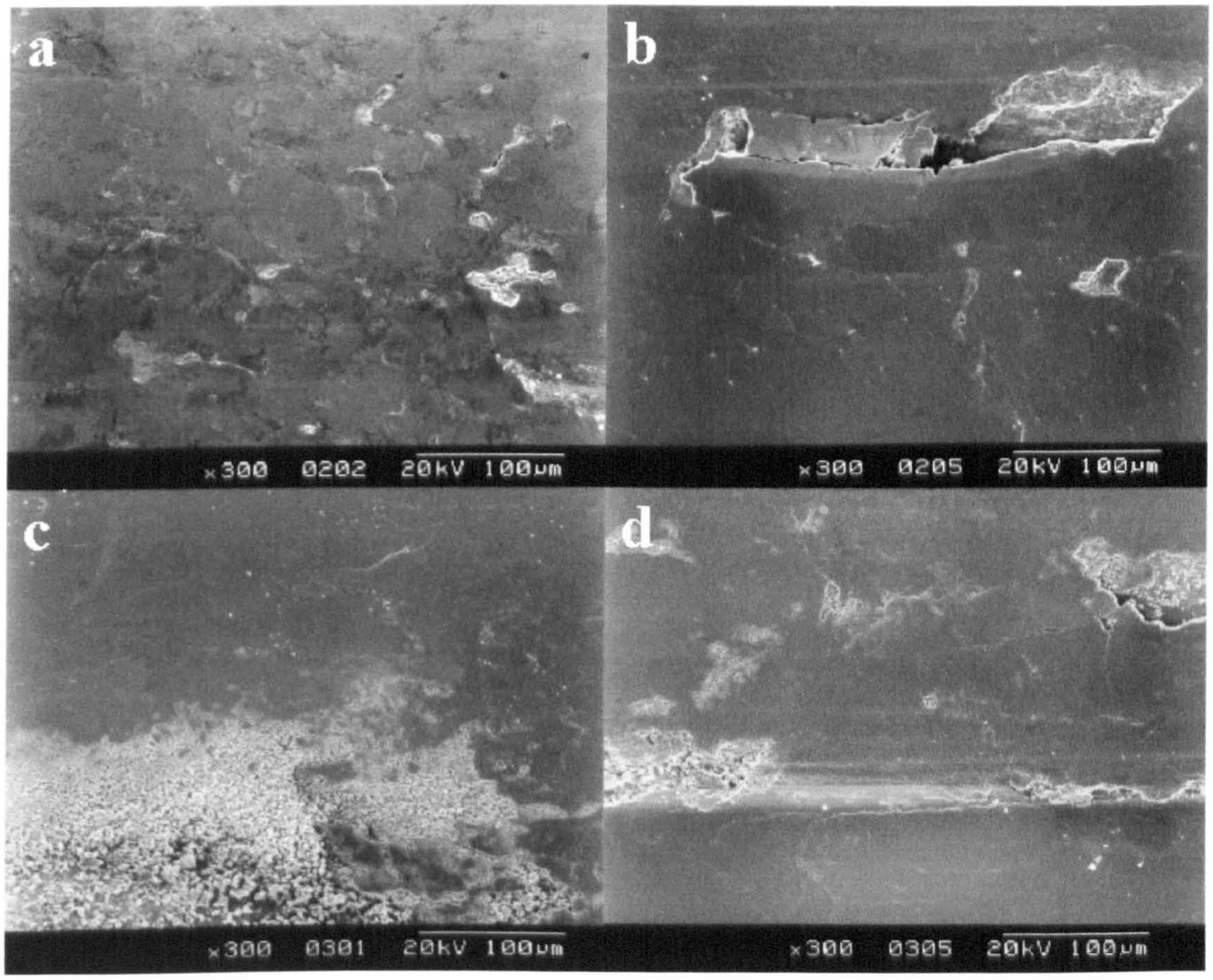

Figure 5.7 Plan views of wear scars formed upon MA956 worn with (a) and (b) Stellite 6 and (c) and (d) Incoloy 800 counterfaces at 7 and 25N load respectively, for 4 hours

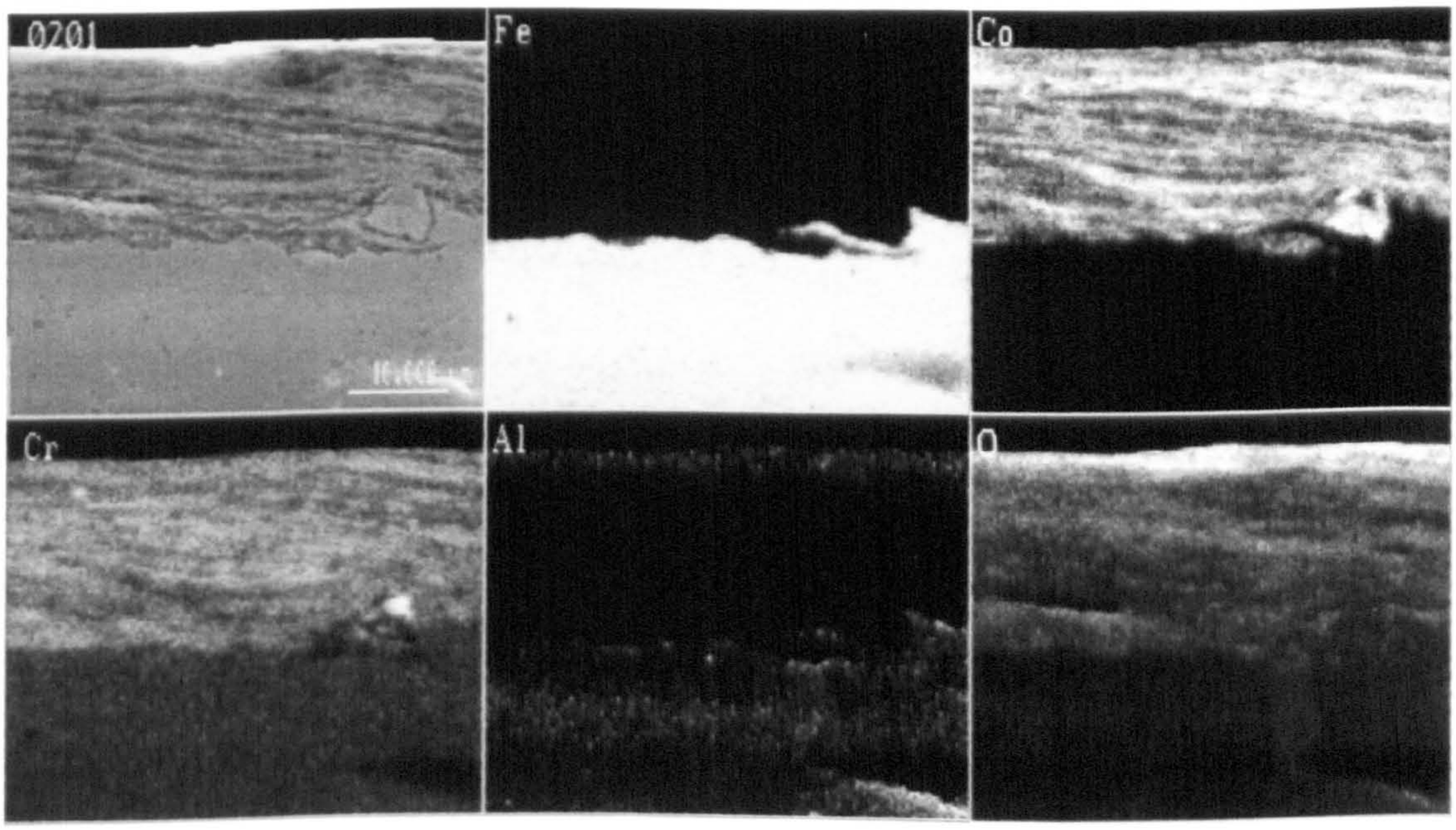

Figure 5.8 Cross-sectional SEM/EDX element map through the wear scar formed upon MA956 worn with Stellite 6 at 750°C for 4 hours

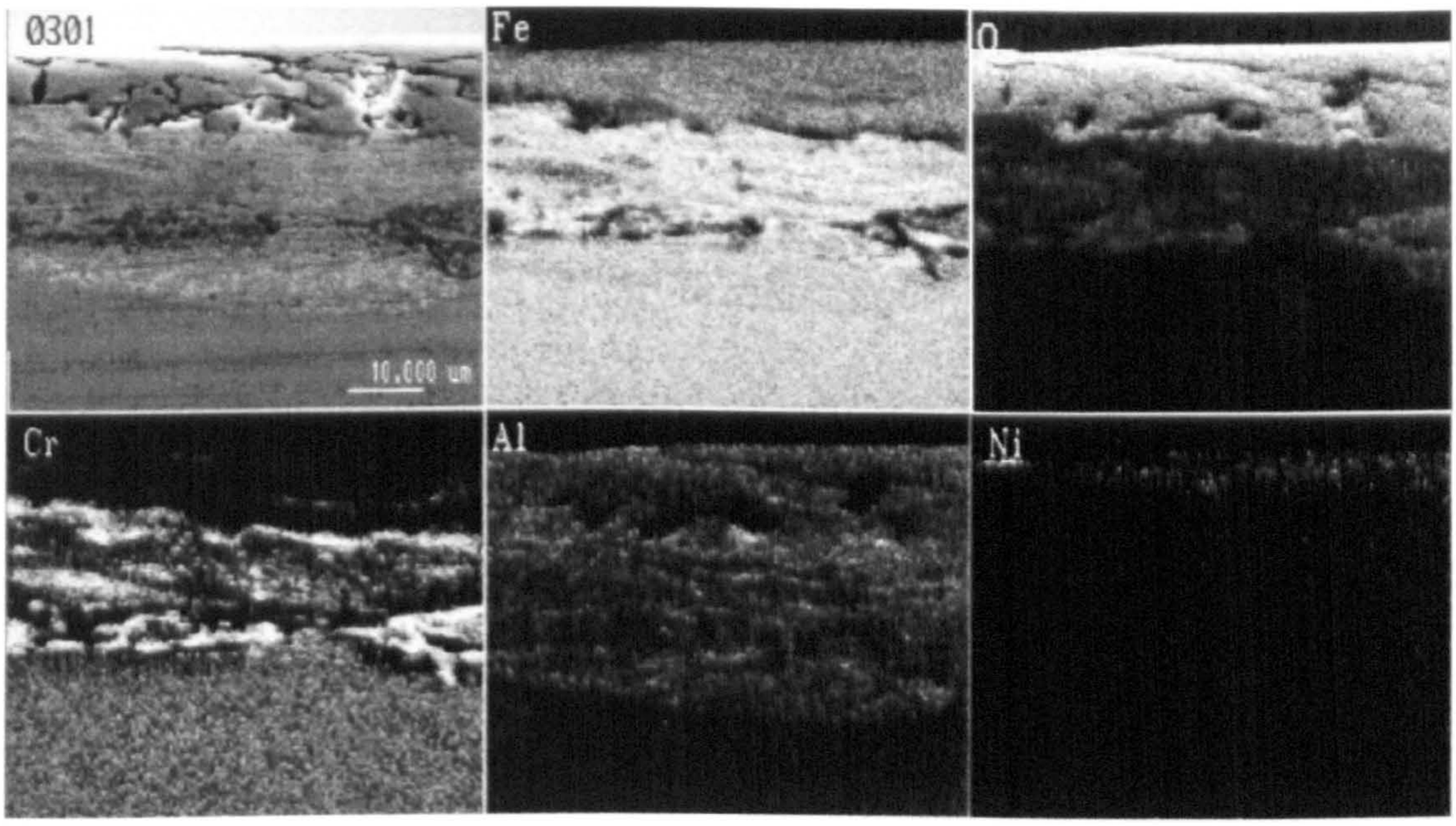

Figure 5.9 Cross-sectional SEM/EDX element map through the wear scar formed upon MA956 worn with Incoloy 800 at 750°C for 4 hours

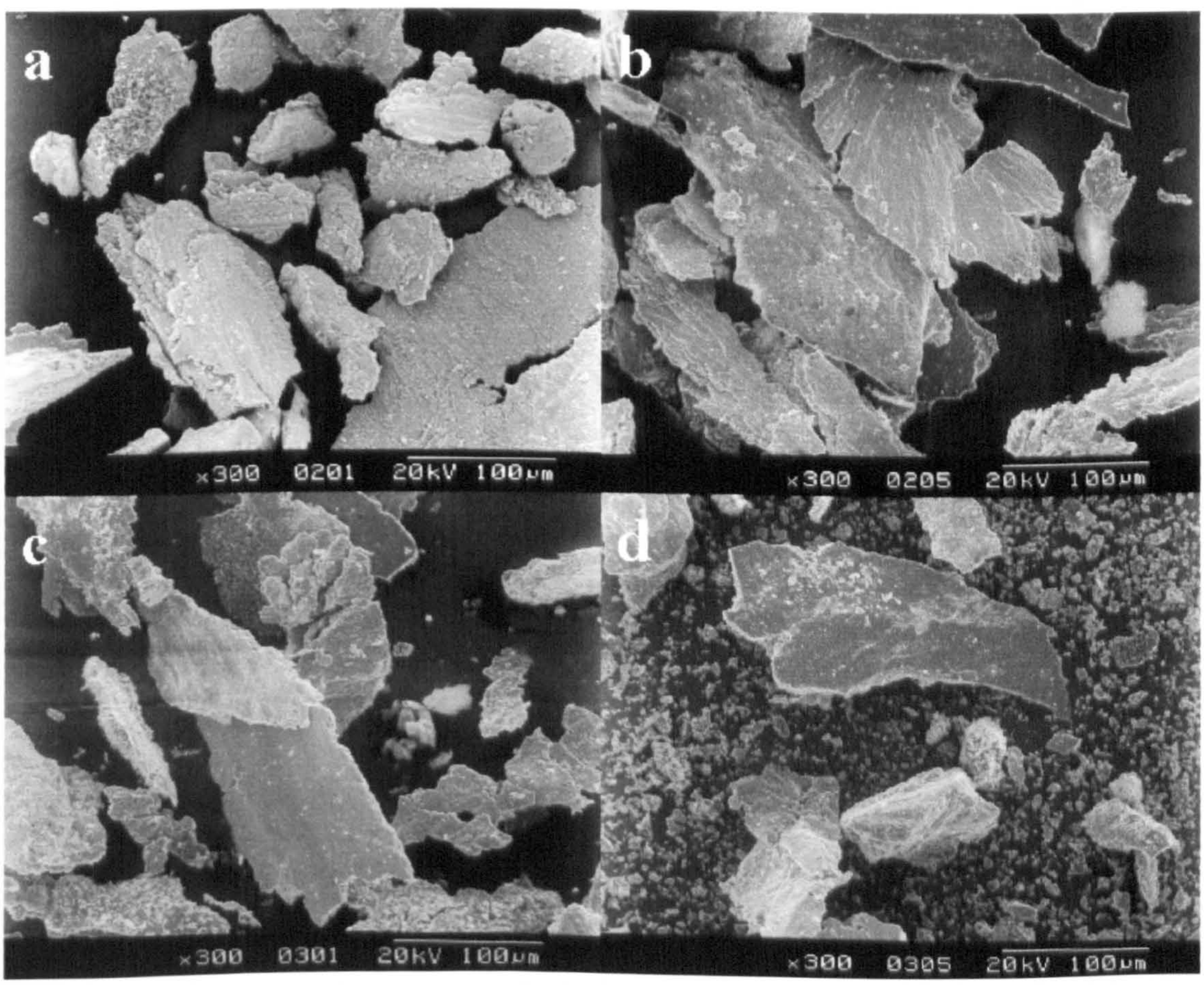

Figure 5.10 Wear debris recovered from the wear of MA956 worn with (a) and (b) Stellite 6 and (c) and (d) Incoloy 800 counterfaces at 7 and 25N load respectively, for 4 hours

5.4 Wear testing of Nimonic 80A with two counterfaces over a range of loads (7 to 25N) at 750°C

5.4.1 Weight changes

Weight loss data for Nimonic 80A worn with Stellite 6 and Incoloy 800 counterfaces are displayed in **Figure 5.11**. At 7 and 10N load there was a marked difference seen between the two counterfaces – Incoloy 800 giving a lower wear rate. Above 15N there was a dramatic increase in the wear rate of Nimonic 80A with both counterfaces. Between 20 and 25N the increase in weight loss was not as great as that between 15 and 20N, although the sample was clearly worn at these loads and the apparent area of contact was much larger than that seen at 7N load.

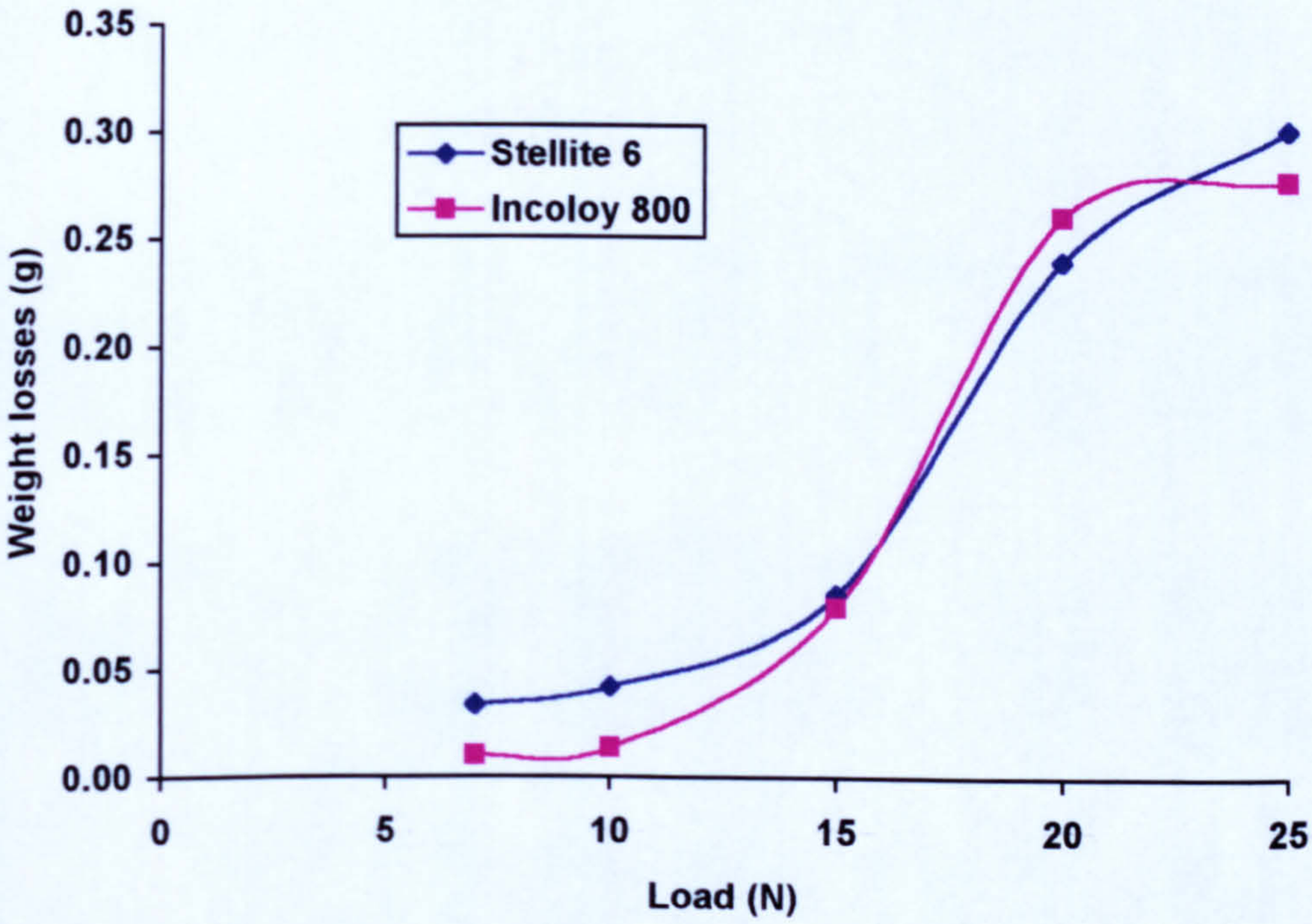

Figure 5.11 Weight losses for Nimonic 80A worn with Stellite 6 and Incoloy 800 counterfaces at 750°C for 4 hours from 7 to 25N normal loads

5.4.2 Coefficients of friction

Coefficient of friction data for Nimonic 80A worn with Stellite 6 and Incoloy 800 counterfaces are presented in **Figures 5.12** and **Figure 5.13** respectively. For Nimonic 80A worn with Stellite 6 the coefficient of friction reached a stable value within the first 10 minutes of the test. This stable value being 0.45 to 0.55 (slightly higher ~0.65 at the 7N load) remained unchanged for the rest of the test.

The coefficient of friction for Nimonic 80A worn with an Incoloy 800 counterface obtained a stable value after ~20 minutes. These value ranges were from 0.69 to 0.37 – the coefficient of friction was generally lower at higher loads. Once established, the coefficient of friction remained stable at all the loads tested.

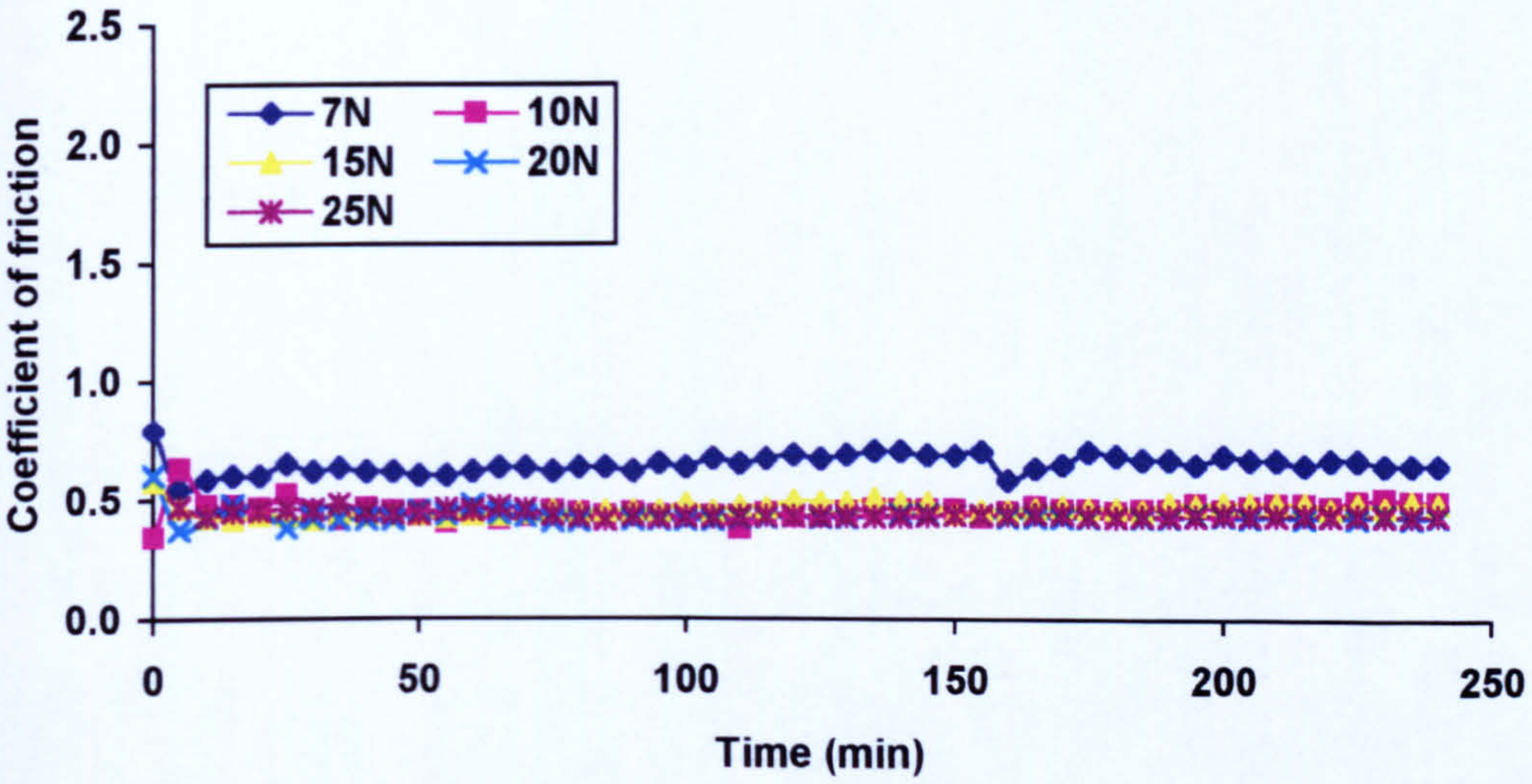

Figure 5.12 Coefficients of friction for Nimonic 80A worn with Stellite 6 at 750°C at normal loads from 7 to 25N

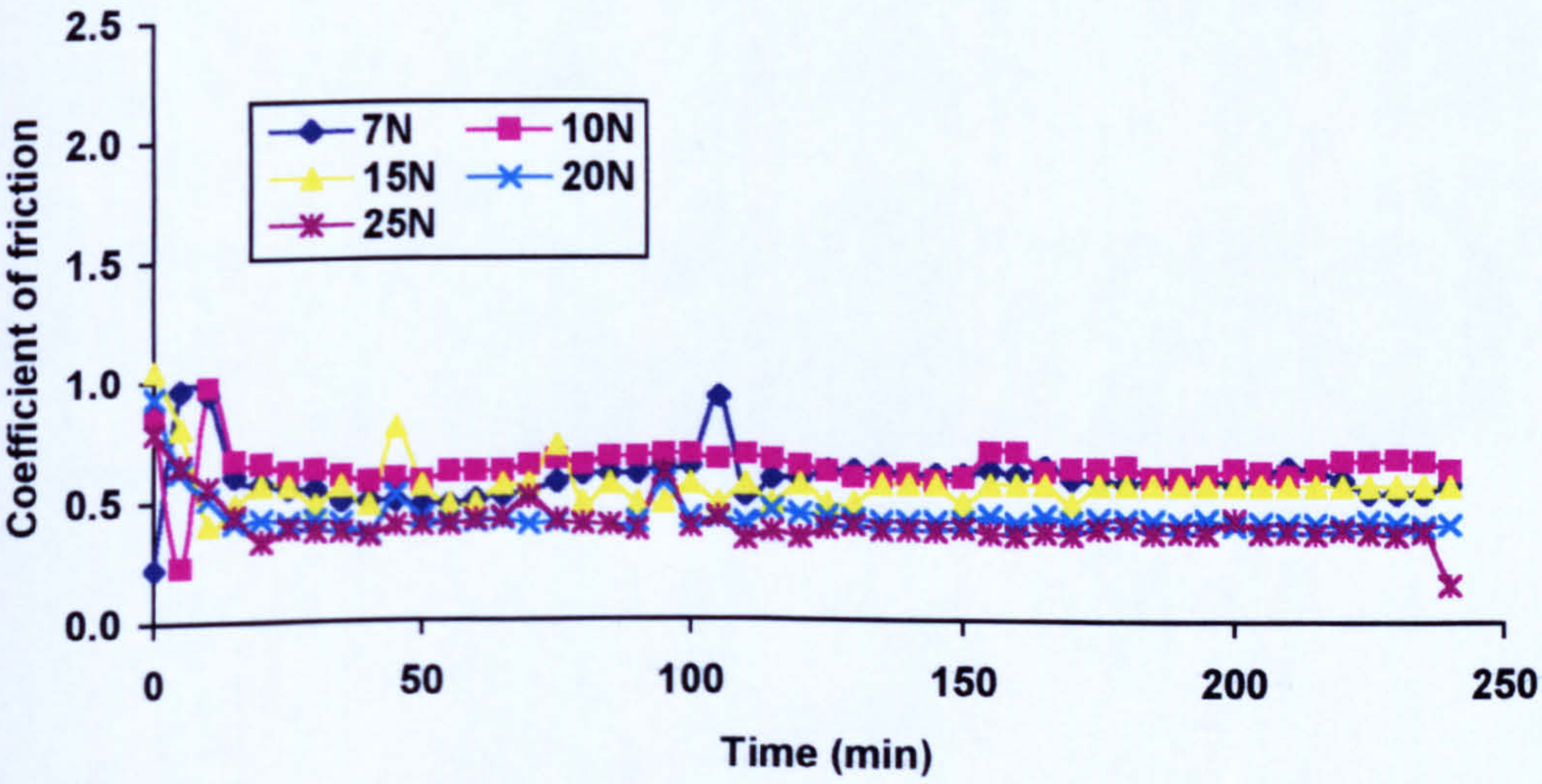

Figure 5.13 Coefficients of friction for Nimonic 80A worn with Incoloy 800 at 750°C at normal loads from 7 to 25N

5.4.3 XRD analysis

Diffractograms for Nimonic 80A samples worn with Stellite 6 and Incoloy 800 are presented in **Figure 5.14** and **Figure 5.15** and the phases identified are shown in **Table 5.3**. For Nimonic 80A worn with a Stellite 6 counterface only the phase corresponding to Nimonic 80A was identified. No cobalt-containing phases were identified.

For Nimonic 80A worn with Incoloy 800, phases were identified corresponding to Nimonic 80A and nickel oxide (NiO) at all loads investigated.

Nimonic 80A worn with Stellite 6 counterfaces	
Phase identified	**Conditions identified / interpretation**
Iron chromium nickel stainless steel phases ($Cr_{0.19}$ $Fe_{0.7}$ $Ni_{0.11}$)	Nimonic 80A substrate, all loads tested
Nimonic 80A worn with Incoloy 800 counterfaces	
Phase identified	**Conditions identified / interpretation**
Iron chromium nickel stainless steel phases ($Cr_{0.19}$ $Fe_{0.7}$ $Ni_{0.11}$)	Nimonic 80A substrate, all loads tested
Nickel oxide (NiO)	7 and 10N only

Table 5.3 XRD analysis of Nimonic 80A samples worn with Stellite 6 and Incoloy 800 at 750°C from 7 to 25N

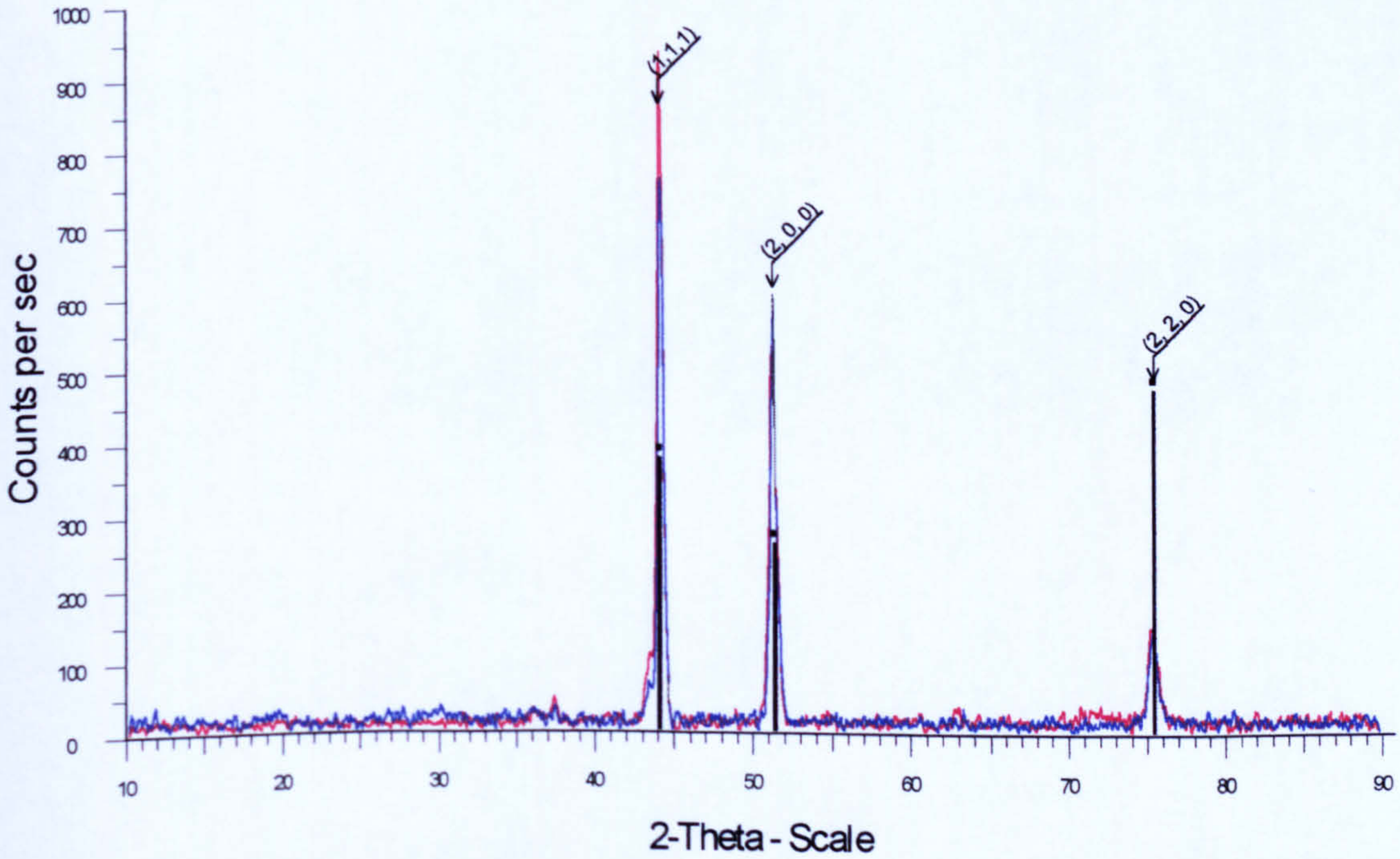

Figure 5.14 XRD data for Nimonic 80A worn with Stellite 6 at 750°C at loads of 7N and 25 N. Phases identified ▣ iron chromium nickel stainless steel phases ($Cr_{0.19}$ $Fe_{0.7}$ $Ni_{0.11}$) (Nimonic 80A)

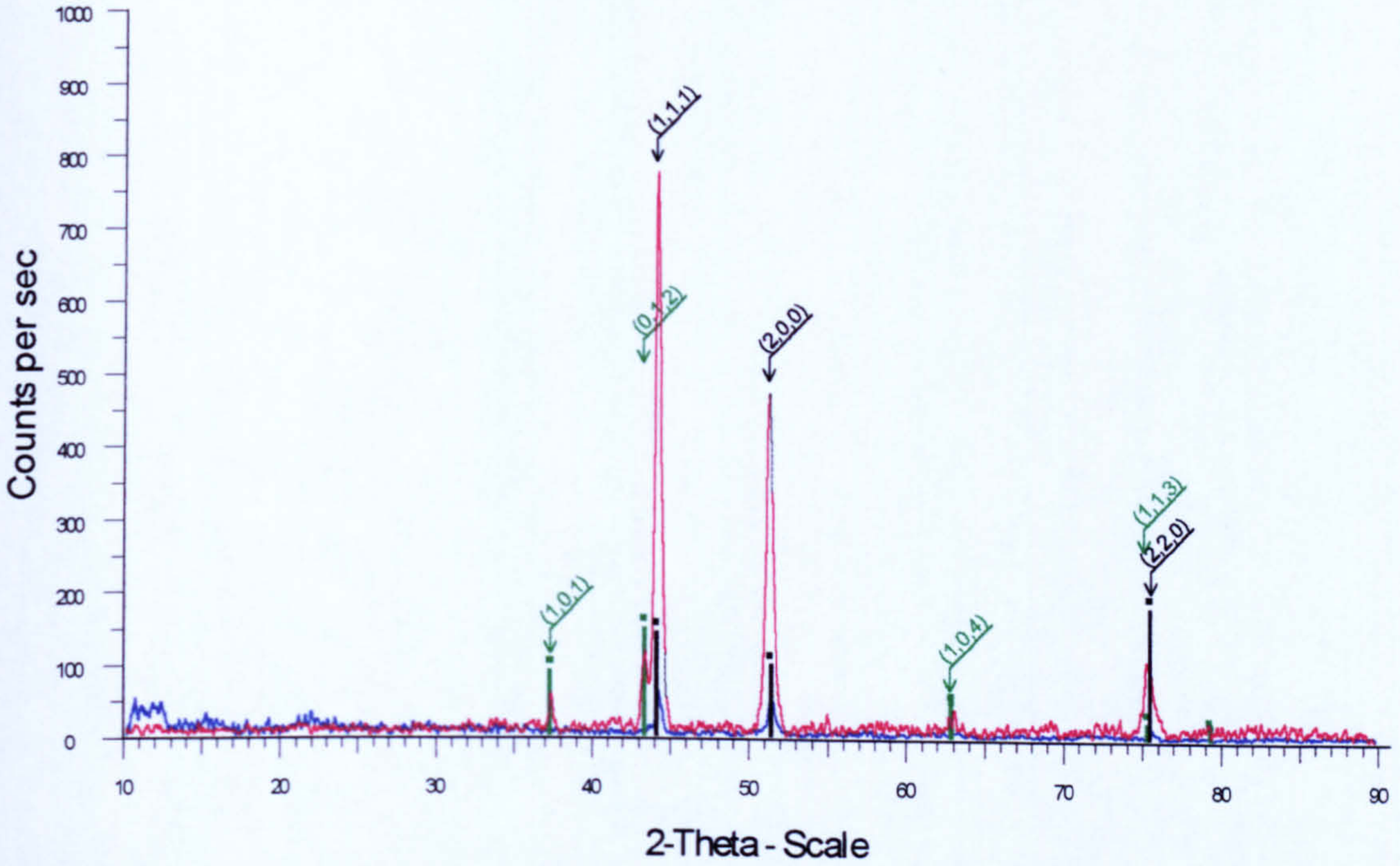

Figure 5.15 XRD data for Nimonic 80A worn with Incoloy 800 at 750°C at loads of 7N and 25N. Phases identified iron chromium nickel stainless steel phases ($Cr_{0.19}$ $Fe_{0.7}$ $Ni_{0.11}$) (Nimonic 80A) and nickel oxide (NiO)

5.4.4 SEM morphological analysis

SEM examination of the wear scars indicates that with the Incoloy 800 counterface, Nimonic 80A forms some limited areas of compacted oxide material at 7 and 10N loads. At higher loads the surfaces became more grooved and no oxide plateaux could be detected. At 20 and 25N there was more loose material on the surfaces than at 15N, this is due to the increases in the apparent area of contact, hence an effective reduction in load per unit area. For the Stellite 6 counterface, the grooved and highly worn appearance was observed at all the loads tested. SEM micrographs of the 7 and 25N wear scars, for both counterfaces, are presented in **Figure 5.16**.

5.4.5 SEM/EDX cross-section analysis

Cross-sectional SEM/EDX element maps – displayed in **Figure 5.17** and **Figure 5.18** – of the wear scars on the Incoloy 800 counterface showed that some oxide layers were present at 7 and 10N load consisting of nickel oxides – these may have originated from the sample or the counterface. No layers could be detected at higher loads. For the Stellite 6 counterface no layers could be detected

at any of the loads investigated (**Figure 5.17**) although some cobalt transferred from the counterface was seen to be present on the surface.

5.4.6 Analysis of wear debris

Micrographs of the wear debris collected from Nimonic 80A worn with Stellite 6 and Incoloy 800 counterfaces are shown in **Figure 5.19**. For Nimonic 80A worn with Stellite 6, the debris comprises two types of wear particle. There were considerable amounts of fine debris – 1 to 5μm – which were often seen to be clumped together. These clumps of debris were identified as being predominately formed from Stellite 6 material (Co/Cr oxides). The larger flakes of material were of varying composition containing both Stellite 6 and Nimonic 80A material and appeared to have delaminated surfaces. Again the larger particles often had finer particles attached to their surfaces.

The wear debris formed when Nimonic 80A was worn with Incoloy 800 consisted mainly of large particles at 7N load (100 to 300μm in size). At higher load the average size of the particles decreased (50 to 100μm at 25N load). With increasing load there were also many more finer fragments associated with the debris. The debris consisted of both Nimonic 80A and Incoloy 800 material.

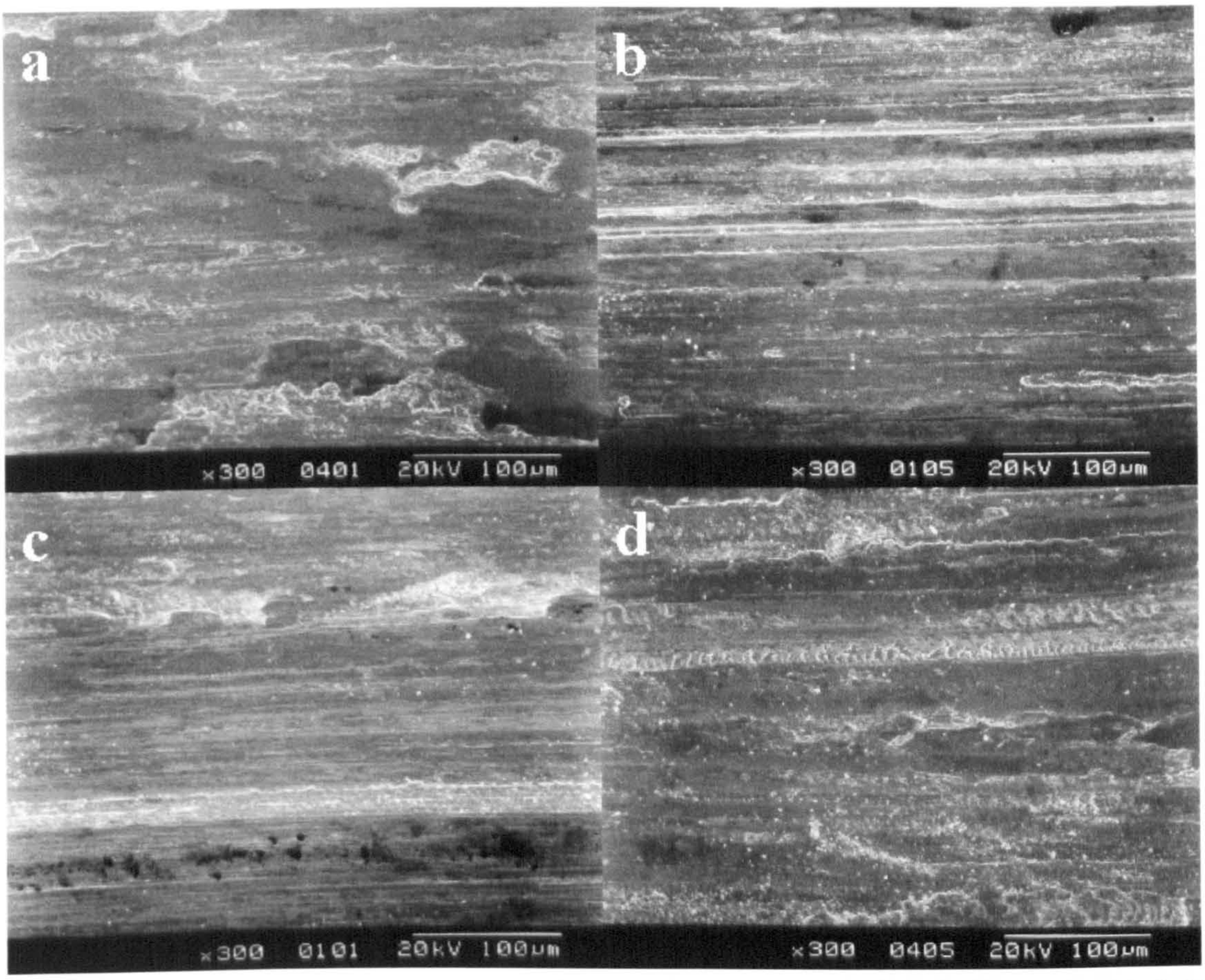

Figure 5.16 Plan views of wear scars formed on Nimonic 80A worn with (a) and (b) Stellite 6 and (c) and (d) Incoloy 800 counterfaces at 7 and 25 N load respectively, for 4 hours

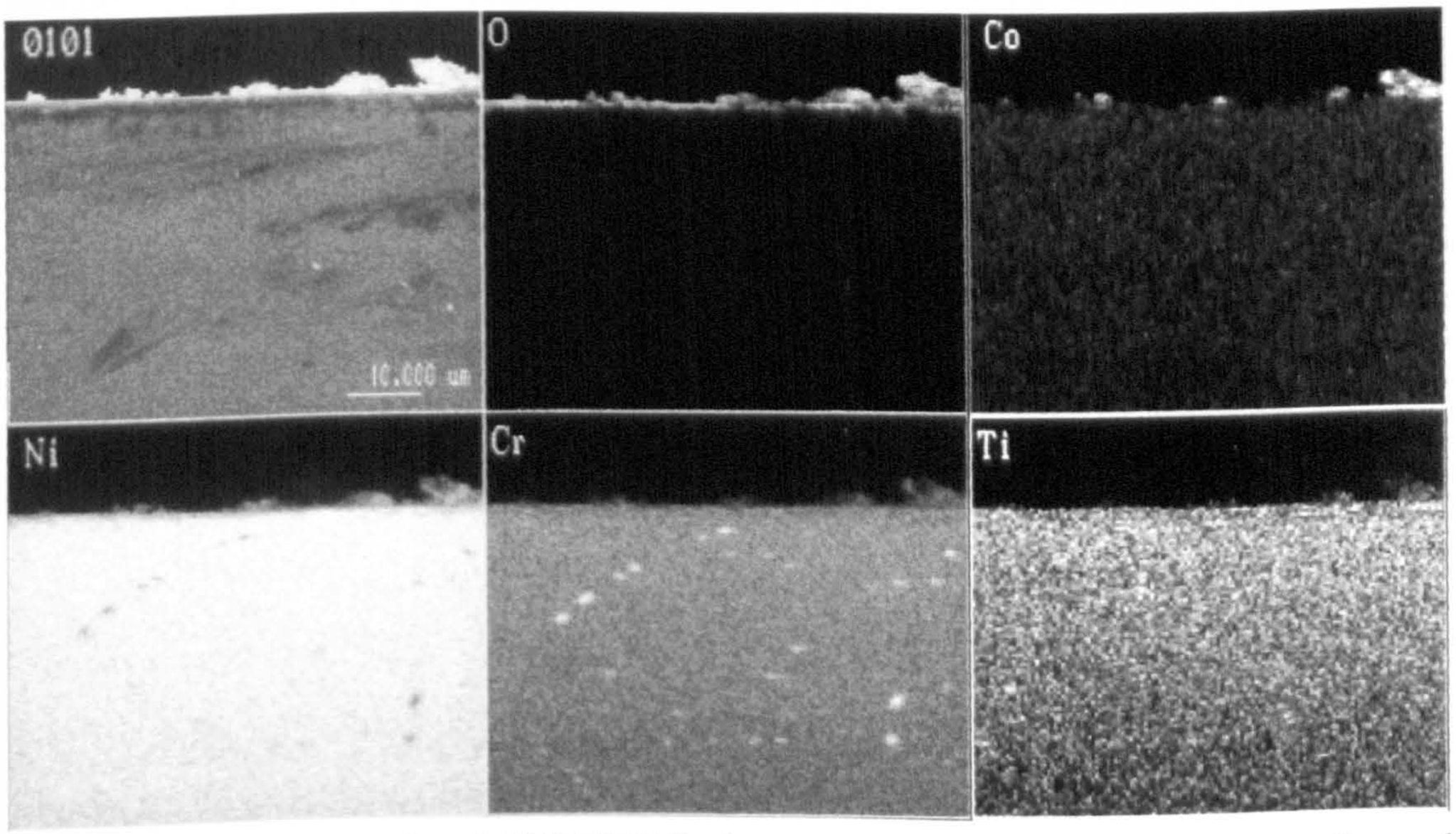

Figure 5.17 Cross-sectional SEM/EDX element map through the wear scar formed upon Nimonic 80A worn with Stellite 6 at 750°C for 4 hours

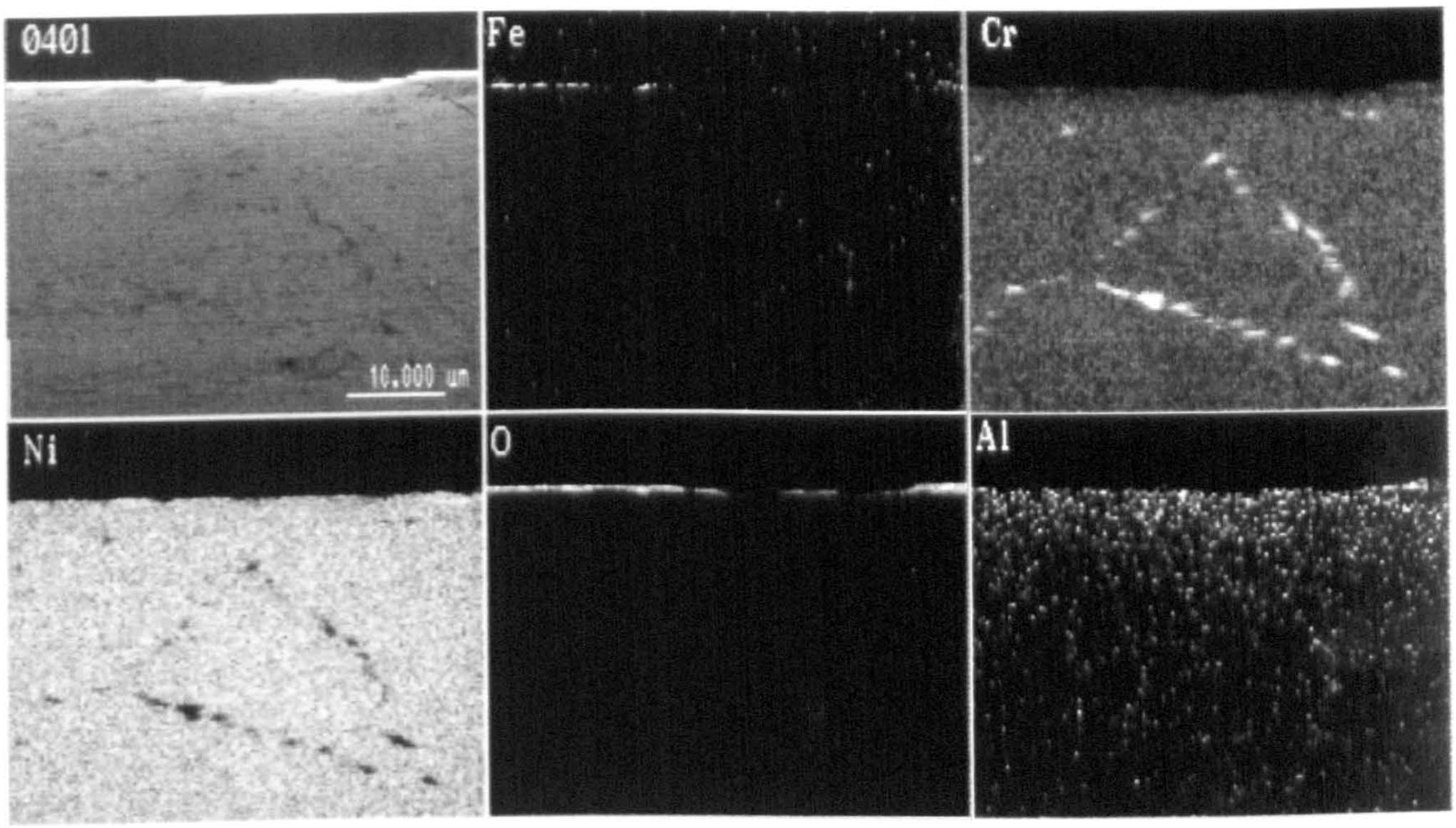

Figure 5.18 Cross-sectional SEM/EDX element map through the wear scar formed upon Nimonic 80A worn with Incoloy 800 at 750°C for 4 hours

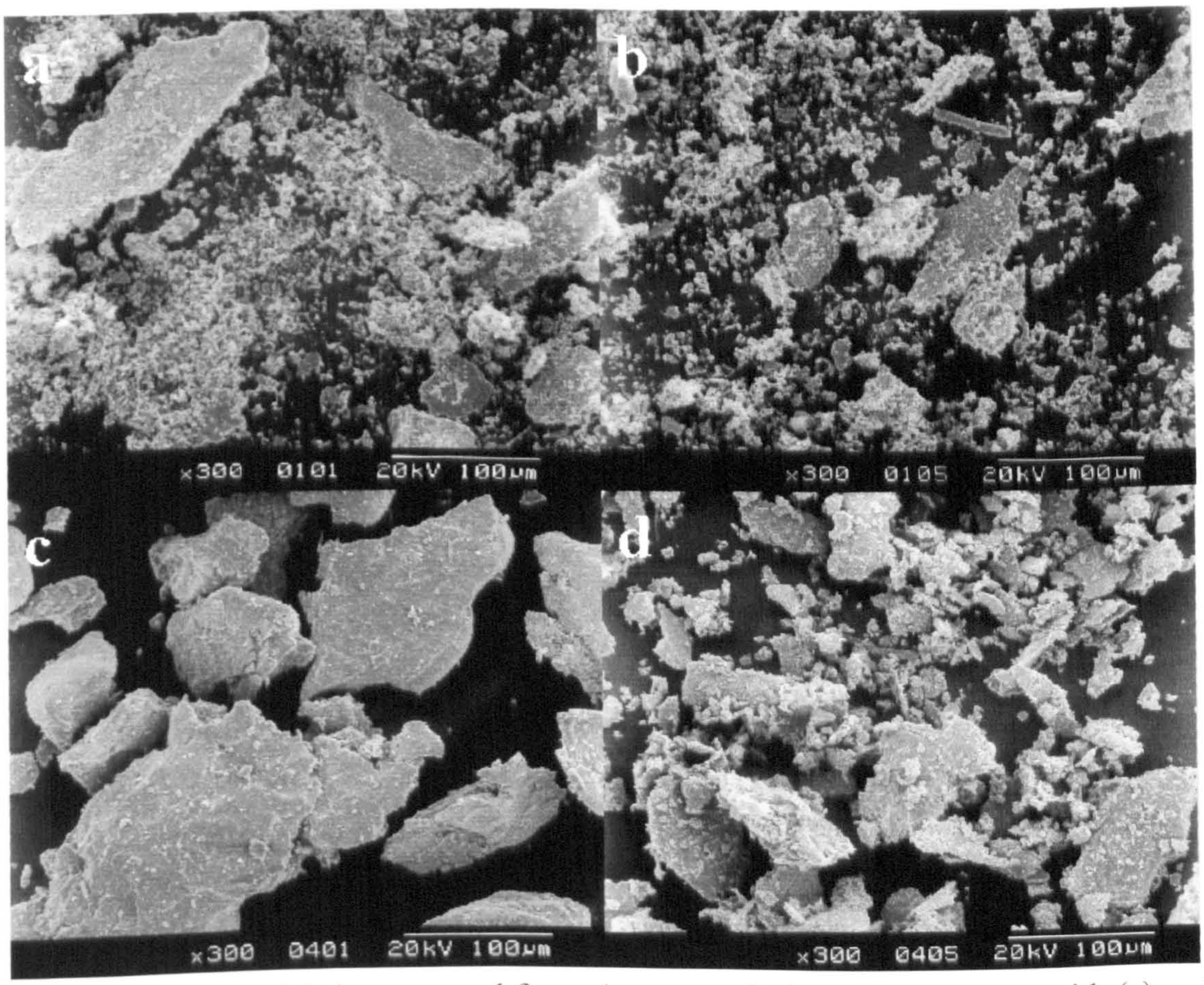

Figure 5.19 Wear debris recovered from the wear of Nimonic 80A worn with (a) and (b) Stellite 6 and (c) and (d) Incoloy 800 counterfaces at 7 and 25 N load respectively, for 4 hours

5.5 MA956 worn with Stellite 6 and Incoloy 800 counterfaces from room temperature to 750°C

5.5.1 Weight changes

Weight losses for MA956 with Stellite 6 and Incoloy 800 at ~25°C were relatively low, (0.011g) for Stellite 6 and (0.002g) for Incoloy 800 counterfaces (**Figure 5.20**).

For Stellite 6 counterfaces, weigh losses from room temperature to 390°C remain very low. With further increases in temperature, weight losses reach a maximum (0.132g) at 510°C. From 630°C to 750°C weight losses decrease with temperature, reaching (0.000(3)g) at 750°C.

For Incoloy 800 counterfaces a similar pattern of weight loss is seen, although here weight losses are constantly higher than those achieved with Stellite 6 counterfaces. Weight losses started to increase from 270°C reaching a maximum (0.656g) at 630°C. At higher temperatures the weight losses fell to lower values reaching a minimum (0.347g) at 750°C.

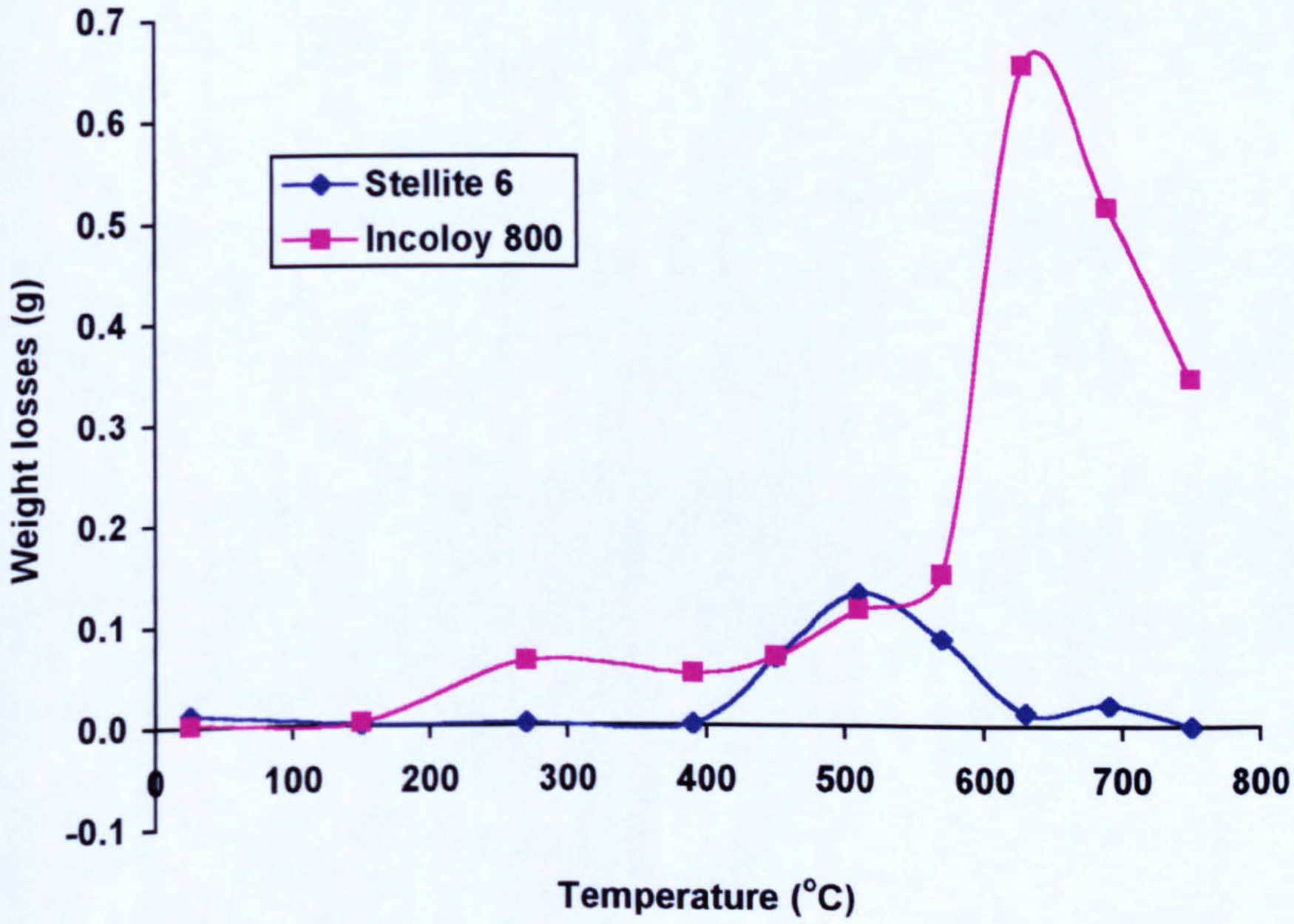

Figure 5.20 Weight losses for MA956 with Stellite 6 and Incoloy 800 counterfaces over a range of temperatures from ~25 to 750°C

5.5.2 Coefficients of friction

Coefficients of friction data for MA956 worn with Stellite 6 and Incoloy 800 counterfaces over the range of temperatures are shown in **Figure 5.21** and **Figure 5.22** respectively.

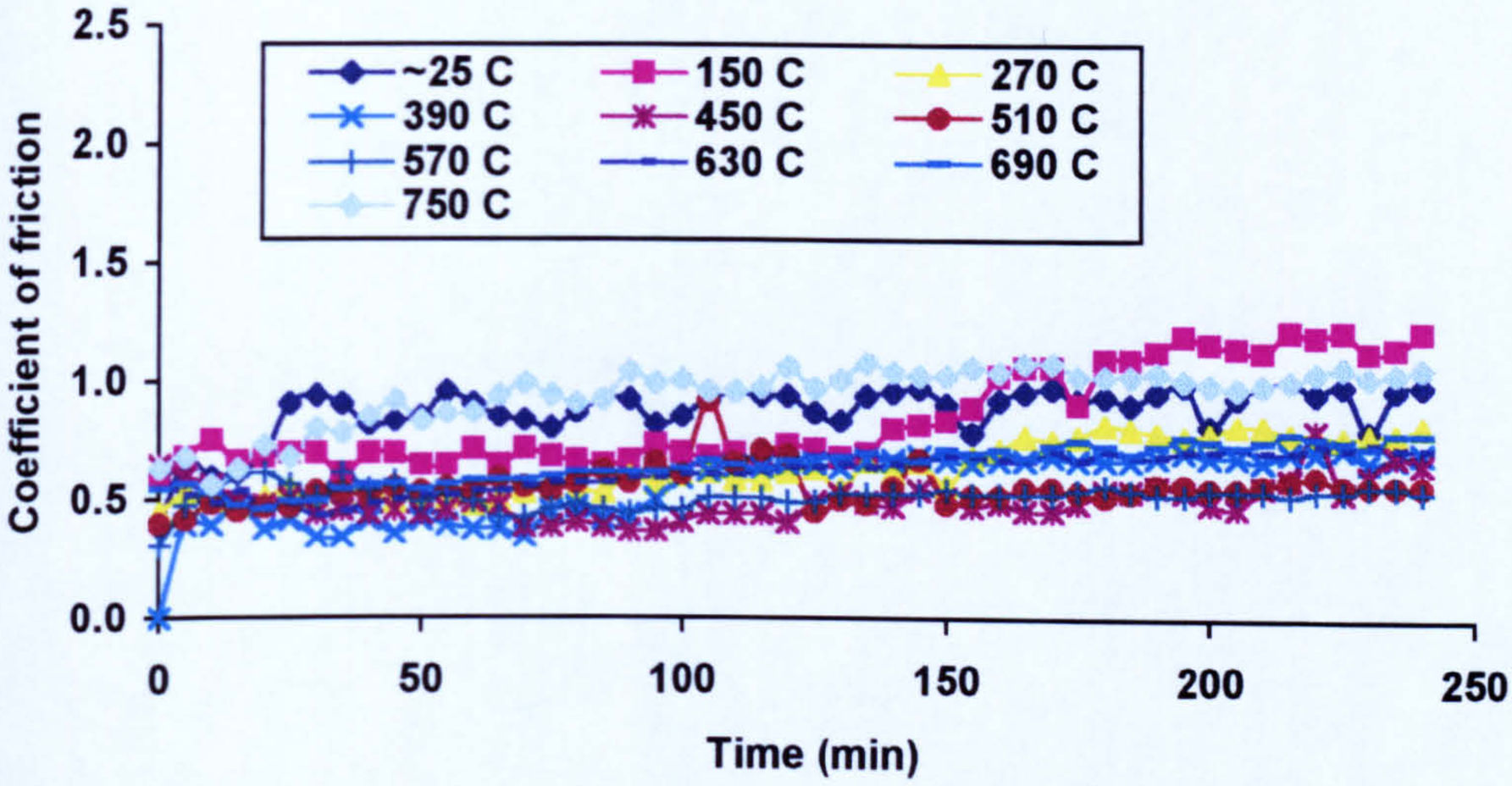

Figure 5.21 Coefficients of friction for MA956 worn with Stellite 6 over a range of temperatures from ~25 to 750°C

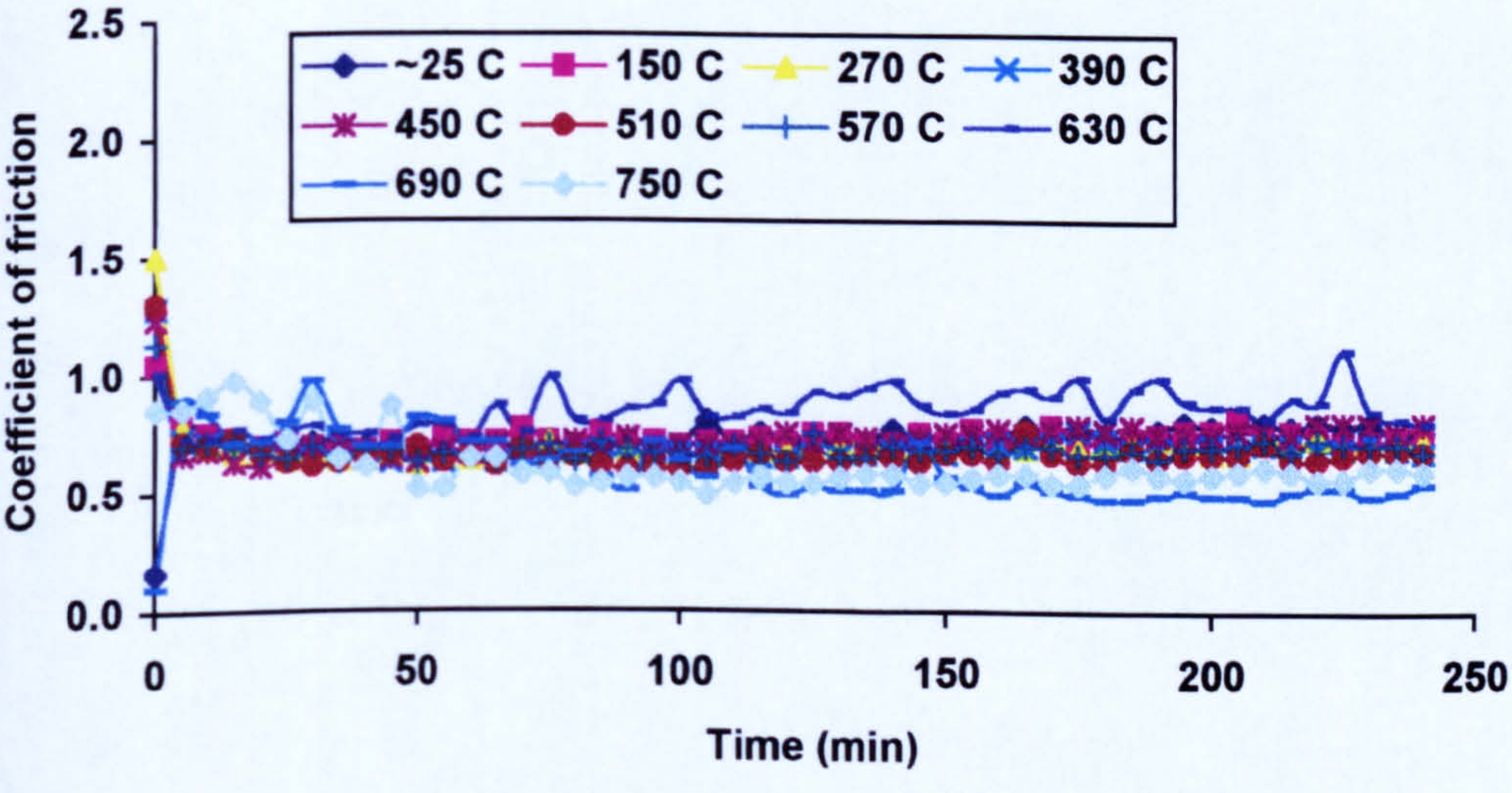

Figure 5.22 Coefficients of friction for MA956 worn with Incoloy 800 over a range of temperatures from ~25 to 750°C

For MA956 worn with Stellite 6 counterfaces it can be seen that the coefficient of friction gave a wide range of values between ~0.40 to 1.00. The coefficient of friction does not reveal any discernible pattern with temperature,

however, the coefficient of friction does rise slowly throughout the test, normally by 0.10 to 0.20.

For MA956 worn with Incoloy 800 counterfaces, the coefficient of friction rapidly reaches a stable value of 0.60 to 0.80 within the first 10 minutes of the tests, a far smaller range than that seen with Stellite 6 counterfaces. The coefficient remains approximately the same at all temperatures tested, no discernible pattern of change with temperature was observed.

5.5.3 XRD analysis

Diffractograms taken of MA956 samples with Stellite 6 and Incoloy 800 counterfaces are displayed in **Figure 5.23** and **Figure 5.24** and the phases identified are shown in **Table 5.4.** For MA956 worn with Stellite 6 only the phase confirming the presence of the MA956 substrate was identified from room temperature to 450°C. From 510°C to 750°C phases for cobalt chromium oxide ($CoCr_2O_4$) transferred from the counterface and chromium iron oxide ($Cr_{1.3}Fe_{0.7}O_3$) originating from the sample were also identified.

For MA956 worn with Incoloy 800 counterfaces, only the phase revealing the presence of MA956 was identified from room temperature to 630°C. At 690°C and 750°C chromium iron oxide ($Cr_{1.3}Fe_{0.7}O_3$) phases were also identified.

MA956 worn with Stellite 6 counterfaces	
Phase identified	**Conditions identified / interpretation**
Iron chromium stainless steel phase (Fe-Cr)	MA956 substrate, all temperatures tested
Cobalt chromium oxide ($CoCr_2O_4$)	From 510°C to 750°C
Chromium iron oxide ($Cr_{1.3}Fe_{0.7}O_3$)	From 510°C to 750°C
MA956 worn with Incoloy 800 counterfaces	
Phase identified	**Conditions identified / interpretation**
Iron chromium stainless steel phase (Fe-Cr)	MA956 substrate, all temperatures tested
Chromium iron oxide ($Cr_{1.3}Fe_{0.7}O_3$)	At 690°C and 750°C

Table 5.4 XRD analysis of MA956 samples worn with Stellite 6 and Incoloy 800 from ~ 25°C to 750°C

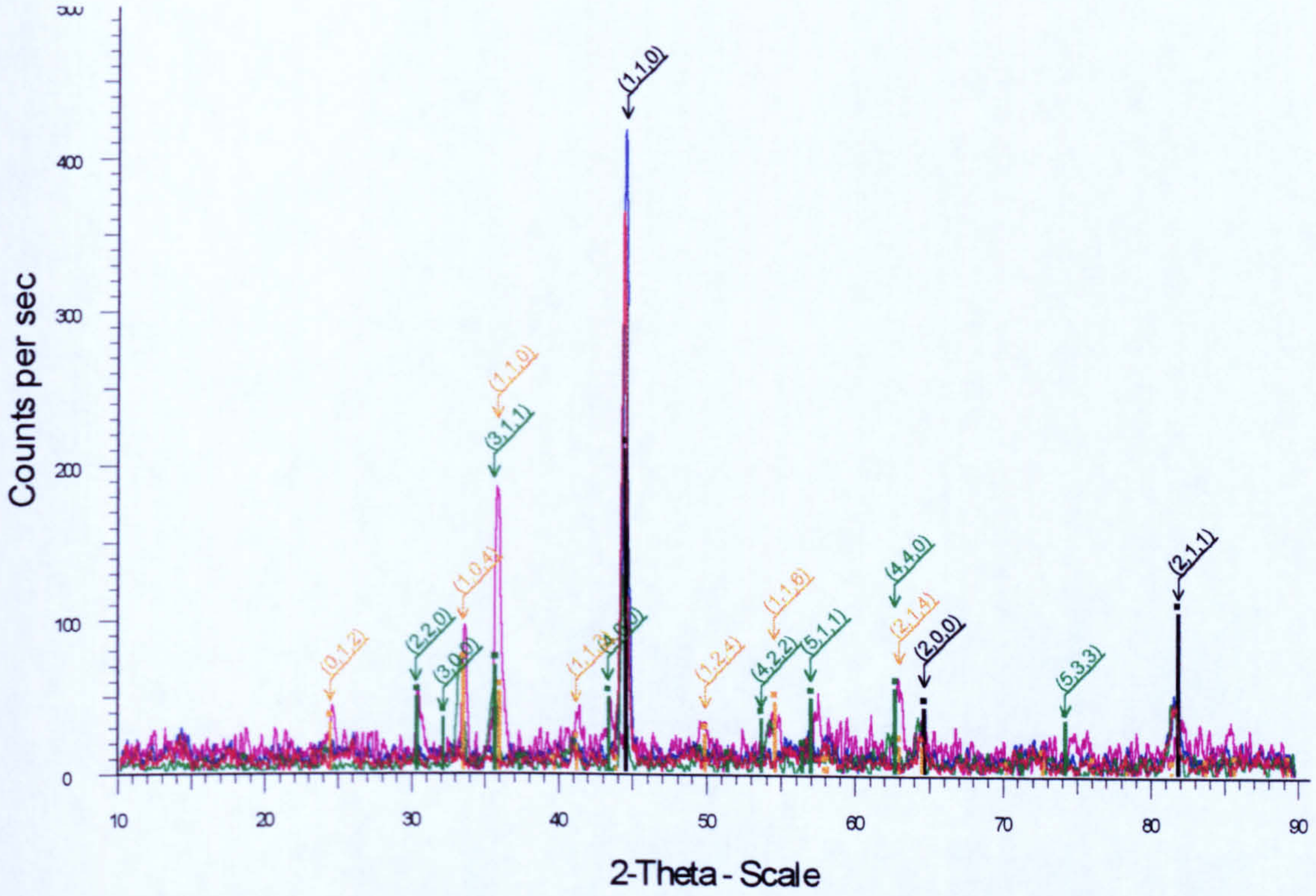

Figure 5.23 XRD data for MA956 worn with Stellite 6 at temperatures of ~25°C, 270, 510 and 750°C. Phases identified iron-chromium phase (Fe-Cr) (MA956), cobalt chromium oxide ($CoCr_2O_4$) chromium iron oxide ($Cr_{1.3}Fe_{0.7}O_3$) for 4 hours at 7N load

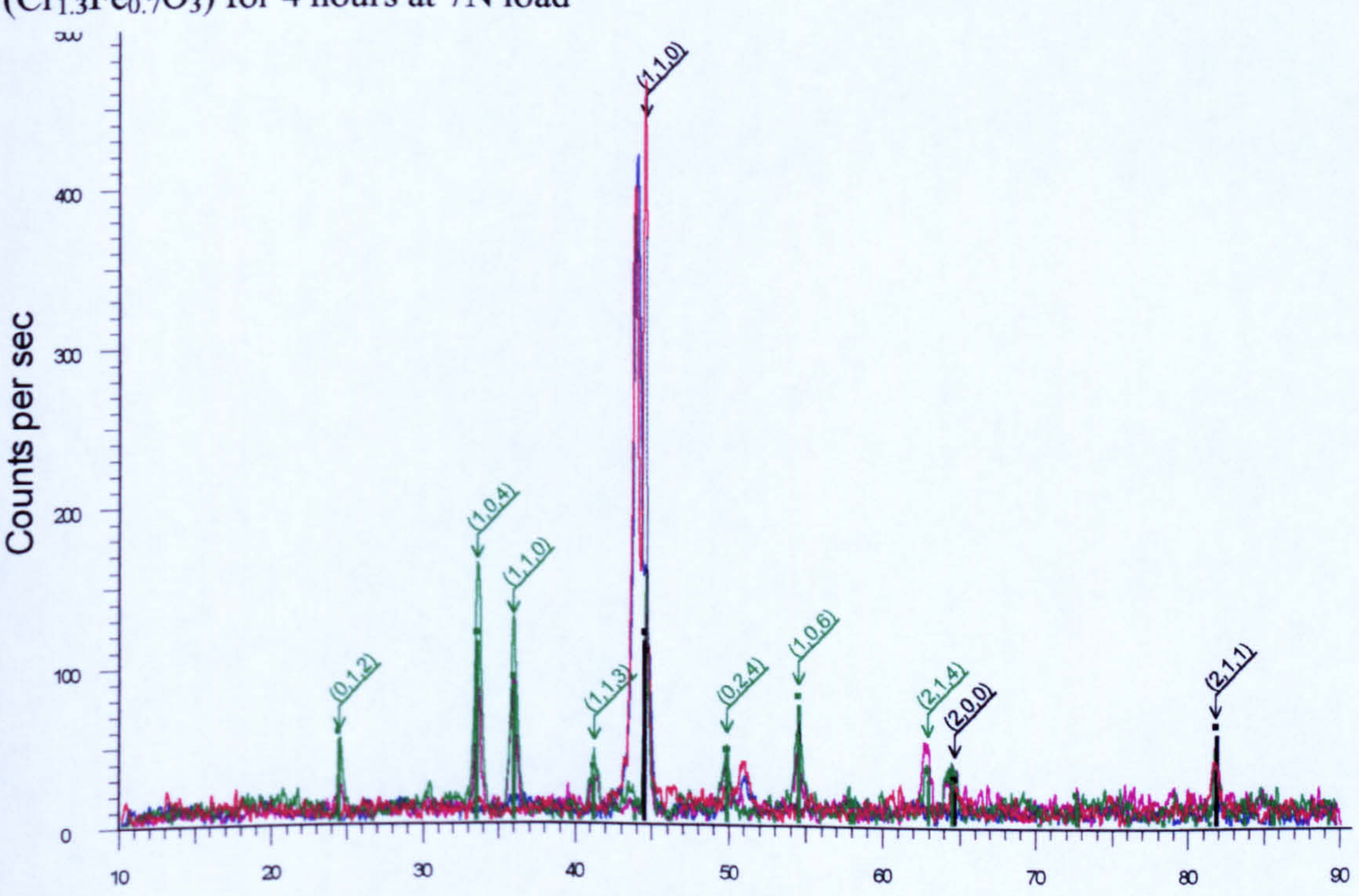

Figure 5.24 XRD data for MA956 worn with Incoloy 800 at temperatures of ~25, 270, 510, 750°C. Phases identified iron-chromium phase (Fe-Cr) (MA956) and chromium iron oxide ($Cr_{1.3}Fe_{0.7}O_3$) for 4 hours at 7N load

5.5.4 SEM morphological analysis

SEM micrographs of the surfaces worn with Stellite 6 at 25, 270, 510 and 750°C are shown in **Figure 5.25.** For MA956 worn with Stellite 6 counterfaces from room temperature to 390°C the wear scar appeared grooved and was covered with fine wear debris particles. SEM/EDX showed the fine particles to comprise Stellite 6 material. However at 450°C the wear scar appeared highly torn and deformed, and the fine wear debris particles present at lower temperatures were absent. The first appearance of the compacted oxide layer occurred at 510°C. From 510°C to 750°C compacted oxide layers ('glazes') were seen covering the wear scars' surface, with a characteristically smooth surface. Between the areas of compacted oxide material there were small areas in which wear debris remained uncompacted and were caught in hollows and depressions in the surface.

Figure 5.26 displays the situation for the MA956 worn with Incoloy 800 counterfaces at temperatures 25, 270, 510 and 750°C. For MA956 worn with the Incoloy 800 counterfaces the wear scars had considerably less attached debris compared to the Stellite 6 counterface. From room temperature to 630°C the surfaces had a broken and grooved appearance, the degree of surface damage increasing with increasing temperature. Between 690°C and 750°C the surfaces were very smooth, characteristic of compacted oxide layers.

5.5.5 Analysis of wear debris

The wear debris collected from MA956 worn with Stellite 6 counterfaces shows two types of particles across the range of temperatures investigated – **Figure 5.27.** From room temperature to 390°C the debris consists almost entirely of fine particles (1-5μm) which tended to agglomerate. This debris was predominately Stellite 6 material – identified as mainly Co-Cr oxide by SEM/EDX analysis.

Between 450°C and 750°C the wear debris consisted of large, predominately flat, angular particles ranging in size from ~50 to 250μm and 10 to 20μm in thickness. Fine wear debris was also seen at these temperatures, the finer material often being attached to the surfaces of the larger fragments.

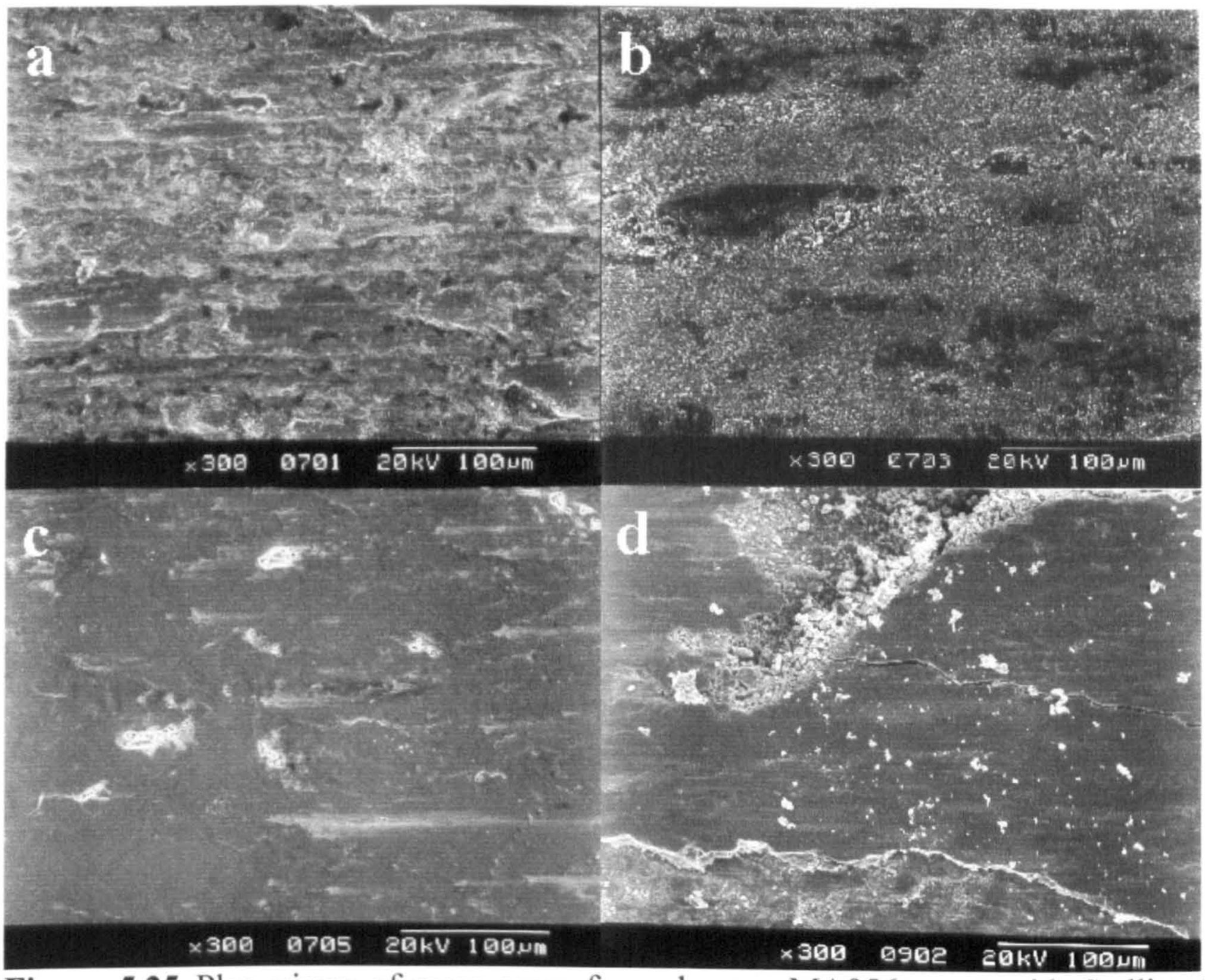

Figure 5.25 Plan views of wear scars formed upon MA956 worn with Stellite 6 counterfaces at temperatures of ~25, 270, 510 and 750°C, (a), (b), (c) and (d) respectively for 4 hours at 7N load

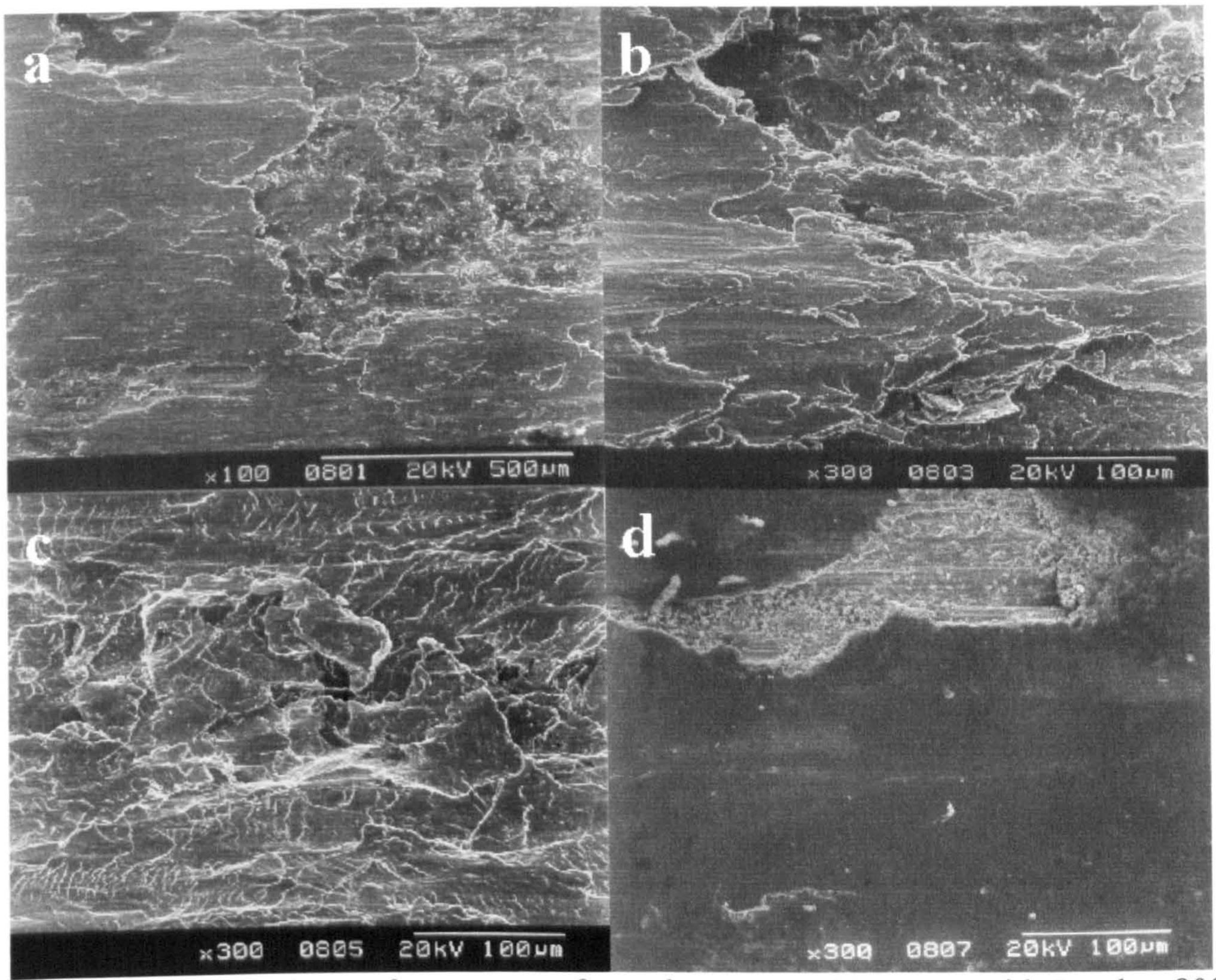

Figure 5.26 Plan views of wear scars formed upon MA956 worn with Incoloy 800 counterfaces at temperatures ~25, 270, 510 and 750°C, (a), (b), (c) and (d) respectively, for 4 hours at 7N load

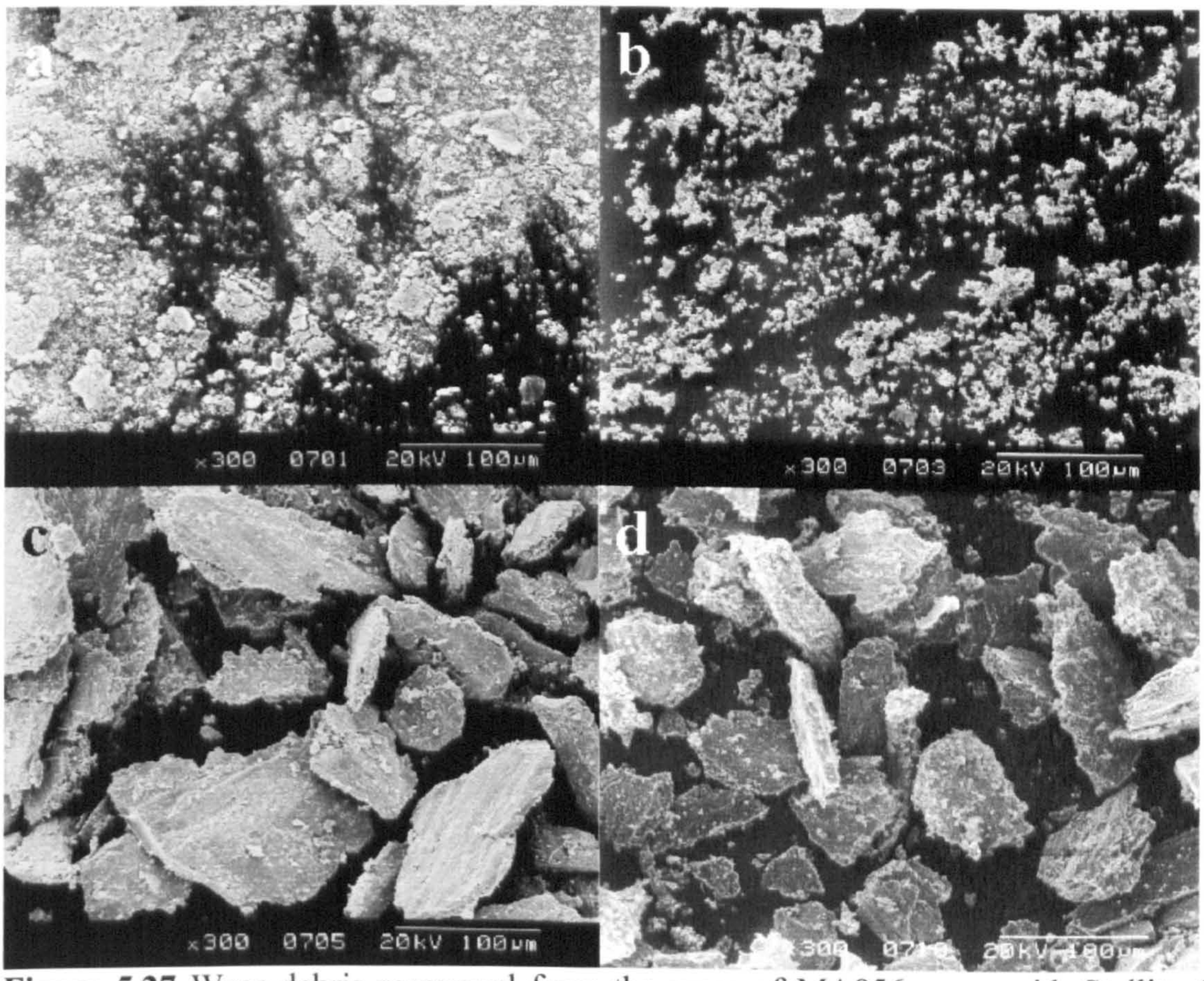

Figure 5.27 Wear debris recovered from the wear of MA956 worn with Stellite 6 counterfaces at temperatures ~25, 270, 510 and 750°C, (a), (b), (c) and (d) respectively, for 4 hours at 7N load

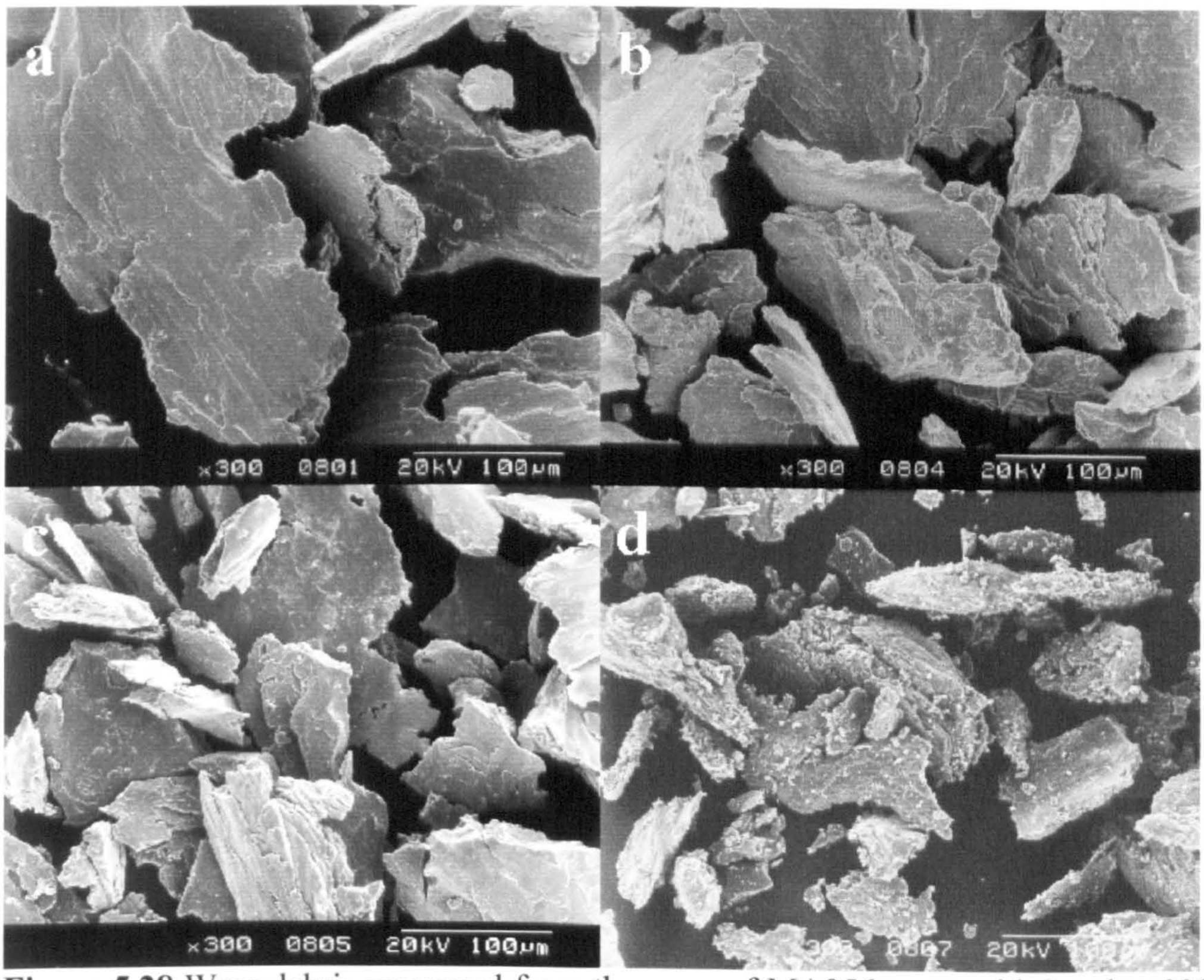

Figure 5.28 Wear debris recovered from the wear of MA956 worn with Incoloy 800 counterfaces at temperatures ~25, 270, 510 and 750°C, (a), (b), (c) and (d) respectively, for 4 hours at 7N load

Wear debris (**Figure 5.28**) collected from MA956 worn with Incoloy 800 counterfaces from room temperature to 630°C – **Figure 5.28 (a)**, **(b)** and **(c)** – consists of flat, angular particles of sizes 50 to 250μm and thickness 20 to 30μm. At 690°C and 750°C large flat particles were present, upon which finer debris was attached (1 to 5μm in size). SEM/EDX showed the debris to be a mixture of MA956 and Incoloy 800 material.

5.5.6 Hardness cross-section profiles for MA956 worn with Stellite 6 and Incoloy 800 counterfaces

Cross-sectional hardness profiles for MA956 worn with Stellite 6 counterfaces at the four temperatures examined are displayed in **Figure 5.29**. Here it can be seen that no hardened layers could be detected beneath the wear scars at any of the temperatures tested.

Cross-section profiles for MA956 worn with an Incoloy 800 counterface are shown in **Figure 5.30**. At room temperature some hardening near the scar's surface (approximately the first 30μm) was seen. At 270 and 510°C there is considerable hardening of the material beneath the substrate, to a depth of ~100μm. Although at 750°C, where a compacted oxide 'glaze' layer was clearly present on the scar's surface, only a small amount of hardening was observed close to the base of the oxide layer. As before, below a depth of approximately 150μm all the samples tested had hardness close to the room temperature hardness recorded for MA956, i.e. 3.43 GPa.

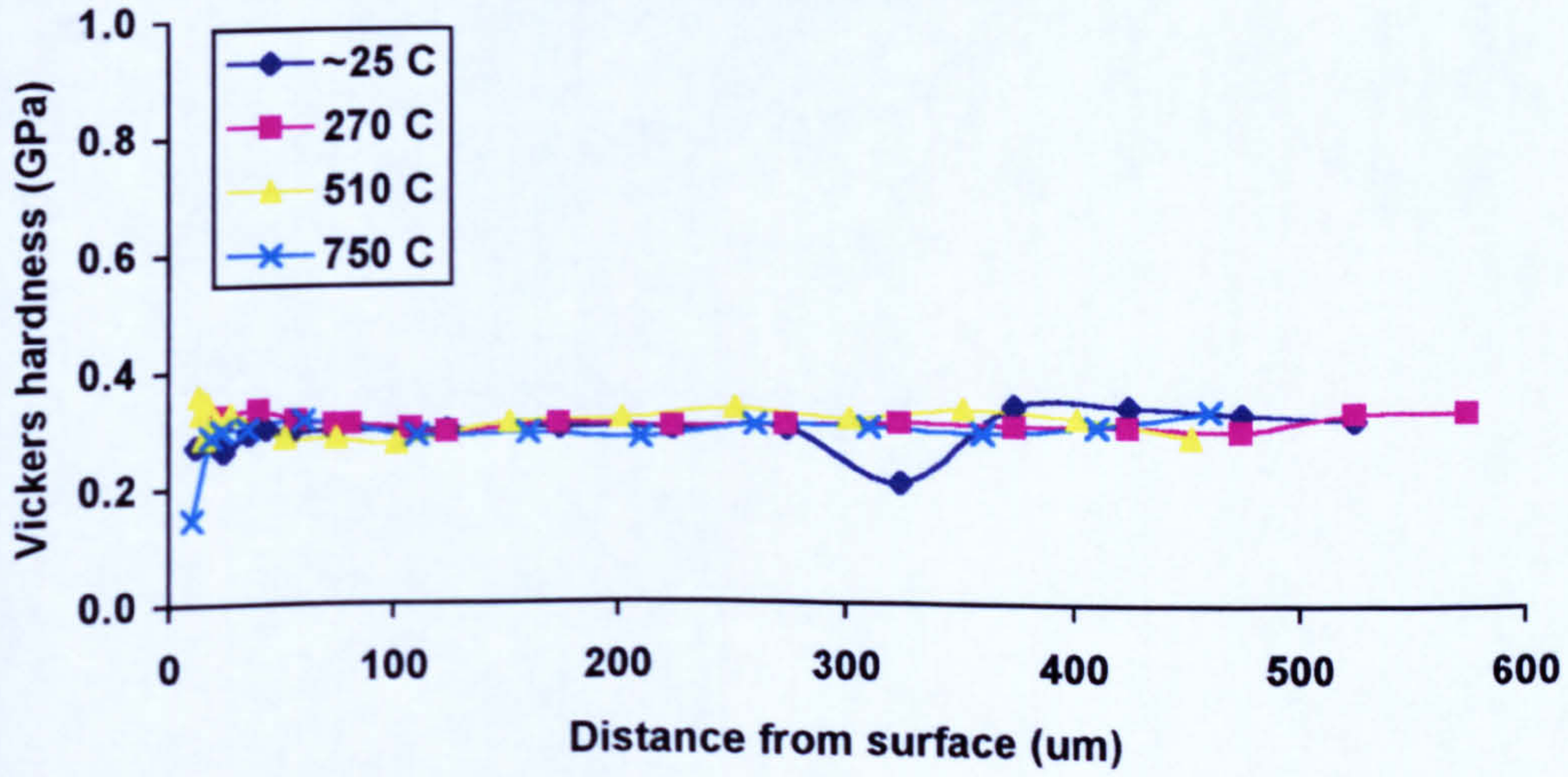

Figure 5.29 Hardness profiles through MA956 sample wear scar worn with Stellite 6 at 7N load for 4 hours. Hardness testing load 50g dwell time 12 seconds

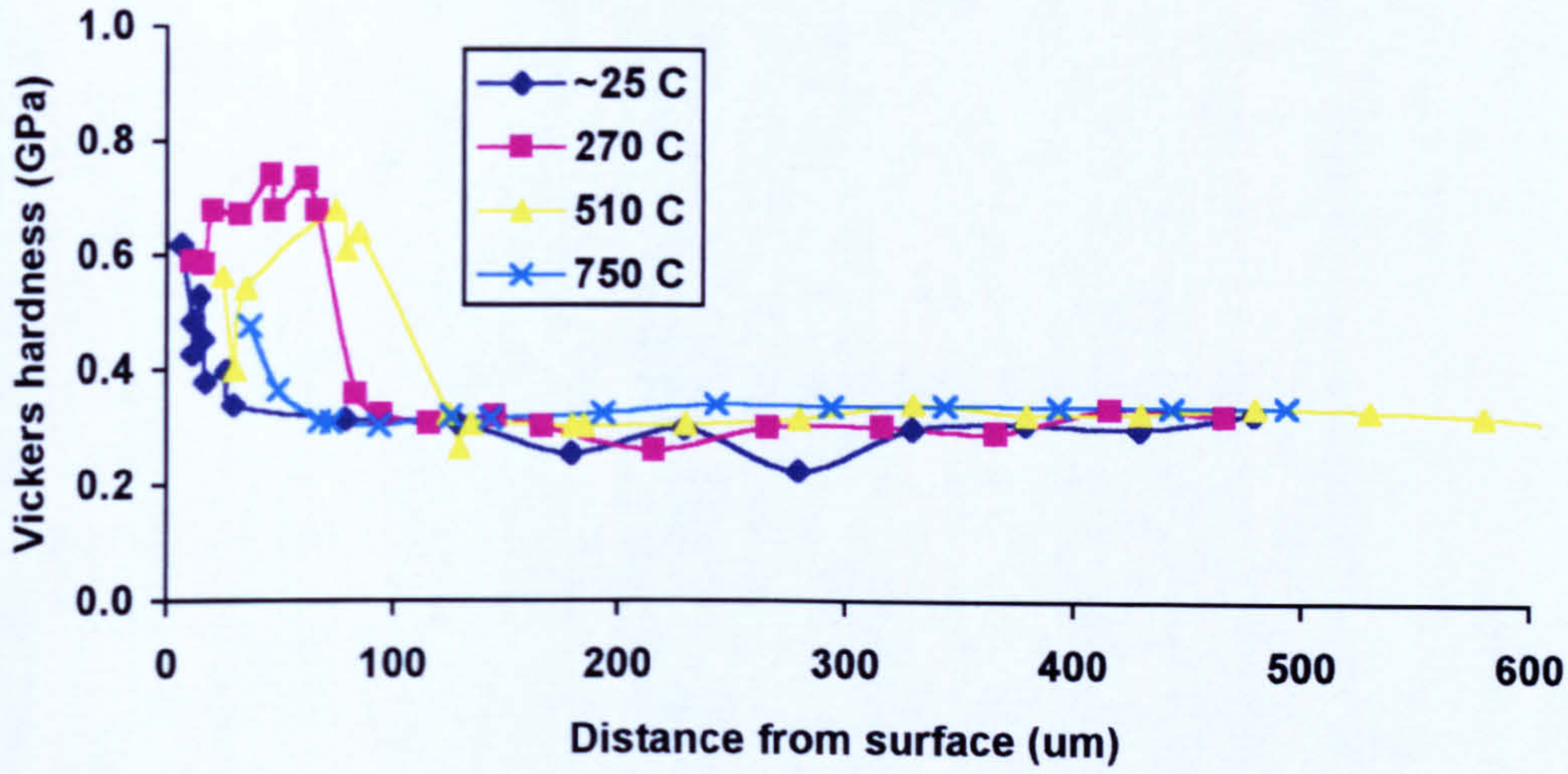

Figure 5.30 Hardness profiles through MA956 sample wear scar worn with Incoloy 800 at 7 N load for 4 hours. Hardness testing load 50g dwell time 12 seconds

5.5.7 Appearance of the counterface

At room temperature Stellite 6 counterfaces appeared only slightly worn, with a fine grooved surface. There was no evidence of oxidation of the counterface and as with the recovered debris, the appearance of the surface was bright and metallic. From 150°C to 510°C the wear tracks become progressively covered with fine oxide debris in the form of a fine black powder, which is easily removed by touch. At 510°C small islands of compacted oxide 'glaze' material begin to appear on the wear track, these are surrounded by loosely adherent oxide powder. At higher temperatures the compacted oxide material progressively covers more of the wear track. At 750°C the wear track is almost completely covered. The overall appearance across the range of temperatures was very similar to the wear scars on the corresponding samples. However considerably more attached debris was seen on the counterface than the corresponding samples.

At room temperature Incoloy 800 counterfaces worn with MA956 showed little wear and were bright and metallic in appearance. From 150°C to 390°C there is a progressive change, as the surfaces become rougher with areas of material appearing smeared across the surface. At 270°C the surface of the whole counterface takes on a light golden brown colour due to the presence of a thin oxide film and the smearing and deformation of the surface becomes more pronounced. At 630°C the wear track was extremely rough and worn – accounting for the lack of smooth running of the rig at these temperatures.

At 690°C and 750°C small islands of shiny compacted oxide material were present on the wear scar and the surface damage was considerably reduced.

Surrounding these areas were loosely attached fine debris powder – much finer than the recovered debris. A greater coverage of the wear track with 'glaze-type' islands of material was observed at the higher temperature. Again the morphology of the Incoloy 800 counterfaces mirror those on the corresponding samples.

5.6 Nimonic 80 A worn with Stellite 6 and Incoloy 800 counterfaces from ~25 to 750°C

5.6.1 Weight changes

The weight losses for Nimonic 80A – shown in **Figure 5.31** – produce two different patterns when worn with Stellite 6 and Incoloy 800 counterfaces. Nimonic 80A worn with Stellite 6 counterfaces gives very low weight losses from ~25 to 450°C. From 510 to 630°C the weight losses increase to a maximum at 630°C (0.5107g). Above 630°C to 750°C the weight losses fall with temperature (e.g. 0.0843g at 750°C).

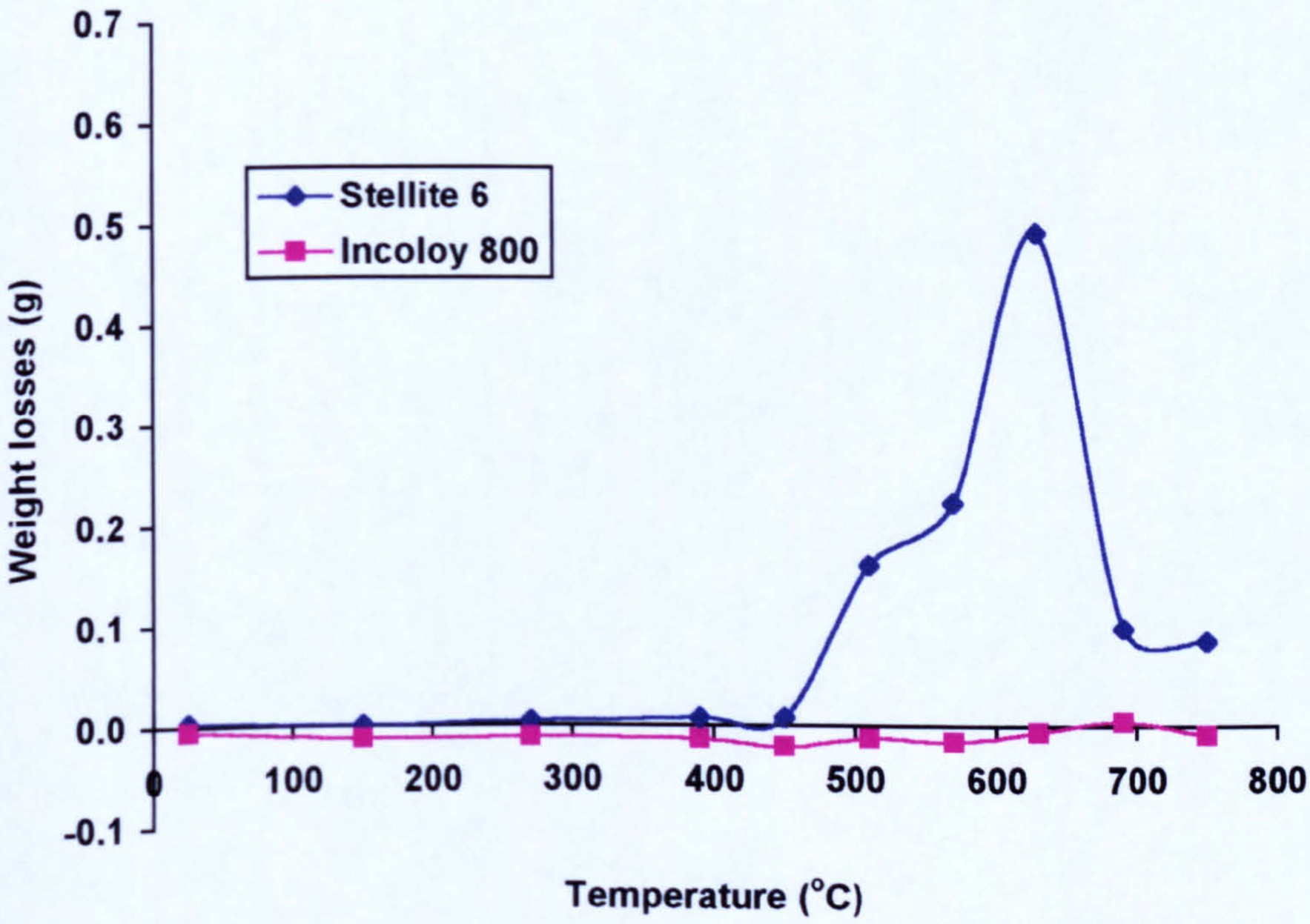

Figure 5.31 Weight losses for Nimonic 80A with Stellite 6 and Incoloy 800 counterfaces over a range of temperatures from ~25 to 750°C, for 4 hours at 7N load

For Nimonic 80A worn with an Incoloy 800 counterface the weight changes all show very small weight gains. However these were generally less than the normal reproducibility of the wear test arrangement.

5.6.2 Coefficients of friction

The coefficient of friction for Nimonic 80A worn with Stellite 6 and Incoloy 800 counterfaces are shown in **Figure 5.32** and **Figure 5.33** respectively. For Nimonic 80A worn with Stellite 6 the coefficient of friction remains between 0.40 to 0.50 for all the temperatures examined for the length of the tests – except at ~25°C. At ~25°C the coefficient of friction fluctuated between 0.40–0.5 and a higher value of 0.75–1.05. The coefficient of friction remained at the higher value for most of the test. The patterns of weight loss and coefficient of friction did not follow each other.

For Nimonic 80A worn with Incoloy 800 the coefficient of friction from ~25 to 570°C fall in a range from 0.60 to 0.80 which remains unchanged for the first 10 minutes of the tests, dropping from initial values of ~1.00. From 630 to 750°C the coefficient of friction undergoes a transition after a given time to a lower stable value of 0.35 to 045. The time for this transition decreased with increasing temperature (100 minutes at 630°C, 15 minutes at 750°C). This corresponds to the appearance of the compacted oxide layer on the contacting surfaces.

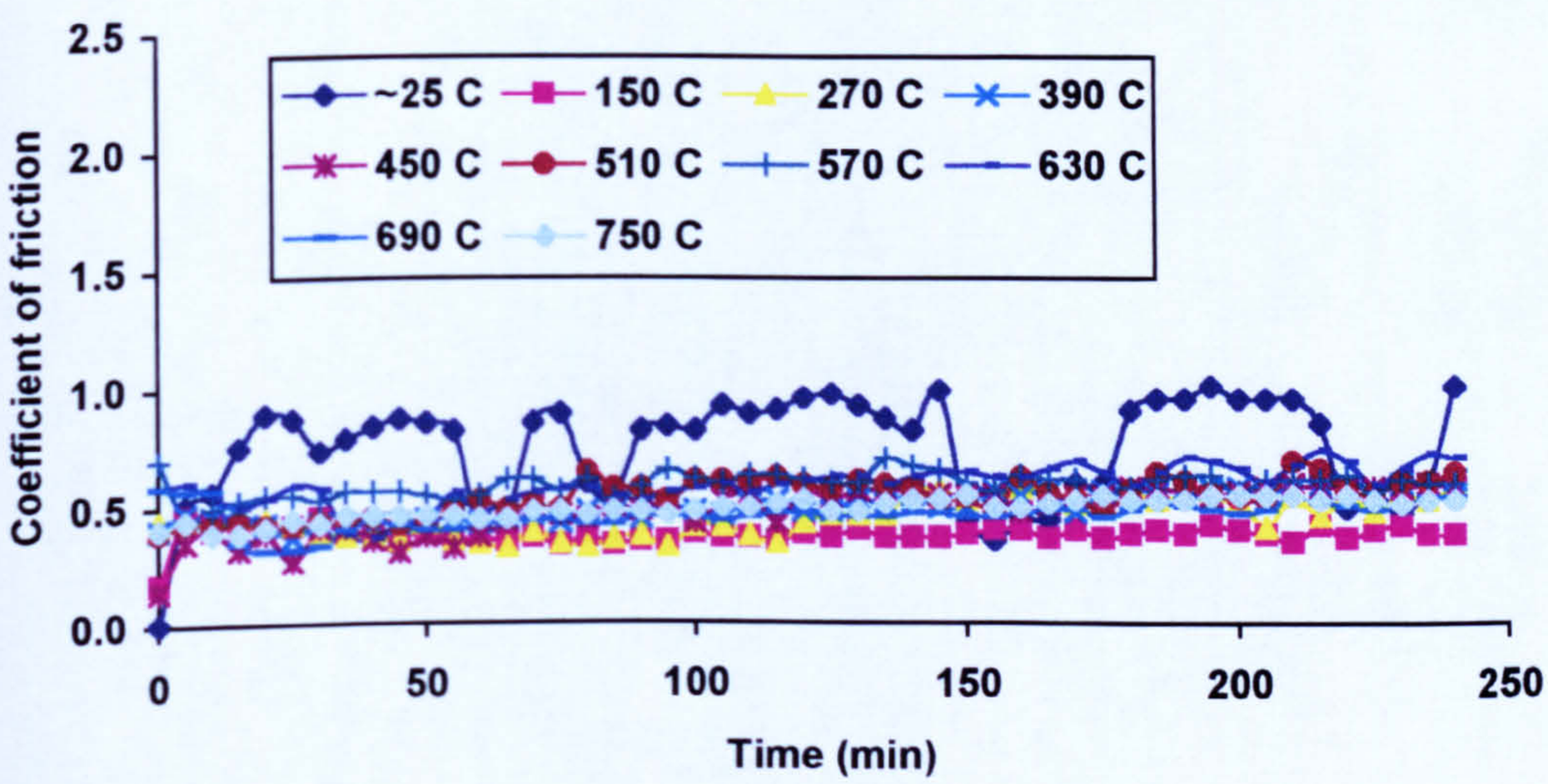

Figure 5.32 Coefficients of friction for Nimonic 80A worn with Stellite 6 counterfaces from ~25 to 750°C at 7N load

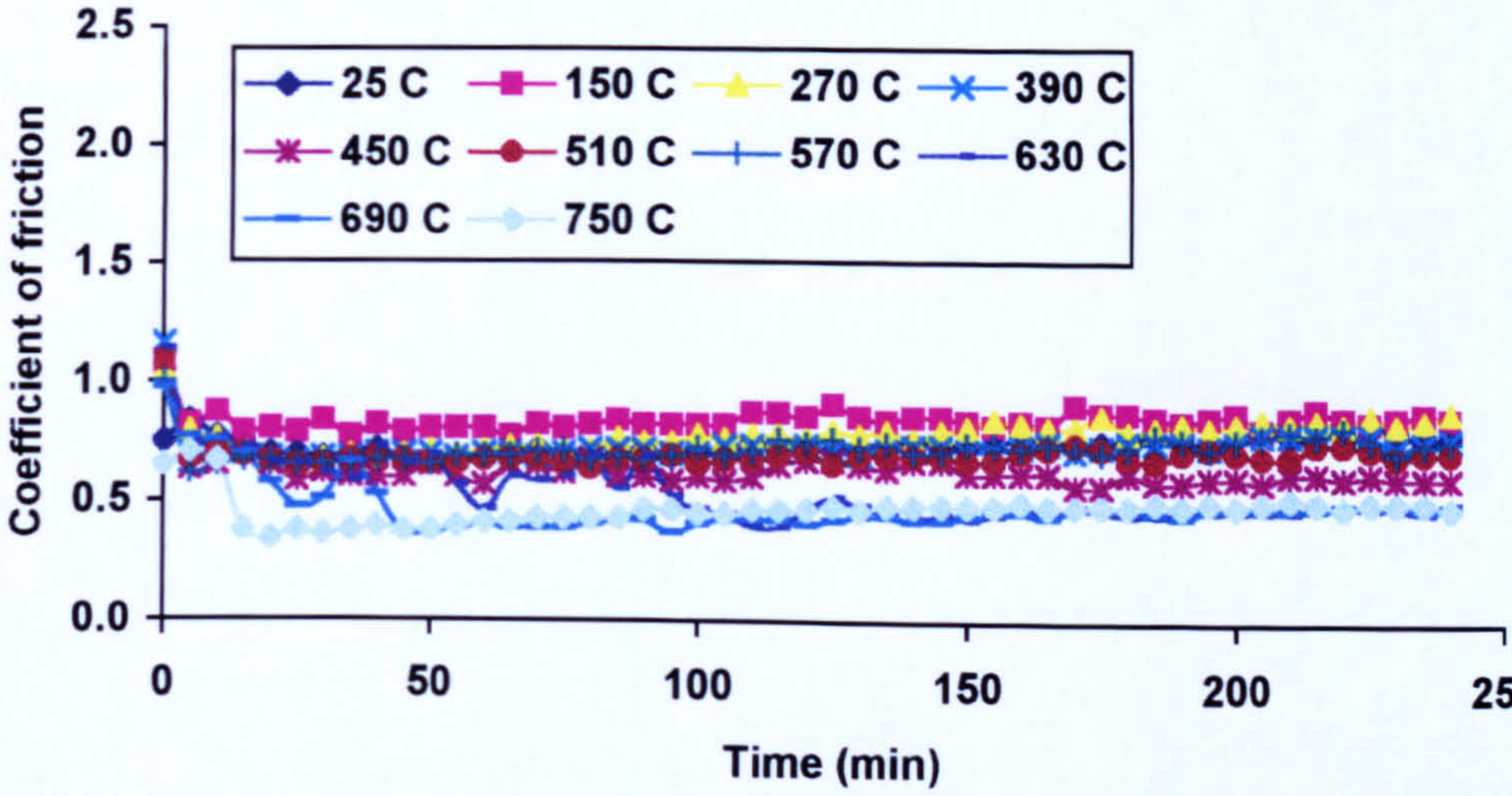

Figure 5.33 Coefficients of friction for Nimonic 80A worn with Incoloy 800 counterfaces from ~25 to 750°C at 7N load

5.6.3 XRD analysis

Diffractograms of the wear scars on Nimonic 80A worn with Stellite 6 are shown in **Figure 5.34**. From ~25 to 630°C only the iron chromium nickel phase corresponding to the Nimonic 80A substrate was identified. At 690 and 750°C the phase for cobalt chromium oxide ($CoCr_2O_4$), transferred from the counterface, was also detected. Data are summarised in **Table 5.5**.

Nimonic 80A worn with Stellite 6 counterfaces	
Phase identified	**Conditions identified**
Iron chromium nickel stainless steel phases ($Cr_{0.19}$ $Fe_{0.7}$ $Ni_{0.11}$)	Nimonic 80A substrate, all temperatures tested
Cobalt chromium oxide ($CoCr_2O_4$)	690°C and 750°C
Nimonic 80A worn with Incoloy 800 counterfaces	
Phase identified	**Conditions identified**
Iron chromium nickel stainless steel phases ($Cr_{0.19}$ $Fe_{0.7}$ $Ni_{0.11}$)	Nimonic 80A substrate, all temperatures tested
Transferred Incoloy 800	270°C and 570°C
Nichromite ($NiCr_2O_4$)	630°C to 750°C

Table 5.5 XRD analysis of Nimonic 80A samples worn with Stellite and Incoloy 800 from ~ 25°C to 750°C

Diffractograms of the wear scars on Nimonic 80A worn with Incoloy 800 are displayed in **Figure 5.35** and in **Table 5.5**. At all temperatures the iron chromium nickel phase revealing the presence of the Nimonic 80A substrate was

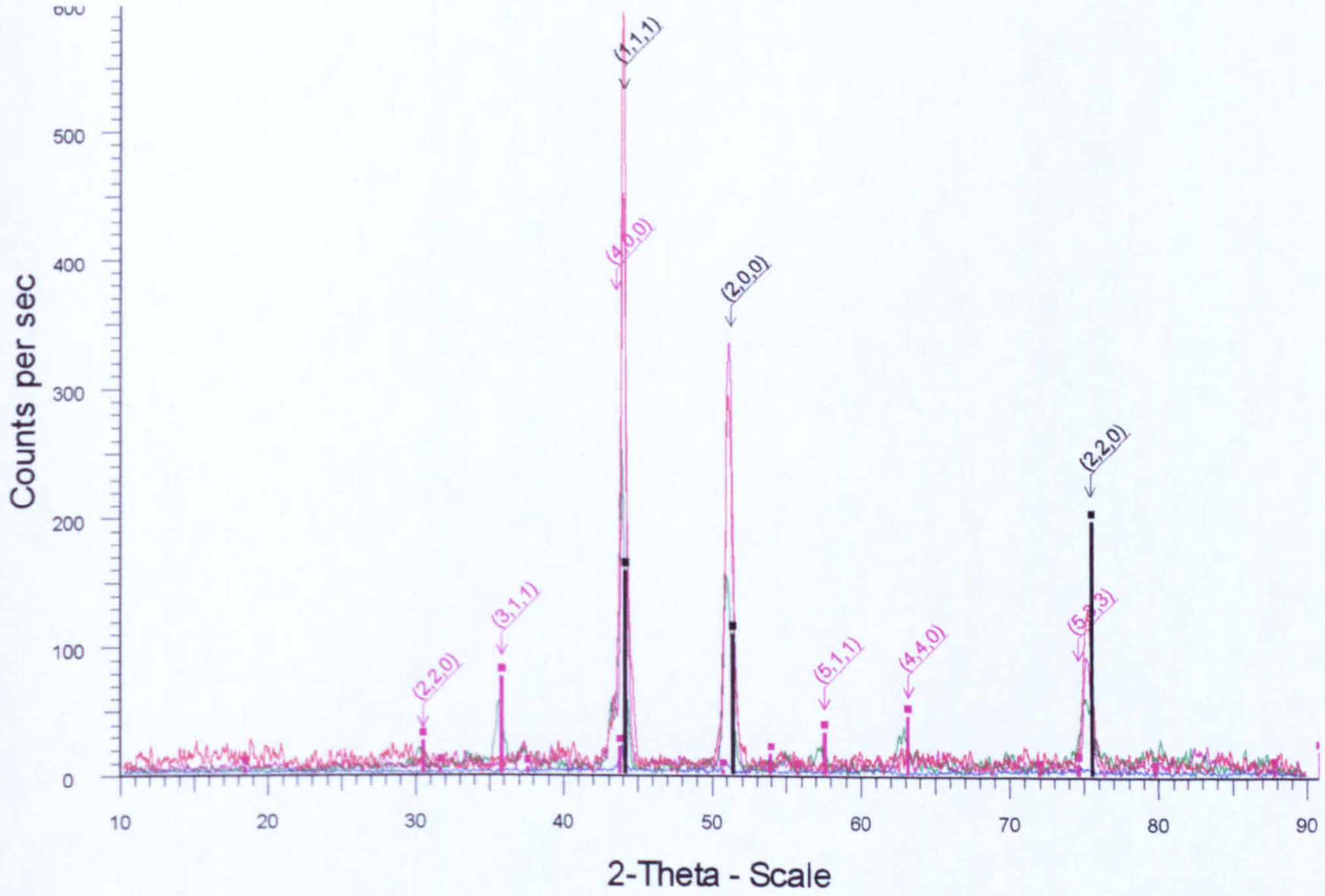

Figure 5.34 XRD data for Nimonic 80A worn with Stellite 6 at temperatures of ~25, 270, 510, 750°C. Phases identified ▣ iron chromium nickel phases ($Cr_{0.19}$ $Fe_{0.7}$ $Ni_{0.11}$) (Nimonic 80A) and ▣ cobalt chromium oxide ($CoCr_2O_4$) at 7N load, for 4 hours

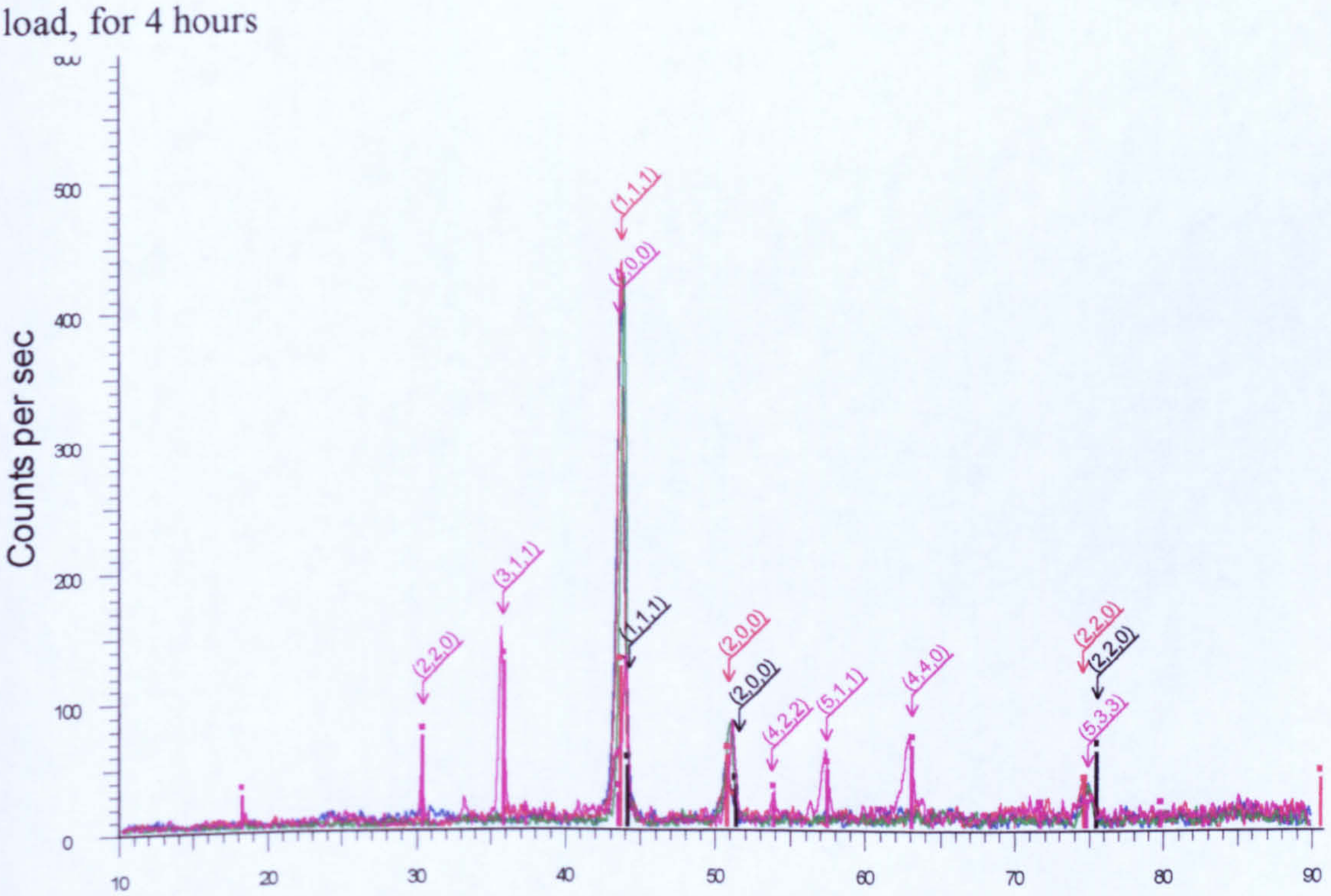

Figure 5.35 XRD data for Nimonic 80A worn with Incoloy 800 at temperatures of ~25, 270, 510, and 750°C Phases identified ▣ iron chromium nickel phases ($Cr_{0.19}$ $Fe_{0.7}$ $Ni_{0.11}$) (Nimonic 80A), ▣ transferred Incoloy 800 and ▣ nichromite ($NiCr_2O_4$) at 7N load, for 4 hours

found. Between 270 to 570°C phases were detected for traces of transferred Incoloy 800 from the counterface and from 630 to 750°C nichromite ($NiCr_2O_4$) was present on the surface.

5.6.4 SEM morphological analysis

Wear scars produced on Nimonic 80A worn with Stellite 6 counterfaces are given in **Figure 5.36**. At ~25°C the surfaces are covered in fine particles of what appear to be Stellite 6 material. These are present on the scars from ~25 to 450°C, although over this temperature range their appearance gradually changes from beds of quite loose particles on the scars' surfaces to a more smeared appearance. At higher temperatures the particles tend to accumulate in hollows and depressions at the surface.

From 510 to 630°C there are no particles on the wear scars and the surfaces appear torn and deformed. In places large wear particles (50 to 250μm) seemed to be forming from the surface. At 690 and 750°C the fine particles of Stellite 6 material are again present on the scars. Here the particles are smeared across the surface and caught in hollows and depressions of the scars – however, this does not constitute a compacted oxide layer.

Wear scars produced on Nimonic 80A worn with Incoloy 800 counterfaces are presented in **Figure 5.37**. From ~25 to 570°C the wear scars have a torn and deformed appearance. SEM/EDX showed these surfaces to contain many areas of transferred Incoloy 800 material.

From 630°C to 750°C the wear scars were covered with highly smooth compacted oxide layers. This covered most of the wear scars with only small areas of loosely compacted particles or exposed substrate where the oxide layer had cracked away.

5.6.5 Analysis of wear debris

The wear debris collected from Nimonic 80A worn with Stellite 6 counterfaces is shown in **Figure 5.38**. At temperatures from ~25 to 750°C fine powdery Stellite 6 material was found (1 to 5μm). However there were some fragments of flat angular particles present in the debris at all the temperatures examined, increasing in number from ~25°C up to a maximum at circa 510°C to 570°C. Above 570°C the debris almost entirely consisted of fine powdery material.

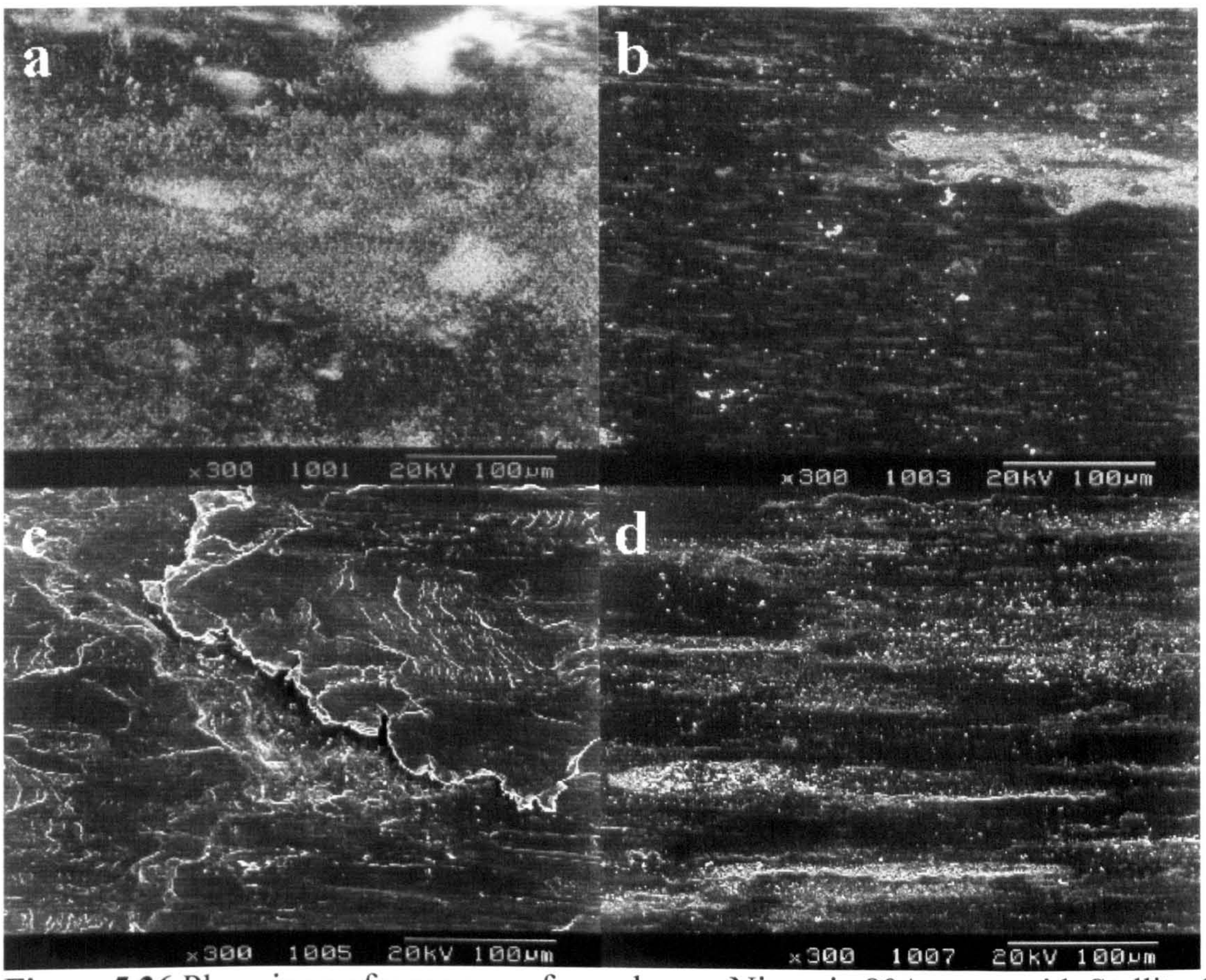

Figure 5.36 Plan views of wear scars formed upon Nimonic 80A worn with Stellite 6 counterfaces at temperatures ~25, 270, 510 and 750°C, (a), (b), (c) and (d) respectively, for 4 hours at 7N load

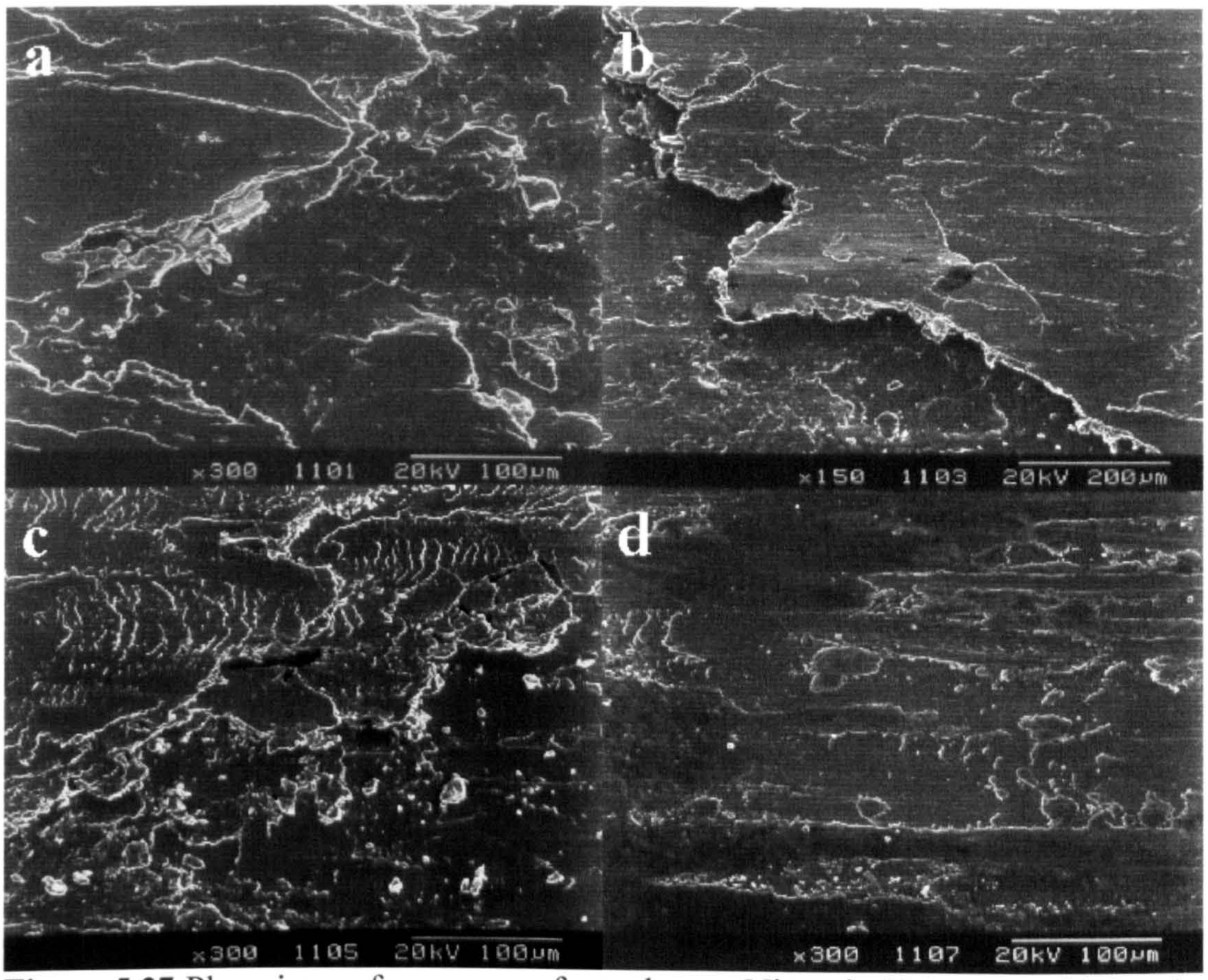

Figure 5.37 Plan views of wear scars formed upon Nimonic 80A worn with Incoloy 800 counterfaces at temperatures ~25, 270, 510 and 750°C, (a), (b), (c) and (d) respectively, for 4hours at 7N load

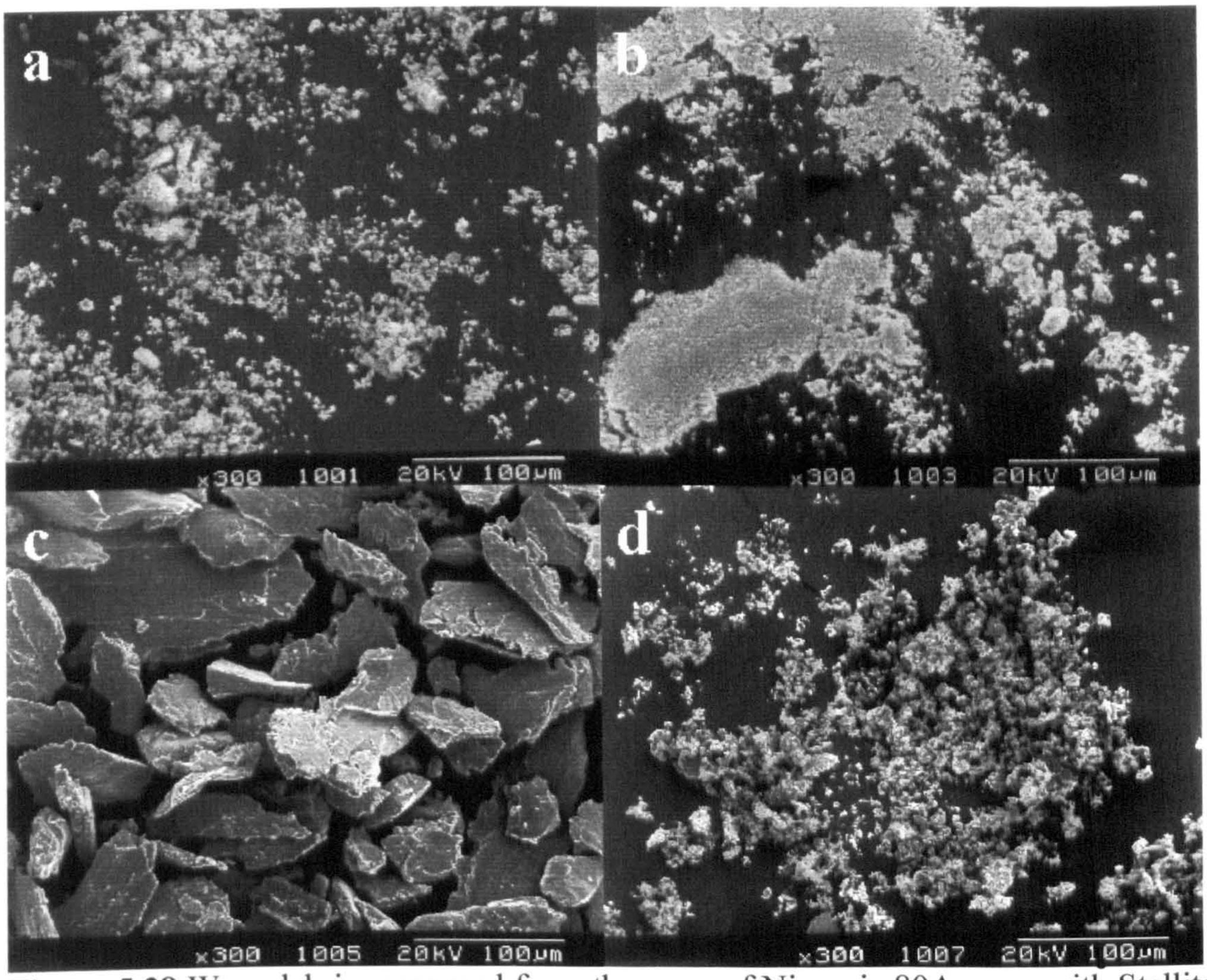

Figure 5.38 Wear debris recovered from the wear of Nimonic 80A worn with Stellite 6 counterfaces at temperatures ~25, 270, 510 and 750°C, (a), (b), (c) and (d) respectively, for 4 hours at 7N load

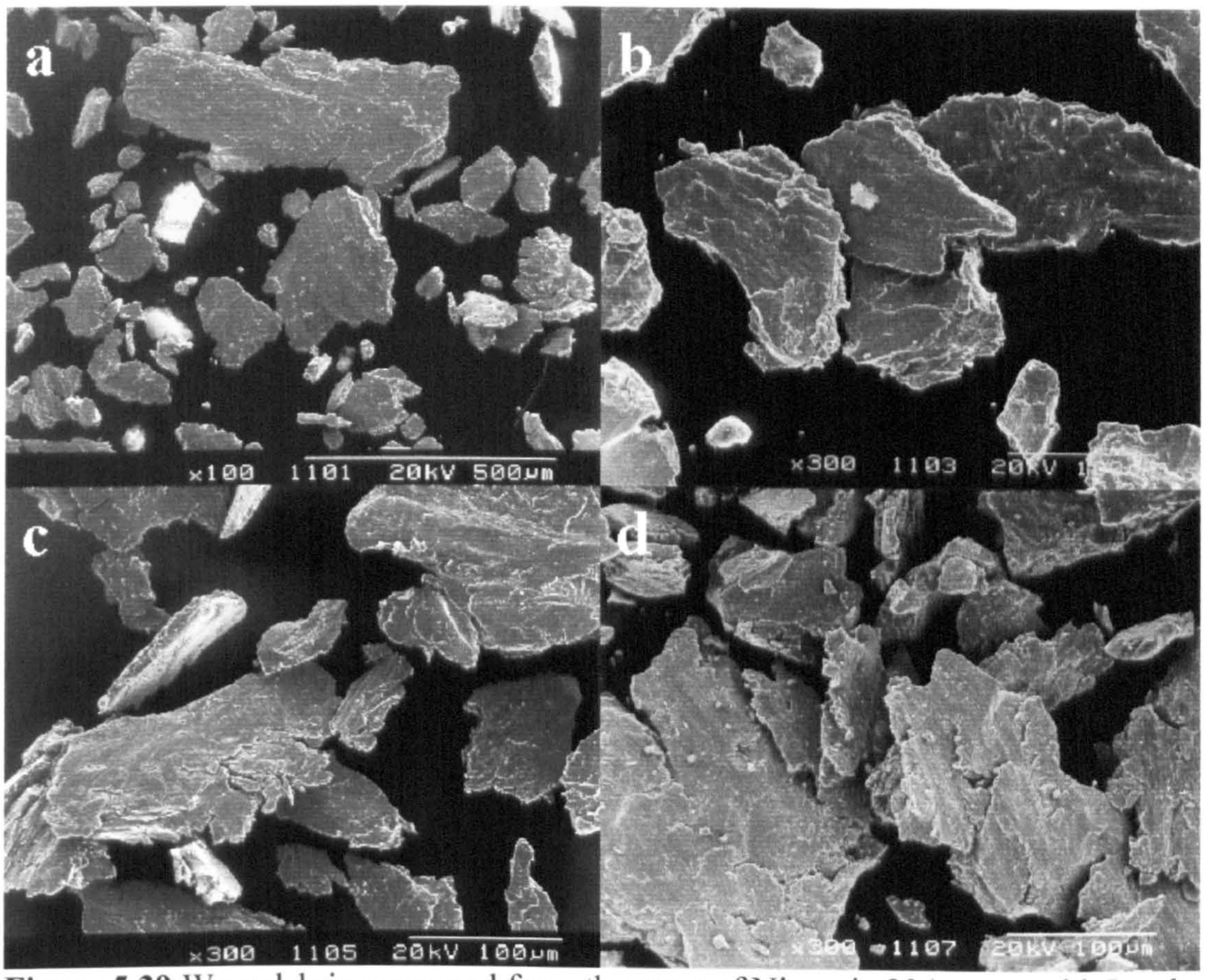

Figure 5.39 Wear debris recovered from the wear of Nimonic 80A worn with Incoloy 800 counterfaces at temperatures ~25, 270, 510 and 750°C, (a), (b), (c) and (d) respectively, for 4 hours at 7N load

Debris collected from Nimonic 80A worn with Incoloy 800 is displayed in **Figure 5.39**. This consisted of mainly large fragments of material (50 to 250μm) which were generally flat and angular in appearance. This type of debris was seen to form from ~25 to 750°C. From 630°C to 750°C these large fragments were observed to have smaller particles (5 to 15μm) attached to their surfaces – these had the same composition as the larger fragments. SEM/EDX revealed that the wear debris to consist of predominantly Incoloy 800 material.

5.6.6 Hardness cross-section profiles for Nimonic 80A worn with Stellite 6 and Incoloy 800 counterfaces

Cross-section hardness profiles for Nimonic 80A worn with Stellite 6 counterfaces are given in **Figure 5.40**. Here it can be seen that for all the temperatures examined there is some hardening – as compared with the as-received value – of the materials beneath the wear scar. The temperatures in which the greatest levels of hardening were detected were 250° and 510°C, where hardness of 0.4 to 0.5 GPa were recorded.

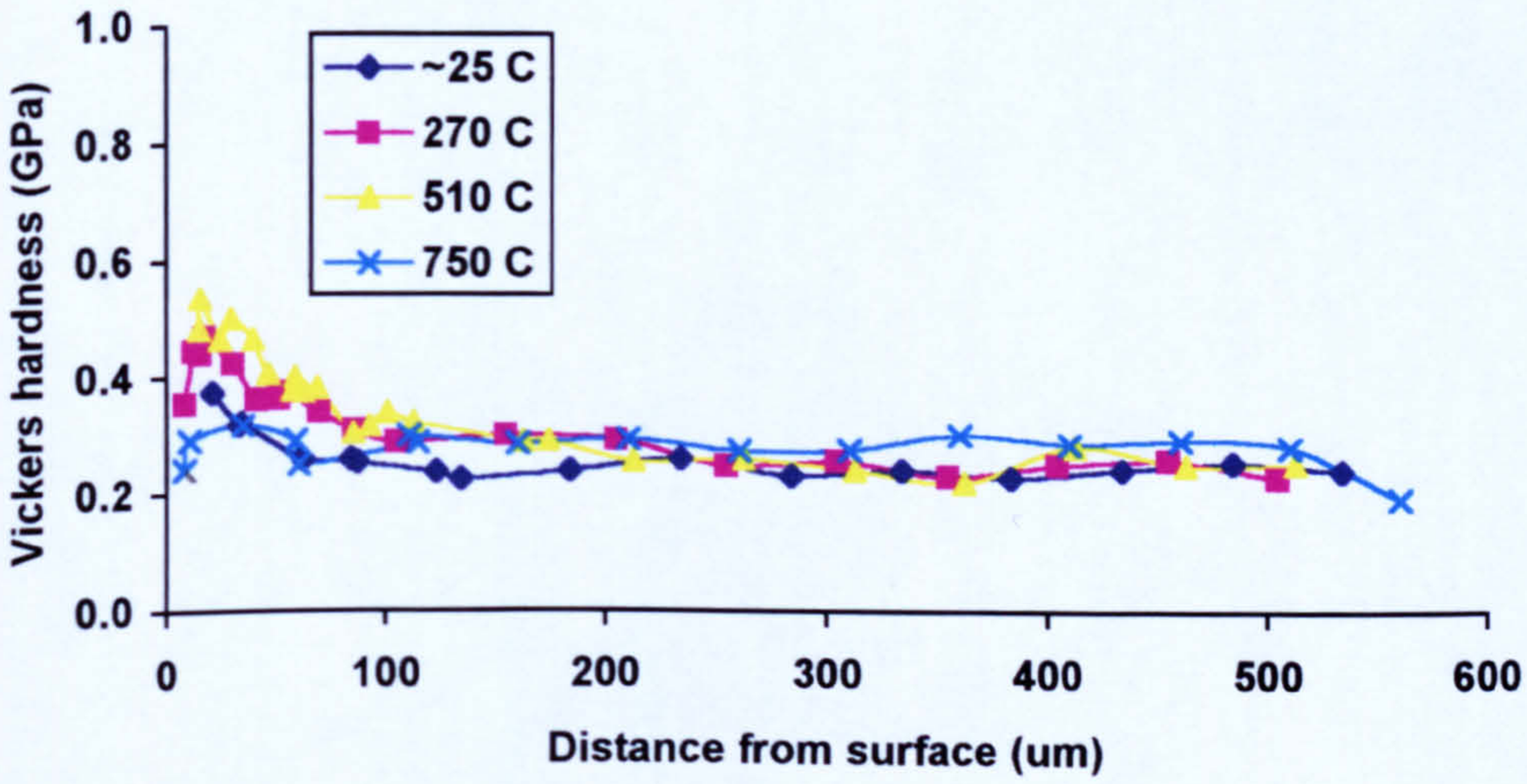

Figure 5.40 Hardness profiles through Nimonic 80A sample wear scar worn with Stellite 6 at 7 N load for 4 hours. Hardness testing load 50g dwell time 12 seconds

Cross-sectional hardness profiles for Nimonic 80A worn with Incoloy 800 counterfaces are shown in **Figure 5.41**. Hardening of the material beneath the wear scar was found at all temperatures investigated. Here the effect can be seen to a depth of up to 200μm, compared with ~100μm for the Stellite 6 counterface. As has been seen before, the two intermediate temperatures gave the greatest

level of hardening, up to 0.7 GPa (Vickers). However these hardened regions are likely to be transferred Incoloy 800 material.

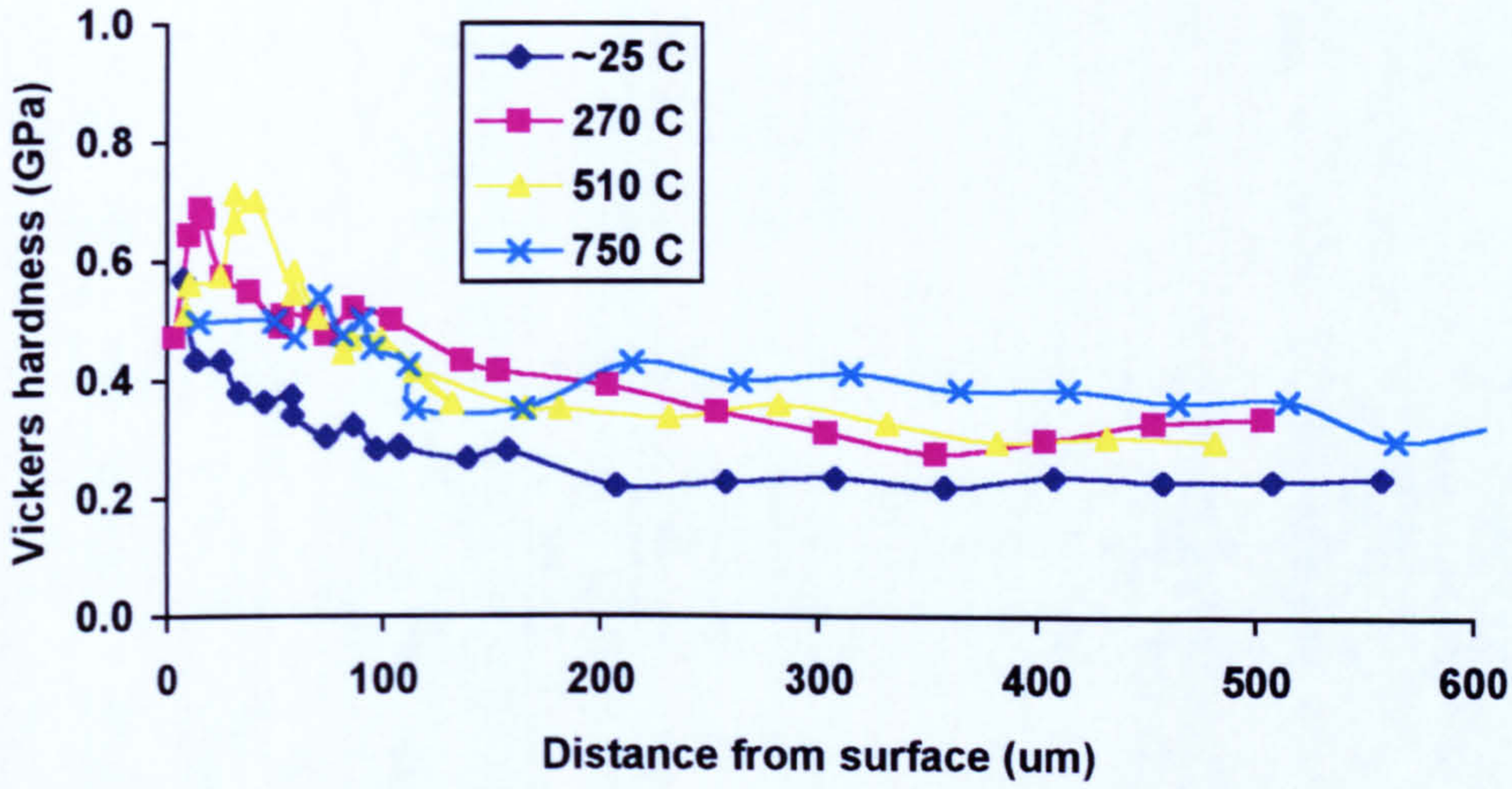

Figure 5.41 Hardness profiles through Nimonic 80A sample wear scar worn with Incoloy 800 at 7 N load for 4 hours. Hardness testing load 50g dwell time 12 seconds

5.6.7 Appearance of the counterface

For the Stellite 6 counterfaces worn with Nimonic 80A, from ~25 to 450°C the wear tracks appear to have undergone relatively little wear, being only slightly grooved. As the temperature was increased the tracks took on a 'blackened' appearance due to the presence of fine black powder which was easily removed by touch. Between 510 and 630°C, where the weight losses of the corresponding samples were high, the tracks showed signs of severe wear, being free from fine oxide debris. Here the counterface seems to have undergone significant material loss.

At 690 and 750°C the wear tracks were grooved and fine oxide powder was again present upon there surface, this powder tended to pile-up at the end of the scar. The appearance of the counterface was quite shiny almost 'glaze'-like in appearance.

From ~25 to 570°C the counterface wear tracks on Incoloy 800 were highly damaged, the damage becoming increasingly severe with increasing temperature. There was also a broadening of the wear track at higher temperatures due to the absence of smooth sliding leading to vibration of the wear rig. No attached debris or powder was present on the surfaces and there appeared to have been considerable material loss from the counterface.

For 630 to 750°C areas of compacted oxide material were seen on the tracks. These constituted of small 'islands' of compacted oxide material surrounded by fine black debris loosely compacted to the track. With increasing temperature the 'islands' covered a greater area of the track. Removing this 'third body', the attached debris revealed a torn and deformed track upon which the 'glaze' areas had formed. This suggests a period of severe wear before the development of the compacted oxide surfaces.

5.7 Sliding of Stellite 6 samples with MA956 counterfaces at 750°C

In this system the samples and counterface materials are reversed and compared to the results obtained in **Section 5.5**.

5.7.1 Weight changes

For a MA956 sample worn with a Stellite 6 counterface, a low weight loss was recorded (0.002(5)g). A Stellite 6 sample worn with a MA956 counterface gave a small negative weight loss (-0.011g), i.e. a slight weight gain. Weight changes are displayed in **Figure 5.42**.

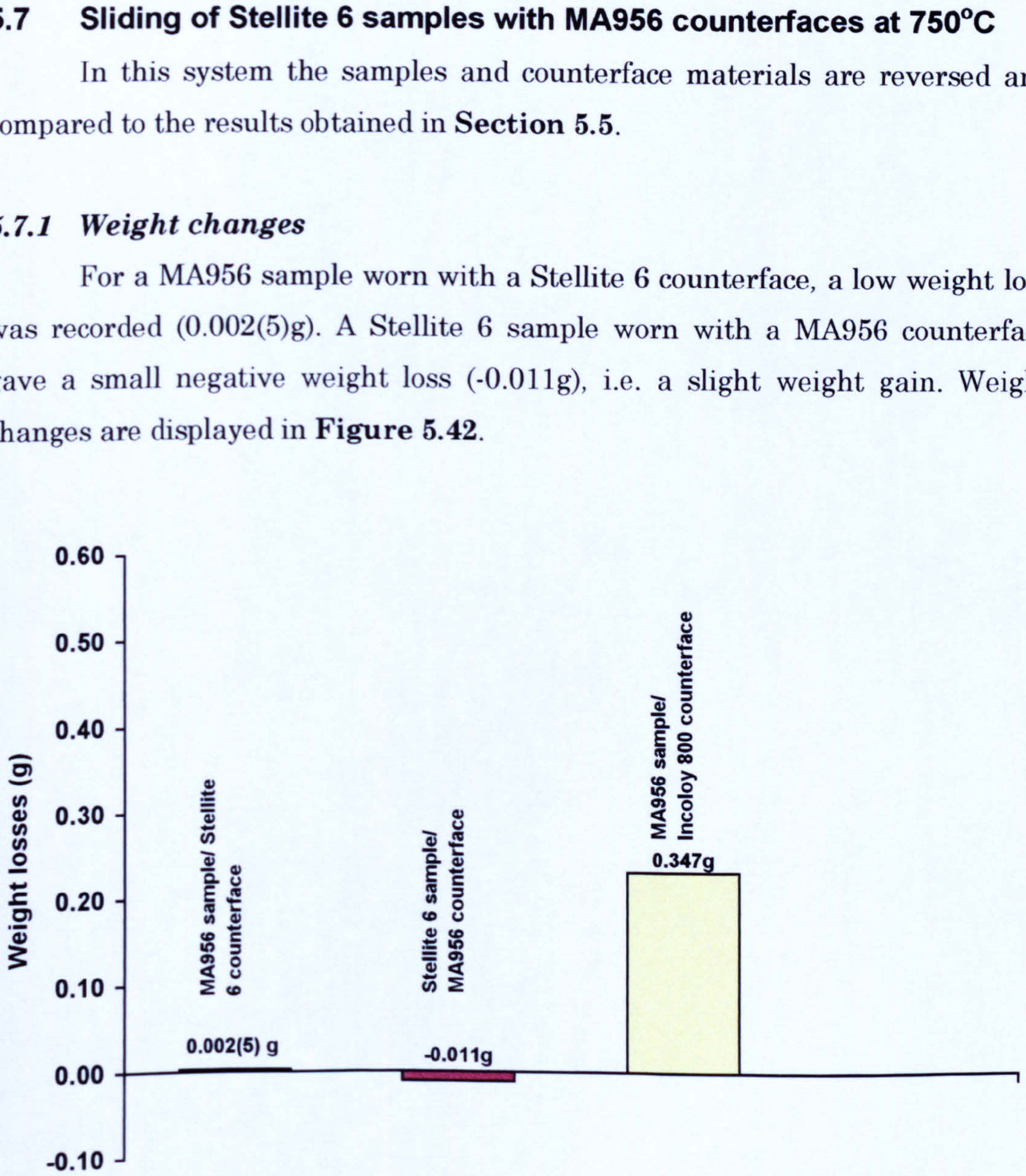

Figure 5.42 Weight losses for wear of the combinations of MA956 as a sample counterface worn with Stellite 6 and Incoloy 800 as counterfaces and sample, at 7N load for 4 hours (Incoloy 800 sample worn with MA956 counterface omitted due to failure of the test)

5.7.2 Coefficients of friction

The coefficient of friction with time for MA956 and Stellite 6 worn with each other are shown in **Figure 5.43**. For the MA956 sample worn with a Stellite 6 counterface the coefficient of friction remained relatively unchanged over the length of the test (0.50 to 0.60). This tended to rise slightly over the duration of the test.

For a Stellite 6 sample worn with a MA956 counterface a short running-in time was observed where the friction fell from an initial value of 1.50 to a stable level of 0.40–0.50 over the first 20 minutes of the test.

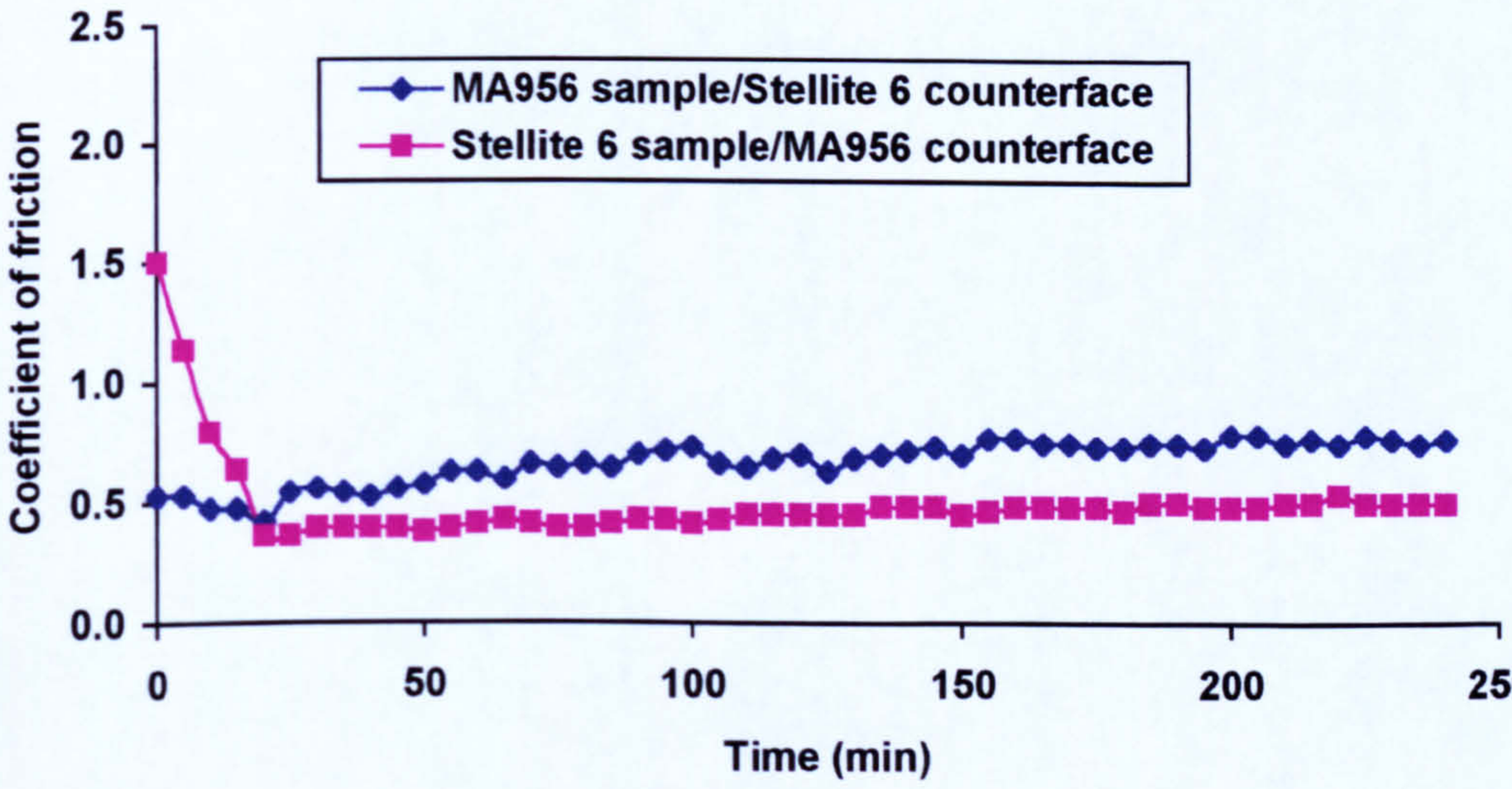

Figure 5.43 Coefficients of friction for MA956 and Stellite 6 as both sample and counterface at 750°C and 7N load

5.7.3 XRD analysis

Diffractograms of the wear scar on MA956 and Stellite 6 samples are displayed in **Figure 5.44** and **Figure 5.45** and the phases identified are shown in **Table 5.6**. For the MA956 sample worn with a Stellite 6 counterface the wear scar showed cobalt chromium oxides ($CoCr_2O_4$) phases on the MA956 substrate transferred from the counterface. Some iron chromium oxides ($Cr_{1.3}Fe_{0.7}O_3$) originating from the sample were also detected.

For a Stellite 6 sample worn with a MA956 counterface the wear scar revealed phases which correspond to the Stellite 6 substrate and transferred material from the counterface in the form of chromium oxide and iron oxide (Cr-O, Fe_2O_3).

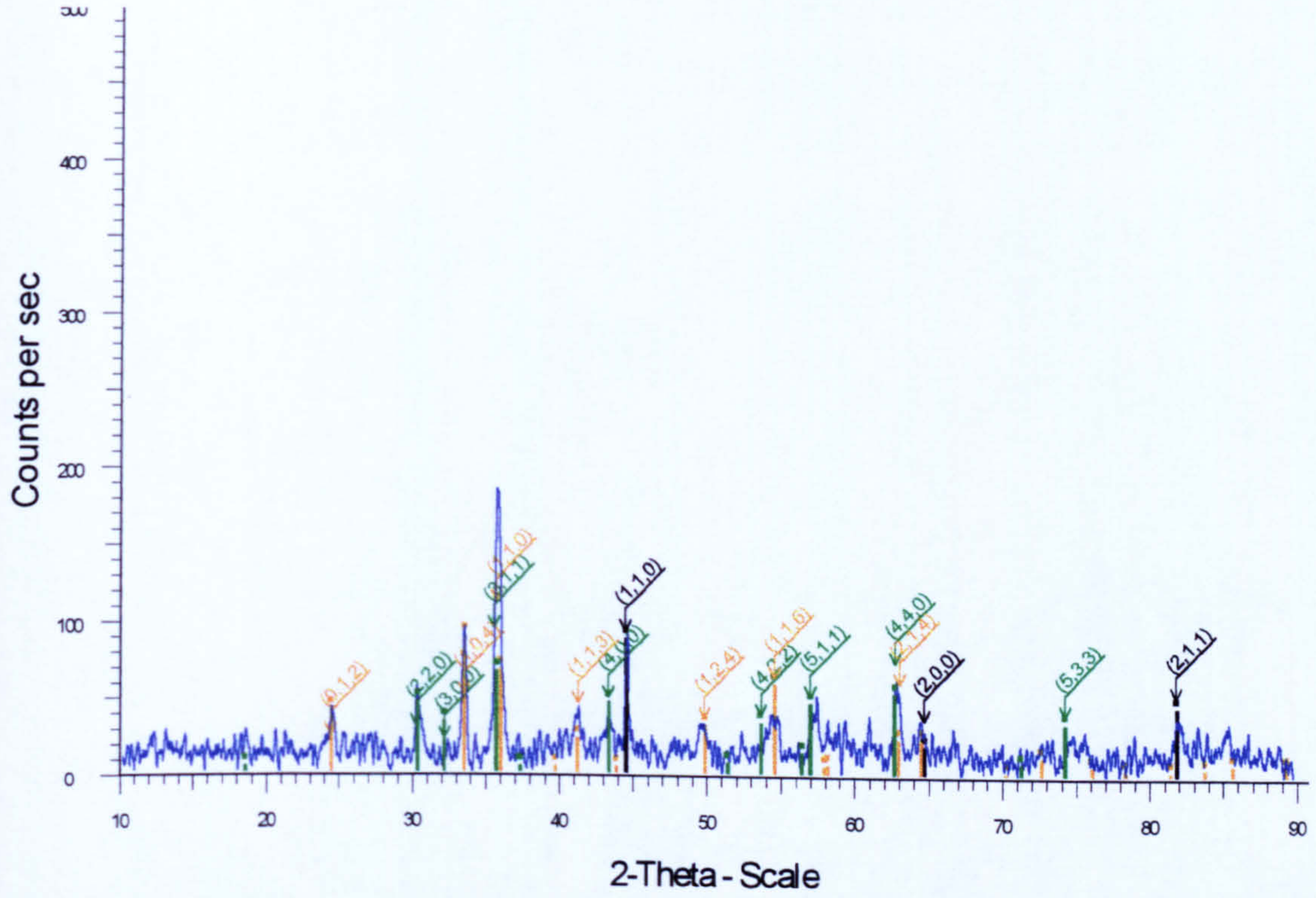

Figure 5.44 XRD data for MA956 worn with a Stellite 6 counterface at 750°C. Phases identified ▣ iron-chromium phase (Fe-Cr) (MA956), ▣ cobalt chromium oxide ($CoCr_2O_4$) and ▣ chromium iron oxide ($Cr_{1.3}Fe_{0.7}O_3$), at 7N load for 4 hours

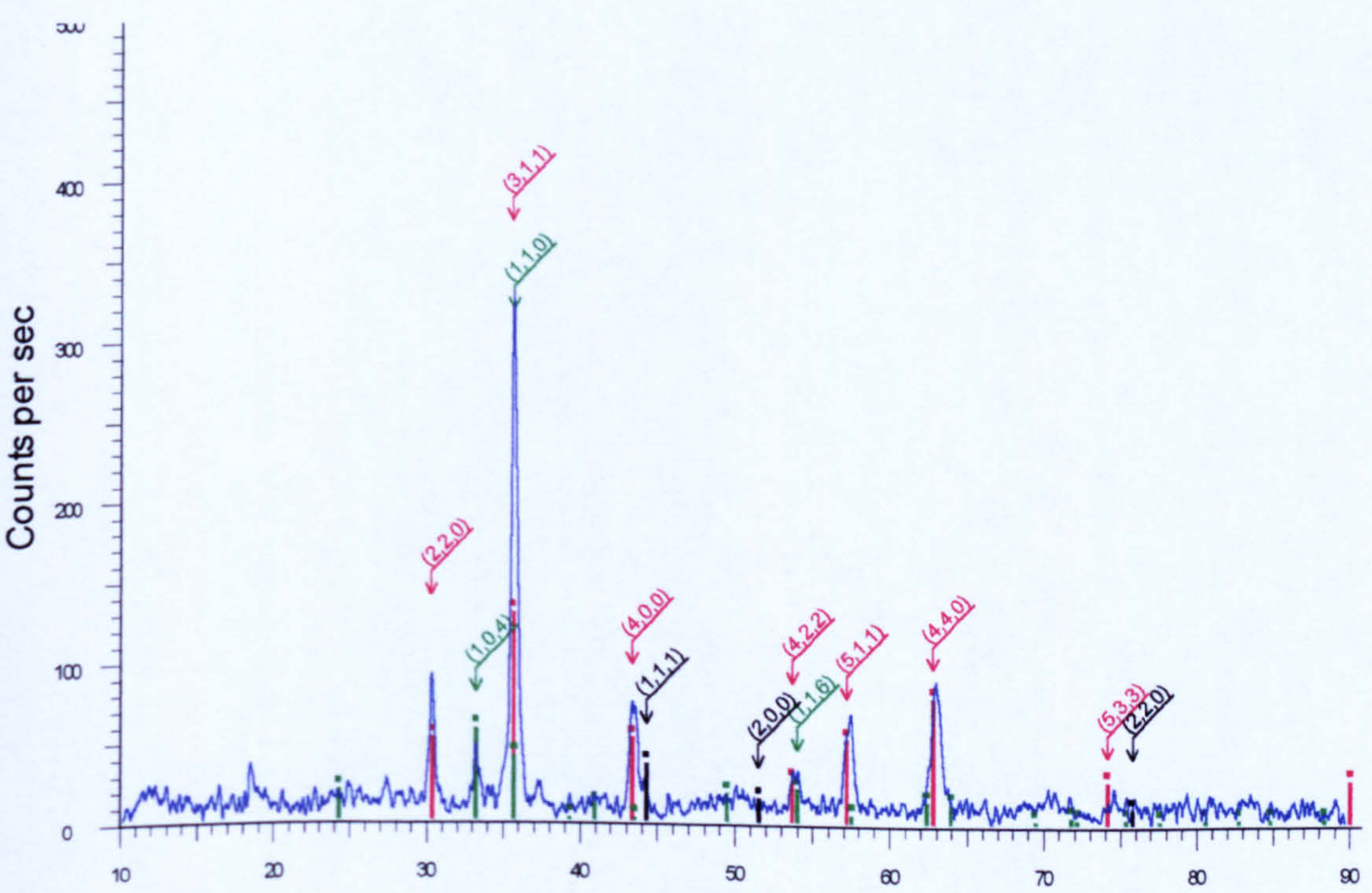

Figure 5.45 XRD data for Stellite 6 worn with a MA956 counterface at 750°C. Phases identified ▣ cobalt-chromium phase (Stellite 6), ▣ chromium oxide (Cr-O) and ▣ hematite (Fe_2O_3) for 4 hours at 7N load

MA956 worn with Stellite 6 counterfaces	
Phase identified	**Conditions identified / interpretation**
Iron-chromium stainless steel phase (Fe-Cr)	MA956 substrate
Cobalt chromium oxides ($CoCr_2O_4$)	Transferred from counterface
Iron chromium oxides ($Cr_{1.3}Fe_{0.7}O_3$)	Originating from sample
Stellite 6 worn with MA956 counterfaces	
Phase identified	**Conditions identified / interpretation**
Cobalt-chromium phase	Stellite 6 substrate
Chromium oxide (Cr-O)	Origin unclear
Iron oxide (Fe_2O_3)	Transferred from counterface

Table 5.6 XRD analysis of MA956 samples worn with Stellite 6 and Stellite 6 samples worn with MA956 at 750°C

5.7.4 SEM morphological analysis

Both combinations of sample and counterface produced compacted oxide layer-type surfaces. That produced upon the MA956 sample worn with a Stellite 6 counterface consisted of a very smooth layer covering almost the entire contact surface as shown in **Figure 5.46 (a)**. There were some areas where the 'glaze-type' layer was absent and fine wear particles had collected in surface hollows. In some areas spallation of the compacted oxide layer had also occurred (probably as a result of cooling).

For the Stellite 6 sample worn with an MA9456 counterface – shown in **Figure 5.46 (b)** – the compacted oxide layer shows evidence of spalling. It is however believed that the compacted oxide layer remained attached to the samples during its formation at the test temperature.

5.7.5 SEM/EDX cross-section analysis

Cross-sectional SEM/EDX element maps of the wear samples in both systems – MA956 worn with Stellite 6 counterface and Stellite 6 worn with MA956 counterface – are presented in **Figures 5.47** and **Figure 5.48** respectively. For the MA956 sample/Stellite 6 counterface the element maps show the presence of iron and aluminium from the sample, cobalt from the counterface and chromium from both sample and counterface.

For the Stellite 6 sample/MA956 counterface the element maps revealed that the compacted oxide layer was formed from oxide initially from the counterface.

5.7.6 Analysis of wear debris

The wear debris recovered from the tests with MA956 worn with Stellite 6 counterface and Stellite 6 worn with MA956 counterface are displayed in **Figure 5.46 (c)** and **(d)** respectively.

For MA956 worn with a Stellite 6 counterface, very little wear debris was generated. The debris generated consisted of a mixture of large particles (50 to 250μm) of MA956 and Stellite 6 material and of finer fragments (1 to 5μm) which were often clumped together, consisting of Stellite 6 material.

For the Stellite 6 worn with an MA956 counterface the wear particles produced were of two types. There were larger particles (50 to 500μm, 20 to 30μm thick) which were generated from the compacted oxide layer. Together with these, there was a large amount of very fine particles often aggregated together or attached to the surface of the larger particles. The wear debris originated predominately from the counterface, MA956.

5.7.7 Appearance of counterfaces

For a Stellite 6 counterface worn with a MA956 sample the wear track was almost entirely covered with compacted oxide 'glaze'-type material. Surrounding these 'glazes' were areas of fine black powder. The compacted oxide areas appeared raised from the sounded track, indicating that these were load-bearing. Hear the appearance of the counterface did not suggest that it had undergone excessive wear.

For the MA956 counterface worn with a Stellite 6 sample, the wear track was covered with a compacted oxide layer. Around these bright shiny areas of 'glaze' material, fine black powder was seen, although it was clear that the glaze areas were load-bearing. Fine grooves were seen upon the compacted oxide areas which appeared to run around the whole counterface – which shows that once established the sliding was smooth enough to allow such features to develop. The overall appearance of the counterface suggests that the wear of the counterface was relatively low.

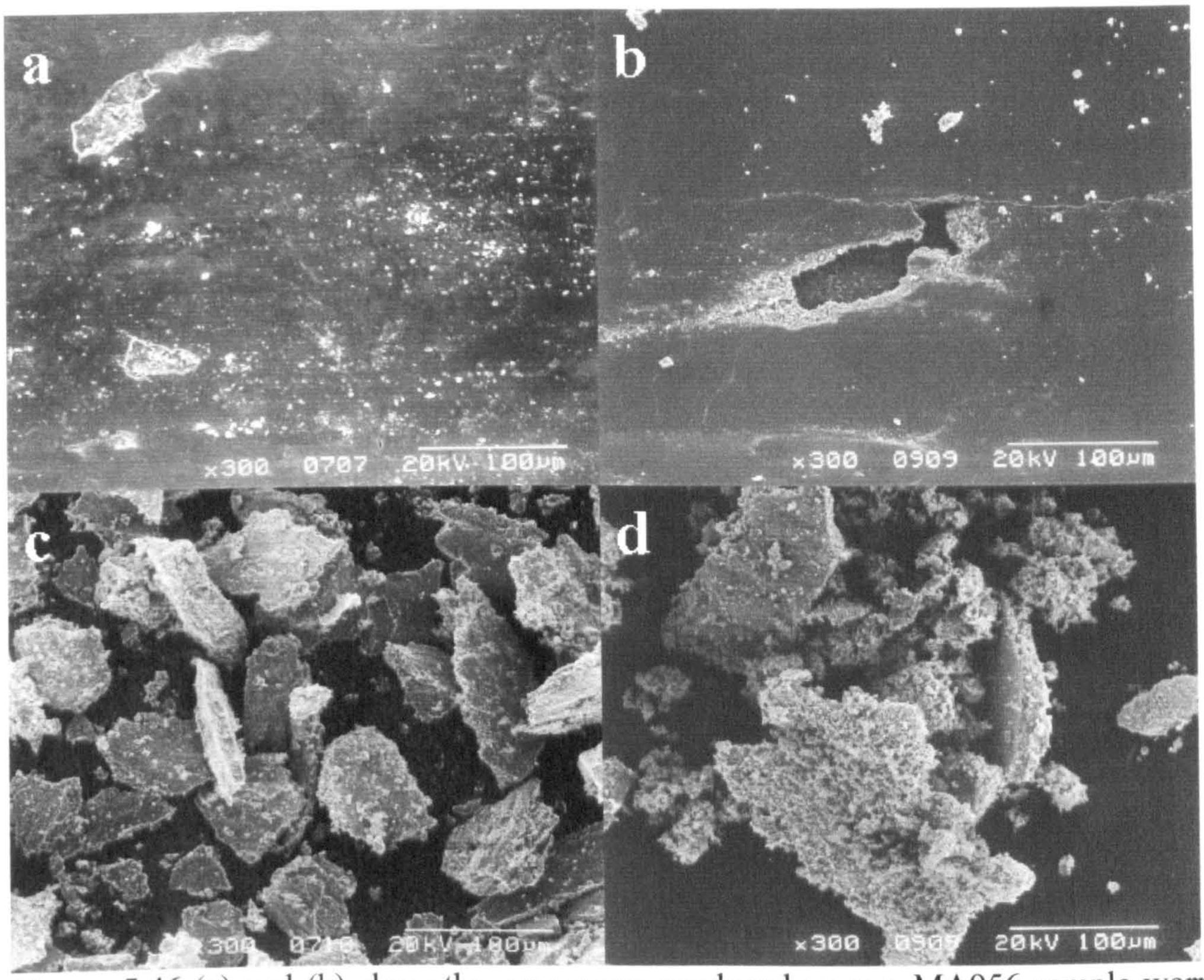

Figure 5.46 (a) and (b) show the wear scars produced upon a MA956 sample worn with a Stellite 6 counterface and the wear debris produced respectively. (c) and (d) show the wear scars produced upon a Stellite 6 sample worn with a MA956 counterface and the wear debris produced respectively, at 7N load for 4 hours

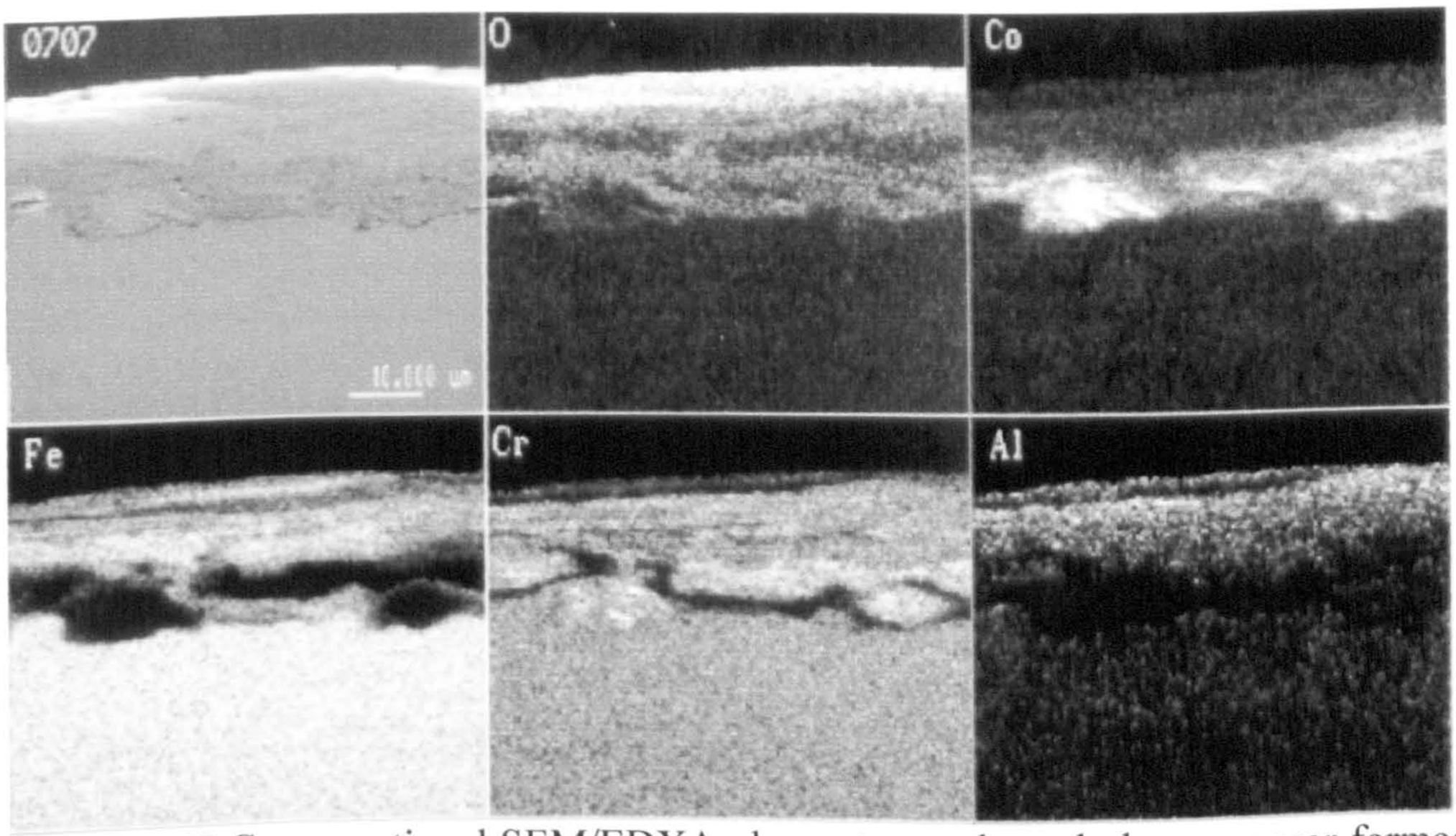

Figure 5.47 Cross-sectional SEM/EDXA element map through the wear scar formed upon MA956 worn with Stellite 6 at 750°C at 7N load for 4 hours

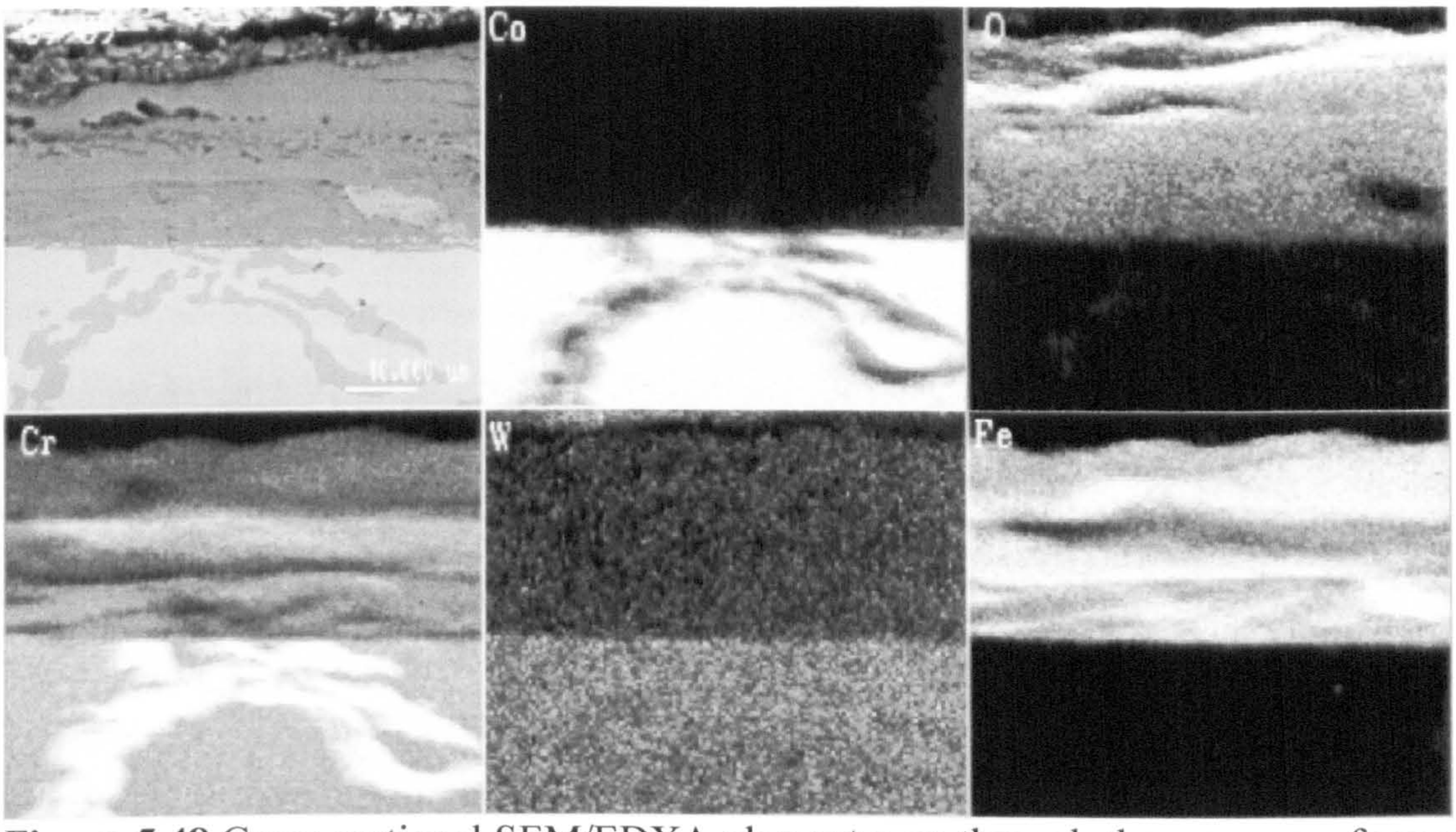

Figure 5.48 Cross-sectional SEM/EDXA element map through the wear scar formed upon Stellite 6 worn with MA956 at 750°C at 7N load for 4 hours

5.8 Sliding of Incoloy 800 samples with MA956 counterfaces at 750°C

5.8.1 Weight changes

For MA956 worn with an Incoloy 800 counterface, the weight loss was relatively high (0.232g) – **Figure 5.42**. However for the reversed system, Incoloy 800 sample/MA956 counterface, the wear rig did not permit the completion of the test due to the very high levels of friction produced.

5.8.2 Coefficients of friction

The coefficients of friction for MA956 and Incoloy 800 worn together are presented in **Figure 5.49**. The coefficient for friction for MA956 worn with an Incoloy 800 counterface starts at an initial value of 0.66, which rises to a maximum of 0.88 after 20 minutes. The coefficient then fell to a steady value of 0.40–0.45 which remains constant for the rest of the test.

For Incoloy 800 worn with a MA956 counterface, the coefficient of friction recorded up to the time of failure of the test shows the friction rapidly rises from an initial value of 1.59 to 1.86 after 10 minutes – at this point the wear rig was unable to cope with the forces acting upon it and the test failed.

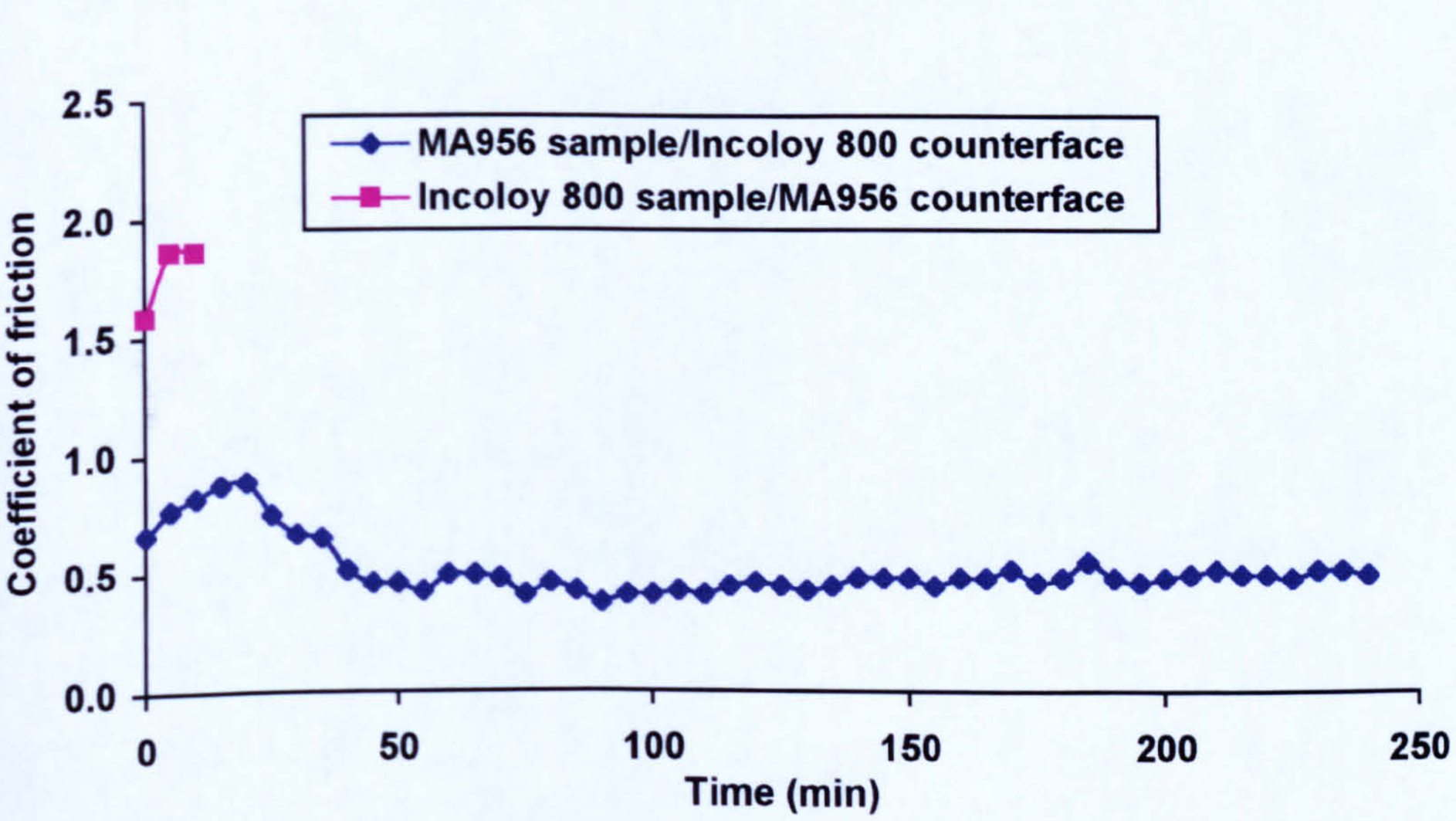

Figure 5.49 Coefficients of friction for MA956 and Incoloy 800 as both sample and counterface at 750°C at 7N load for 4 hours

5.8.3 XRD analysis

Diffractograms of the wear scars on MA956 and Incoloy 800 samples are displayed in **Figure 5.50** and **Figure 5.51** and the phases identified are shown

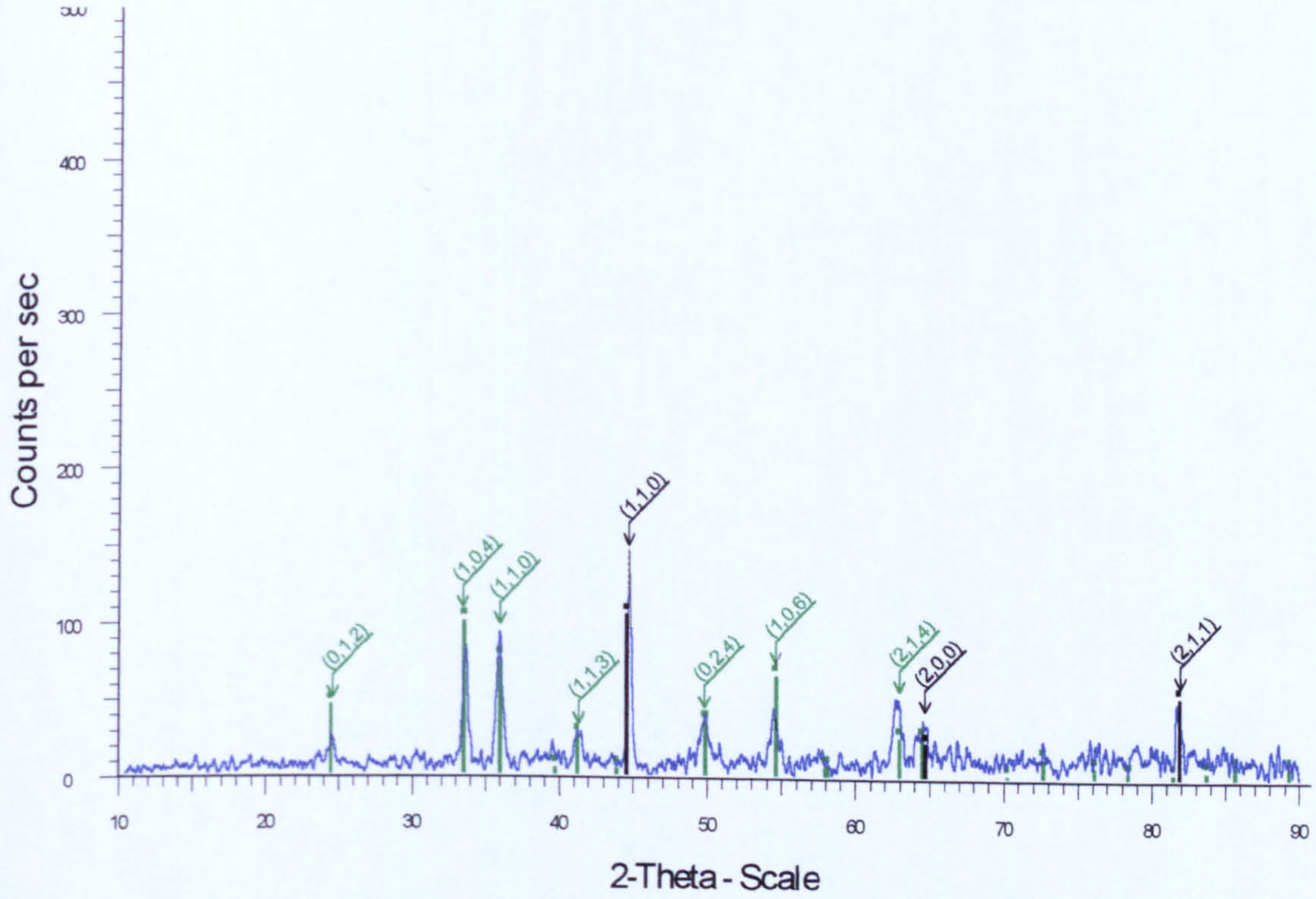

Figure 5.50 XRD data for MA956 worn with a Incoloy 800 counterface at 750°C. Phases identified ▣ iron-chromium phase (Fe-Cr) (MA956) and ▣ chromium iron oxide ($Cr_{1.3}Fe_{0.7}O_3$) at 7N load for 4 hours

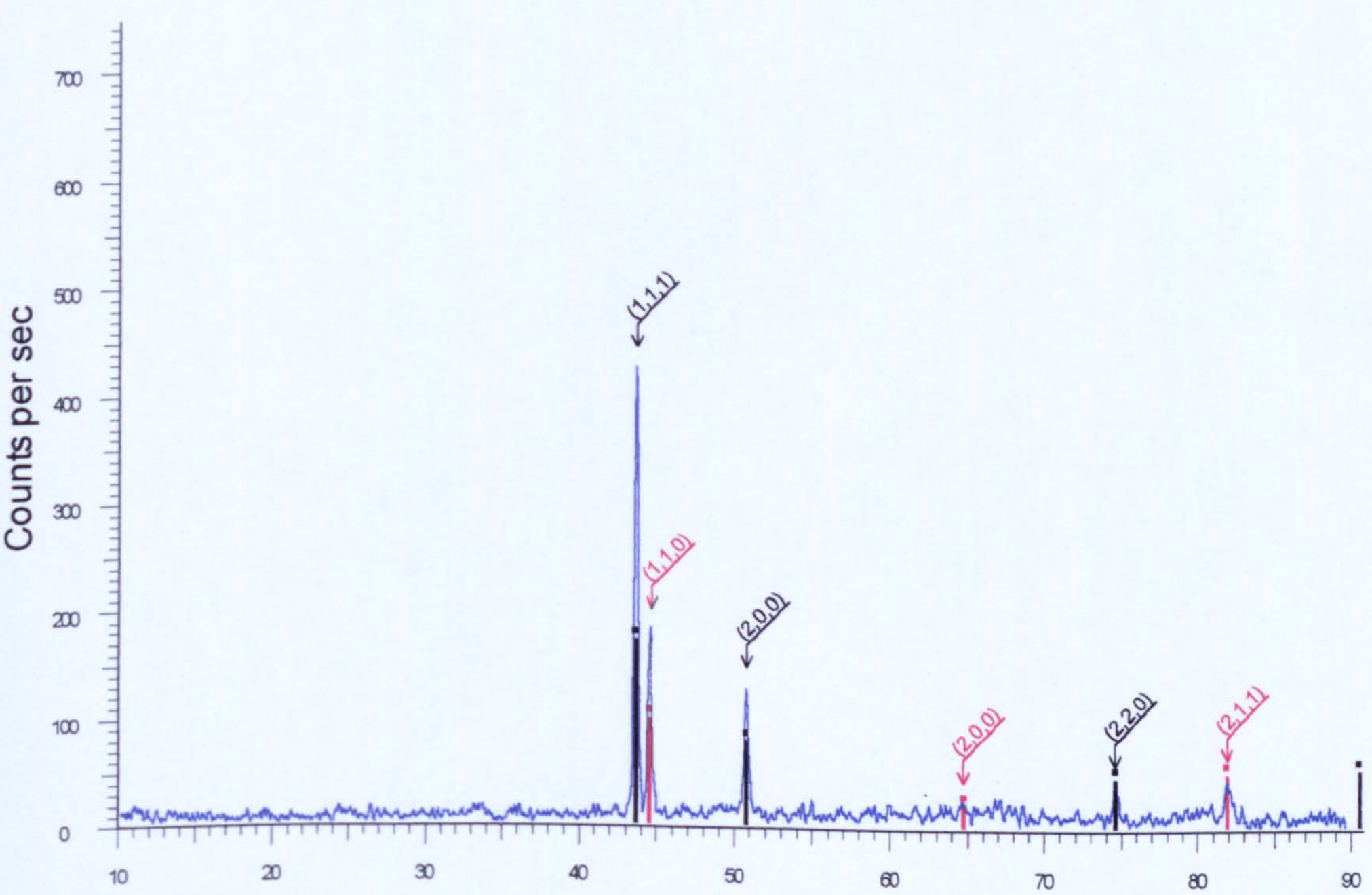

Figure 5.51 XRD data for Incoloy 800 worn with a MA956 counterface at 750°C. Phases identified ▣ iron chromium nickel phase (Cr -Fe-Ni) (Incoloy 800) and ▣ iron-chromium phase (Fe-Cr) (transferred MA956) at 7N load for 4 hours

in **Table 5.7**. The MA956 sample worn with Incoloy 800 system shows iron-chromium phases corresponding to the MA956 substrate and chromium iron oxide ($Cr_{1.3}Fe_{0.7}O_3$) only.

For the Incoloy 800 sample worn with a MA956 counterface (which failed after 15 to 20 minutes) the diffractograms show iron-chromium-nickel phases revealing the presence of the Incoloy 800 samples and a marked amount of transferred MA956 material. Here no oxides were detected on the wear scar.

MA956 worn with Incoloy 800 counterfaces	
Phase identified	**Conditions identified / interpretation**
Iron-chromium stainless steel phase (Fe-Cr)	MA956 substrate
Chromium iron oxide ($Cr_{1.3}Fe_{0.7}O_3$)	Oxides produced from sample
Incoloy 800 worn with MA96 counterfaces	
Phase identified	**Conditions identified / interpretation**
Iron chromium nickel stainless steel phase (Cr -Fe-Ni)	Incoloy 800 substrate
Iron-chromium stainless steel phase (Fe-Cr)	MA956,transferred from counterface

Table 5.7 XRD analysis of MA956 samples worn with Incoloy 800 and Incoloy 800 samples worn with MA956 at 750°C

5.8.4 SEM morphological analysis

Plan-view micrographs of the wear scars formed on MA956 worn with an Incoloy 800 counterface and Incoloy 800 worn with an MA956 counterface are shown in **Figure 5.52 (a)** and **(b)**.

For MA956 worn with an Incoloy 800 counterface the wear scar had the highly smooth surface characteristic of a compacted oxide layer. Some areas show a grooved appearance, these areas were covered with a large amount of fine wear debris. Closer examination of the scar reveals both areas of layer formation, characterised by fine agglomerating debris, and layer breakdown – cracking and break up of the layers – can be observed on the scar (not shown here).

The wear scar formed on Incoloy 800 worn with an MA956 counterface, up until the test failed, reveals a highly torn and deformed surface which appears to have undergone a great deal of adhesion and deformation. Some wear particles remain on the surface (10 to 20μm in size).

5.8.5 SEM/EDX cross-section analysis

Cross-sectional SEM/EDX element maps of the wear scars formed on a MA956 sample worn with an Incoloy 800 counterface – displayed in **Figure 5.53** – demonstrate that a compacted oxide layer had formed. This layer consisted of iron and chromium oxides with a small amount of aluminium and nickel. For an Incoloy 800 sample worn with a MA956 counterface no surface oxide layers were detected within the time of the test (approximately 20 minutes duration).

5.8.6 Analysis of wear debris

Micrographs of the wear debris collected from the two sliding couples are displayed in **Figure 5.52 (c)** and **(d)**. Wear debris collected from MA956 worn with an Incoloy 800 counterface shows large angular particles, many of which appear to be removed areas of compacted oxide layer. Other particles seem highly deformed, these were probably formed during metal-to-metal contact at the beginning of the test, these range in size from 50 to 250μm. Many of these larger fragments are covered in finer debris (1 to 5μm) – SEM/EDX analysis reveal that this wear debris to be comprised of both MA956 and Incoloy 800 material.

Wear debris collected from Incoloy 800 worn with the MA956 counterface – up to the time of failure – consisted of very large wear particles of size range 100 to 500μm or more. These particles are generally of the flat angular type and have a similar appearance to that of the wear scar. However, there are also particles present that have clearly been rolled within the interface. Their shape shows cylinders or balls of material that have clearly been produced after detachment from the surface by movement within the wearing interface.

5.8.7 Appearance of counterfaces

For an Incoloy 800 counterface worn with a MA956 sample, small islands of compacted oxide material were seen to be protruded through the large amount of fine black powder on the wear tracks' surface. Removing the 'third body' of black powder revealed a wear track characteristic of severe wear upon which the glaze areas had developed, surrounded by the fine debris.

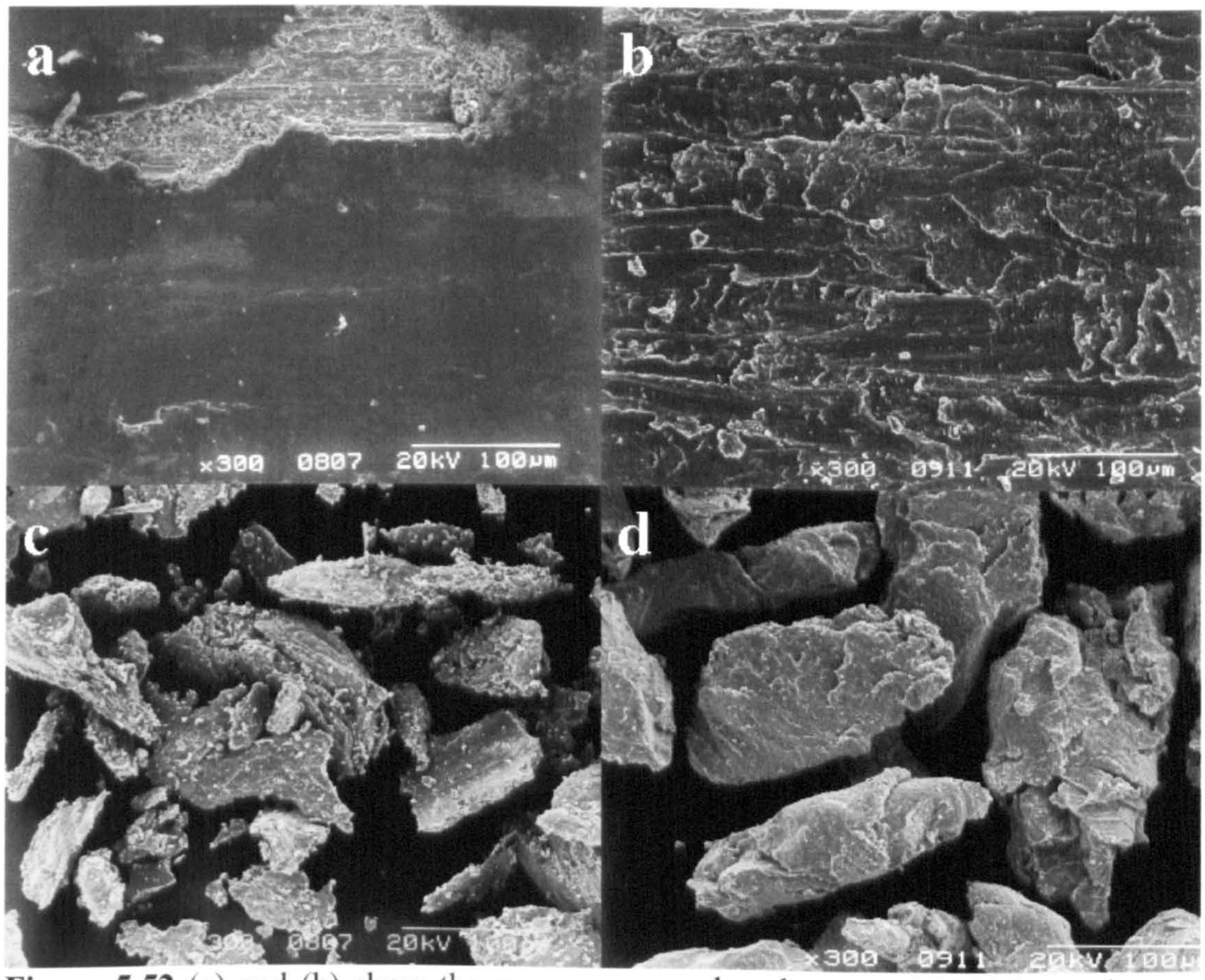

Figure 5.52 (a) and (b) show the wear scars produced upon a MA956 sample worn with a Incoloy 800 counterface and the wear debris produced respectively. (c) and (d) show the wear scars produced upon a Incoloy 800 sample worn with a MA956 counterface and the wear debris produced respectively, at 7N load for 4 hours

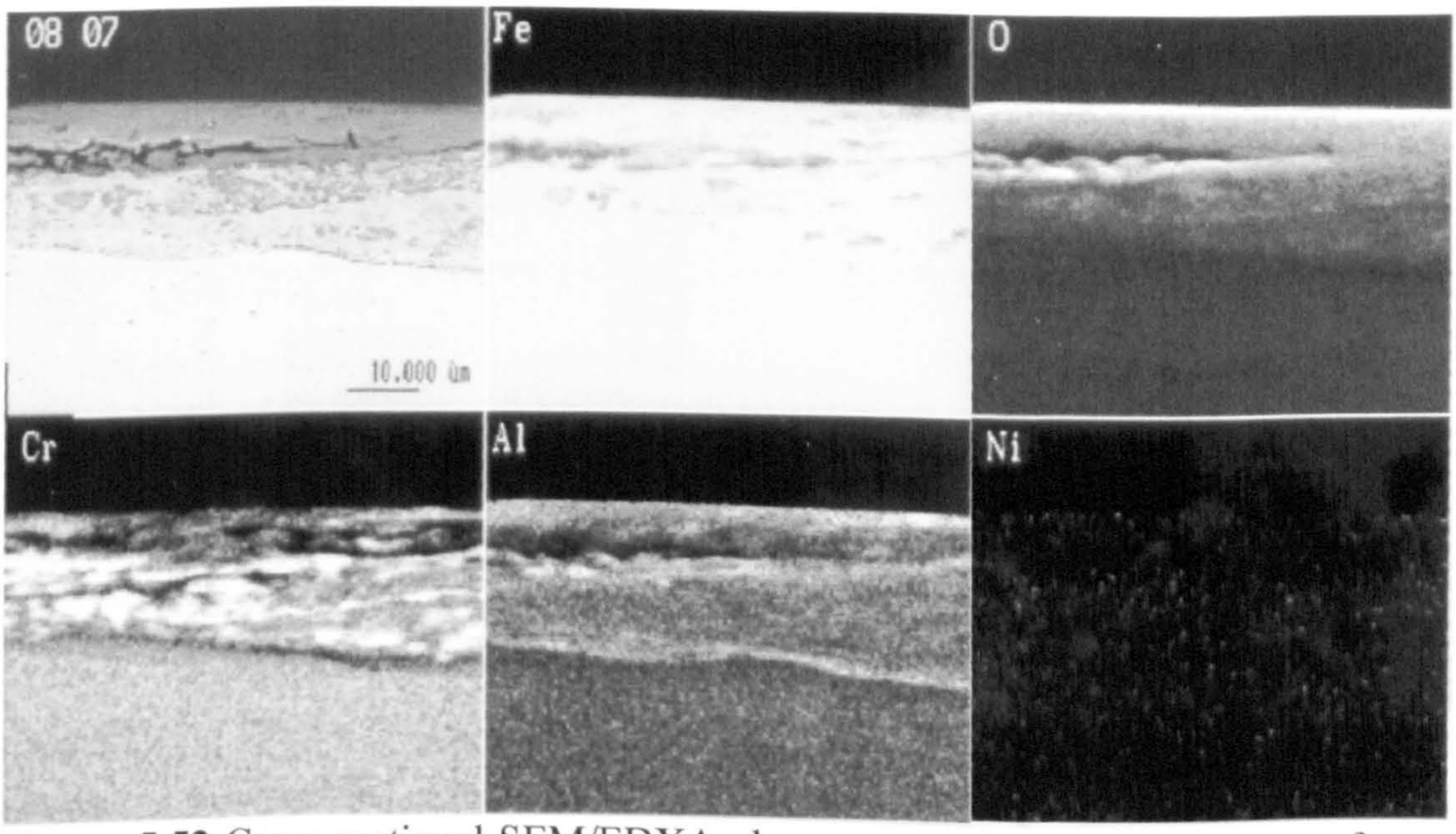

Figure 5.53 Cross-sectional SEM/EDXA element map though the wear scar formed upon MA956 worn with Incoloy 800 at 750°C at 7N load for 4 hours

For the MA956 counterface worn with an Incoloy 800 sample, the test was stopped to prevent damage to the rig after ~20 minutes. At his point the wear track was broader than the sample being around 6 to 7mm across, due to the high levels of vibration incurred in the test. Third-body type oxides were not seen on the track, which was highly torn and deformed in appearance. Some large fragments of material were present on the track which appear to have been transferred from the sample.

5.9 Sliding of Stellite 6 samples with Nimonic 80A counterface at 750°C

5.9.1 Weight changes

Nimonic 80A samples worn with a Stellite 6 counterface gave a moderately high weight loss (0.135g). Stellite 6 sample worn with a Nimonic 80A counterface underwent a small negative weight loss (-0.004g) (i.e. slight weight gain). Weight loss data are given in **Figure 5.54**.

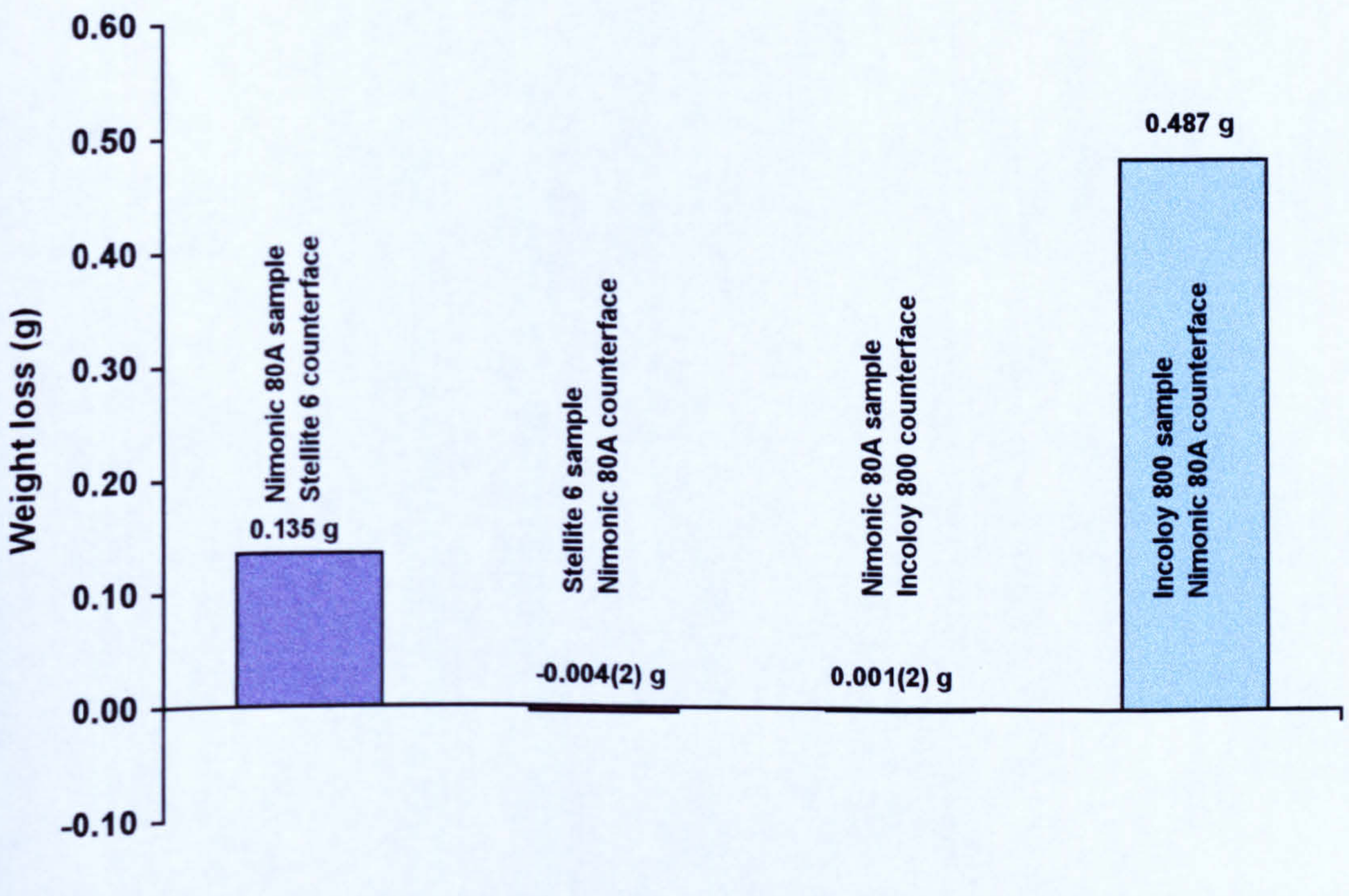

Figure 5.54 Weight losses for wear of the combinations of Nimonic 80A as a sample counterface worn with Stellite 6 and Incoloy 800 as counterfaces and samples at 750°C for 4 hours at 7N load

5.9.2 Coefficients of friction

The recorded coefficient of friction for Nimonic 80A worn with a Stellite 6 counterface and Stellite 6 worn with a Nimonic 80A counterface are shown in **Figure 5.55**. Both systems showed steady values of coefficient of friction between 0.40 to 0.50 within the first 10 minutes of the test. However the initial values differed – the initial values for the Nimonic 80A/Stellite 6 counterface was 0.47 while that for Stellite 6/Nimonic 80A was 0.88.

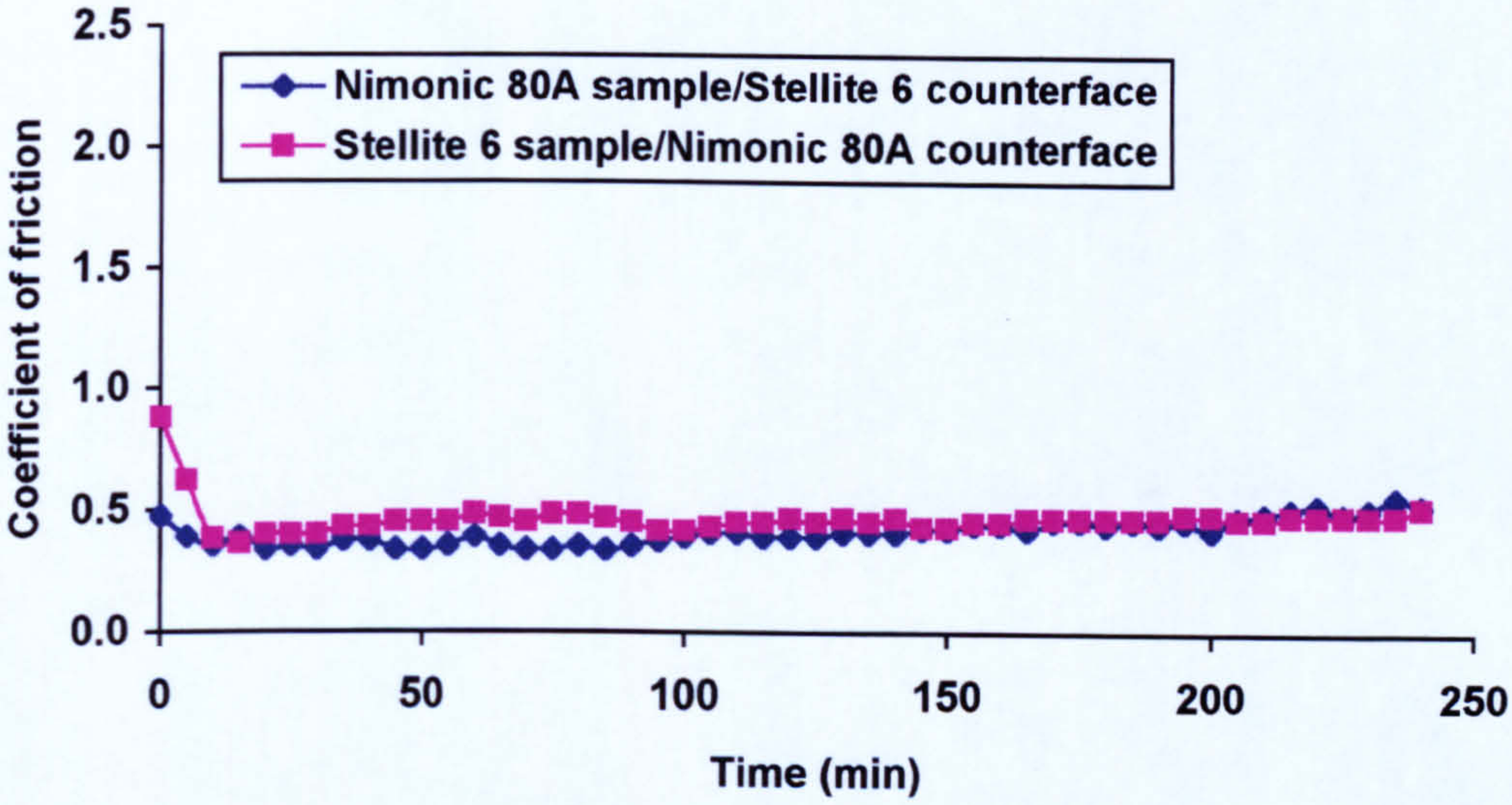

Figure 5.55 Coefficients of friction for Nimonic 80A and Stellite 6 as both sample and counterface at 750°C at 7N load

5.9.3 XRD analysis

Nimonic 80A worn with Stellite 6 counterfaces	
Phase identified	**Conditions identified / interpretation**
Iron chromium nickel phases ($Cr_{0.19}$ $Fe_{0.7}$ $Ni_{0.11}$)	Nimonic 80A substrate
Stellite 6 worn with Nimonic 80A counterfaces	
Phase identified	**Conditions identified / interpretation**
Cobalt-chromium phase	Stellite 6 substrate
Nickel oxide (NiO)	Oxides from Nimonic 80A (counterface)
Cochromite ($CoCr_2O_4$ / CoO Cr_2O_3)	Oxides from Stellite 6 (sample) Only small response

Table 5.8 XRD analysis of Nimonic 80A samples worn with Stellite 6 and Stellite 6 samples worn with Nimonic 80A at 750°C

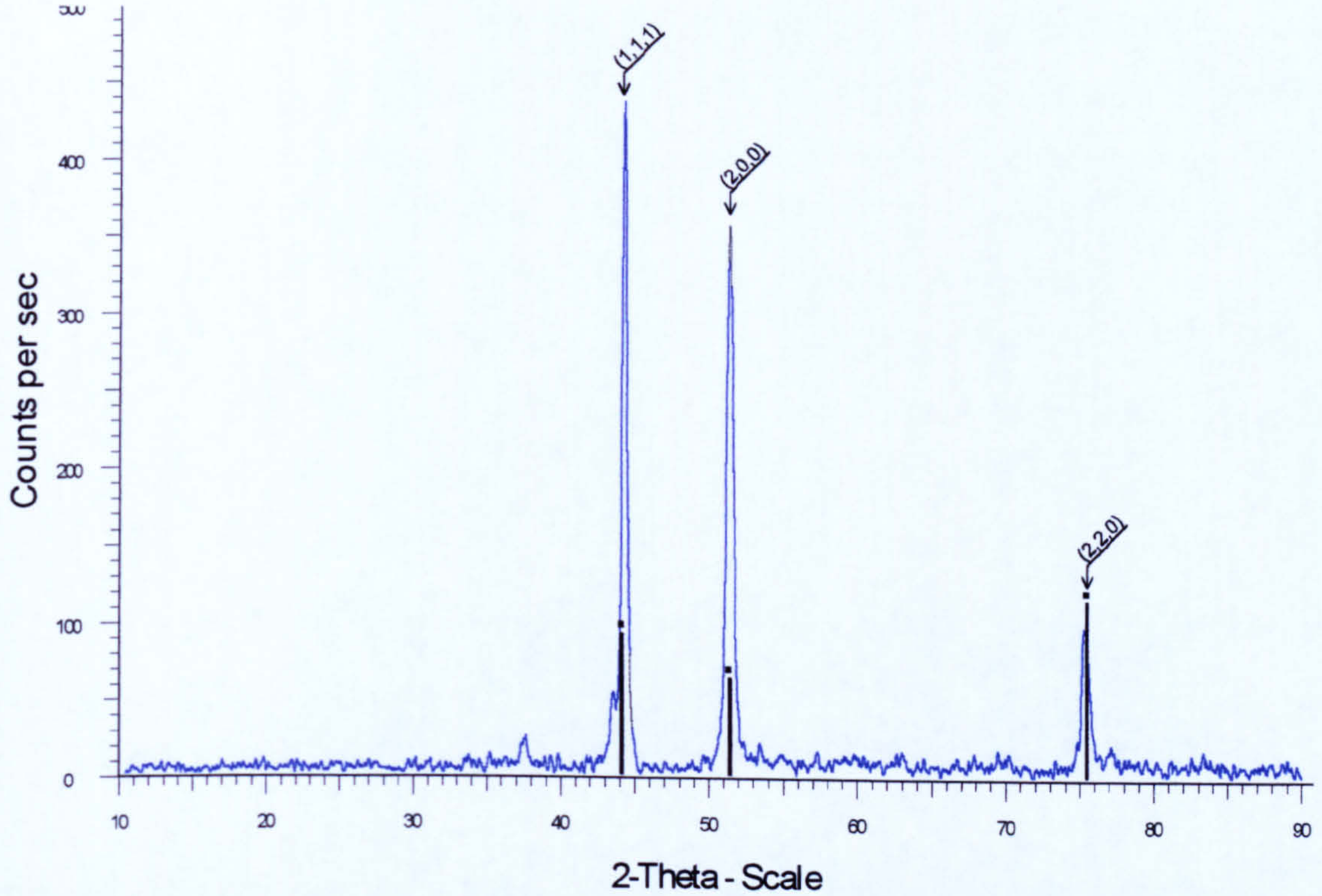

Figure 5.56 XRD data for Nimonic 80A worn with a Stellite 6 counterface at 750°C for 4 hours at 7N load. Phases identified ▣ iron chromium nickel phases ($Cr_{0.19}$ $Fe_{0.7}$ $Ni_{0.11}$) (Nimonic 80A)

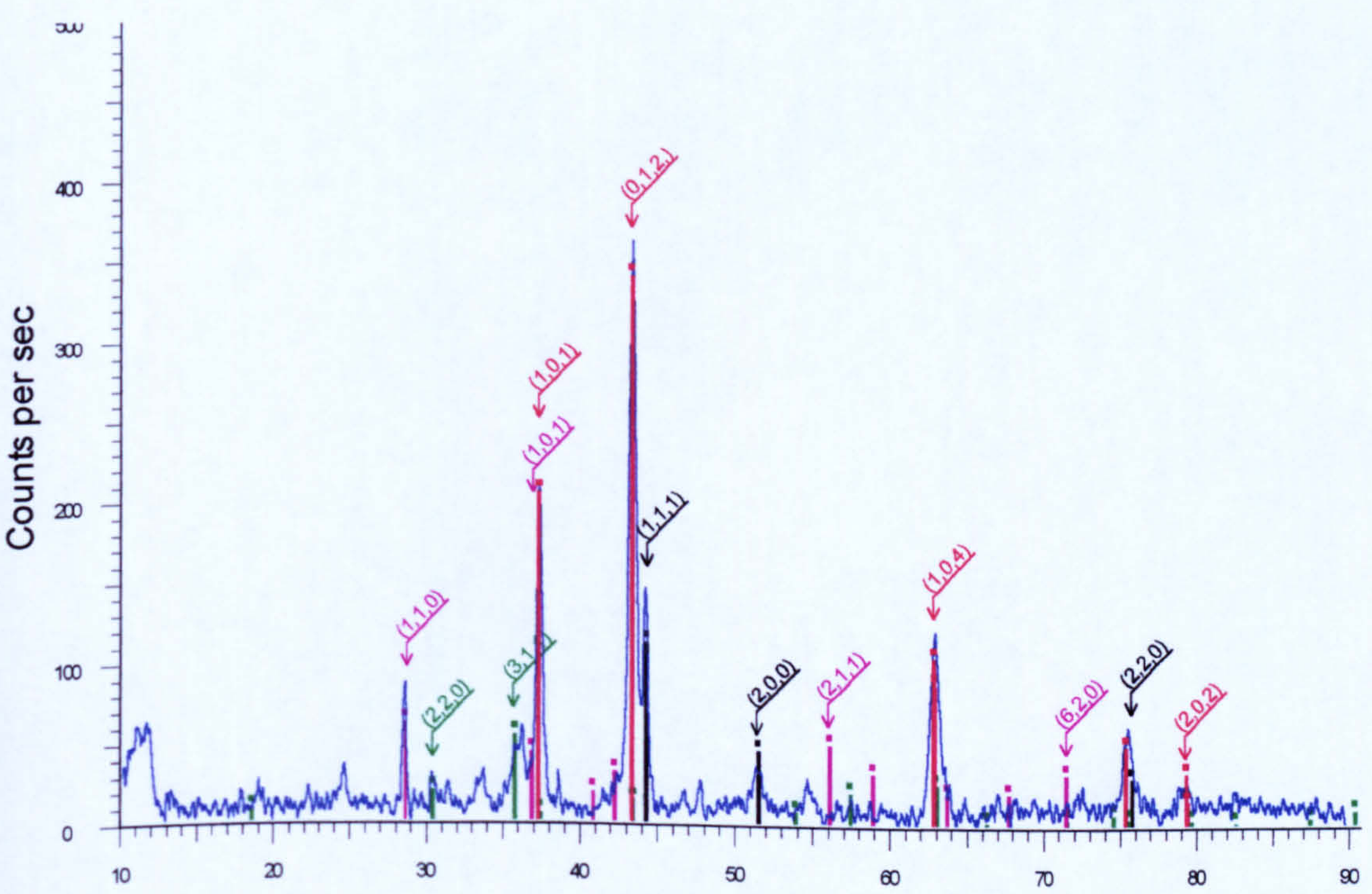

Figure 5.57 XRD data for Stellite 6 worn with a Nimonic 80A counterface at 750°C for 4 hours at 7N load. Phases identified ▣ cobalt-chromium (Stellite 6), ▣ nickel oxide (NiO), ▣ cochromite ($CoCr_2O_4/CoO{\cdot}Cr_2O_3$) and ▣ chromium oxide ($CrO_2$)

Diffractograms for Nimonic 80A and Stellite 6 samples are displayed in **Figure 5.56** and **Figure 5.57** and the phases identified are shown in **Table 5.8.** For Nimonic 80A worn with a Stellite 6 counterface the diffractogram showed only the presence of an iron chromium nickel phase, which corresponds to Nimonic 80A alloy. No oxides of transferred material were detected.

For Stellite 6 worn with a Nimonic 80A counterface the diffractogram revealed, together with a cobalt chromium phase characteristic of the Stellite 6 alloy, the presence of nickel oxide and chromium oxide from the counterface (NiO, CrO_2) and the cobalt/chromium oxides from the sample ($CoCr_2O_4$ / CoO Cr_2O_3).

5.9.4 SEM morphological analysis

SEM micrographs of the wear scars on the surface of Nimonic 80A worn with Stellite 6 and Stellite 6 worn with Nimonic 80A are displayed in **Figures 5.58 (a)** and **(b)** respectively.

The wear scar on the Nimonic 80A sample worn with a Stellite 6 counterface appears worn and grooved. There are large numbers of fine (1 to 5μm) particles on the surface which had accumulated in surface depressions and hollows. In places these particles are bonded although they do not appear as a fully compacted oxide layer.

The Stellite 6 sample worn with Nimonic 80A counterface has a large amount of debris at the surface. Other areas appear to have formed more substantial compacted particle layers, despite the layer seeming to have suffered from repeated breakdown and failure.

5.9.5 SEM/EDX cross-section analysis

Cross-sectional ESM/EDX element maps of Nimonic 80A worn with a Stellite 6 counterface revealed no oxide layers (not shown here). Stellite 6 worn with a Nimonic 80A counterface, presented in **Figures 5.59**, exhibits the presence of a typical surface layer, consisting of nickel and chromium oxides. These layers were present only in limited areas of the scar.

5.9.6 Analysis of wear debris

Wear debris recovered from Nimonic 80A worn with a Stellite 6 counterface – shown in **Figure 5.58 (c)** – consisted of fine debris (1 to 5μm) which tended to agglomerate and of some larger particles (25 to 100μm). These

larger particles were flat and angular in appearance and some could be seen to be removed fragments of the wear scar or track. SEM/EDX analysis demonstrated the particles to consist of both Stellite 6 and Nimonic 80A material.

Wear debris recovered from the Stellite 6 sample worn with a Nimonic 80A counterface – displayed in **Figure 5.58 (d)** – consists of fine wear debris particles (1 to 5μm). These fine debris were coalesced as larger particles, which were interspersed with larger 'solid' fragments some clearly parts of removed compacted oxide layer. These larger particles were covered with finer particles adhering to their surfaces – SEM/EDX analysis of these particles showed them to be formed of nickel and chromium with traces of aluminium and titanium, which corresponds to Nimonic 80A. No cobalt was detected indicating the debris to be Nimonic 80A material.

5.9.7 Appearance of counterfaces

For the Stellite 6 counterface worn with a Nimonic 80A sample the wear track was relatively smooth but having a grooved appearance. Some fine green debris was present upon the surface although this was not a compacted oxide layer, not having the characteristic glaze appearance. Material loss and damage did not seen great.

For the Nimonic 80A counterface worn with a Stellite 6 sample, the wear track was, again, similar in appearance to the scar found on the sample. Most of the scar was covered with semi-compacted fine green powder, in some areas this appeared to have been further compacted to form a 'true' compacted oxide 'glaze' layer, having the distinctive bright shiny surface. The overall level of damage to the counterface suggested that weight losses from the counterface were relatively low.

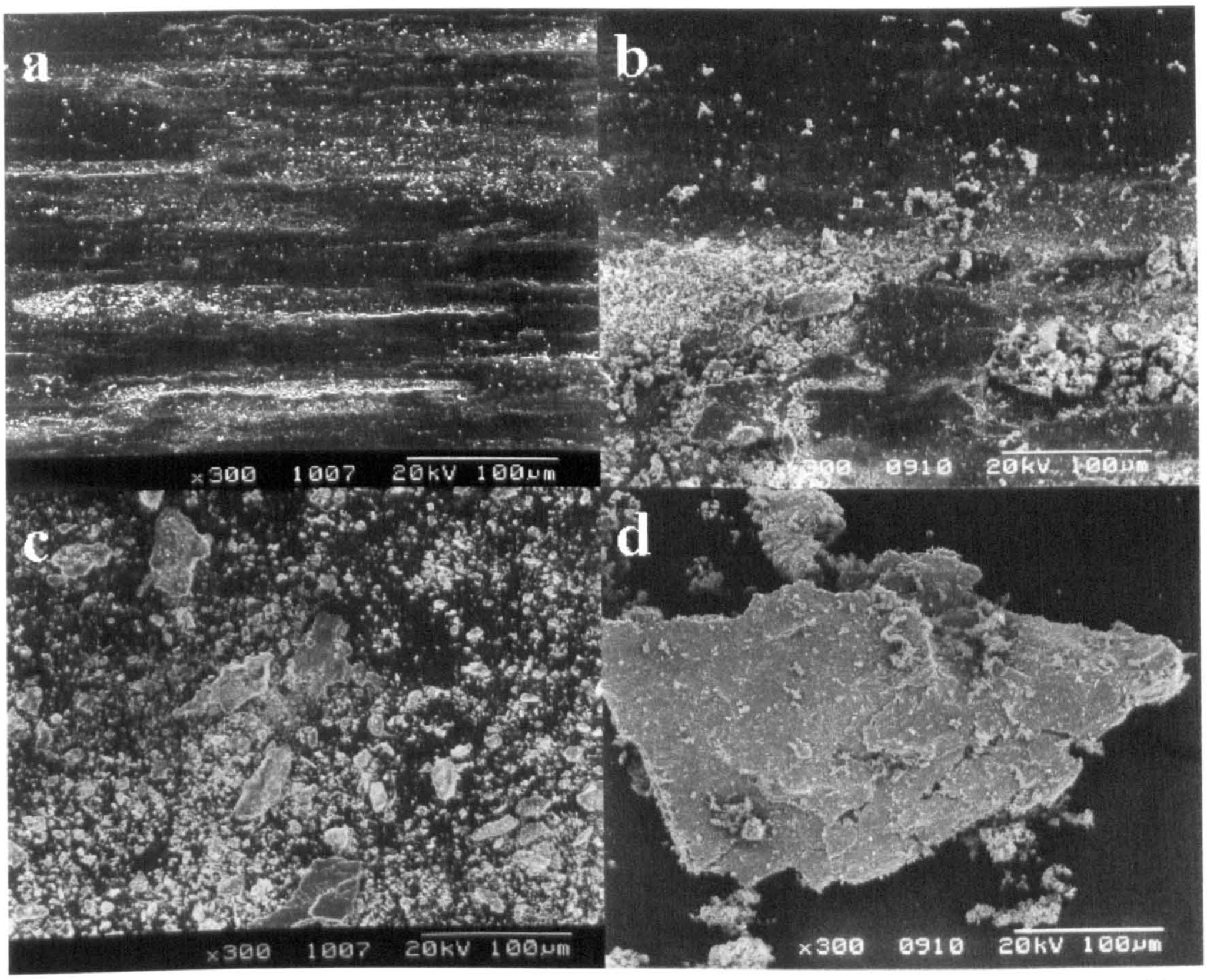

Figure 5.58 (a) and (b) wear scars produced on a Nimonic 80A sample worn with a Stellite 6 counterface and the wear debris produced respectively. (c) and (d) show the wear scars produced on a Stellite 6 sample worn with a Nimonic 80A counterface and the wear debris produced respectively. At 750°C for 4 hours at 7N load

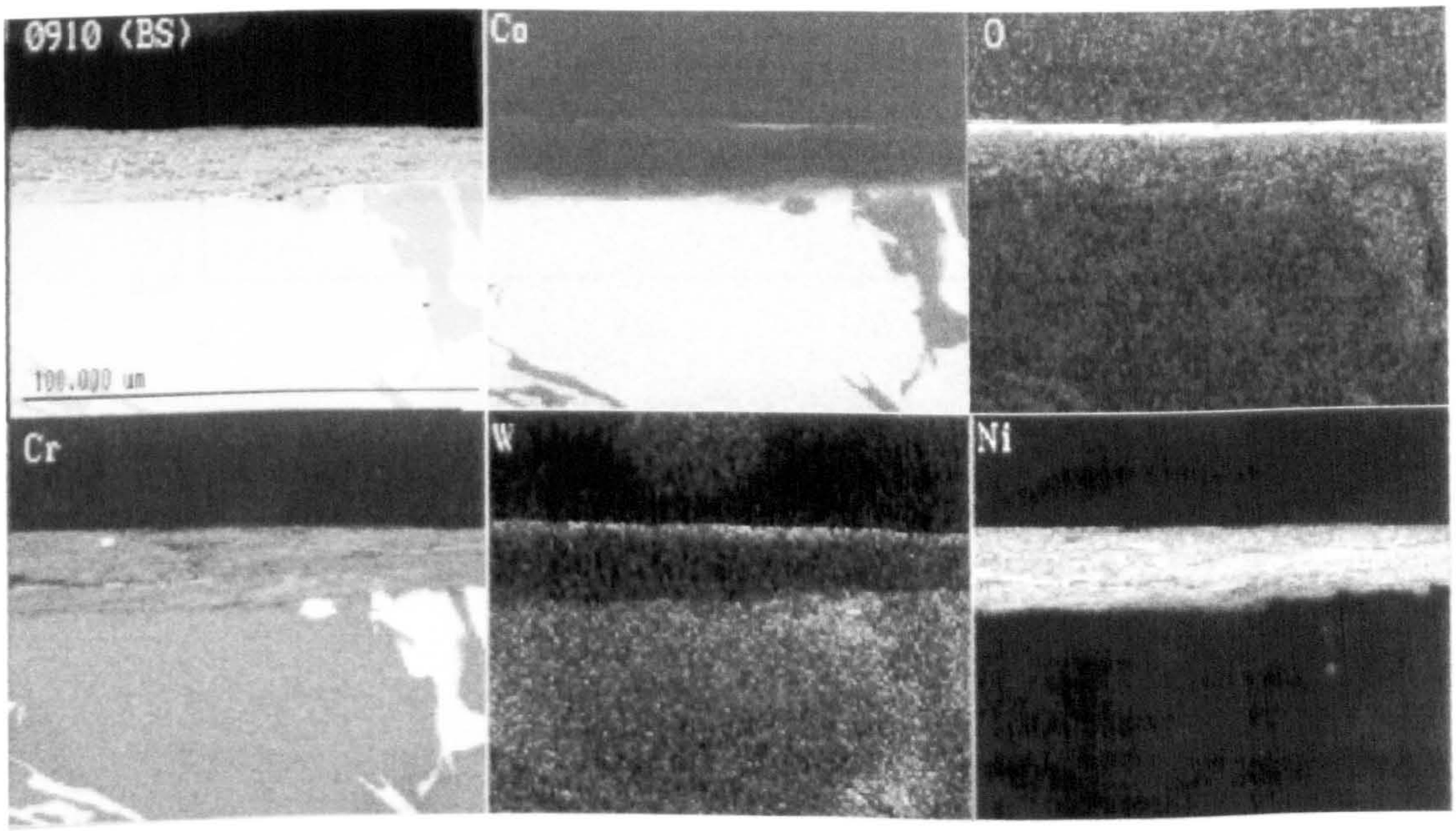

Figure 5.59 Cross-sectional SEM/EDX element map through the wear scar formed on Stellite 6 worn with Nimonic 80A at 750°C for 4 hours at 7N load

5.10 Sliding of Incoloy 800 sample with Nimonic 80A counterface at 750°C

5.10.1 Weight changes

For Nimonic 80A worn with an Incoloy 800 counterface at 750°C the weight change was low, a small negative weight loss (-0.001(2)g) (i.e. small weight gain). For Incoloy 800 worn with a Nimonic 80A counterface a large weigh loss was recorded (0.487g). Weight loss data are presented in **Figure 5.54**.

5.10.2 Coefficients of friction

Both Nimonic 80A and Incoloy 800 samples worn with their respective counterfaces showed similar behaviour in terms of coefficient of friction. The coefficient of friction fell from an initial value of approximately 1.10 to stable values of around 0.40. These stable values were achieved after 25 to 30 minutes and remained constant for the rest of the test. Coefficient of friction data are displayed in **Figure 5.60**.

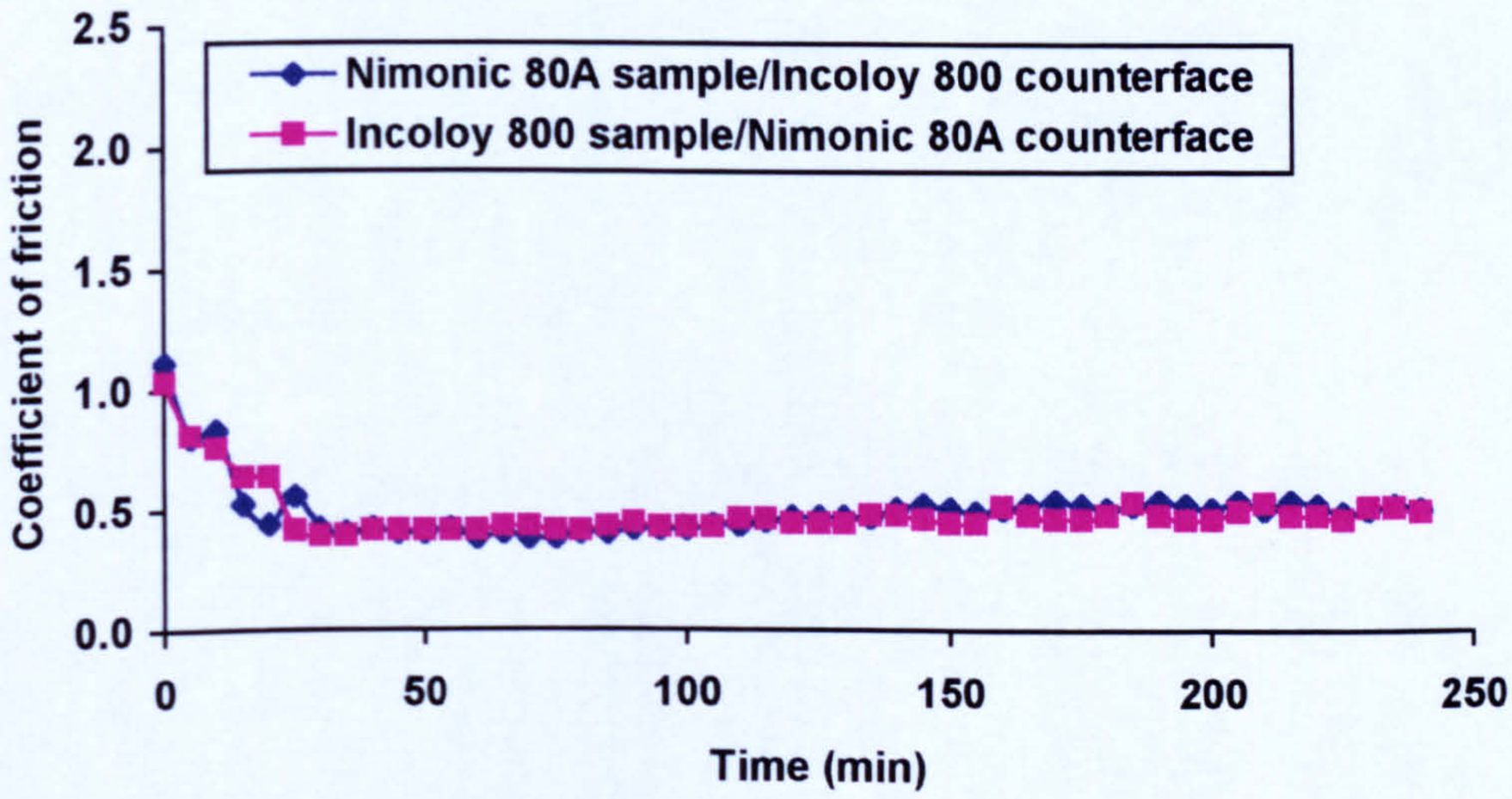

Figure 5.60 Coefficients of friction for Nimonic 80A and Incoloy 800 as both sample and counterface at 750°C and 7N load

5.10.3 XRD analysis

Diffractograms of Nimonic 80A and Incoloy 800 samples are presented in **Figure 5.61** and **Figure 5.62** and the phases identified are listed in **Table 5.9**. The scar on Nimonic 80A shows iron-chromium-nickel phase revealing the presence of Nimonic 80A, nickel chromium oxide ($NiCr_2O_4$) and a small amount of transferred Incoloy 800.

The wear scar formed upon Incoloy 800 worn with Nimonic 80A gave iron-chromium-nickel phases corresponding to the Incoloy 800 substrate and nickel chromium oxide ($NiCr_2O_4$).

Nimonic 80A won with Incoloy 800 counterfaces	
Phase identified	**Conditions identified / interpretation**
Iron chromium nickel phases ($Cr_{0.19}$ $Fe_{0.7}$ $Ni_{0.11}$)	Nimonic 80A substrate
Iron chromium nickel phase (Cr-Fe-Ni)	Transferred Incoloy 800
Nichromite ($NiCr_2O_4$)	
Incoloy 800 worn with Nimonic 80A counterfaces	
Phase identified	**Conditions identified / interpretation**
Iron chromium nickel phase (Cr -Fe-Ni)	Incoloy 800 substrate
Nichromite ($NiCr_2O_4$)	

Table 5.9 XRD analysis of Nimonic 80A samples worn with Incoloy 800 and Incoloy 800 samples worn with Nimonic 80A at 750°C

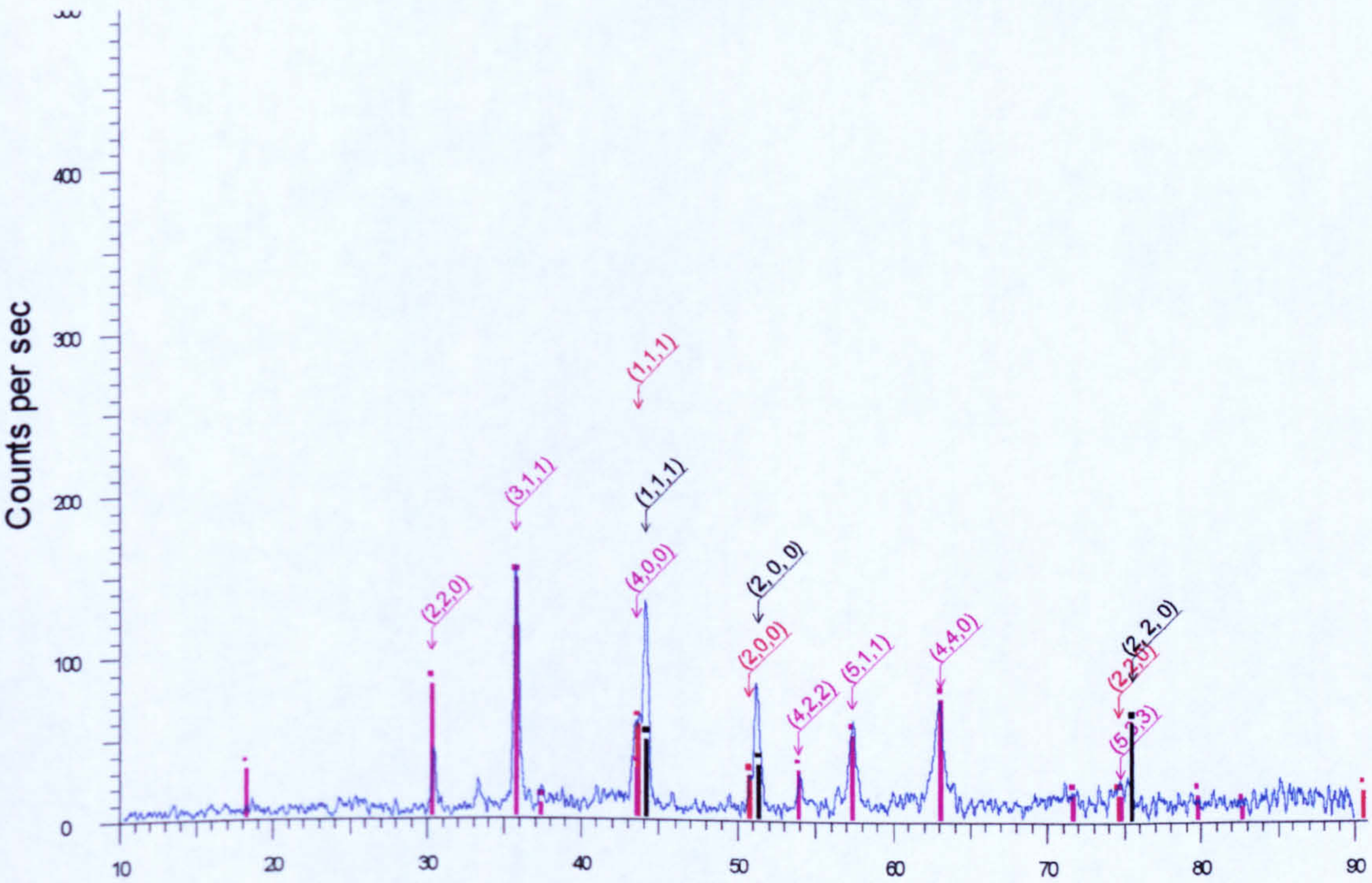

Figure 5.61 XRD data for Nimonic 80A worn with an Incoloy 800 counterface for 4 hours at 750°C and 7N load. Phases identified ▣ iron chromium nickel phases ($Cr_{0.19}$ $Fe_{0.7}$ $Ni_{0.11}$) (Nimonic 80A), ▣ iron chromium nickel phase (Cr-Fe-Ni) (transferred Incoloy 800) and ▣ nichromite ($NiCr_2O_4$)

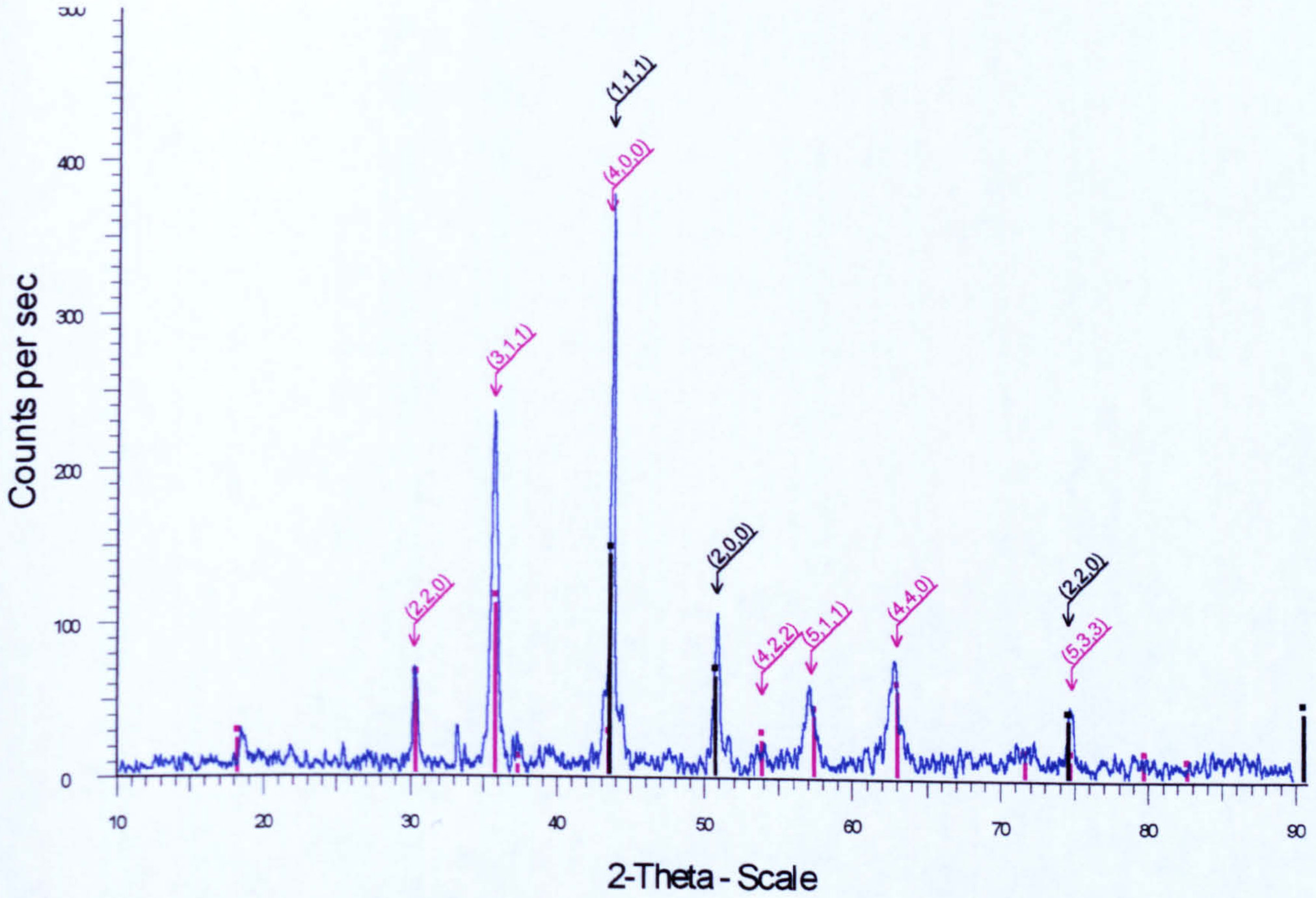

Figure 5.62 XRD data for Incoloy 800 worn with a Nimonic 80A counterface for 4 hours at 750°C and 7N load. Phases identified ▣ iron chromium nickel phase (Cr-Fe-Ni) (Incoloy 800) and ▣ nichromite ($NiCr_2O_4$)

5.10.4 SEM morphological analysis

Plan-view micrographs of the surface of Nimonic 80A worn with Incoloy 800 are shown in **Figure 5.63 (a)**. This reveals a smooth surface characteristic of a compacted oxide layer covering most of the wear scar. In places, development of compacted surfaces took place layer by layer. There are also loose particles on the surface caught in depressions and hollows.

Micrographs of the surface of Incoloy 800 worn with a Nimonic 80A counterface are presented in **Figure 5.63 (b)**. The scar here had the smooth surface characteristic of a compacted oxide layer. A large amount of loose debris was also present at the surface (more than was seen for Nimonic 80A worn with an Incoloy 800 counterface). Again this debris is caught within depressions upon the surface.

5.10.5 SEM/EDX cross-section analysis

Cross-sectional SEM/EDX element maps of the wear scars on Nimonic 80A and Incoloy 800 are shown in **Figure 5.64** and **Figure 5.65** respectively. For Nimonic 80A worn with an Incoloy 800 counterface a thick compacted oxide layer is seen upon the wear scar's surface. Cross-sectional mapping of the scar reveals

a single layer consisting of iron, chromium and nickel oxides that relates to transfer of Incoloy 800 material.

SEM/EDX cross-sectional element maps of the wear scar formed on Nimonic 80A worn with an Incoloy 800 counterface indicate a thin and patchy compacted oxide layer which consists of iron, chromium and nickel oxides. The presence of iron suggests that material was transferred from the counterface.

5.10.6 Analysis of wear debris

The wear debris recovered from Nimonic 80A worn with an Incoloy 800 counterface is displayed in **Figure 5.63 (c)**. The debris consisted of flat, angular type debris, most of which was in the size range 50 to 550μm. However there were also some very large particles, up to 1mm in length. Some fine particles were observed adhering to the larger debris. SEM/EDX analysis showed the wear debris to consist of iron, chromium and nickel suggesting that the most of the debris was formed from Incoloy 800.

Wear debris recovered from Incoloy 800 worn with an Nimonic 80A counterface is given in **Figure 5.63 (d)** The debris consisted of particles of a wide range of sizes (25 to 100μm). The larger particles are flat and angular in shape and covered with many smaller debris fragments (1 to 10μm). SEM/EDX indicated the debris to consist of iron, nickel and chromium, suggesting that the majority of debris is comprised of Incoloy 800 material (the nickel content of the particles being consistently lower than Nimonic 80A).

5.10.7 Appearance of counterfaces

The Incoloy 800 counterface worn with a Nimonic 80A sample showed 'islands' of compacted oxide material surrounded by fine debris attached to the counterface's surface. When the fine black powder was removed the underlying surface was highly damaged which strongly suggested that a severe wear mechanism had operated before the oxide layers had become established. It would appear that the counterface was severely damage and significant material loss had occurred before the establishment of the compacted oxide layer.

With the Nimonic 80A counterface worn with an Incoloy 800 sample, again a thick layer of black powder was present upon the wear track. Protruding through this 'third-body' were 'islands' of compacted oxide material. When the loose material was removed the underlying surface was grooved and highly worn, suggesting that significant material loss had taken place from the counterface.

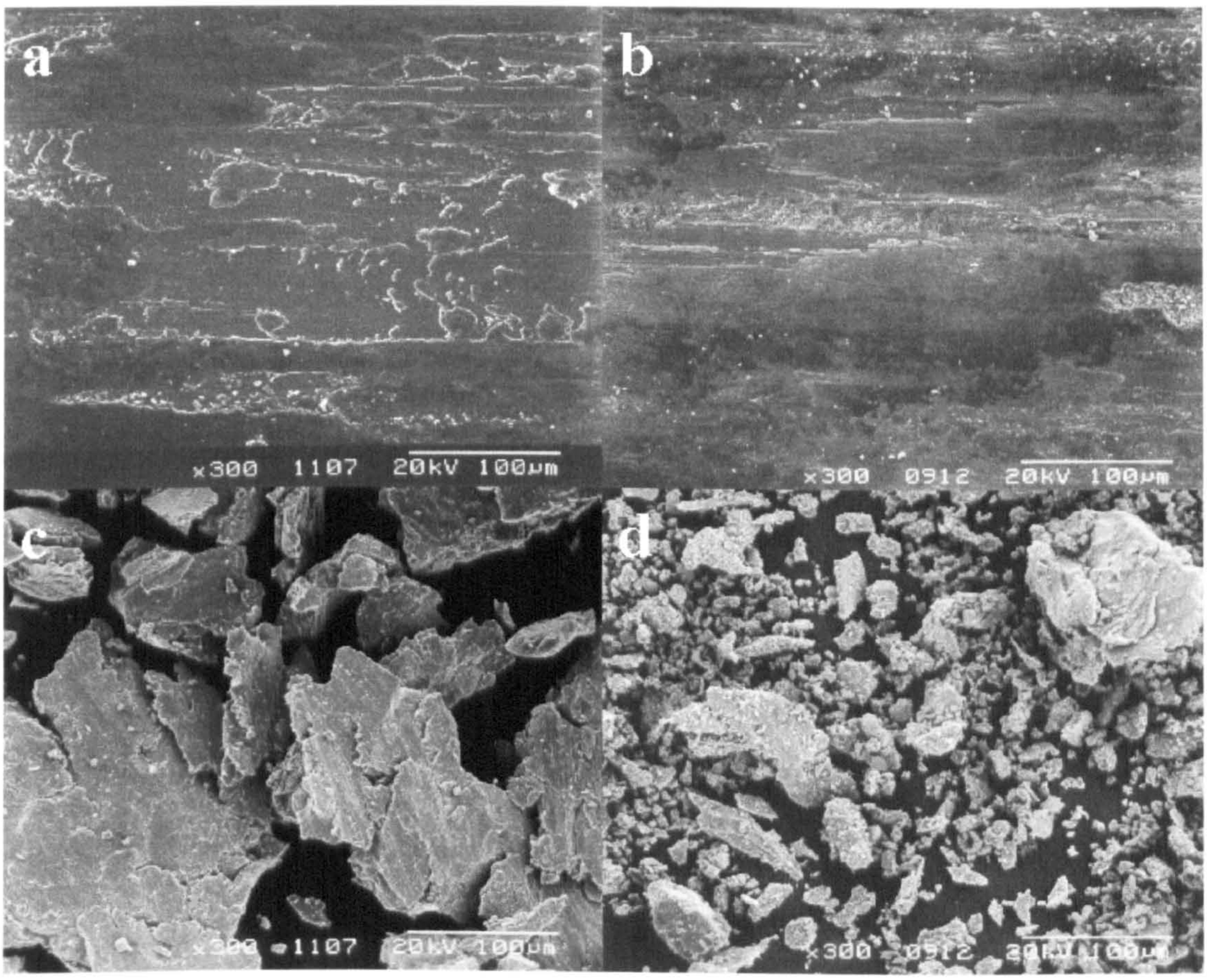

Figure 5.63 (a) and (b) show the wear scars produced on a Nimonic 80A sample worn with an Incoloy 800 counterface and the wear debris produced respectively for 4 hours at 750°C and 7N load. (c) and (d) show the wear scars produced on an Incoloy 800 sample worn with a Nimonic 80A counterface and the wear debris produced respectively

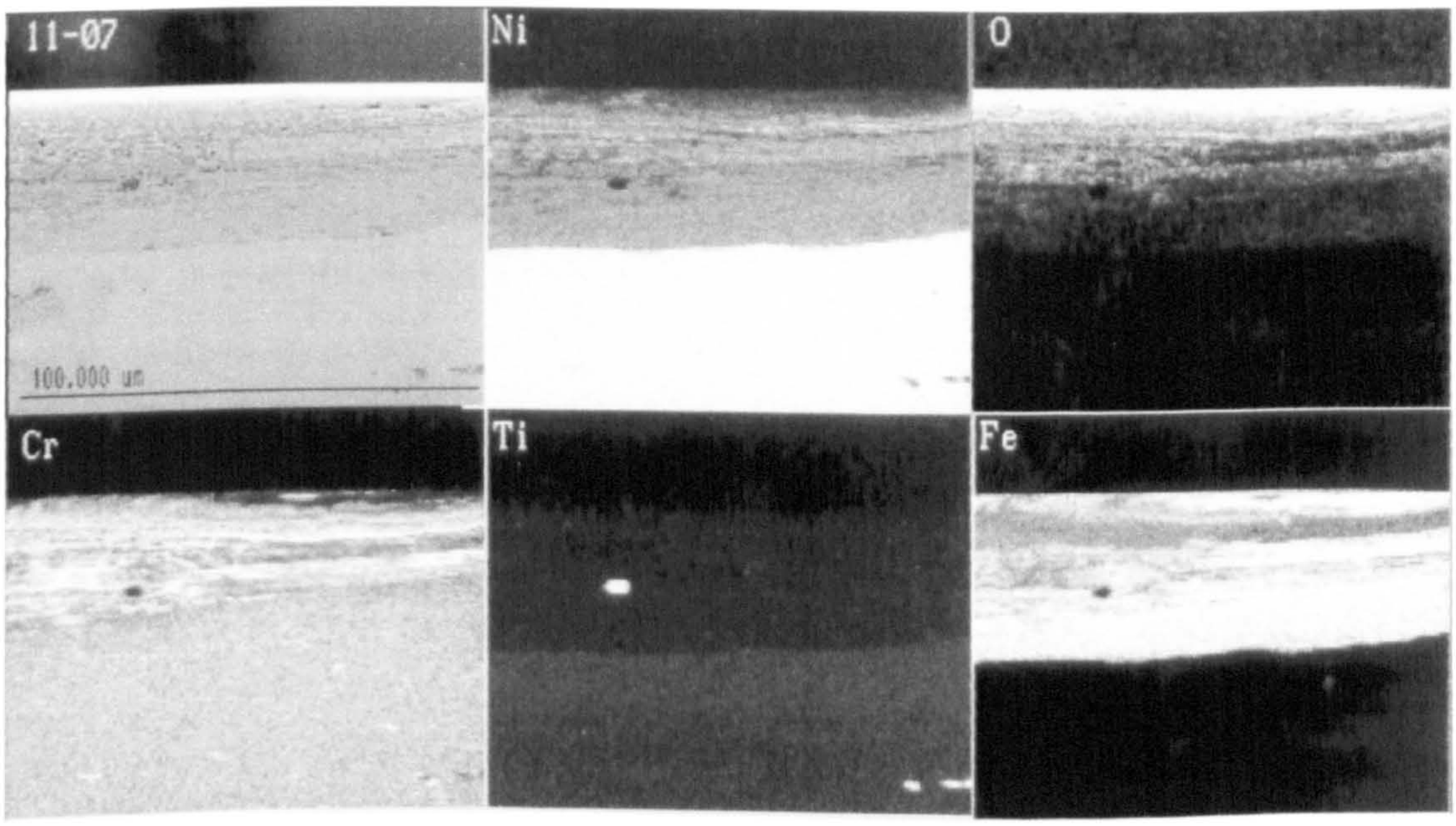

Figure 5.64 Cross-sectional SEM/EDX element map through the wear scar formed on Nimonic 80A worn with Incoloy 800 at 750°C and 7N load for 4 hours

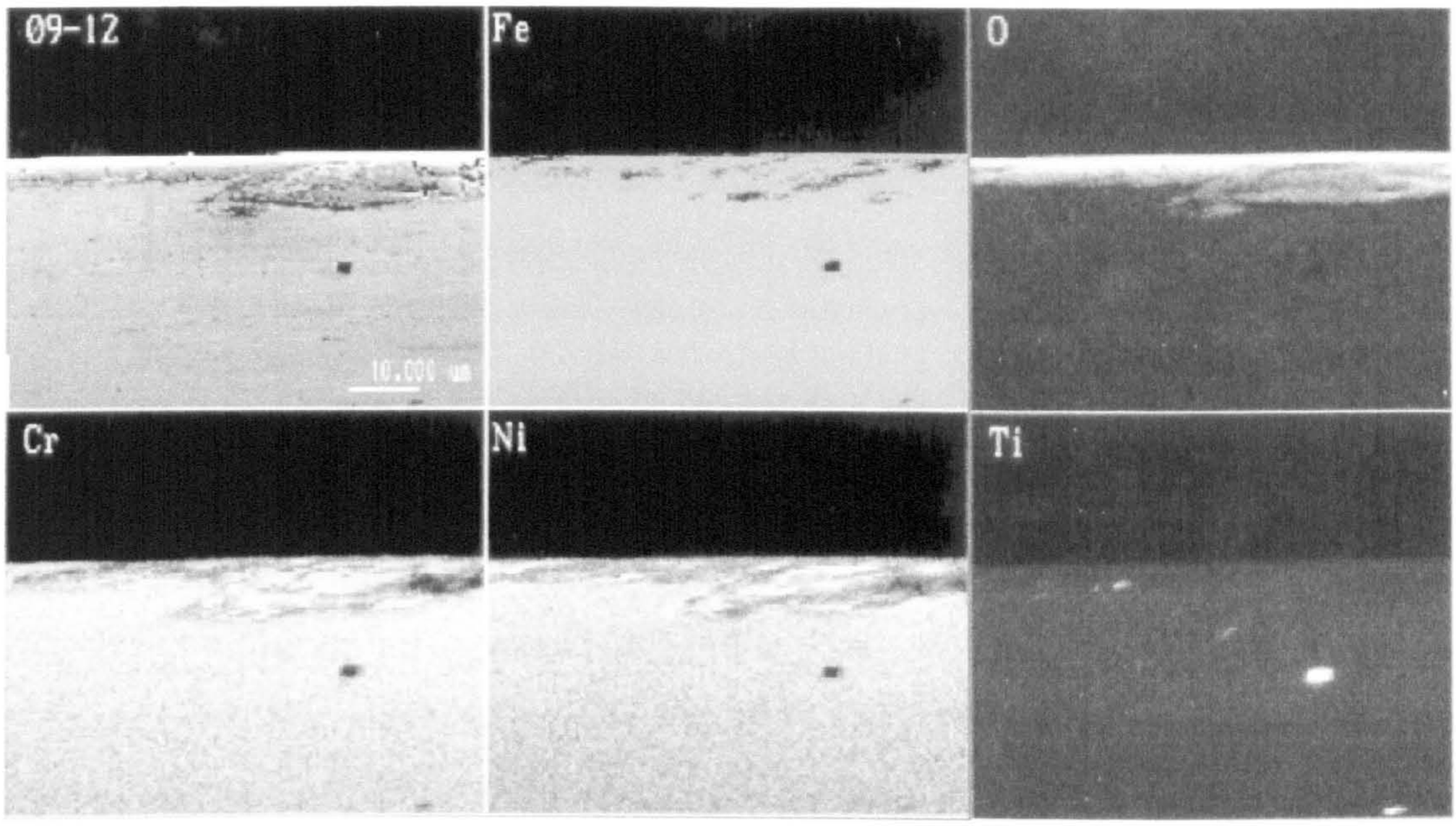

Figure 5.65 Cross-sectional SEM/EDX element map through the wear scar formed on Incoloy 800 worn with Nimonic 80A at 750°C and 7N load for 4 hours

5.11 Like-on-like sliding at 750°C

Like-on-like sliding was carried out at 750°C for the four alloys used. Here three of the tests were successful (Nimonic 80A, Incoloy 800 and Stellite 6). However, like-on-like sliding of MA956 led to gross adhesion between the samples and the counterface and failure of the test.

5.11.1 Weight changes

Weight changes for the three like-on-like tests are shown in **Figure 5.66**. For MA956/MA956 no weight change was recorded due to the failure of the test. Nimonic 80A/Nimonic 80A and Incoloy 800/Incoloy 800 both gave relatively high weight losses (0.282g and 0.535g respectively). Stellite 6/Stellite 6 underwent very small negative weight loss (-0.000(6)g, i.e. slight weight gain).

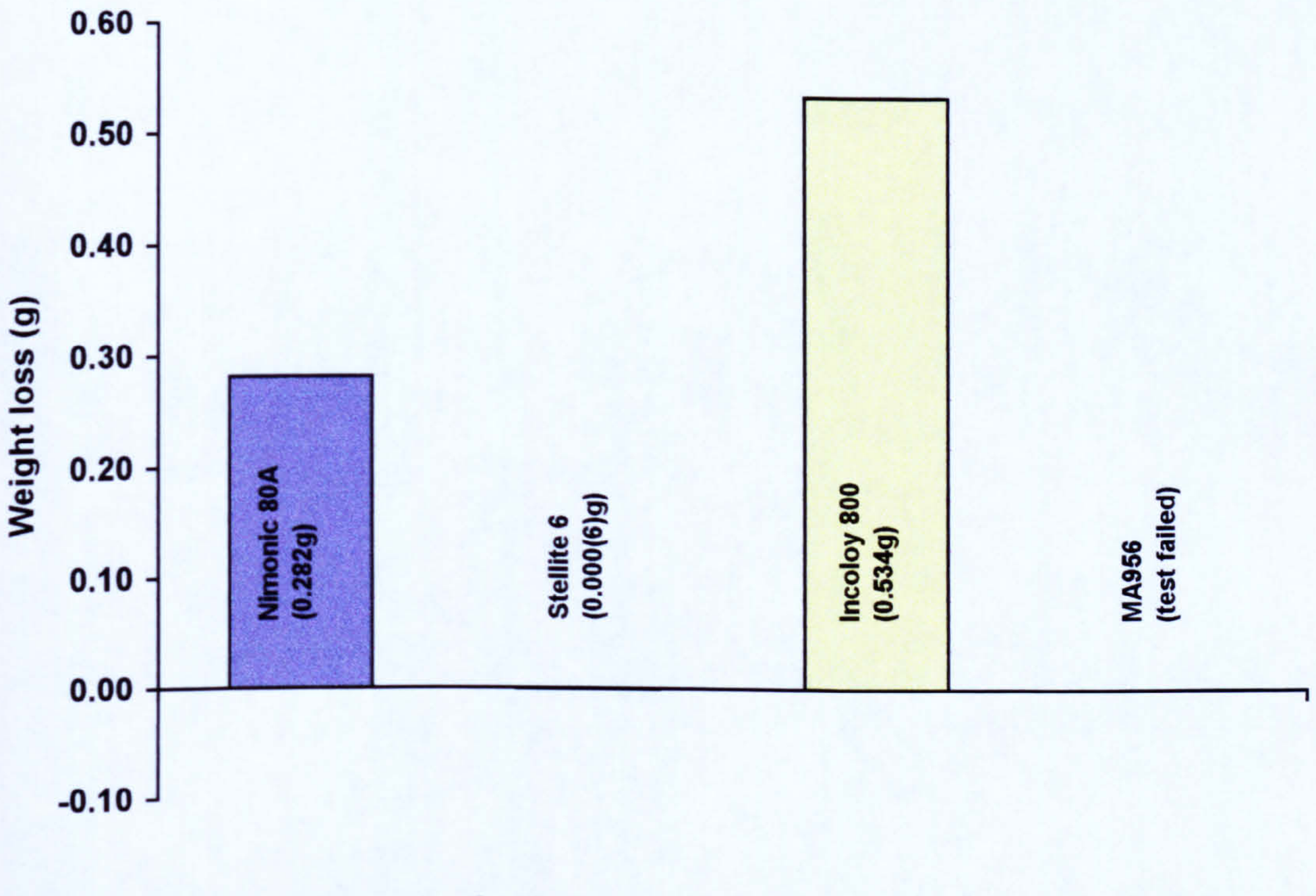

Figure 5.66 Weight changes for like-on-like wear of Nimonic 80A, Stellite 6 and Incoloy 800 at 750°C and 7N load for 4 hours [Failed MA956 test omitted]

5.11.2 Coefficients of friction

Coefficient of friction data for the three like-on-like couples tested are shown in **Figure 5.67**. No friction data were recovered for MA956/MA956 (the friction probably rose rapidly from the start of the test to a high value causing failure of the rig).

Nimonic 80A/Nimonic 80A and Incoloy 800/Incoloy 800 both showed similar patterns. Here the coefficient of friction values fell rapidly from an initial level of near unity (0.88 and 1.02 for Nimonic 80A and Incoloy 800 respectively) to a stable value (0.45 to 0.50) in the first 40 to 50 minutes of the test, where it remained for the rest of the test.

Stellite 6 showed a lower initial coefficient of friction (0.42), which fell to a stable value (0.25 to 0.35) in the first 20 minutes of the test. It was noted that Stellite 6 gave very smooth sliding throughout the test.

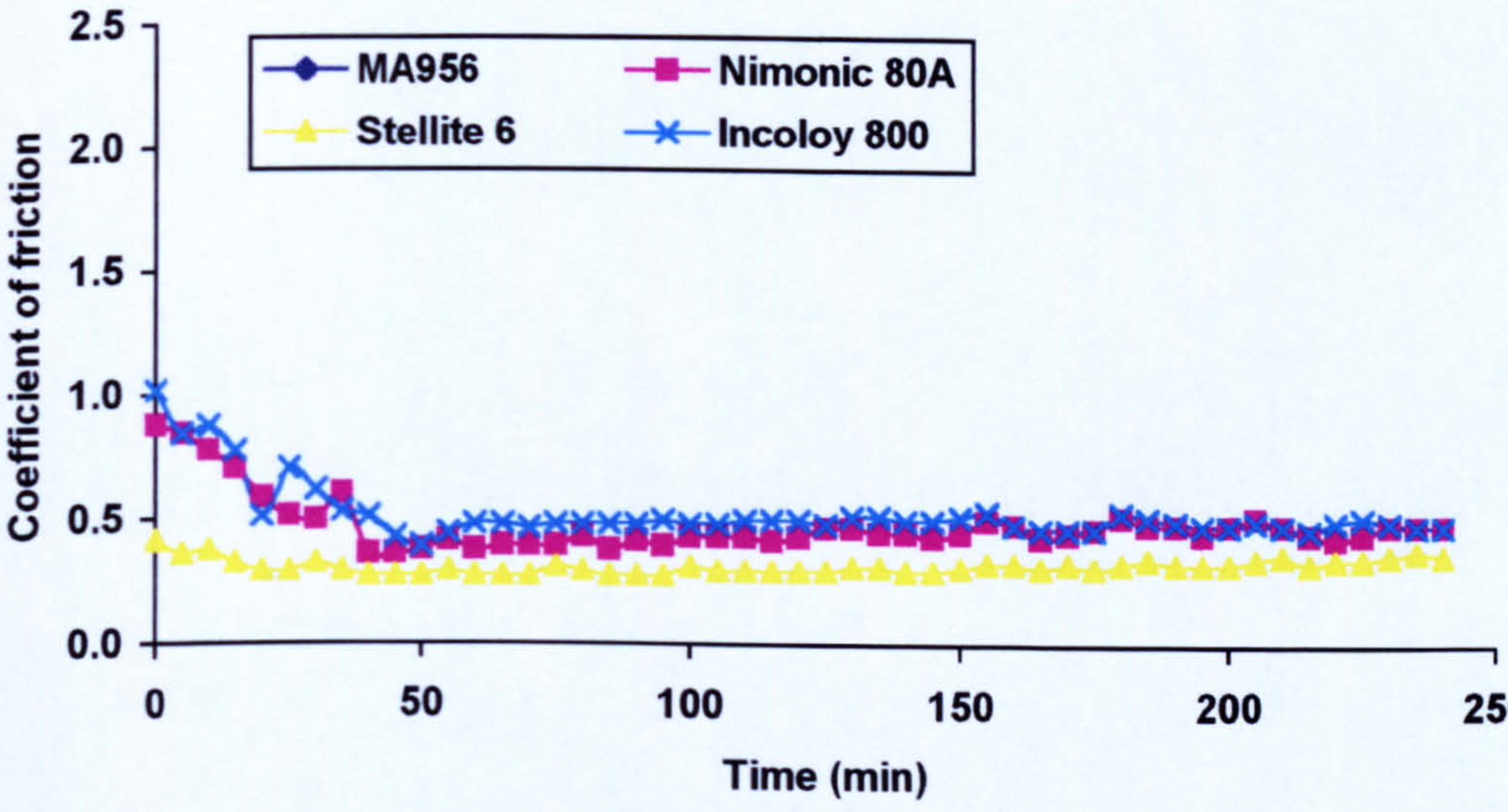

Figure 5.67 Coefficients of friction for like-on-like sliding of MA956, Nimonic 80A, Stellite 6 and Incoloy 800 at 750°C and 7N load for 4 hrs

5.11.3 XRD analysis

Diffractograms for the wear samples produced in like-on-like sliding are displayed in **Figures 5.68** to **5.71**: the phases identified are given in **Table 5.10**. The wear scars produced on the failed like-on-like sliding of MA956 showed only the phases for the MA956 substrate – no oxide phases were detected. For like-on-like sliding of Nimonic 80A, phases were detected for the Nimonic 80A substrate and for nickel oxide (NiO). For Stellite 6 in addition to cobalt chromium oxide (Co_2CrO_4), phase were identified from the Stellite 6 substrate. Incoloy 800 revealed phases from the substrate, maghemite (Fe_2O_3) and nickel chromium oxide ($NiCr_2O_4$).

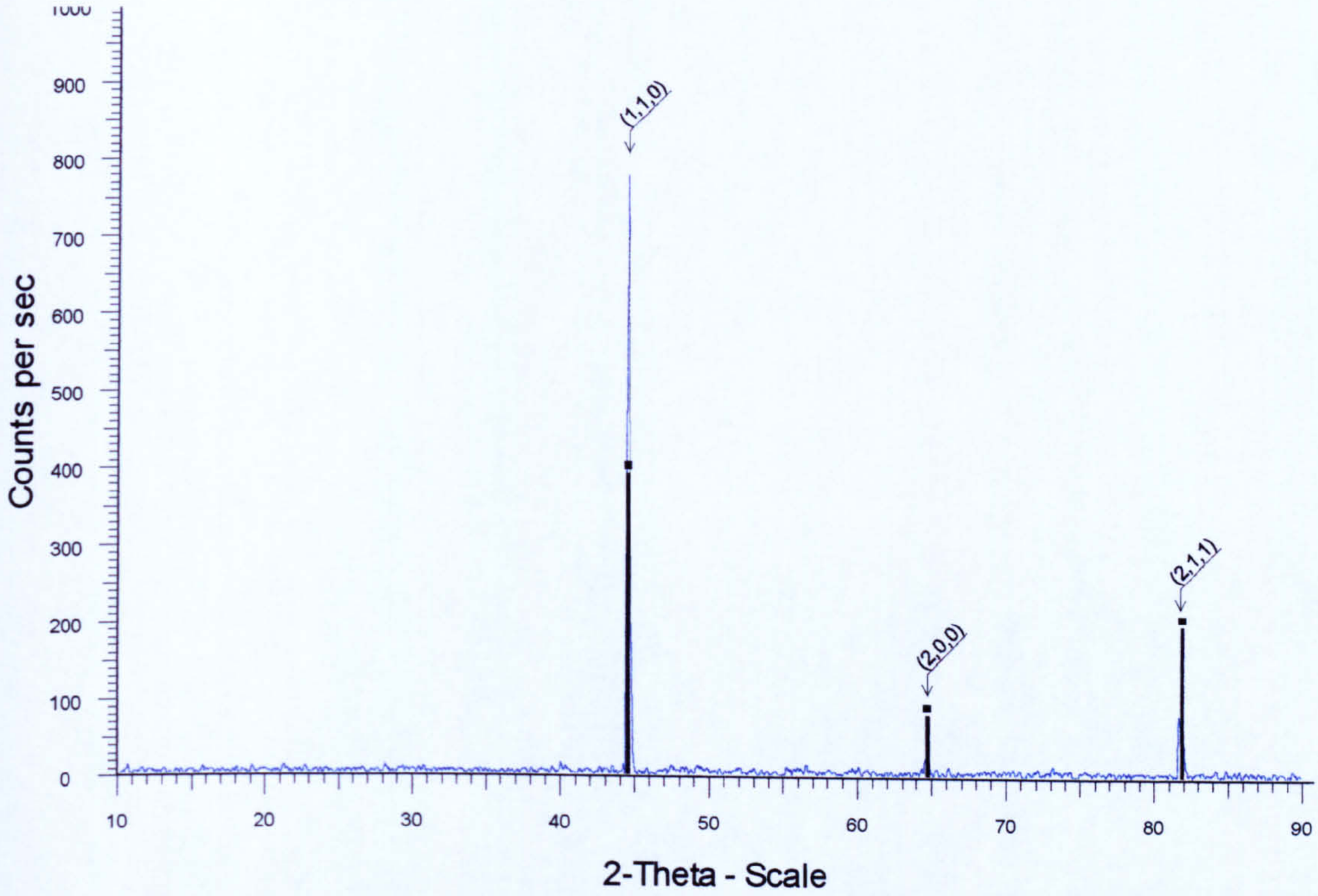

Figure 5.68 XRD data for like-on-like sliding of MA956 at 750°C and 7N load for 4 hours. Phases identified ▣ iron chromium phase (Fe-Cr) only (MA956)

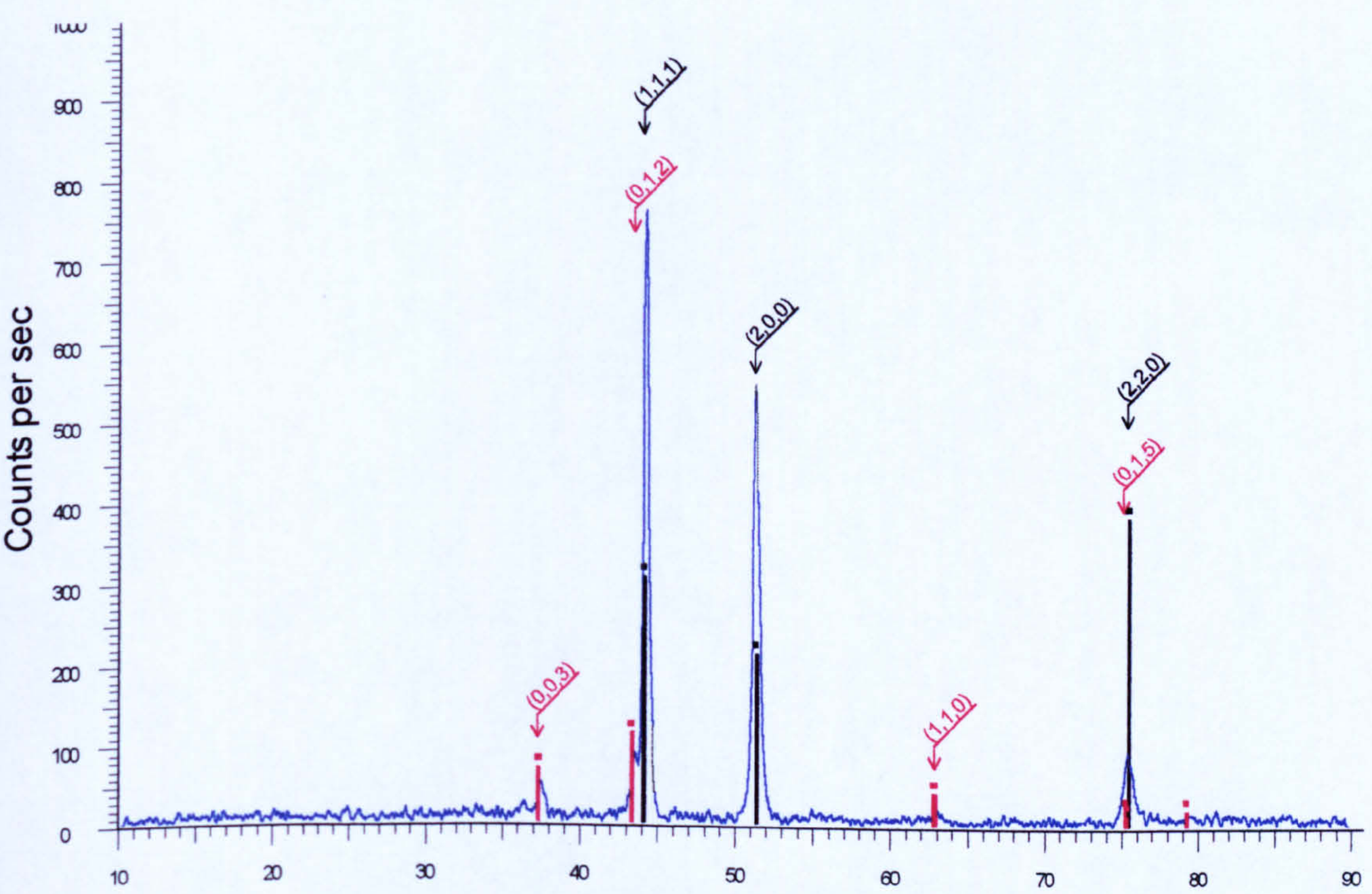

Figure 5.69 XRD data for like-on-like sliding of Nimonic 80A at 750°C and 7N load for 4 hours. Phases identified ▣ iron chromium nickel phases ($Cr_{0.19}$ $Fe_{0.7}$ $Ni_{0.11}$) (Nimonic 80A) and ▣ nickel oxide (NiO)

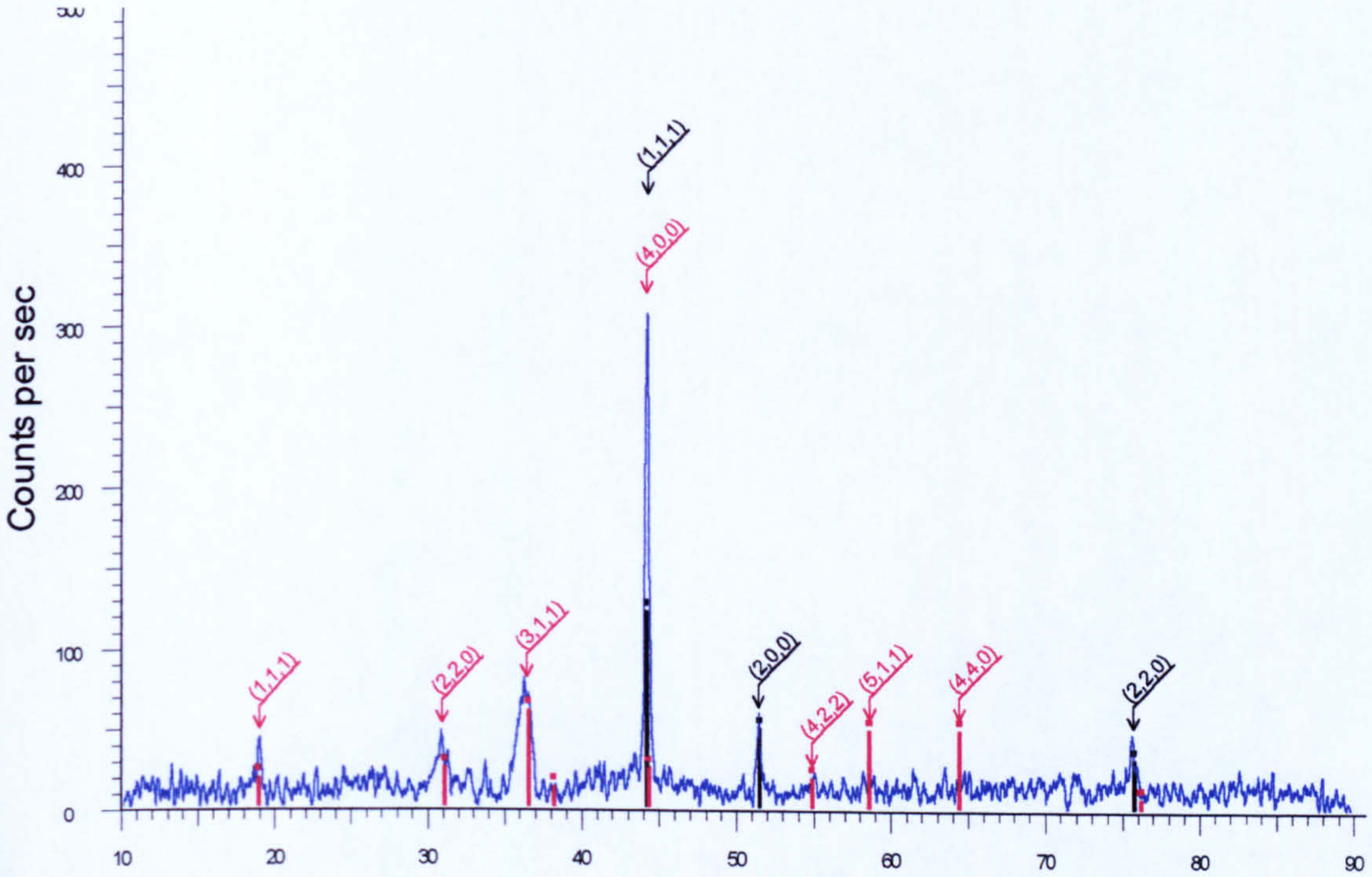

Figure 5.70 XRD data for like-on-like sliding of Stellite 6 at 750°C and 7N load for 4 hours. Phases identified ▣ cobalt chromium phase (Stellite 6) and ▣ cobalt chromium oxide (Co_2CrO_4)

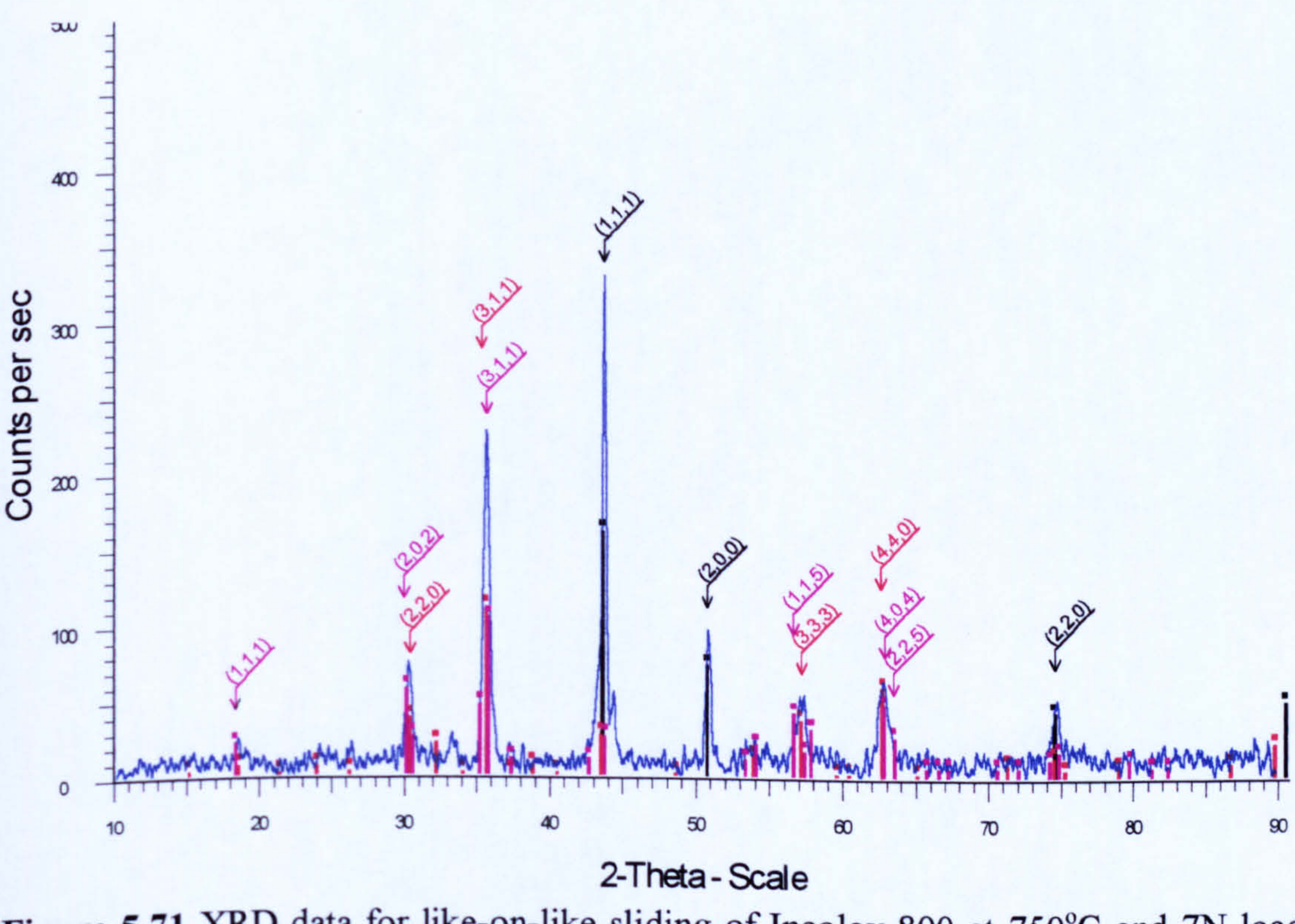

Figure 5.71 XRD data for like-on-like sliding of Incoloy 800 at 750°C and 7N load for 4 hours. Phases identified ▣ iron chromium nickel phase (Cr-Fe-Ni) (Incoloy 800), ▣ maghemite (Fe_2O_3) and ▣ nickel chromium oxide ($NiCr_2O_4$)

Like-on-like sliding of MA956	
Phase identified	**Conditions identified / interpretation**
Iron chromium stainless steel phase (Fe-Cr)	MA956 substrate
Like-on-like sliding of Nimonic 80A	
Phase identified	**Conditions identified / interpretation**
Iron chromium nickel stainless steel phases ($Cr_{0.19}$ $Fe_{0.7}$ $Ni_{0.11}$)	Nimonic 80A substrate
Nickel oxide (NiO)	
Like-on-like sliding of Stellite 6	
Phase identified	**Conditions identified / interpretation**
Cobalt chromium phase	Stellite 6 substrate
Cobalt chromium oxide (Co_2CrO_4)	
Like-on-like sliding of Incoloy 800	
Phase identified	**Conditions identified / interpretation**
Iron chromium nickel stainless steel phase (Cr-Fe-Ni)	Incoloy 800 substrate
Maghemite (Fe_2O_3)	
Nickel chromium oxide ($NiCr_2O_4$)	

Table 5.10 XRD analysis of MA956, Nimonic 80A, Stellite 6 and Incoloy 800 samples worn under like-on-like sliding at 750°C

5.11.4 SEM morphological analysis

Micrographs of the wear scars produced on the four alloys are presented in **Figure 5.72**. The MA956 sample recovered from the failed test revealed (**Figure 5.72 (a)**) that the sample had undergone significant amounts of wear during the test (which probably only amounted to 20 minutes). Transfer of large metallic fragments of material appeared to have taken place between both the sample and the counterface. No compacted oxide layer or surface oxides were detected.

The scars on Nimonic 80A and Incoloy 800 worn under like-on-like sliding both had compacted oxide layer-type surfaces (**Figures 5.72(b)** and **5.72(d)**). In both cases there was also fine wear debris present at the surfaces, and the surfaces had a smeared appearance.

For like-on-like sliding of Stellite 6 (**Figure 5.72 (c)**) the surface oxide layer formed appeared very smooth, solid and well compacted with no loose debris. Some areas of the sample were not covered by the compacted oxide layer,

these areas appeared grooved and worn due to damage done prior to the establishment of the oxide layer.

5.11.5 SEM/EDX cross-section analysis

SEM/EDX cross-sectional element maps for Nimonic 80A, Stellite 6 and Incoloy 800 worn under like-on-like sliding are shown in **Figure 5.73**, **Figure 5.74** and **Figure 5.75** respectively. Like-on-like sliding of MA956 generated no surface oxide layers.

Nimonic 80A had a very thin oxide layer on the sample surface. This layer consists of nickel and chromium oxides. The Incoloy 800 sample gave a more substantial layer, which consisted of oxides of iron, chromium and nickel. The layer on Stellite 6 was again very thin and formed from chromium and cobalt oxides.

5.11.6 Analysis of wear debris

Wear debris was only recovered from Nimonic 80A and Incoloy 800 tests – micrographs of this debris are displayed in **Figure 5.76.** little debris was generated and no debris was recovered from the Stellite 6 tests. In the MA956 test the debris was lost in the resulting damage caused by failure of the rig.

For like-on-like wear of Nimonic 80A the collected debris consisted of two types. The predominant type of the debris was very fine particles (1 to 5μm) together with a small number of larger flat and angular particles (50 to 100μm). SEM/EDX analysis of both large and small wear fragments revealed them to have approximately the same composition as Nimonic 80A.

The debris generated from the like-on-like sliding of Incoloy 800 consisted of large angular particles of various shapes, predominantly flat and angular debris (50 to 250μm), together with finer particles (1 to 5μm). SEM/EDX analysis showed these particles to consist of all the elements present in Incoloy 800. However, many fragments were enriched in chromium and aluminium at the expense of nickel, which implies that the oxides were formed by oxidation of the substrate leading to preferential oxidation of chromium and aluminium.

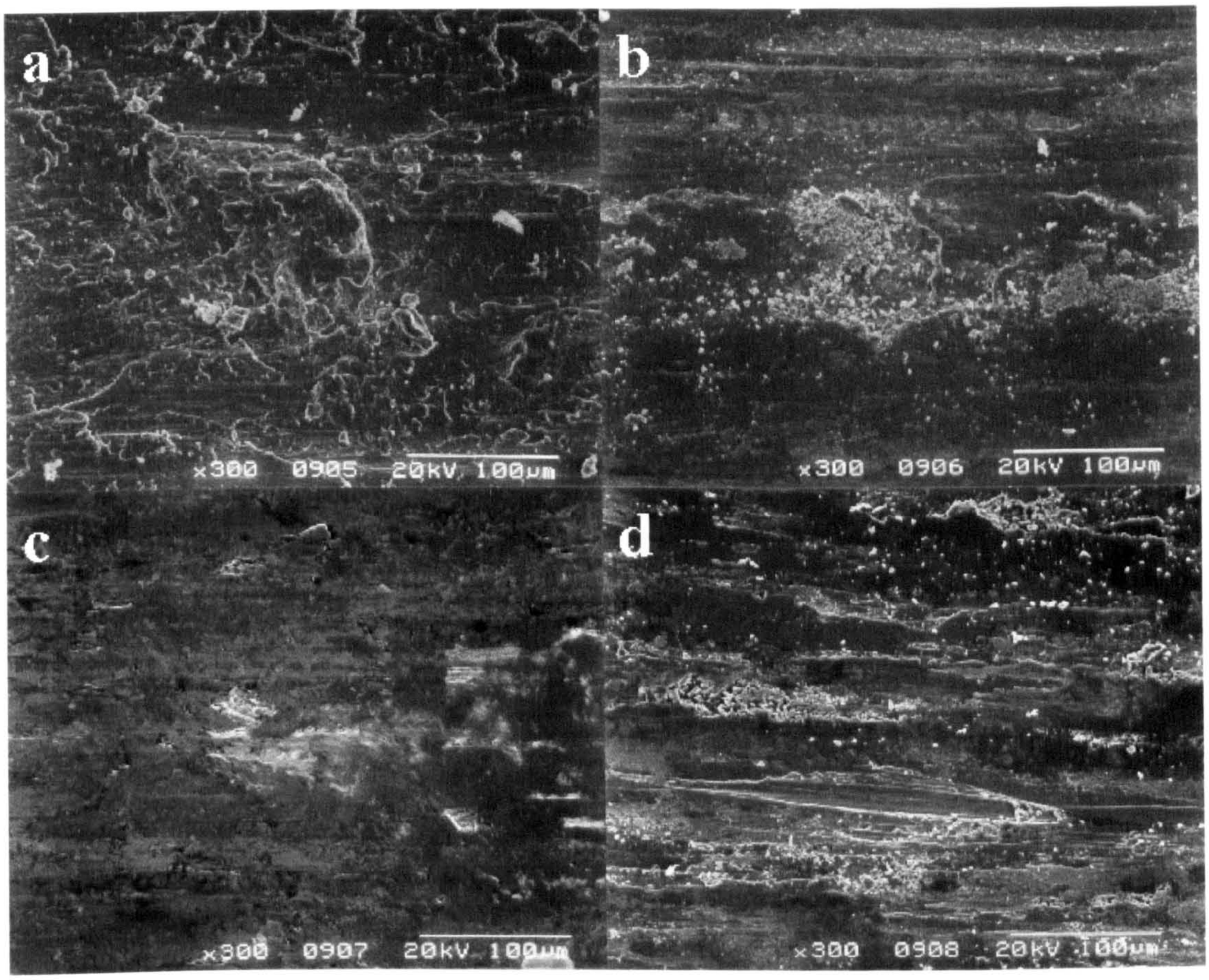

Figure 5.72 Wear scars produced via like-on-like sliding of (a) MA956 (b) Nimonic 80A, (c) Stellite 6 and (d) Incoloy 800 at 750°C and 7N load for 4 hours [Note that the MA956 test failed after approximately 30 minutes, the sample examined being recovered from the rig]

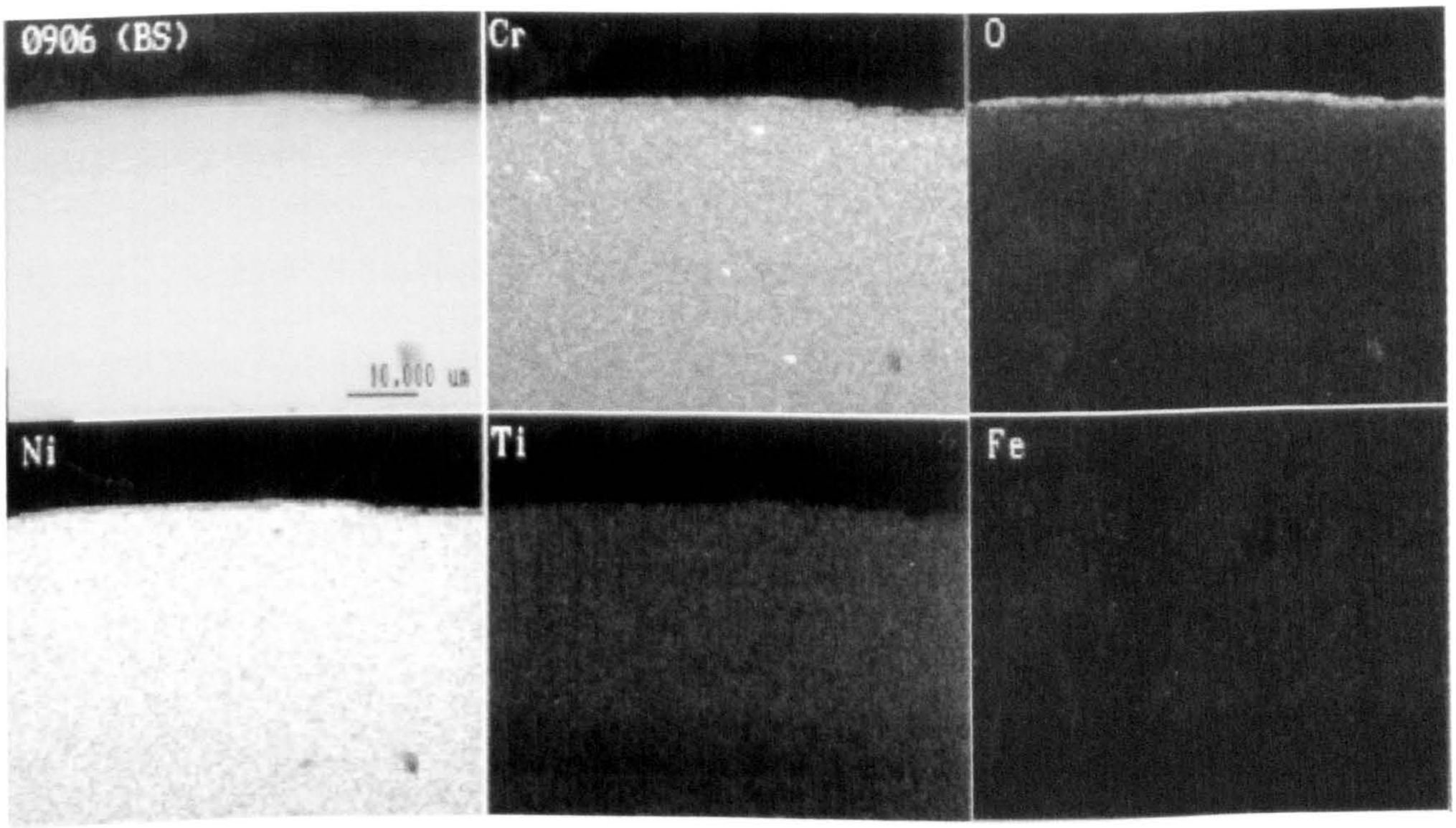

Figure 5.73 Cross-sectional SEM/EDX element map through the wear scar formed upon Nimonic 80A under like-on-like sliding at 750°C and 7N load for 4 hours

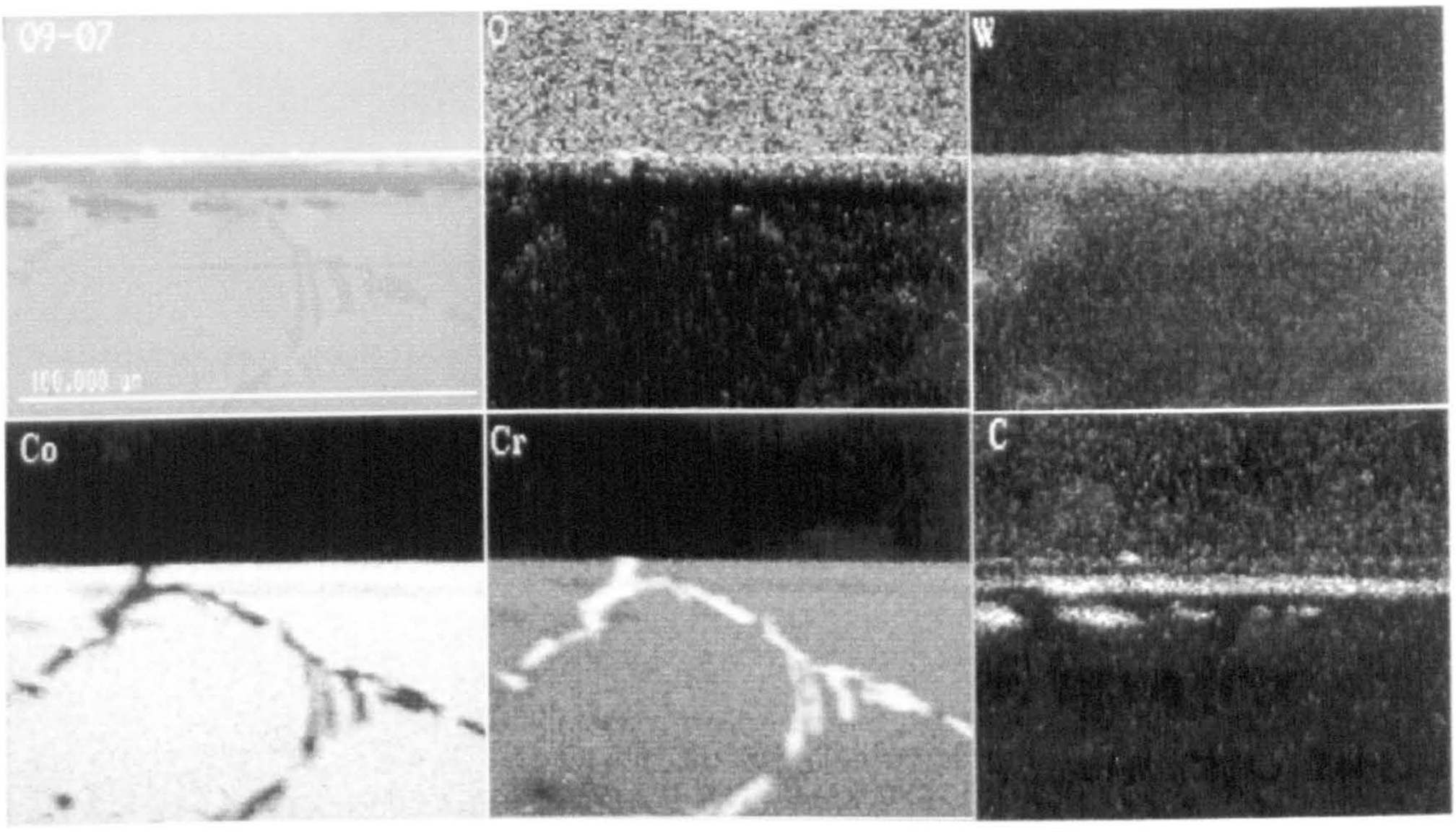

Figure 5.74 Cross-sectional SEM/EDX element map though the wear scar formed upon Stellite 6 under like-on-like sliding at 750°C and 7N load for 4 hours

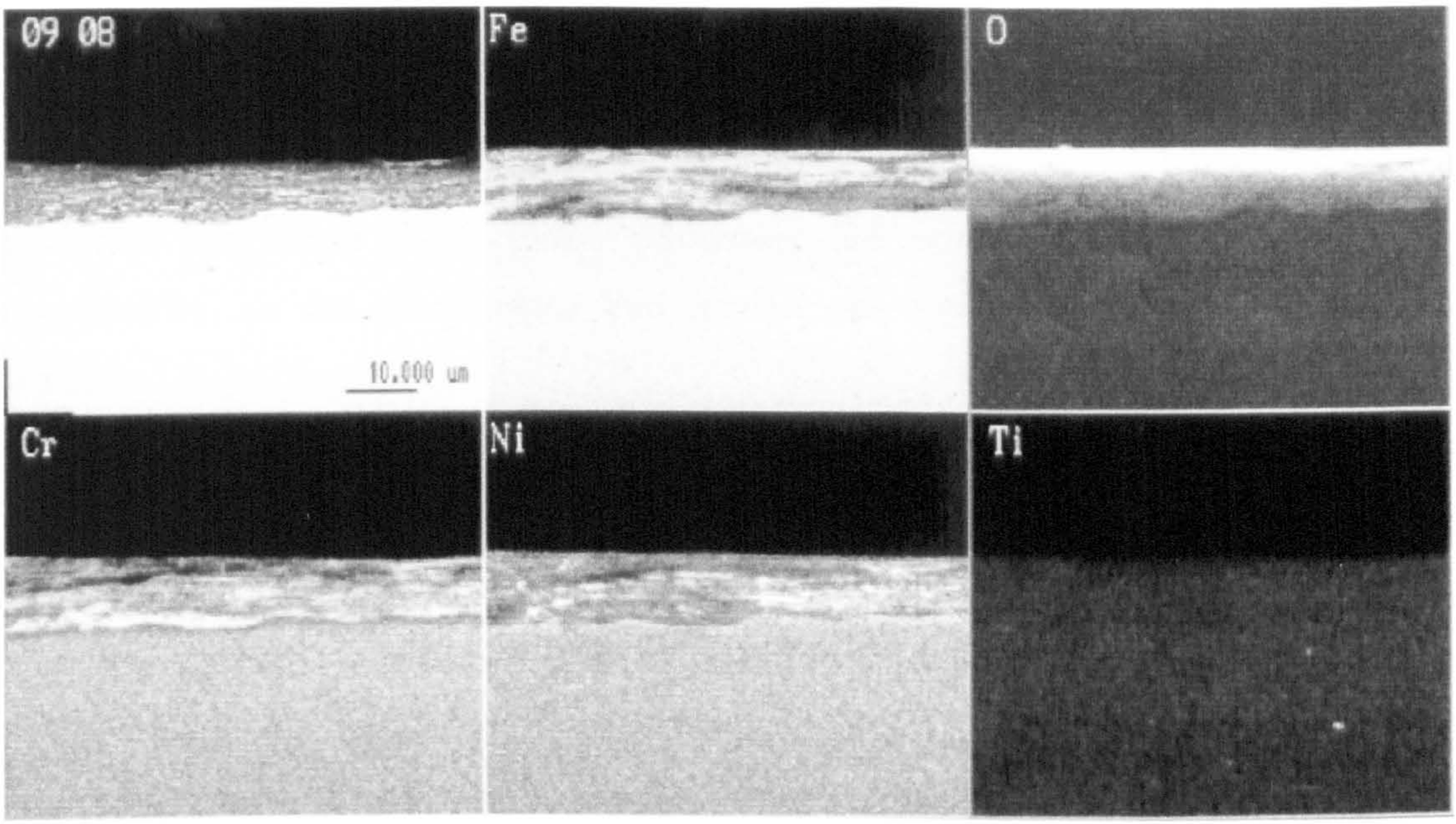

Figure 5.75 Cross-sectional SEM/EDX element map through the wear scar formed upon Incoloy 800 under like-on-like sliding at 750°C and 7N load for 4 hours

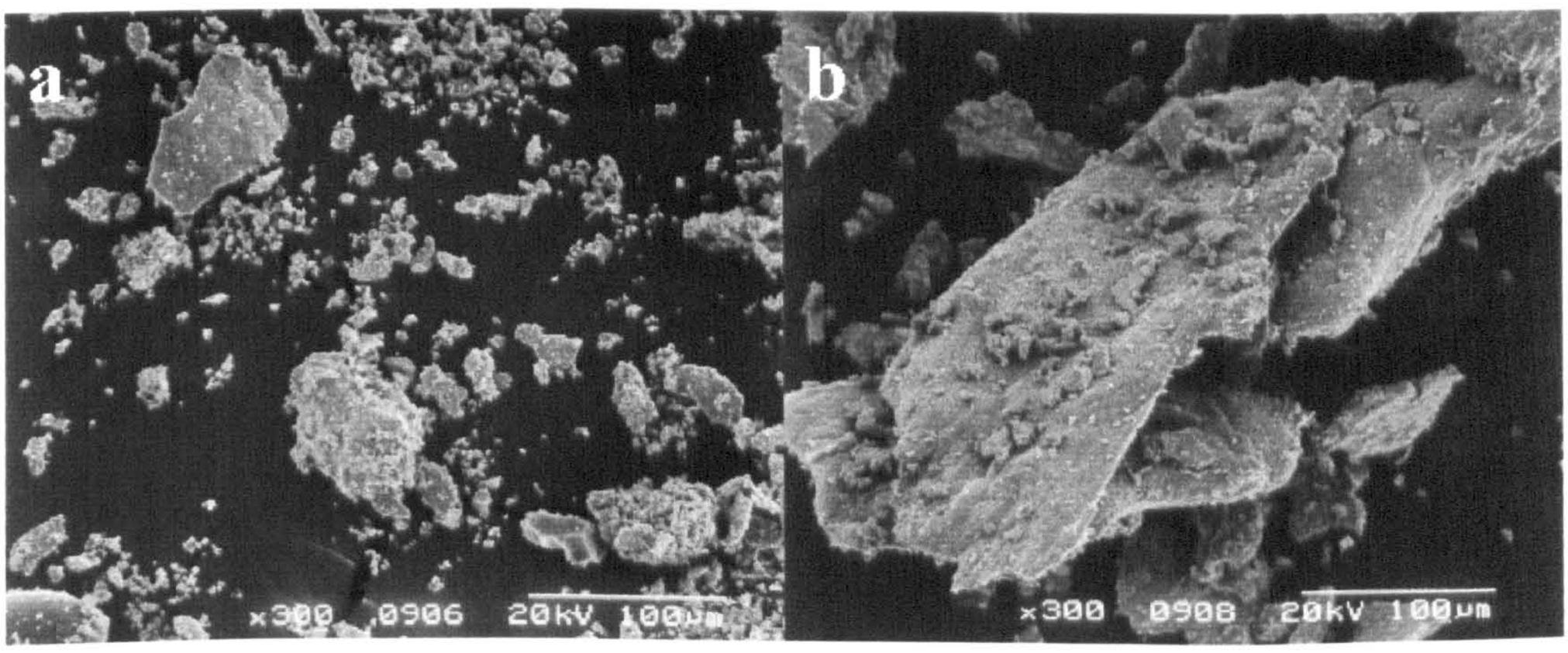

Figure 5.76 Wear debris produced from like-on-like sliding of (a) Nimonic 80A, (b) Incoloy 800 at 750°C and 7N load for 4 hours [No wear debris was recoverable from the failed MA956 test or the wear of Stellite 6 with itself]

5.11.7 Appearance of counterfaces

The wear scar produced from the like-on-like sliding of MA956 was highly damaged and free from attached oxide debris. It also appeared that transfer of material may have taken place. (However the scar was extended across the counterface, as the counterface had moved sideways during the failure of the test).

For like-on-like sliding of Nimonic 80A, most of the wear track was covered with green oxide powder which was attached to the counterface. This fine debris material when removed revealed a fairly deformed wear track, which suggested severe wear in the early stages of the test. This implies that significant material loss took place from the counterface in these early stages.

The wear track on the Stellite 6 counterface appears to be completely covered with a compacted oxide layer, the track having the characteristic shiny, 'glaze' surface. Here the track was free of debris. Here the counterface shows no sign of having undergone material loss.

The wear track on the Incoloy 800 counterface consisted of a very rough surface. Upon this highly damaged wear track there were areas of black powder which surrounded small 'islands' of compacted oxide material. Approximately only half the tracks' surface was covered by these areas of attached debris. The fine debris appeared to have accumulated around the high points on the wear track where the compacted oxide island developed and became load-bearing. Here the counterface appears to have undergone significant material loss.

5.12 Formation of compacted oxide layers: MA956 worn with Incoloy 800 at 690°C

5.12.1 Weight changes

The weight losses for MA956 worn with Incoloy 800 are presented in **Figure 5.77**. After 10 minutes the weight loss was relatively small (0.006g) then from 10 to 90 minutes the weight loss increases with time in a linear fashion. After 90 minutes the rate of material loss decreased. The weight loss at 240 minutes (0.516g) was not double the losses at 120 minutes (0.341g).

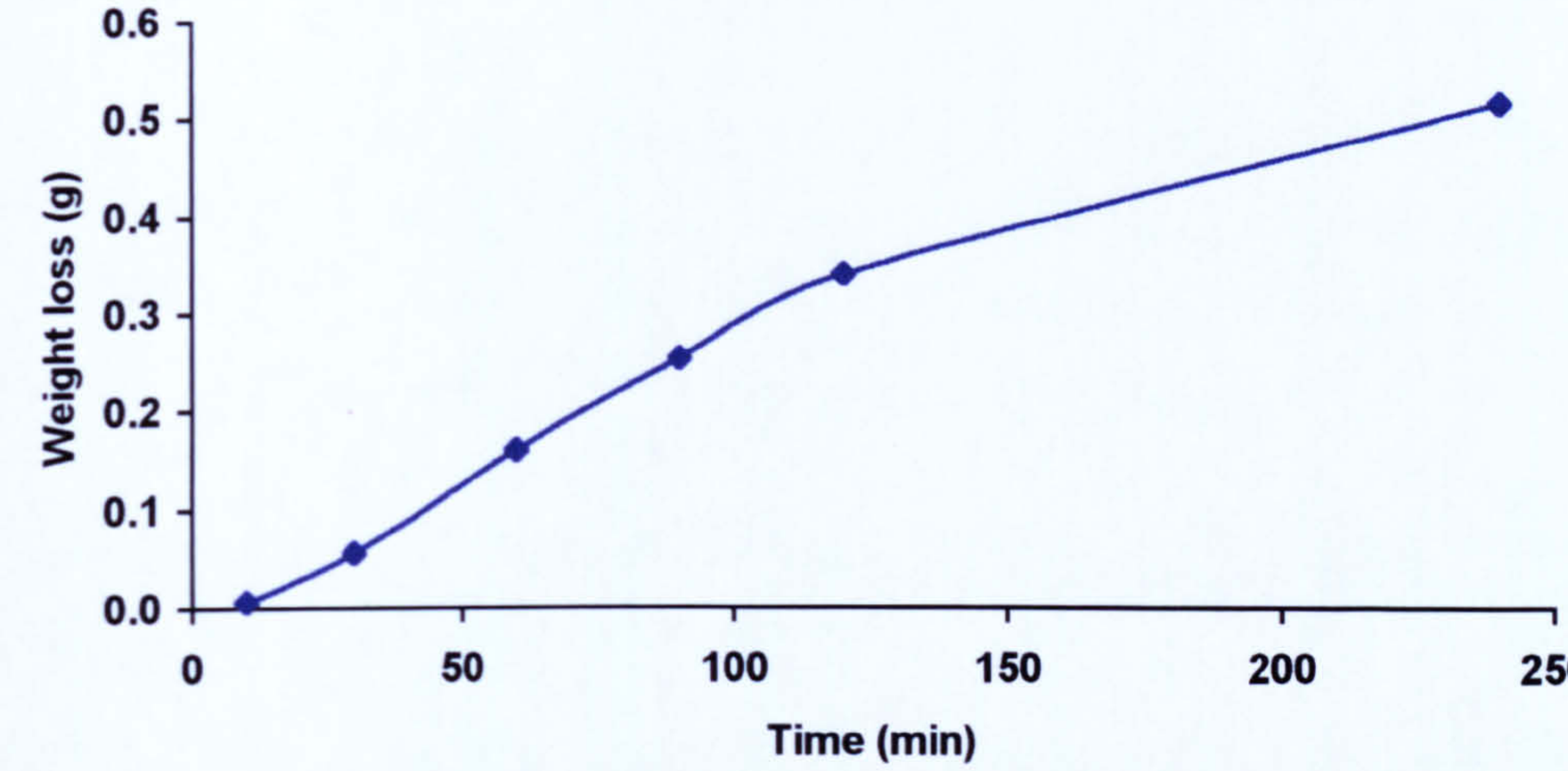

Figure 5.77 Weight loss for MA956 worn with Incoloy 800 over a range of times at 690°C and 7N load

5.12.2 Coefficients of friction

The coefficient of friction data for MA956 worn with Incoloy 800 at 690°C are displayed in **Figure 5.78**. For all the tests the coefficient of friction starts at a value of 0.75 to 0.95. This is maintained for approximately the first 60 minutes after which it falls to 0.45 to 0.50 – this becomes the stable value by 90 minutes.

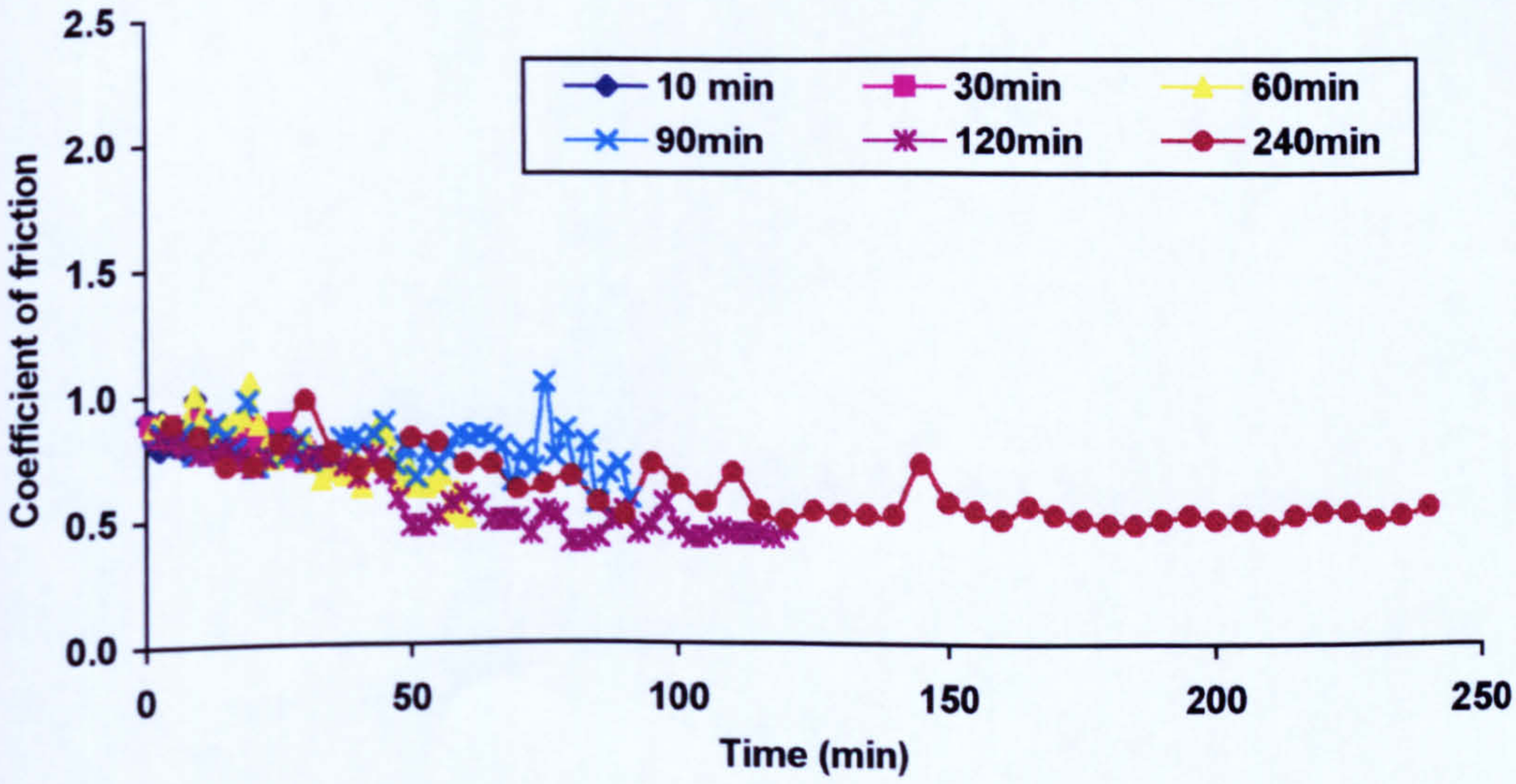

Figure 5.78 Coefficients of friction for MA956 worn with Incoloy 800 over a range of times at 690°C and 7N load

This change in the friction coefficient was also seen for MA956 worn with Incoloy 800 counterface at 750°C, and would appear to be associated with the formation of a compacted oxide layer upon their surfaces.

5.12.3 XRD analysis

Diffractograms of the wear samples run for 10, 30 120 and 240 minutes are presented in **Figure 5.79** and the phases identified are given in **Table 5.11**. At all the times tested the phase for the MA956 substrate was found. From 30 minutes onwards chromium/iron oxide was also detected.

Phase identified	**Conditions identified / interpretation**
Iron chromium stainless steel phase (Fe-Cr)	MA956 substrate
Chromium/iron oxide ($Cr_{1.3}Fe_{0.7}O_3$)	From 30 minutes onwards, origin unclear

Table 5.11 XRD analysis of MA956 worn with Incoloy 800 at 690°C, from 10 to 240 minutes

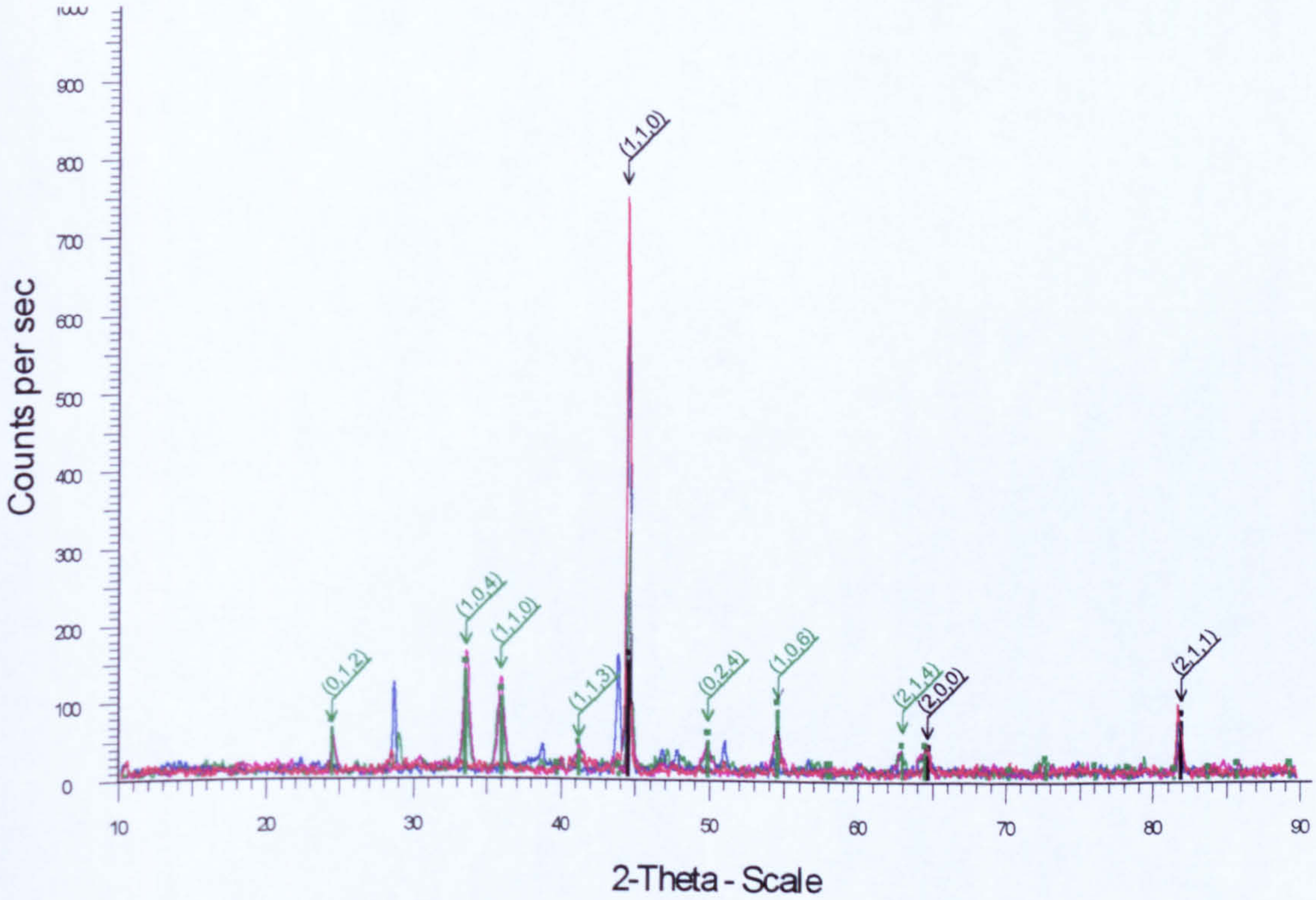

Figure 5.79 XRD data for MA956 worn with Incoloy 800 at 690°C at times of 10, 30, 120 and 240 minutes at 7N load. Phases identified ▣ iron-chromium phase (Fe-Cr) (MA956) and ▣ chromium iron oxide ($Cr_{1.3}Fe_{0.7}O_3$)

5.12.4 SEM morphological analysis

Plan views of the wear scars formed on MA956 worn with Incoloy 800 at 690°C are given in **Figure 5.80.** These show that after 10 minutes the scars are torn and deformed and there was no evidence of a build-up of oxide debris material upon the surface.

After 30 minutes, there were two types of features seen on the surface. Some areas of the wear scar remained similar to those observed after 10 minutes – i.e. torn, deformed and free from debris material. In other areas, islands of compacted oxide material had started to form with the characteristic 'glaze-type' surface. Around these areas and in hollows and depressions upon the surface the 'pile-up' of uncompacted fine debris was seen.

From 60 to 240 minutes there was a progressive increase in the areas of compacted oxide and 'glaze-type' surfaces – these gradually expanded laterally as debris piles-up in front and around the load-.
bearing areas to cover the whole scar area.

5.12.5 Analysis of wear debris

Micrographs of the wear debris recovered are shown in **Figure 5.81.** Wear debris recovered from initial stages of wear consisted of large angular particles characteristic of adhesive/severe wear (50 to 250μm).

Debris recovered from longer duration tests are of similar appearance to those recovered at 10 and 30 minutes. However there was some finer material attached to the particle's surfaces and occasional debris fragments appeared to contain features that were once part of the scar's or track's surface.

Analysis of the debris via SEM/EDX revealed the debris to consist of iron, chromium and nickel indicating wear of both the counterface and sample.

5.12.6 Appearance of counterfaces

At times of 10 to 60 minutes the wear tracks become progressively damaged, giving the appearance of severe wear (as seen with this couple at lower temperatures). At longer times areas of loosely attached fine powder were present upon the track, which surrounded areas with the characteristic shinny surfaces, 'glaze' areas which progressively covered the surface at longer times of sliding.

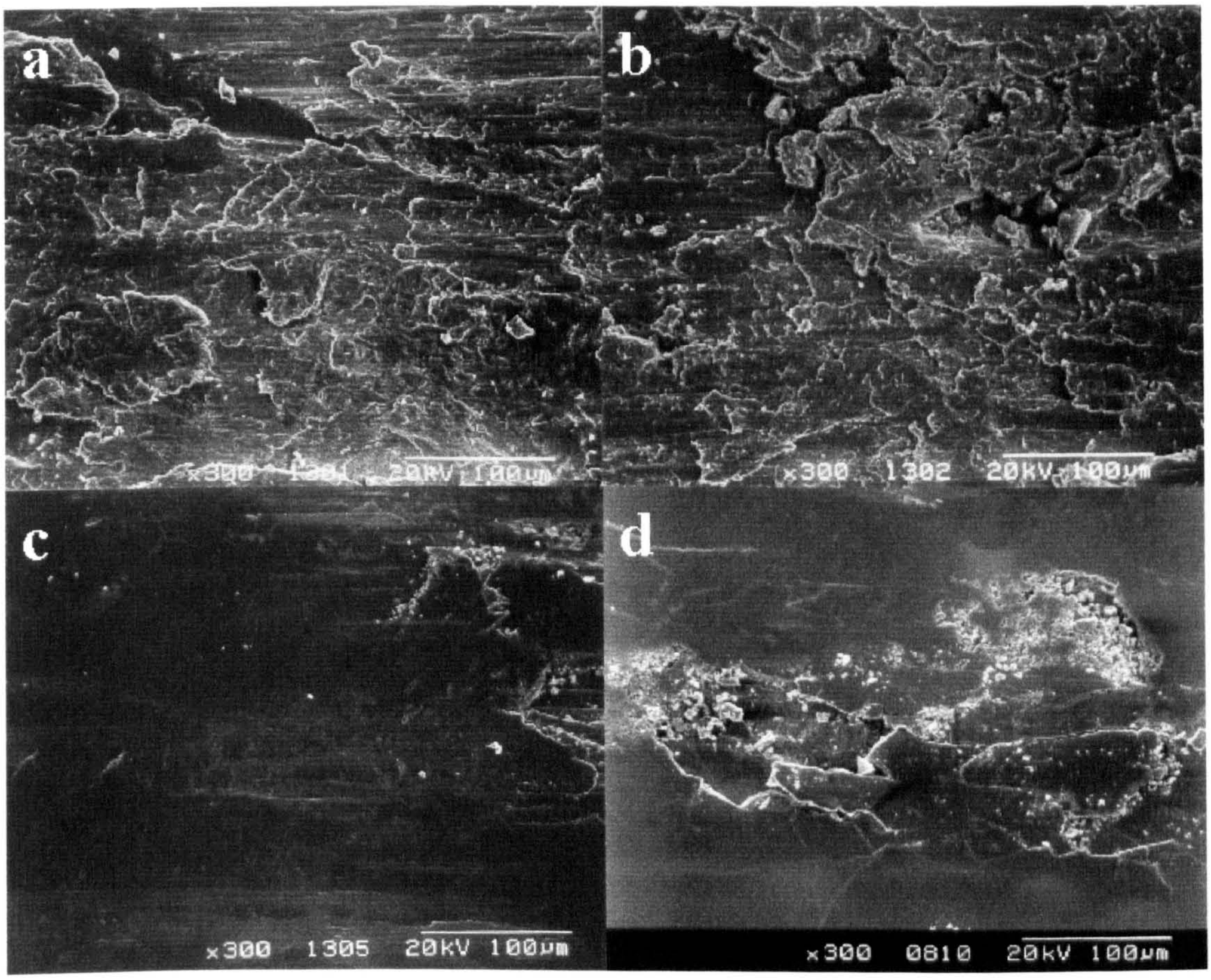

Figure 5.80 Wear scars produced upon MA956 worn with Incoloy 800 at 690°C and 7N load at times of (a) 10, (b) 30, (c) 120 and (d) 240 minutes

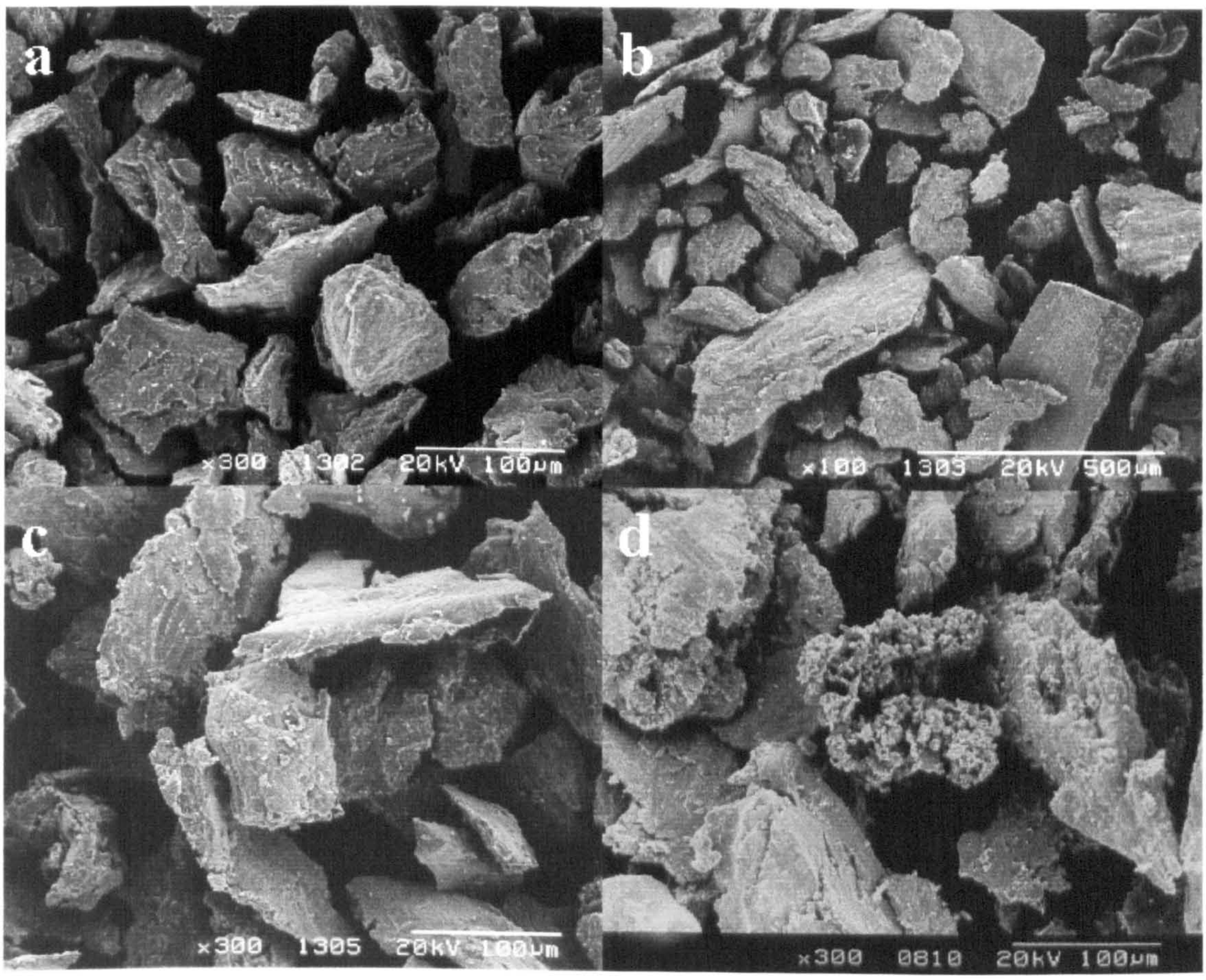

Figure 5.81 Debris recovered from the wear of MA956 samples with Incoloy 800 counterfaces at 690°C and 7N load at times of (a) 30, (b) 60, (c) 120 and (d) 240 minutes

5.13 Formation of compacted oxide layers: Nimonic 80A worn with Incoloy 800 at 630°C

5.13.1 Weight changes

The weight losses for Nimonic 80A worn with Incoloy 800 at 630°C are displayed in **Figure 5.82**. This figure shows small negative weight losses up to ~60 minutes (-0.025g) which then decrease again. At the end of the test the negative weight loss (weight gain) had fallen to (-0.006g).

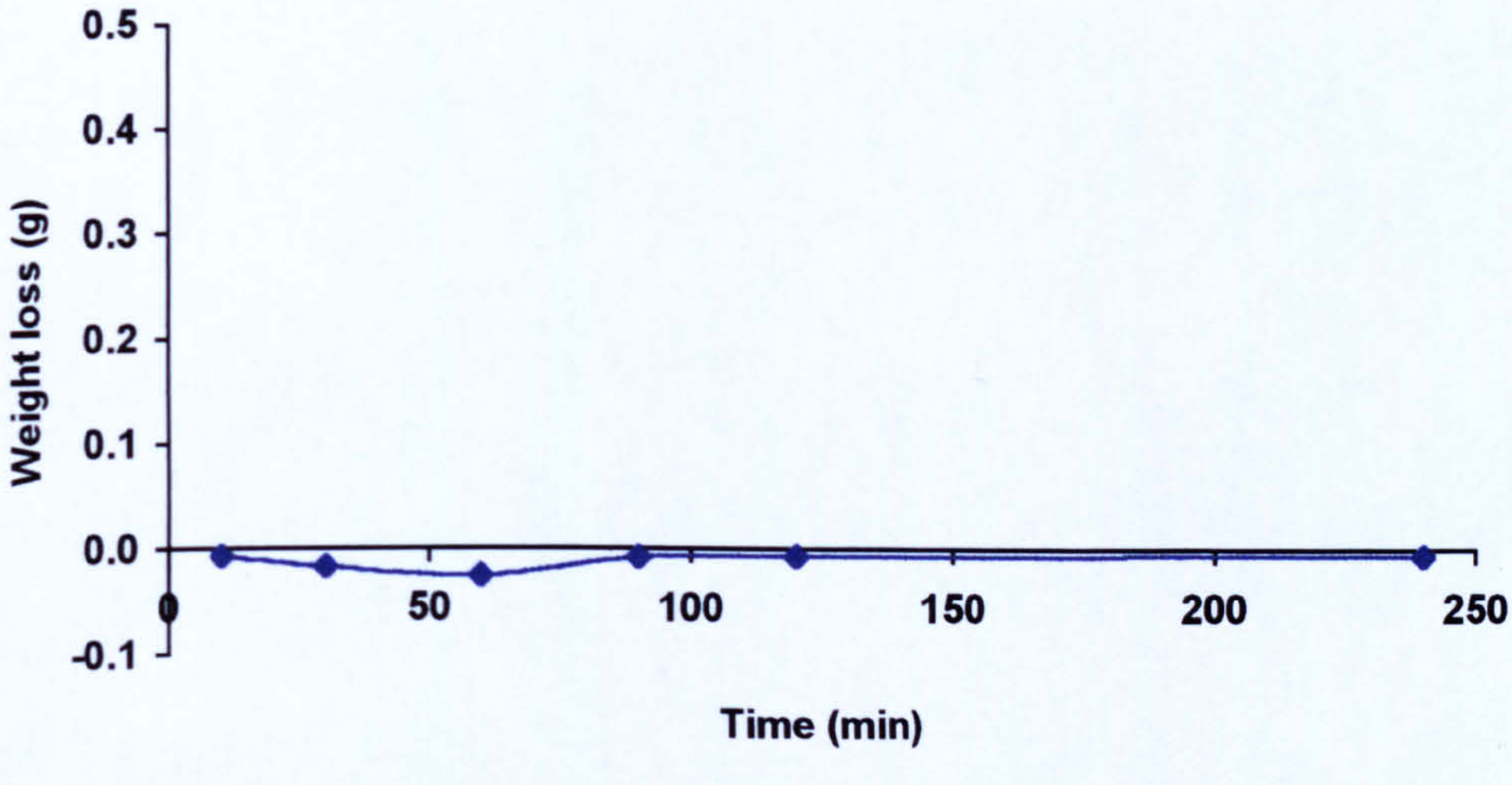

Figure 5.82 Weight loss for Nimonic 80A worn with Incoloy 800 over a range of times at 630°C and 7N load

5.13.2 Coefficients of friction

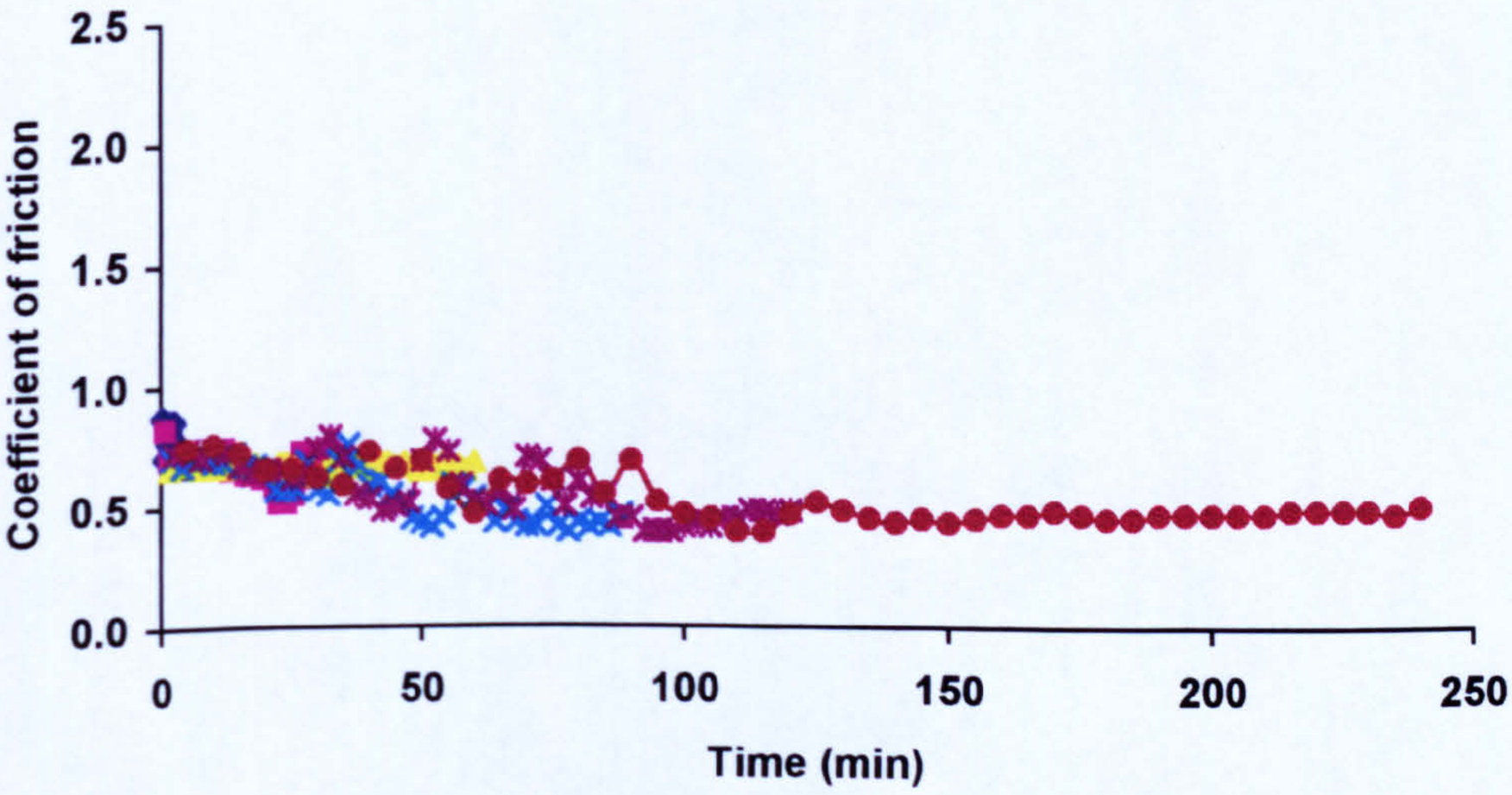

Figure 5.83 Coefficients of friction for Nimonic 80A worn with Incoloy 800 over a range of times at 630°C at 7N load

The coefficients of friction are displayed in **Figure 5.83**. It can be seen that the initial coefficients of friction, 0.65–0.75, are maintained for approximately the first 30 minutes of the test. After about 30 to 90 minutes the friction falls to a lower value of 0.35 to 0.50. During the intermediate time the friction fluctuates between the two ranges. This transition in the coefficient of friction appears to be associated with the formation of a compacted oxide layer on the sample's surface.

5.13.3 XRD analysis

Diffractograms of the wear samples run for 10, 30, 120 and 240 minutes are presented in **Figure 5.84** – phases identified are shown in **Table 5.12**. At all the times tested phases from the Nimonic 80A substrate were identified. For tests of duration 30 minutes and longer, nichromite ($NiCr_2O_4$) phase was also detected, the origin of which was unclear. At 10 and 30 minutes there appeared to also be transferred Incoloy 800 present upon the sample.

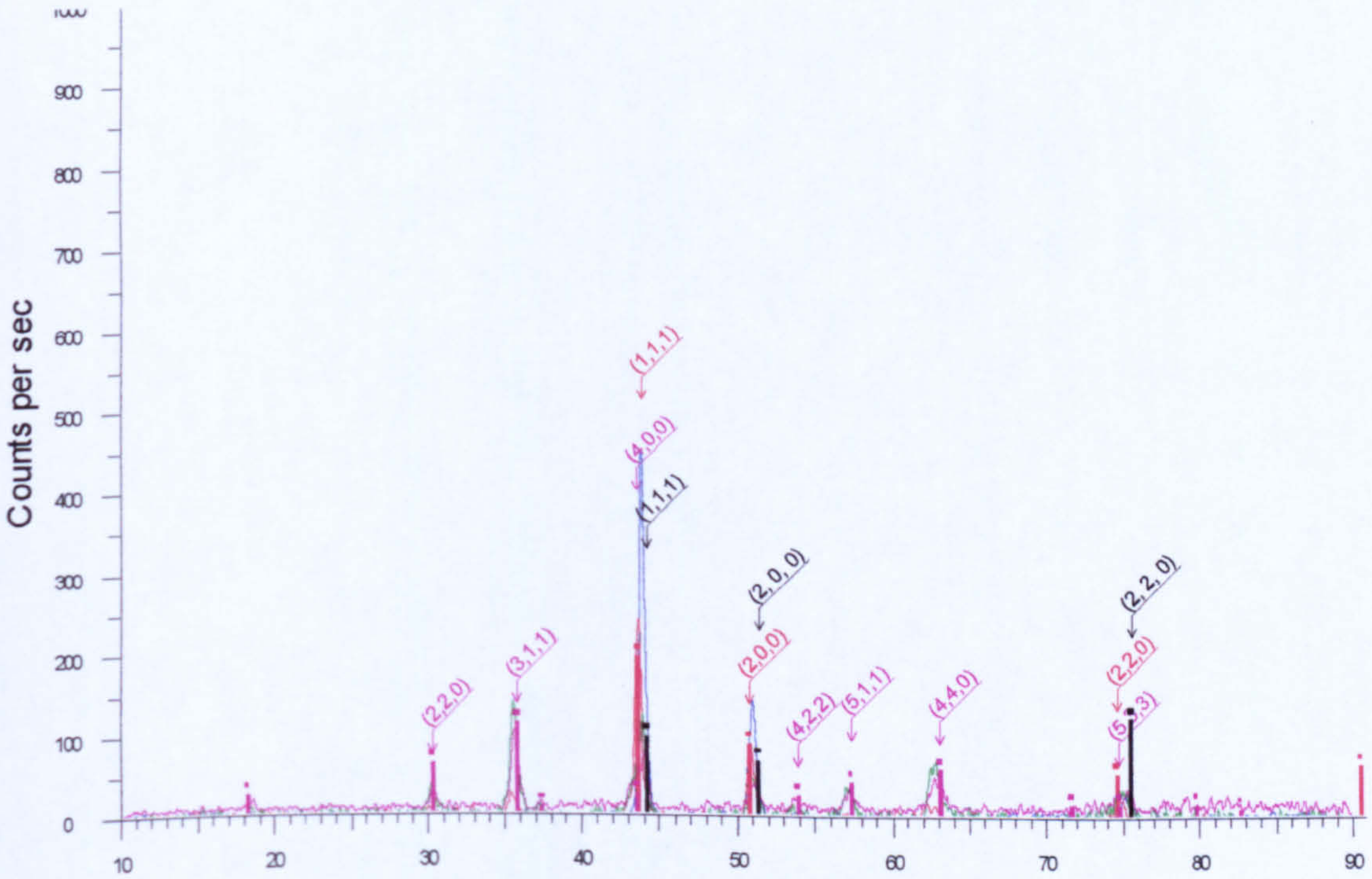

Figure 5.84 XRD data for Nimonic 80A worn with Incoloy 800 at 630°C at 7N load and times of 10, 30, 120 and 240 minutes. Phases identified ▣ iron chromium nickel phases ($Cr_{0.19}$ $Fe_{0.7}$ $Ni_{0.11}$) (Nimonic 80A), ▣ iron chromium nickel phase (Cr-Fe-Ni) (transferred Incoloy 800) and ▣ nichromite ($NiCr_2O_4$).

Phase identified	Conditions identified / interpretation
Iron chromium nickel stainless steel phases ($Cr_{0.19}$ $Fe_{0.7}$ $Ni_{0.11}$)	Nimonic 80A substrate all tests
Transferred Incoloy 800	From 10 and 30 minutes
Nichromite ($NiCr_2O_4$)	From 30 minutes onwards, origin unclear

Table 5.12 XRD analysis of Nimonic 80A worn with Incoloy 800 at 630°C, from 10 to 240 minutes

5.13.4 SEM morphological analysis

Micrographs of the wear scars formed on Nimonic 80A worn with Incoloy 800 at 630°C are given in **Figure 5.85**. The figure reveals that after 10 minutes the surface showed signs of deformation and was covered with some fine wear particles.

At 30 and 60 minutes patches of particles (1 to 10μm) begin to appear, some of these seem to be flattened onto the surface and partially compacted. In some discrete areas a 'glaze'-type surface was seen.

At longer times, 120 and 240 minutes, the areas of particles and 'glaze' layer gradually cover more of the surface, at 240 minutes almost the whole surface was covered with only a few areas of deformed substrate material present.

5.13.5 Analysis of wear debris

SEM micrographs of the wear debris collected from Nimonic 80A worn with Incoloy 800 are shown in **Figure 5.86**. The debris collected after 10 minutes consists of very large particles, 100 to 500μm, which appear flat, angular and highly deformed.

Debris recovered at 30 and 60 minutes has a similar appearance to that recovered at 10 minutes, although the average size of the particles is significantly smaller, 50 to 250μm. At these longer times there were also fine particles attached to the surfaces of the larger debris.

At 120 and 240 minutes the trend continues with a further decrease in the average particle size (not withstanding that debris generated in earlier stages of wear will be present in the debris from tests of longer times). The debris size at these times is approximately 50 to 100μm and there is a significant amount of fine debris (1 to 5μm) attached to the surfaces of these particles.

SEM/EDX analysis identifies the debris as comprising of iron, chromium and nickel, suggesting that it was formed from the Incoloy 800 counterface.

5.13.6 Appearance of counterfaces

At times from 10 to 60 minutes the wear tracks were torn and deformed, showing no evidence of attached debris or oxide layers. After longer times of sliding areas of shiny compacted oxide-type material surrounded by fine powdery debris (loosely attached to the wear track) began to develop.

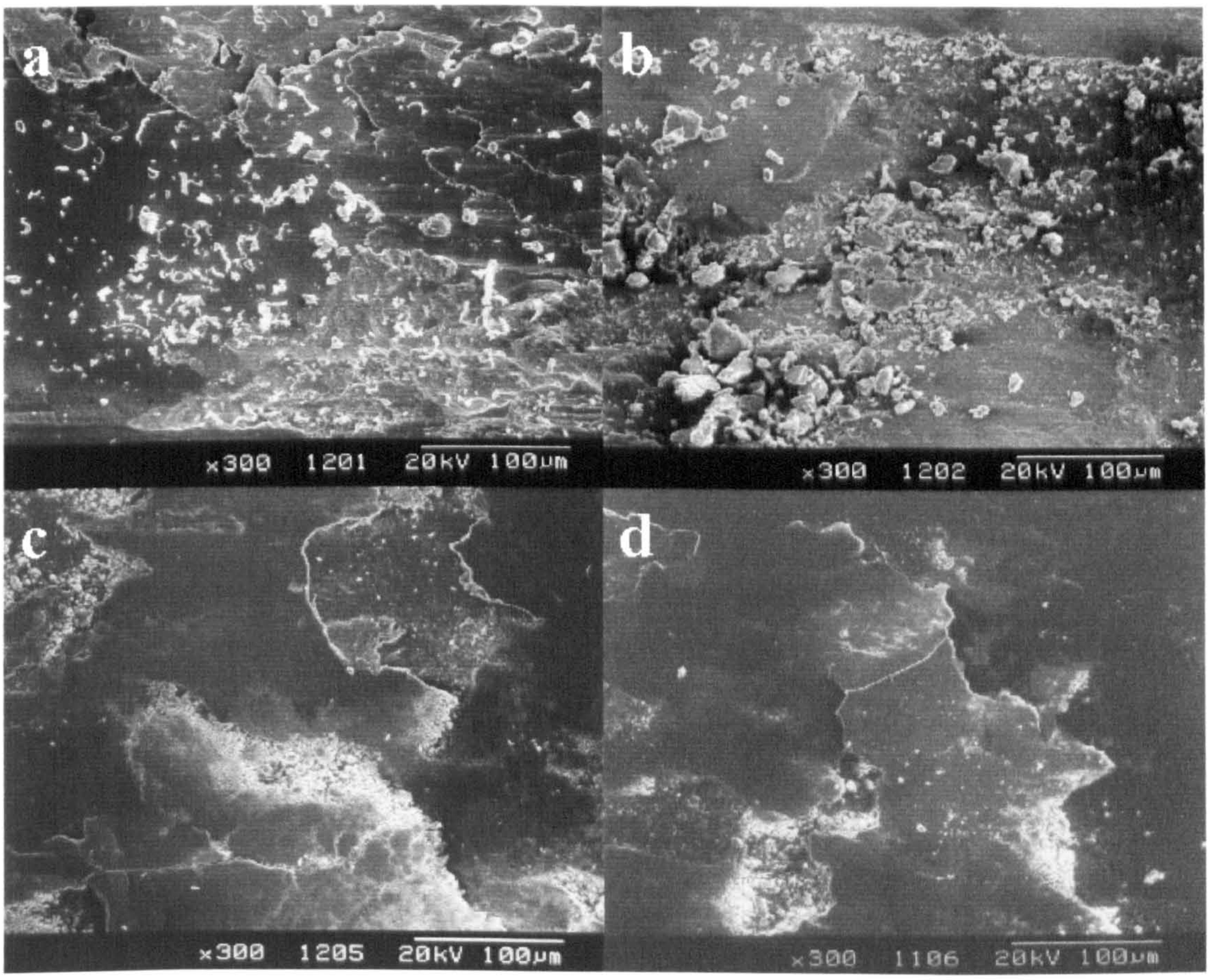

Figure 5.85 Wear scars produced on Nimonic 80A worn with Incoloy 800 at 630°C and 7N load at times of (a) 10, (b) 30, (c) 120 and (d) 240 minutes

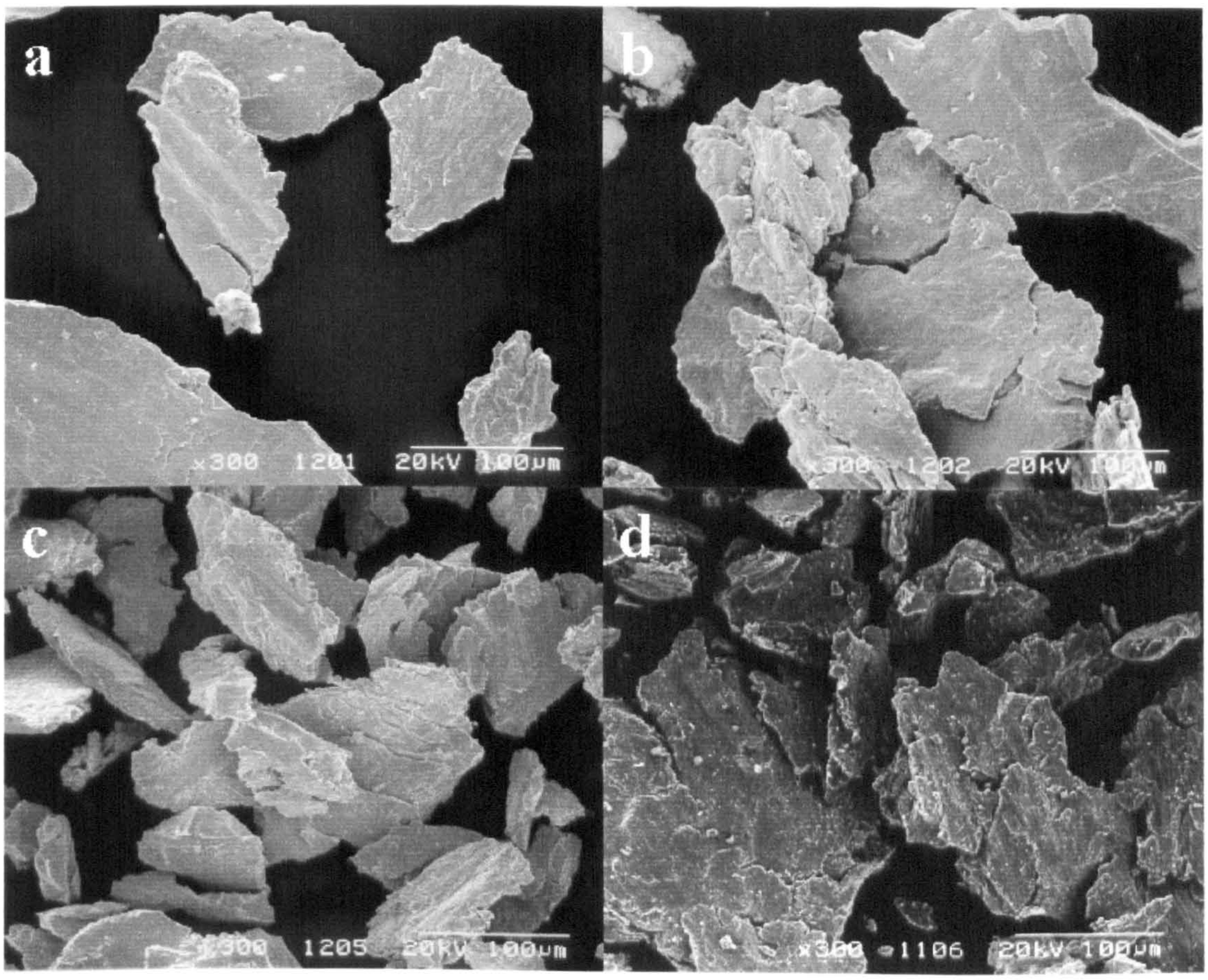

Figure 5.86 Debris recovered from the wear of Nimonic 80A samples with Incoloy 800 counterfaces at 630°C and 7N load at times of (a) 10, (b) 30, (c) 120 and (d) 240 minutes

6. Discussion

6.1 Introduction

This chapter is divided into nine sections following the approach adopted in the experimental programme, vis:

(1) Introduction.

(2) Oxidation of the alloys

(3, 4) Wear of MA956 and Nimonic 80A with Stellite 6 and Incoloy 800 counterfaces at 750°C at normal loads of 7 to 25N.

(5, 6) Wear of the four alloy combinations from room temperature to 750°C, here covering the effect of hot-hardness on the wear of the materials.

(7) Like-on-like and reversing of the samples and counterface pairs at 750°C.

(8, 9) Wear of Nimonic 80A and MA956 with Incoloy 800 at the minimum temperature of compacted oxide layer formation over a range of times.

It is important to note that the formation of compacted oxide layers and the subsequent wear resistance of these layers are highly dependent upon the sliding conditions. Differences which are due to the configuration of the sliding couple – which in turn effects the retention of debris, the out-of-contact oxidation of the samples and counterfaces together with the effects of frictional heating – can only be estimated by comparison with other high temperature wear studies.

6.2 High temperature properties of the test alloys

6.2.1 Oxidation properties of the test alloys

The materials employed in this project are described as 'oxidation resistant' up to ~1000°C. At the temperatures of the present study all the test alloys form protective oxide scales. The four alloys used have been shown not to undergo any significant weight changes at the times and temperatures of the wear tests used [7].

The high (5% wt) aluminium content of MA956 leads to the formation of an alumina scale under air oxidation, which due to the presence of yttrium in the alloy has a very low growth rate [93, 94]. Nimonic 80A, Stellite 6 and Incoloy 800 developed predominately chromina scales with some proportion of the scale formed from other alloying elements. In the case of Nimonic 80A and Incoloy 800, this would be nickel oxide (NiO) [95-97]. For Stellite 6 a chromina scale combined with various cobalt chromium oxides were reported [98] during air oxidation.

Unfortunately no directly comparable data appear to allow the quantitative comparison of the oxidation rates of the four alloys employed in this study. However for the purpose of understanding wear it is important to realise that steady-state oxidation kinetics will not be reached before the oxide film is affected by the wearing processes. The action of the wearing processes will also influenced the materials producing, increases in the oxidation rates.

6.2.2 High temperature strength properties of the test alloys

Hot hardness data collected for the four alloys show a steady decrease in the hardness from room temperature to ~450°C. At 510°C – the highest temperature at which hardness data could be obtained – a marked decline in hardness took place.

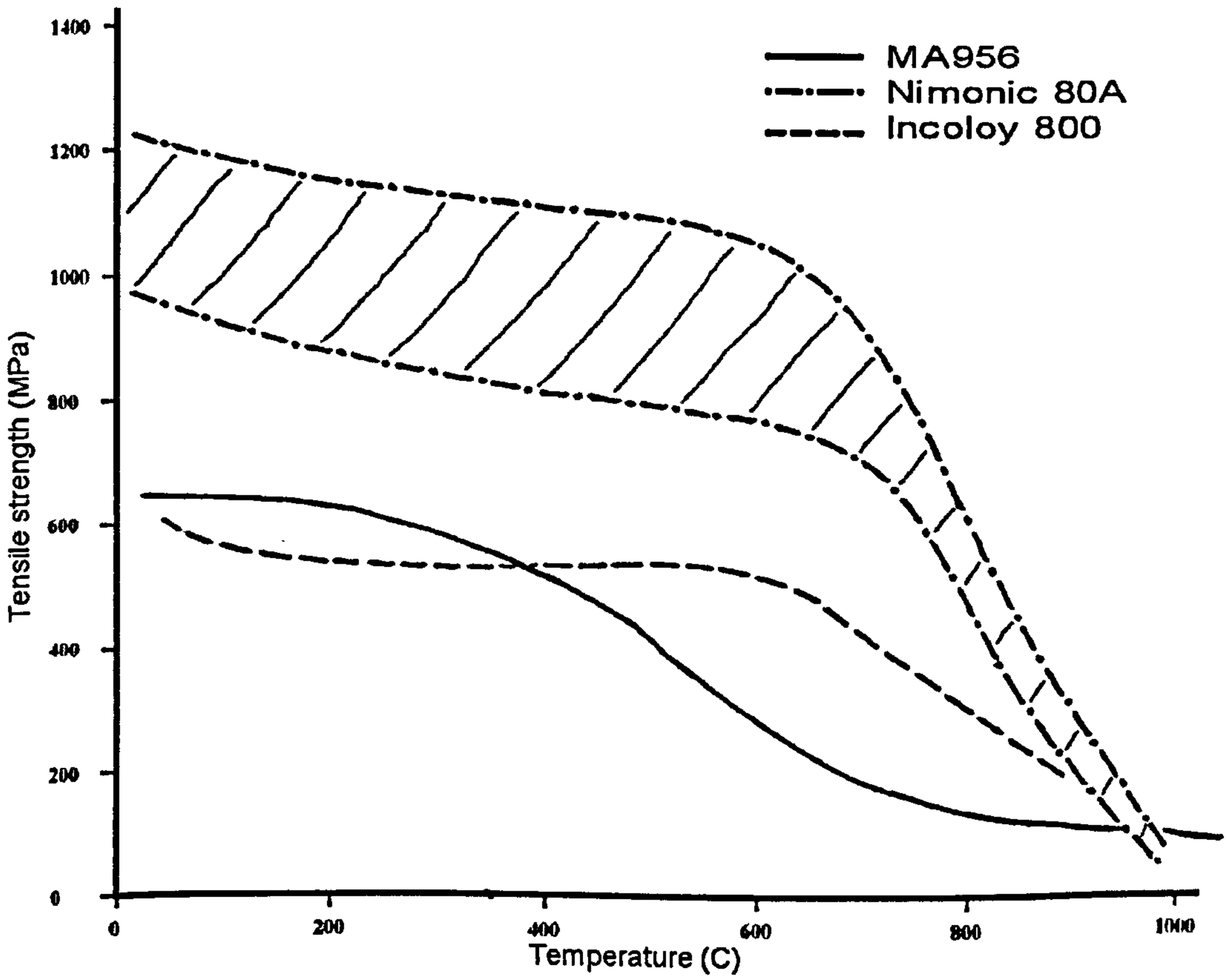

Figure 6.1 High temperature tensile strength of MA956 (cold-rolled sheet) [94], extruded Nimonic 80A bar. Heat treated 8 hours at 1080°C and air cooled, plus 16 hours at 700°C and air cooled 98% confidence region calculated on 13 casts [98] and Incoloy 800 (hot-rolled rod) [99]

However, for MA956, Nimonic 80A and Incoloy 800 the tensile strength of the alloys decreased considerably from ~500°C. This coincided with the fall in

hardness seen with the highest temperature measured with the hot hardness data. Tensile strengths of MA956, Nimonic 80A and Incoloy 800 are shown in **Figure 6.1**.

For Stellite 6 a similar decline in hardness and tensile strength would be expected. It is known that cobalt undergoes a phase change, circa 417°C, from a close-packed hexagonal structure to a face-centred cubic structure [100]. This change leads to a marked decrease in the wear resistance and an increase in the coefficient of friction, as was demonstrated by Burckley [72] – shown in **Figure 6.2.** It is known that this phase transition is rather sluggish and for cobalt-based alloys the addition of alloying elements has the effect of raising this transition temperature [72].

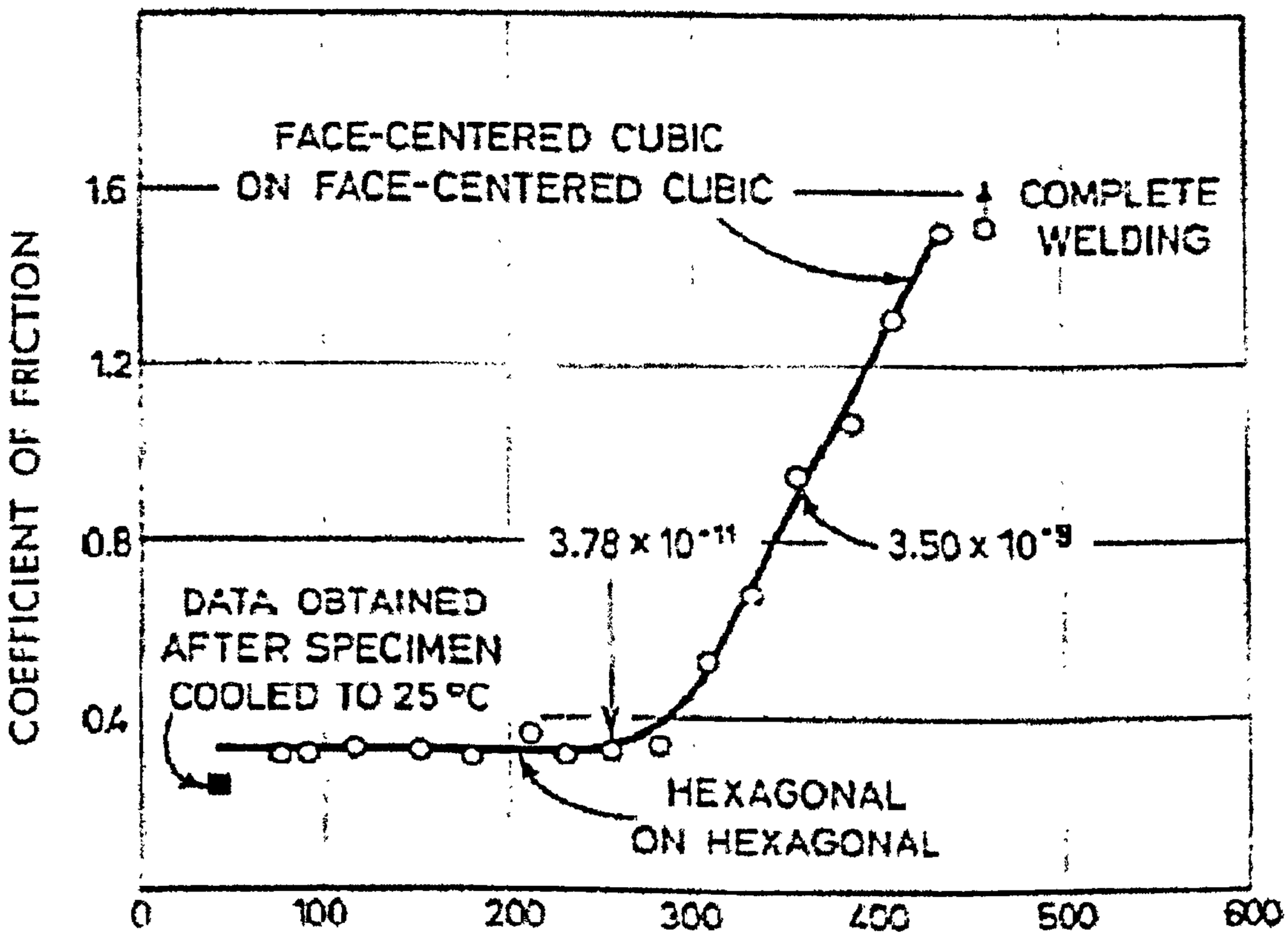

Figure 6.2 Coefficient of friction of cobalt sliding on cobalt in vacuum at various temperatures. 10^{-9} torr, 198 com/sec, 1000g Rider wear rates are in cm^3/cm of sliding [72].

However this phase transition led to a marked change in the wear properties of cobalt, as greater adhesion is given by the face-centred cubic structure c.f. the hexagonal close-paced structure which is present at room

temperature. With further increases in temperature the friction continues to rise until complete welding is obtained.

6.3 Wear testing of MA956 with two counterfaces over a range of loads (7 to 25N) at 750°C

MA956 worn with Stellite 6 and Incoloy 800 counterfaces from 7 to 25N at 750°C showed similar wear/load characteristics for both counterfaces (**Figure 5.2**). Both systems allowed the formation of compacted oxide layers. The Stellite 6, however, gave consistently lower weight losses than the Incoloy 800 counterface.

The oxide layers formed across the range of loads for both counterfaces were of similar appearance, although not exactly identical (**Figure 5.7**). For both counterfaces the wear increased linearly with load up to 20N, which suggests that there was no change in the wear mechanism across this range [17]. At 25N there was a marked increase in the weight losses for samples worn with both counterfaces. This increase in weight loss coincided with increased cracking of the surface layers, implying greater break-up of the layers.

For samples worn with Stellite 6 counterface the compacted oxide layers formed comprised almost wholly cobalt/chromium oxides transferred from the counterface. The layers on MA956 worn with an Incoloy 800 counterface were predominantly formed of MA956 material – iron and chromium oxides – only traces of transferred material were detected (**Table 5.2**).

Another important difference between the two systems was that the coefficient of friction recorded for the MA956/Stellite 6 system (0.75–1.00) (**Figure 5.3**) was consistently higher than that seen for the MA956/Incoloy 800 system (0.45–0.65) (**Figure 5.4**).

For the MA956/Stellite 6 system in the initial stages of wear, pre-formed oxides were removed, and the effects of temperature and relative motion produced wear debris [73]. The higher oxidation rate of the Stellite 6 led to the production of large quantities of Co/Cr debris under 'oxidational wear' conditions by the processes of oxidation, oxide removal, reoxidation. This debris produced from the Stellite 6 rapidly adhered to the contacting surfaces. The high temperature facilitated rapid compaction and sintering of the debris resulting in the formation of 'glaze'-type layers on the contacting surfaces, so protecting the MA956 from further wear.

The cobalt/chromium oxide layer also appeared to possess good adhesion (to the MA956 samples) and cohesion enabling a substantial layer to build-up. This adhesion of the oxide layers on the counterface and sample also led to the higher coefficient of friction compared to the MA956/Incoloy 800 counterface. The processes described above are presented in **Figure 6.3 (a)**.

(a) MA956 worn with Stellite 6 counterfaces from 7 to 25N at 750°C

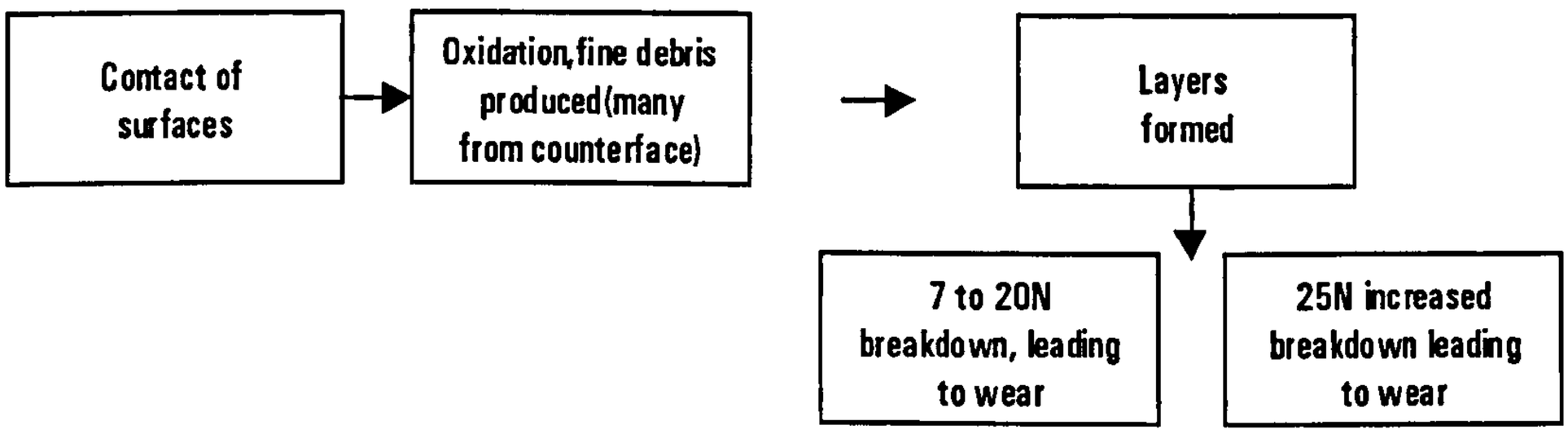

(b) MA956 worn with Incoloy 800 counterfaces from 7 to 25N at 750°C

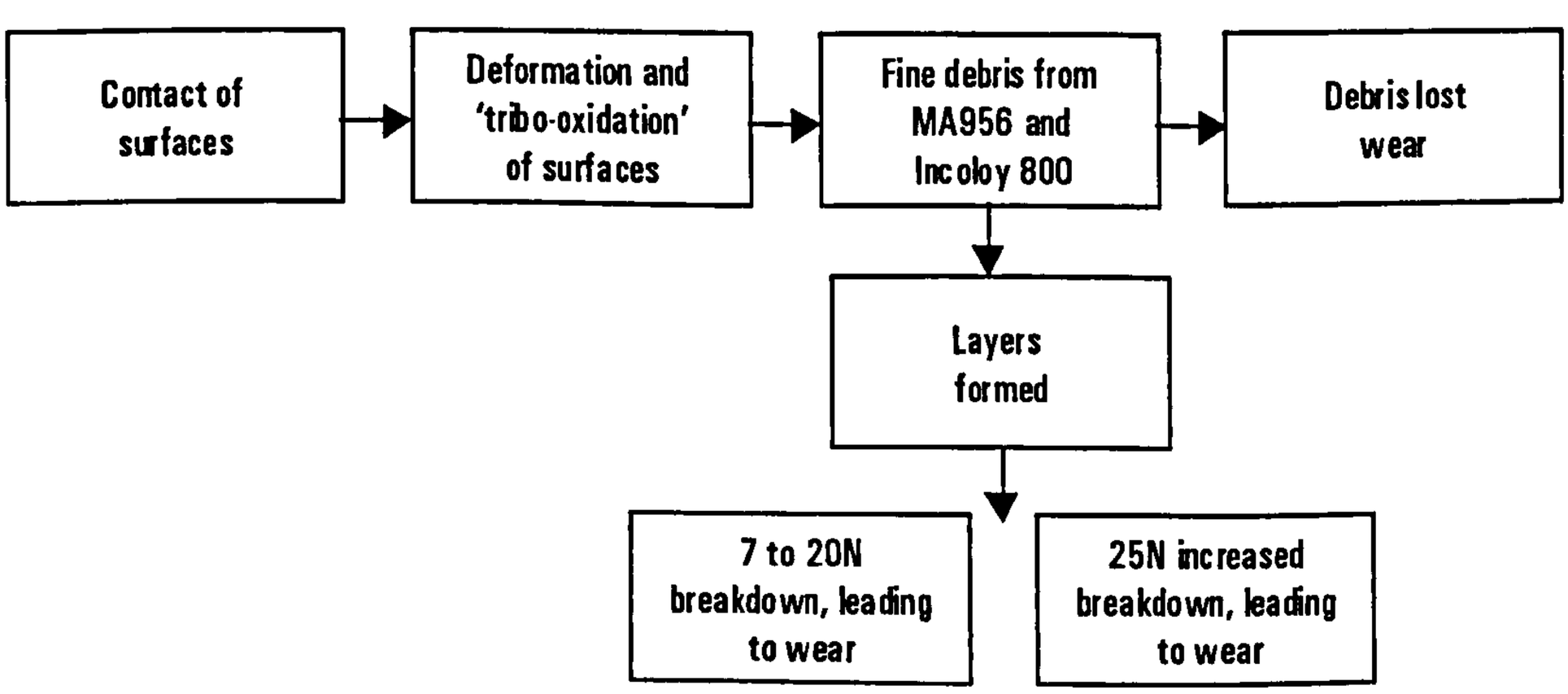

From 7 to 20N load, wear is proportional to load and compacted oxide layers form. For Stellite 6 counterfaces there is a greater level of transfer so resulting in lower weight losses. For Incoloy 800 counterface greater deformation of the sample gives rise to sufficient oxidation for layers to form. At 25N load both counterfaces show a greater level of layer breakdown.

Figure 6.3 Mechanisms of wear identified for MA956 worn with Stellite 6 and Incoloy 800 counterfaces at 750°C at loads 7 to 25N

The MA956/Incoloy 800 counterface system showed a similar wear mechanism to the MA956/Stellite 6 counterface system. Here the iron/chromium oxides which the layer comprised are generated from the sample, and to a limited extent from the counterface. Fine oxide debris were produced in the initial stages

of wear, by the deformation and subsequent oxidation of the surfaces [35] – again via oxidation-scrape-reoxidation [73]. This debris was then able to adhere to the contacting surfaces so enabling a compacted oxide layer to form. However due to the lack of significant transfer from the counterface, the samples worn with an Incoloy 800 counterface experience a greater weight loss than those worn with Stellite 6. This mechanism is displayed schematically in **Figure 6.3 (b)**.

Above 25N the compacted layers formed upon the MA956 samples worn with both counterfaces appeared to undergo an enhanced rate of layer break-down. When an area of the layer was broken-up by the action of the counterface (or sample) material was lost before the layer was able to regenerate, so leading to a higher wear rate. This would appear to relate to the ability of MA956 to support the layer as the break-down occurs at the same load for both counterfaces. Note: large fragments of compacted oxide layer seen in the wear debris (**Figure 5.11**) are too large to be retained within the system once they are detached from the wear scars.

6.4 Wear testing of Nimonic 80A with two counterfaces over a range of loads (7 to 25 N) at 750°C

For Nimonic 80A worn with Stellite 6 and Incoloy 800 counterfaces a similar pattern of weight losses was seen over the range of loads (**Figure 5.11**). At 7 and 10N load, weight losses were low for both counterfaces. The weight losses given with Incoloy 800 were significantly lower than those observed for the Stellite 6 counterface. From 15 to 25N the weight losses increased rapidly with load. At these loads the weight losses were not significantly different between the two counterfaces.

For Nimonic 80A/Stellite 6 counterface, XRD analysis showed no oxide present upon the sample's surfaces at any of the loads tested (**Table 5.5**) only the peaks corresponding to the phases characteristic of Nimonic 80A were found. However SEM/EDX analysis revealed many of the fine wear particles present on the surface were cobalt-chromium material from the counterface. From the appearance of the wear scar it would appear that an oxidational wear mechanism was in operation (**Figure 5.16**), although the formation of a compacted oxide layer was unable to take place.

This wear mechanism remained unchanged across the range of loads examined. The weight loss/load profile gained its shape from the changing area of contact, due to the loss of material from the sample, leading to a levelling-off of

weight losses at higher loads. (Reciprocation of the sample could not be used when the sample arm was operating under increased load).

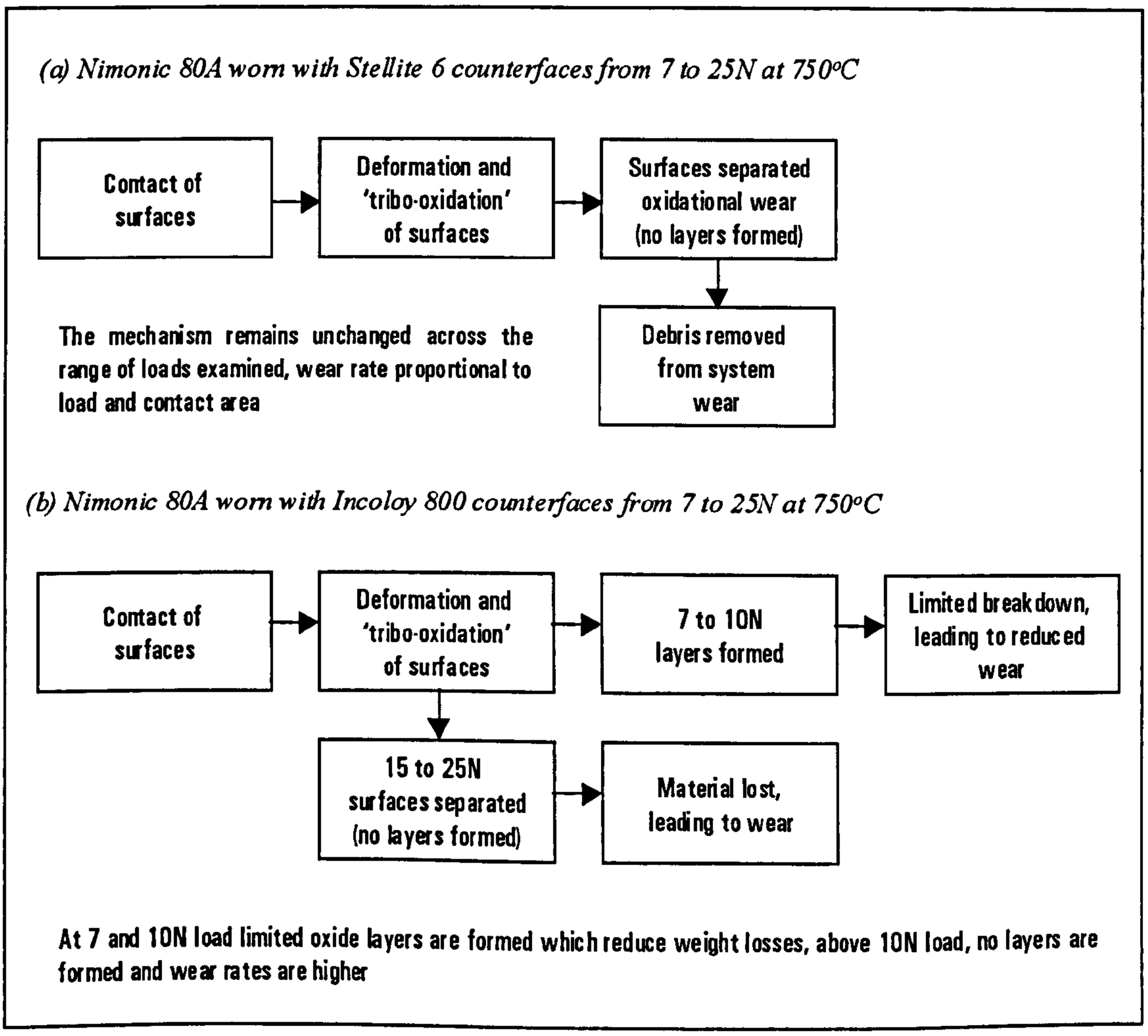

Figure 6.4 Mechanisms of wear identified for Nimonic 80A worn with Stellite 6 and Incoloy 800 counterfaces at 750°C at loads 7 to 25N

The absence of layer formation would appear to relate to insufficient adhesion and cohesion of debris upon the contacting surface together with the ploughing effect of the counterface. This lack of layer formation led to the 'smeared' appearance of the debris on the sample surface. This mechanism is shown in **Figure 6.4 (a)**.

For the Nimonic 80A/Incoloy 800 counterface system, compacted oxide layers were seen to form at 7 and 10N load (**Figures 5.16** and **5.18**). Here, the presence of fine oxide debris within the interface facilitated layer formation. The debris was produced by an oxidational-type mechanism, equating to oxidation-scrape-reoxidation. The layer was shown to be nickel oxide (NiO) originating from either the sample or counterface (**Table 5.5**).

It would appear that up to 10N load the debris was able to undergo compaction and sintering. Cohesion and adhesion of the layer appeared to be relatively poor as the layer did not appear to cover the whole scar, and was unstable at higher loads. At higher loads an oxidational wear mechanism similar to that seen with a Stellite 6 counterface operated and compacted debris layers were unable to form. The mechanisms for Nimonic 80A/Incoloy 800 counterface are presented in **Figure 6.4 (b)**.

6.5 MA956 worn with Stellite 6 and Incoloy 800 counterfaces at ~25 to 750°C

6.5.1 Sliding of MA956 samples worn with Stellite 6 counterface at ~25 to 750°C

MA956 worn with Stellite 6 counterfaces over the range of temperatures ~25 to 750°C showed three distinct wear regimes. The temperature ranges were marked by low wear between ~25 and 390°C (**Figure 5.20**), increased weight losses were given, between 450 and 510°C. Then from 510°C the weight loss decreased with increasing temperature. This reduction in weight loss coincided with the formation of compacted oxide layers on the surfaces (**Figure 5.25**) up to 750°C.

In the low temperature range, ~25 to 390°C, the samples' weight losses were low and their surfaces were covered with fine debris particles (**Figure 5.25**). These particles on the contacting surfaces – comprising cobalt/chromium oxide – behaved as a 'third-body' which prevented direct metal-to-metal contact of the sample and the counterface so reducing deformation and adhesion. The absence of hardened surface layers (**Figure 5.29**), the low weight losses and the presence of small particles on the samples' surface confirmed this. No evidence could be found for the debris within the interface behaving as an abrasive [43].

The nature of the debris (**Figure 5.27**), fine particles from 1 to 5μm, implied an oxidational-type mechanism where oxides are produced on the surfaces and removed by subsequent traverses of the counterface/sample. The collected debris were similar in size and constitution to the particles present on the wear-affected surfaces. The absence of sample/counterface adhesion was caused by the presence of the particles between the two surfaces. Hence work hardening and formation of large particles were prevented (**Figure 5.29**). This

type of mechanism produced low wear, although without the formation of a 'compacted' layer. This wear mechanism is shown in **Figure 6.5 (a)**.

The marked increases in weight loss (**Figure 5.20**) observed from 450 to 510°C were accompanied by the absence of fine wear particles on the scars' surface and the presence of highly torn and deformed surface features (**Figure 5.25**). This indicated increased deformation caused by the reduction in strength of the materials at ~500°C, favouring a severe wear mechanism and the production of large wear particles (**Figure 5.27**). Hence the change in mechanism related to the reduction in the resistance to deformation giving rise to a situation where an oxidational mechanism was unable to become established, and the fine oxide debris required to separate the surfaces was not generated.

This direct contact of the sample and counterface led to deformation and working of the wear scars and tracks (**Figure 5.29**), so producing large fragments of debris. The plate-shape of the wear particles suggested a delamination-type mechanism [28], so giving rise to the high rates of material loss. This mechanism is shown schematically in **Figure 6.5 (b)**.

From 510°C to 750°C, compacted oxide layers were seen to form upon the samples' surface and the weight losses were reduced with increasing temperature. From 510°C fine wear debris consisting of predominantly cobalt-chromium material was produced and so able to adhere [58] to the samples' surfaces and undergo layer formation. The appearance of the first, fine oxide material promoted separation of the surfaces, further encouraging oxidational wear and layer formation.

The reduced wear observed with increasing temperature in the range 510 to 750°C was accompanied by the formation of compacted oxide layers. Over this temperature interval the production of fine wear debris – having the ability to adhere at high temperature to the surfaces – facilitated layer formation. Increased oxidation at high temperature led to the production of a large amount of small oxide particles which had strong adherence to the surface, these particles underwent sintering and compaction promoting the formation of surface 'glaze' layers.

The layer contained significant amounts of cobalt (**Table 5.6**), transferred from the counterface, although the layer also contained iron and chromium originating from the sample. This showed that large amounts of cobalt/chromium debris generated from the counterface went to form the layer on the samples, as was seen in the study on the effect of load (**Section 6.2**). This transfer effect

appeared to relate to the 'out-of-contact' oxidation time of the counterface and the track's larger surface area compared to that of the sample's wear scar. This enabled production of more suitable debris for the formation of the compacted layer to be supplied to the sample by the counterface.

(a) MA956 worn with Stellite 6 counterfaces from ~25 to 390°C

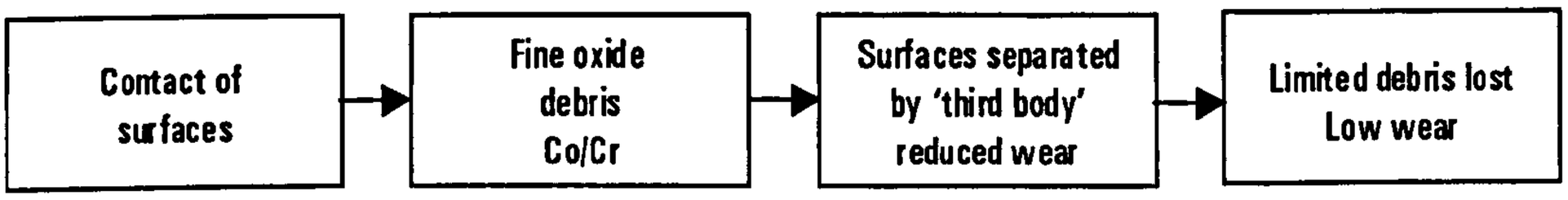

Separation of the surfaces by oxide debris leads to low adhesion and low wear

(b) MA956 worn with Stellite 6 counterfaces from 450 to 510°C

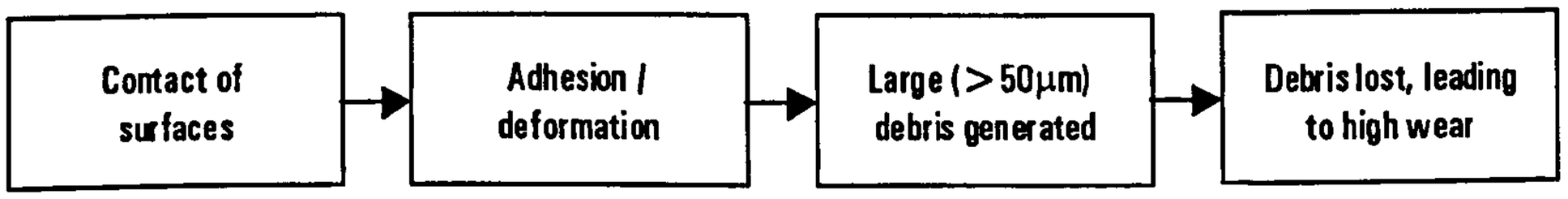

Large debris unable to remain in the interface leading to adhesion and high wear rate and highly damaged surfaces. Flat angular debris suggests delamination wear

(c) MA956 worn with Stellite 6 counterfaces from 510 to 750°C

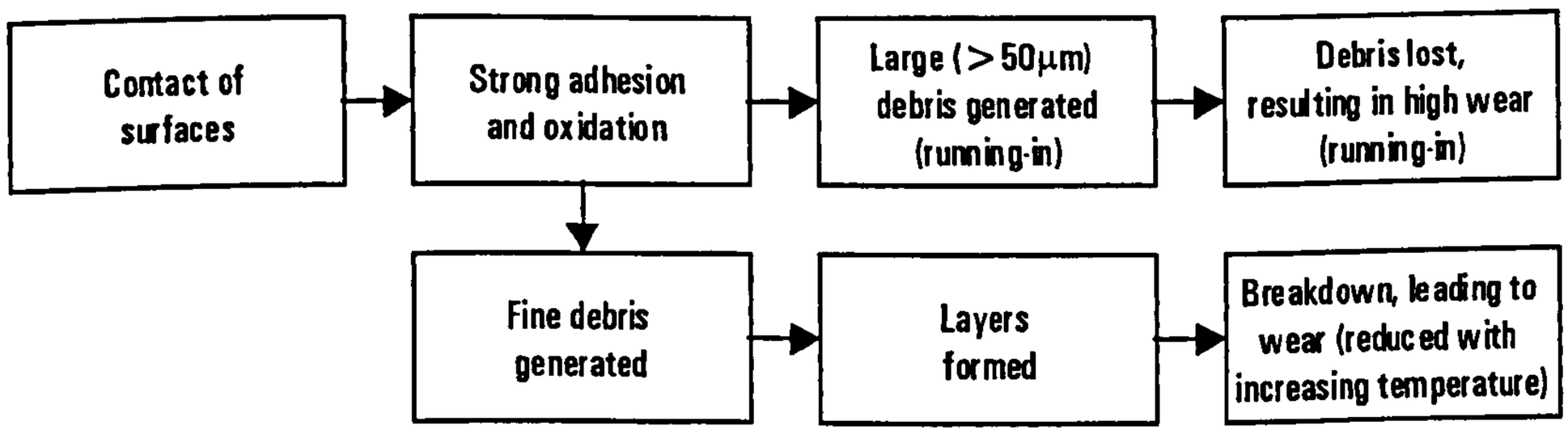

After the initial running-in period of high wear, compacted layer separates the surfaces preventing adhesion and the production of large debris particles so giving rise of low wear

Figure 6.5 Wear mechanisms for MA956 worn with Stellite 6 counterfaces from ~25 to 750°C at 7N load

Large fragments of debris (**Figure 5.27**), some of which showed features of the compacted oxide layer surface, were found in the wear debris. This offers an explanation to the high weight losses recorded at temperatures at which oxide

layers are seen to form. A period of 'running-in' severe wear occurred before the layers are established – this 'running-in' step become shorter with increasing temperature. At higher temperatures the layers were more stable, so leading to reduced break-down and reformation [62]. This mechanism is shown in **Figure 6.5 (c)**.

6.5.2 Sliding of Stellite 6 samples with MA956 counterface at 750°C

For Stellite 6 worn with MA956 counterfaces at 750°C the weight loss data showed a small weight gain (**Figure 5.42**) and a stable coefficient of friction from the start of the test (**Figure 5.43**). A smooth compacted oxide layer formed upon the sample, of iron/chromium material (**Figure 5.48**), transferred from the counterface in an oxidised state. XRD data (**Table 5.6**) showed this to be chromium iron oxide. The debris generated (**Figure 5.46**), consisted of broken-up fragments of compacted oxide material and fine debris.

Here the wear mechanism was strongly influenced by the transfer of oxide material from the counterface to the sample to generate a compacted oxide layer. The compacted oxide layer comprised oxides of iron and chromium transferred from the counterface. The oxidational wear mechanism was rapidly established indicated by the presence of low coefficients of friction achieved soon after the start of the test (**Figure 5.43**). This observation was consistent with the view that deformation and oxidation [35] of the surface led to the generation of fine oxidational-type wear debris from the counterface which gave rise to the rapid formation of a compacted oxide layer at the sample surface. This compacted layer lost its stability when cooled from 750°C to room temperature as indicated by the spallation of the layer (**Figure 5.46**) which was not seen in other cases. The mechanism responsible for this type of behaviour is shown in **Figure 6.6**.

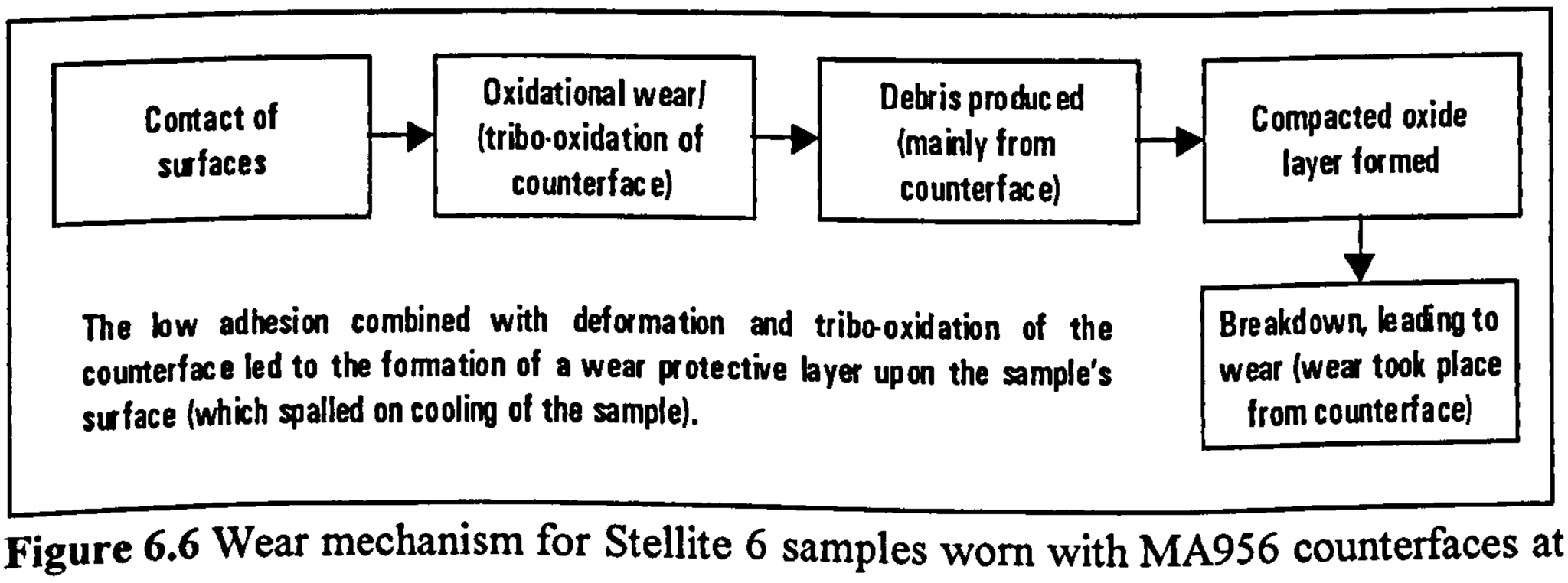

Figure 6.6 Wear mechanism for Stellite 6 samples worn with MA956 counterfaces at 750°C and 7N load

6.5.3 Sliding of MA956 samples worn with Incoloy 800 counterface at ~25 to 750°C

The wear of MA956 with Incoloy 800 counterfaces showed two distinct wear regimes in the range of temperatures examined. Low weight losses in the range 25 to 150°C and high weight losses in the range 270 to 630°C, both equated to a severe wear mechanism. The decrease in weight losses between 690 and 750°C (**Figure 5.20**) coincided with the onset of compacted oxide layer formation (**Figure 5.26**).

(a) MA956 worn with Incoloy 800 counterfaces from ~25 to 630°C

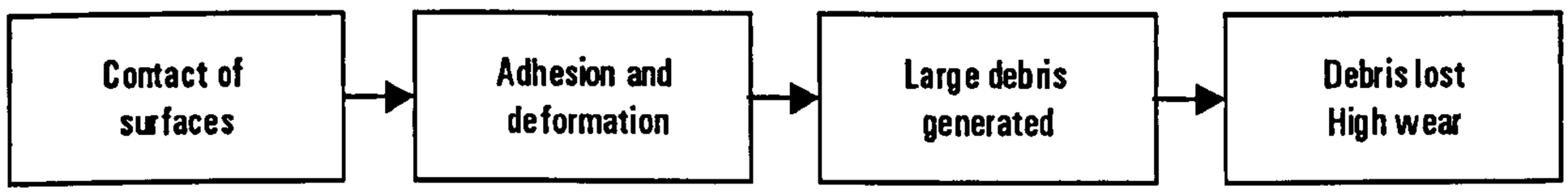

The wear mechanism remains unchanged from ~25 to 630°C, although the wear rates increase significantly with the loss of strength of the alloys with increasing temperature. Large debris unable to remain in the interface leading to adhesion and high wear rate and highly damaged surfaces

(b) MA956 worn with Incoloy 800 counterfaces at 690 and 750°C

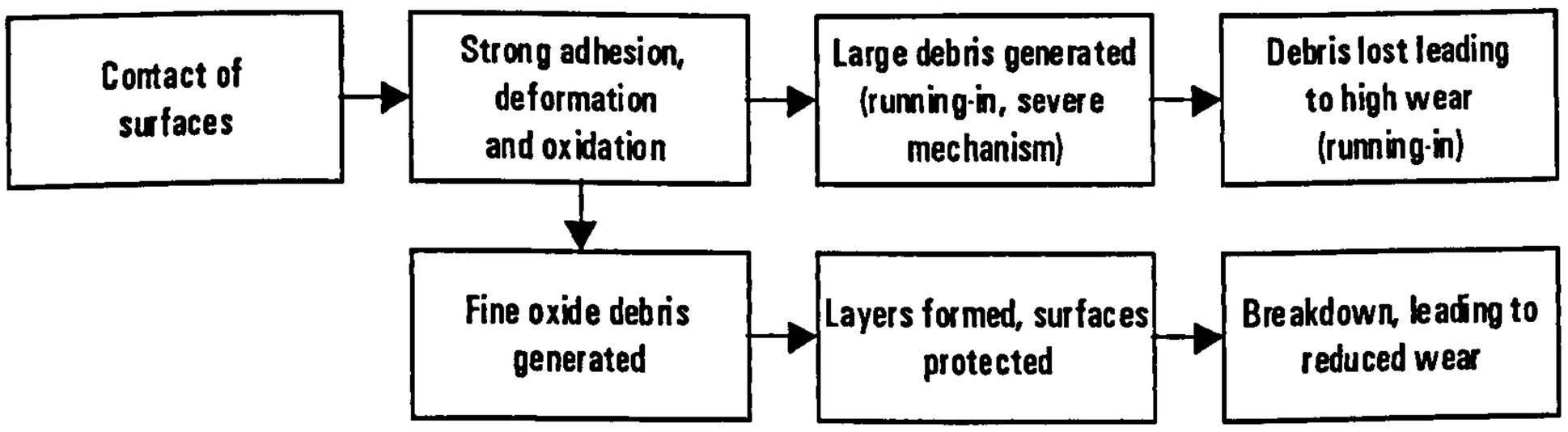

After the initial running-in period of high wear, compacted layer separates the surfaces preventing adhesion and the production of large (> 50μm) debris particles so giving rise to low wear. The compacted layers formed on the oxidised highly deformed layers (from which the debris was generated) giving the appearance of a double layer, the origins of each layer are revealed by the transferred material presence and absence

Figure 6.7 Wear mechanism for MA956 worn with Incoloy 800 counterfaces from ~25 to 750°C at 7N load

At ~25 and 150°C the wear mechanism was of a severe-type where insufficient production of oxide debris led to the formation of large wear debris (**Figure 5.28**) and gave rise to highly deformed surfaces. However due to the

relatively high strength of the materials at these temperatures, giving a high resistance to deformation, the wear rates were relatively low. This was demonstrated by the hardened surface layers only extending to a depth of 20μm from the surface (**Figure 5.30**).

The increased weight losses observed at 270 to 630°C were caused by the decrease in strength with increasing temperature (**Figure 6.1**). From 510°C the marked increase in weight losses coincided with further decreases in the strength of the alloys. The higher hardness of the surface layers (~6.5 MPa, **Figure 5.30**) indicated a higher degree of work hardening. The wear mechanism which operated between ~25 to 150°C did not change up to 630°C. The plate-like debris originating from the deformed layer led to the higher rates of material loss.

At 690 and 750°C further increases in material loss and possible run-away adhesion and junction growth were arrested by the formation of compacted oxide layers on the contacting surfaces, the appearance of fine debris attached to the large wear particles (**Figure 5.28**) indicated a change in wear mechanism. The highly deformed surfaces produced in the 'running-in' period, responsible for the high weight losses, were able to oxidise. The oxidised surfaces participated in the production of fine debris, from which layer formation took place. The double layer (**Figure 5.53**) comprising a compacted layer on the top of a partially oxidised layer demonstrated the stages of the development of compacted layers in this range (690 to 750°C). The rapid formation of compacted layers produced marked reductions in weight losses.

With further increases in temperature the generation of layers took place more rapidly giving further reductions in weight losses. A more detailed study of the formation of the surface layers at 690°C is given in **Section 6.8**. A schematic summary of the wear mechanisms, in the temperature range 25 to 630°C and 690 to 750°C, is presented in **Figure 6.7**.

6.5.4 Sliding of Incoloy 800 samples with MA956 counterface at 750°C

The rapid development of a very high coefficient of friction (**Figure 5.49**) occurred with this sliding couple and to prevent damage to the wear rig the test was stopped after ~ 20 minutes.

The high levels of friction were associated with the formation of a highly deformed wear scar containing transferred metallic material from the counterface (identified via XRD analysis – **Table 5.7**). Together with the absence

of oxide material on the sample surface, the production of large debris indicated a severe wear mechanism was caused by the high compatibility of the surfaces and there low oxidation rates.

The lower friction coefficient observed with the Incoloy 800/MA956 counterface system but not with the MA956/Incoloy 800 counterface system (**Figure 5.49**) was caused by the rapid production of oxide debris, strongly suggested a higher oxidation rate of Incoloy 800 wear damage surfaces compared to MA956 [101-102]. This effect was due to the relatively larger surface area of the Incoloy 800 (counterface) with this configuration so preventing metal-to-metal contact and formation of adhesive junctions. This mechanism is shown in **Figure 6.8**, the mechanism for the MA956/Incoloy 800 system is given in **Figure 6.7 (b)**.

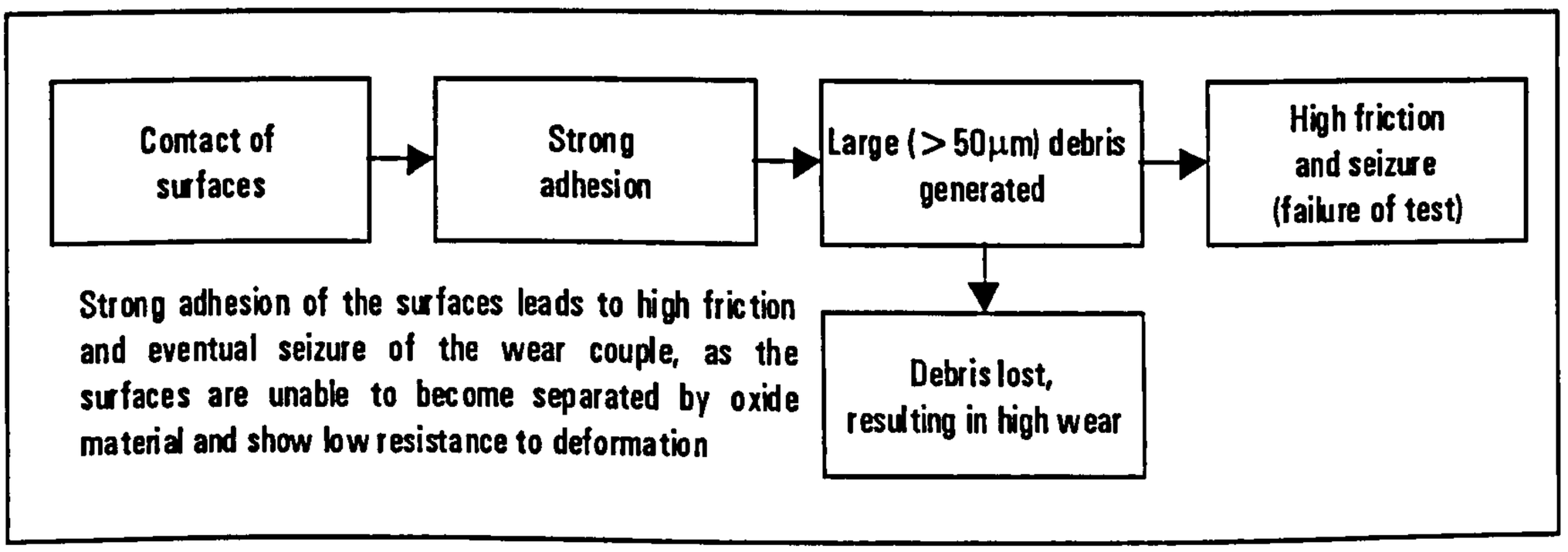

Figure 6.8 Wear mechanism of Incoloy 800 with MA956 counterface at 750°C at 7N load

6.6 Nimonic 80A worn with Stellite 6 and Incoloy 800 counterfaces at ~25 to 750°C

6.6.1 Sliding of Nimonic 80A samples worn with Stellite 6 counterface at ~25 to 750°C

The three wear regimes displayed by Nimonic 80A worn with a Stellite 6 counterface over the temperature range ~25 to 750°C are reflected in the weight losses (**Figure 5.31**). In the temperature range ~25 to 450°C the formation of fine wear debris (containing cobalt) originating from the counterface was seen to cover the surfaces (**Figure 5.36**). This separated the sample and counterface and so prevented metal-to-metal contact via a third-body mechanism and thereby reduced wear.

From ~25 to 450°C the wear rates were low and the sample surfaces were covered with fine oxide debris (**Figure 5.36**). SEM/EDX examination showed the

wear samples to contain cobalt originating from the counterface. However no cobalt-containing material was detected by X-ray diffraction – only phases corresponding to Nimonic 80A alloy were present (**Table 5.8**). The fine debris on the surfaces, combined with the low weight losses, demonstrated that the surfaces were separated by the fine cobalt/chromium debris. This prevented metal-to-metal contact by behaving as a 'third-body' thus preventing adhesion and severe wear.

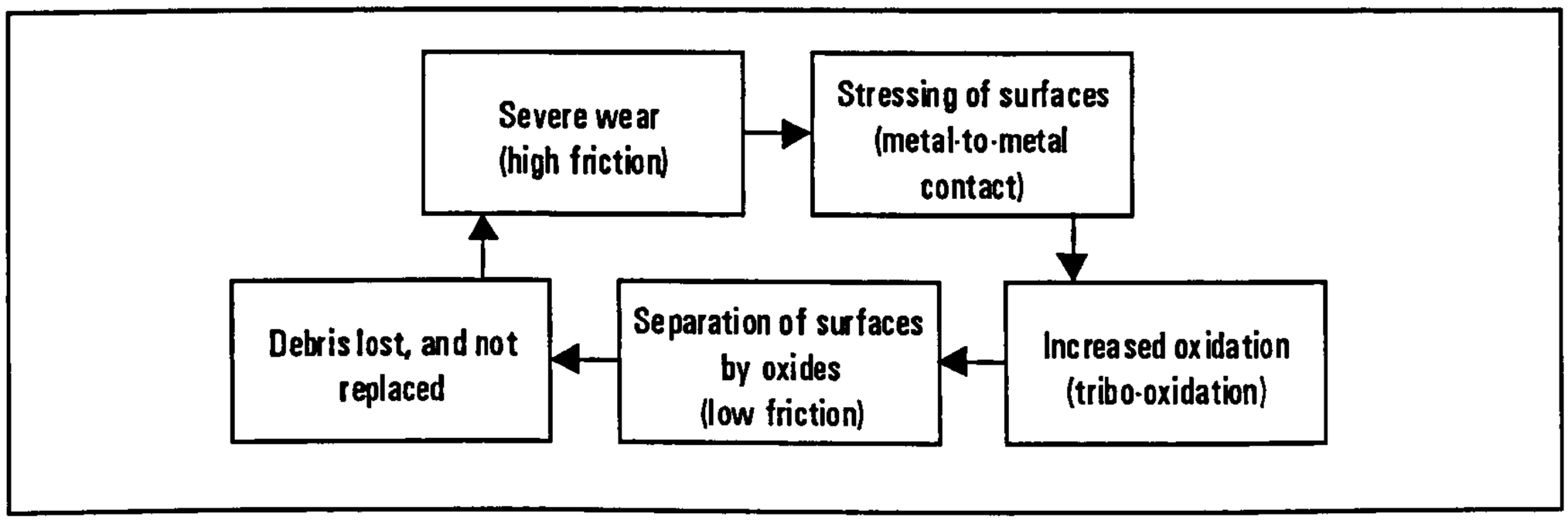

Figure 6.9 Possible processes occurring with Nimonic 80A worn with Stellite 6 at ~25°C accounting for the fluctuations in coefficient of friction

At 25°C (**Figure 6.9**) the mechanism probably underwent a cyclic process of metal-to metal and oxide-to-oxide contact, as shown by the friction coefficient fluctuations between two ranges of 0.40–0.50 and 0.75–1.05. From 150 to 450°C there was sufficient oxidation to keep the surfaces separated and the friction remained low. The were mechanism for Nimonic 80A/Stellite 6 counterface system from ~25 to 450°C is shown in **Figure 6.10 (a)**.

From 510 to 630°C the appearance of the wear surface in a deformed and torn state, the absence of attached debris on this surface, and the production of both large and small debris (**Figure 5.38**) indicated the operation of a severe wear mechanism due to metal-to-metal contact. The formation of a deformed surface layer (**Figure 5.40**) led to the production of large wear debris.

This change in the wear mechanism at ~500°C indicated that increasing weight losses were associated with a marked reduction (**Figure 6.1**) in the strength of Nimonic 80A, and a phase change occurred with cobalt-based alloys. Once the severe mechanism was established, insufficient fine debris was produced to separate the surfaces. These processes are shown in **Figure 6.10 (b)**.

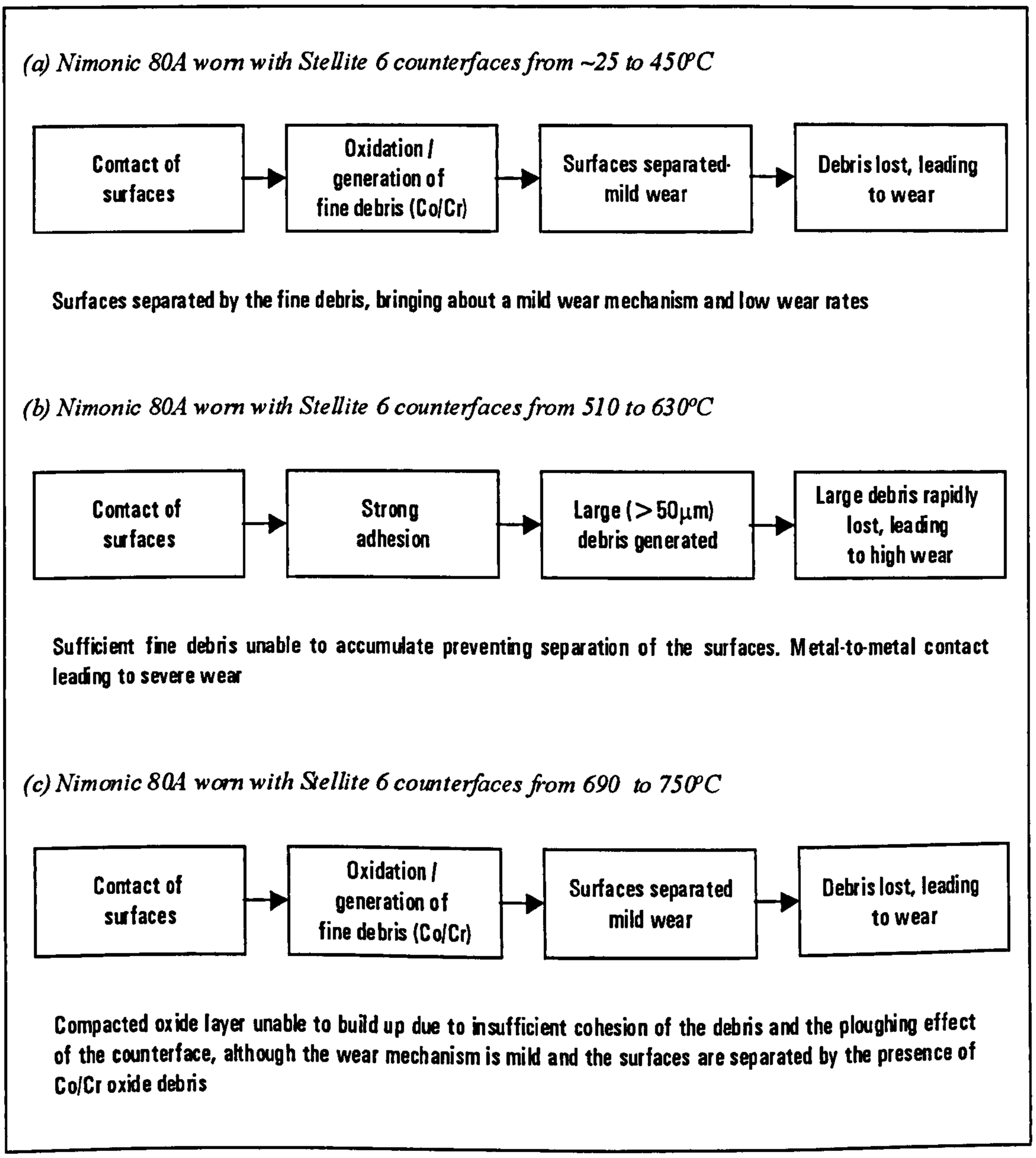

Figure 6.10 Wear mechanisms for Nimonic 80A worn with Stellite 6 from ~25 to 750°C at 7N load

A second transition in the wear mechanism, indicated by decreasing weight loss (**Figure 5.31**), in the temperature range 690 to 750°C, appeared to be brought about by an increase in the oxidation rate of the highly deformed wear surfaces of the materials involved favouring an oxidational-wear mechanism. Under these conditions sufficient oxide was present between the contacting surfaces to bring about a 'mild' wear mechanism. This prevented metal-to-metal contact and adhesion between the surfaces, thereby reducing the weight losses. The Nimonic 80A/Stellite 6 counterface system was unable to form a compacted oxide layer. This appeared due to the lack of adhesion of the debris to the scar

surface combined with the increased ploughing effects of the Stellite 6 counterface [7]. This wear mechanism is shown in **Figures 6.10 (c)**.

6.6.2 Sliding of Stellite 6 samples with Nimonic 80A counterface at 750°C

The formation of a compacted debris layer from counterface-generated material – indicated by the presence of nickel oxide (**Table 5.8**) – resulted in low wear (**Figure 5.54**) and a low coefficient of friction throughout the test (**Figure 5.55**).

The initial stages of wear resulted in the generation of oxide material from the counterface, which rapidly adhered to the sample surface to form a compacted oxide layer (**Figure 5.58**). The friction coefficient results indicated oxide-to-oxide contact. The sample damage was minimal, as the surface rapidly became protected by the oxide debris layer, as demonstrated by the slight weight gain (**Figure 5.54**).

This mechanism is confirmed by the wear debris (**Figure 5.58**) generated, which consisted of fine 'oxidational wear'-type debris – fine particles – and removed fragments of the compacted oxide layer. Although this layer was not as thoroughly compacted and sintered as the other systems studied (for example, MA956/Stellite 6 at 750°C), the sample was protected from wear, at the expense of the counterface. This mechanism, which showed strong similarities to the Stellite 6/MA956 counterface system (**Section 6.5.2**), is displayed in **Figure 6.11**.

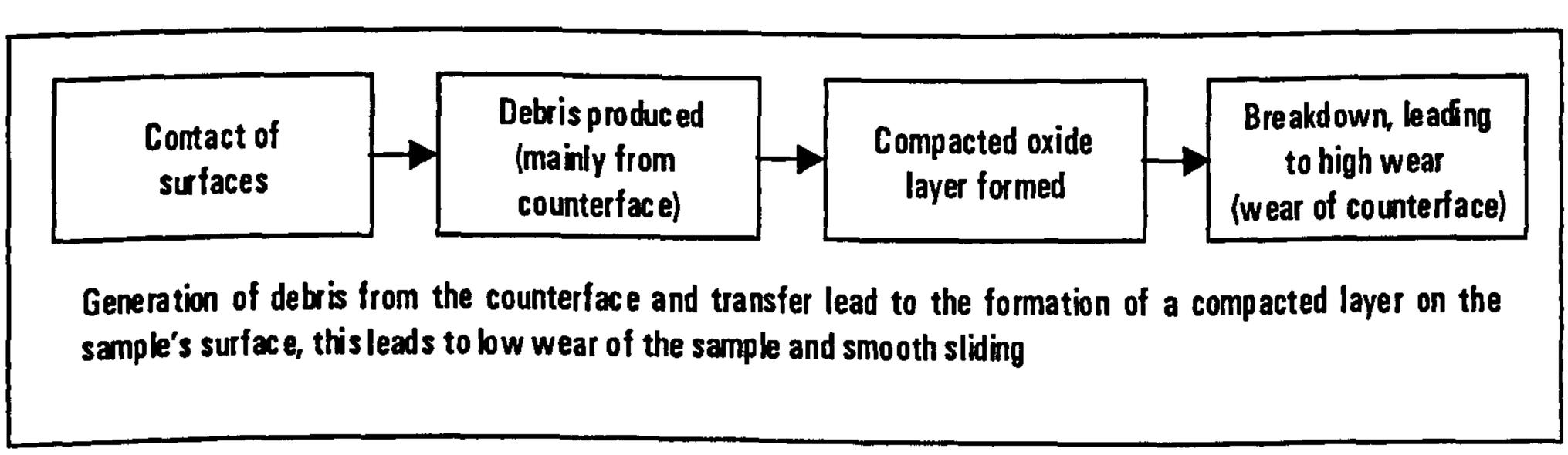

Figure 6.11 Wear mechanism for Stellite 6 worn with Nimonic 80A at 750°C at 7N load

6.6.3 Sliding of Nimonic 80A samples worn with Incoloy 800 counterface at ~25 to 750°C

Nimonic 80A worn with an Incoloy 800 counterface was characterised by two wear regimes (**Figure 5.31**) across the range of temperatures investigated. From ~25 to 570°C a severe wear mechanism operated typified by high friction coefficients (0.6–0.8) and the absence of compacted layer formation. The low weight losses were caused by protection of the sample by transferred material from the counterface.

From ~25 to 570°C wear took place by the transfer of Incoloy 800 from the counterface to the sample – in metallic not oxide form – where it formed a highly work hardened layer upon the surface. This was confirmed by: (a) diffraction data showing evidence for the transfer of Incoloy 800 (**Table 5.5**); (b) the hardness profiles which revealed hardened layers at 270 and 510°C (**Figure 5.41**); and (c) SEM/EDX analyses which revealed a transferred iron-containing layer on the surface (not presented). Although the wear of the sample always showed very slight weight gains – due to the transfer of counterface material – damage to the counterface increased with temperature from ~25 to 570°C indicating a highly damaging wear mechanism.

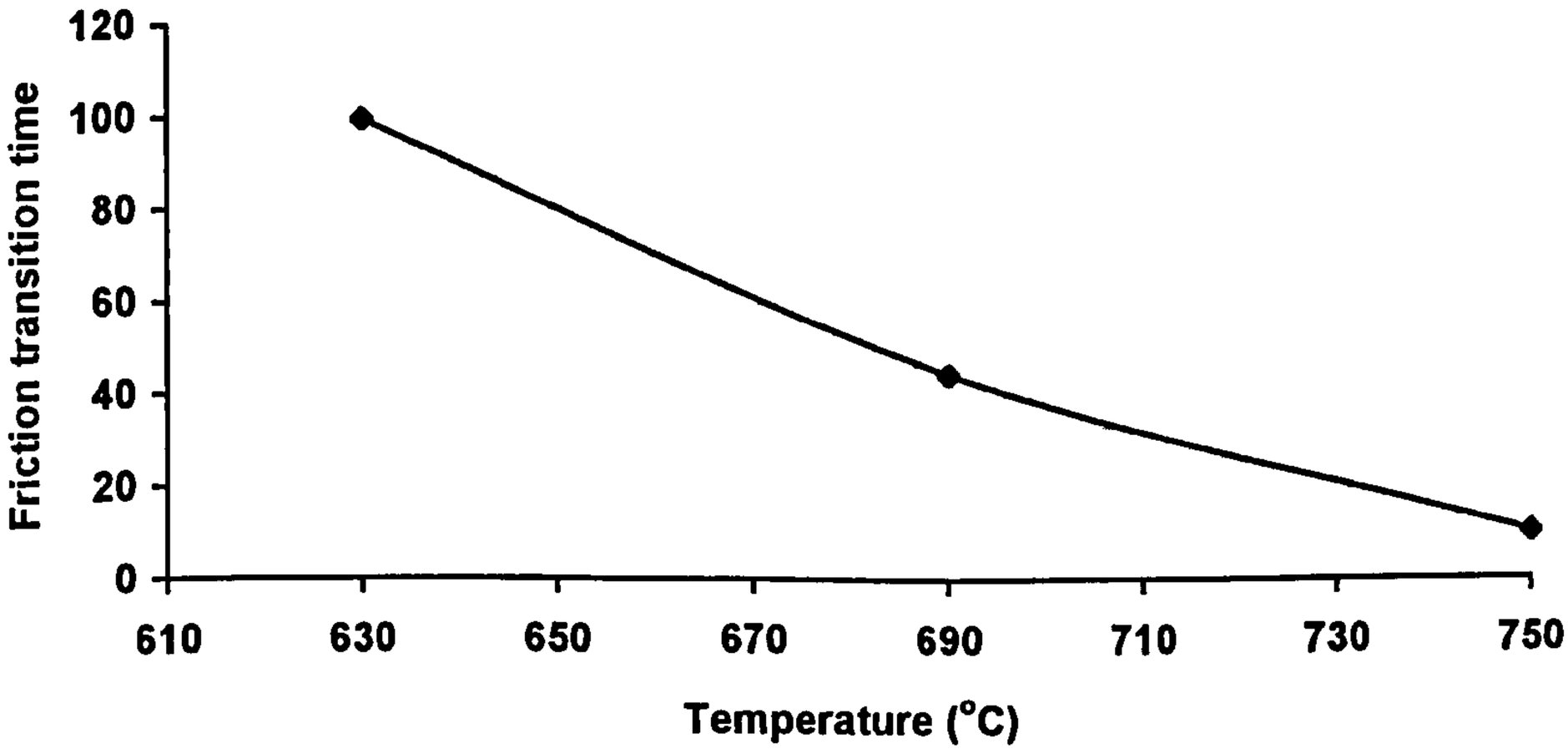

Figure 6.12 Friction transition (drop) temperature of the test for Nimonic 80A sample worn with Incoloy 800 counterface at 7 N load

The wear debris collected from experiments at ~25 to 570°C (**Figure 5.39**) consisted of large flakes of Incoloy 800 – these were formed either directly from the highly deformed and work hardened layer produced from the counterface which broke to generate debris, or the transferred layer on the sample. Fine oxide

material was unable to develop between the surface to establish a milder wear mechanism. Such protective debris was not produced at these temperatures. This mechanism is summarised in **Figure 6.13 (a)**.

(a) Nimonic 80A worn with Incoloy 800 from ~25 to 570°C

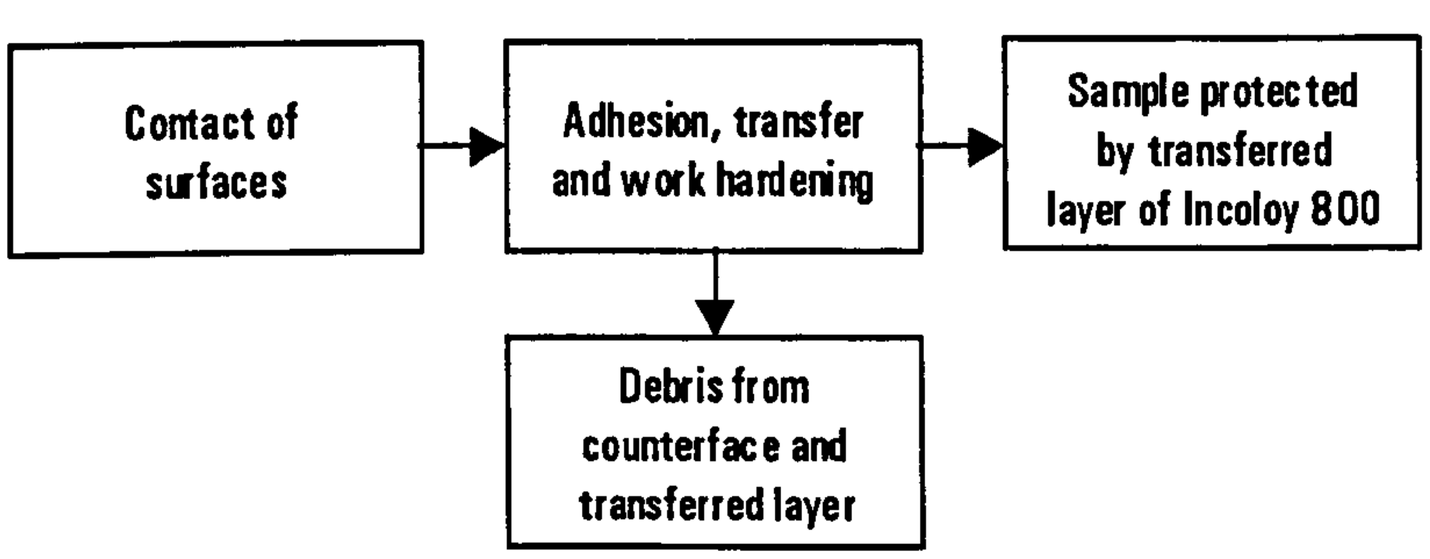

The counterface undergoes progressively higher wear rates with increasing temperature (due to reduced strength with temperature). The sample is protected from wear by the transferred layer.

(b) Nimonic 80A worn with Incoloy 800 from 360 to 750°C

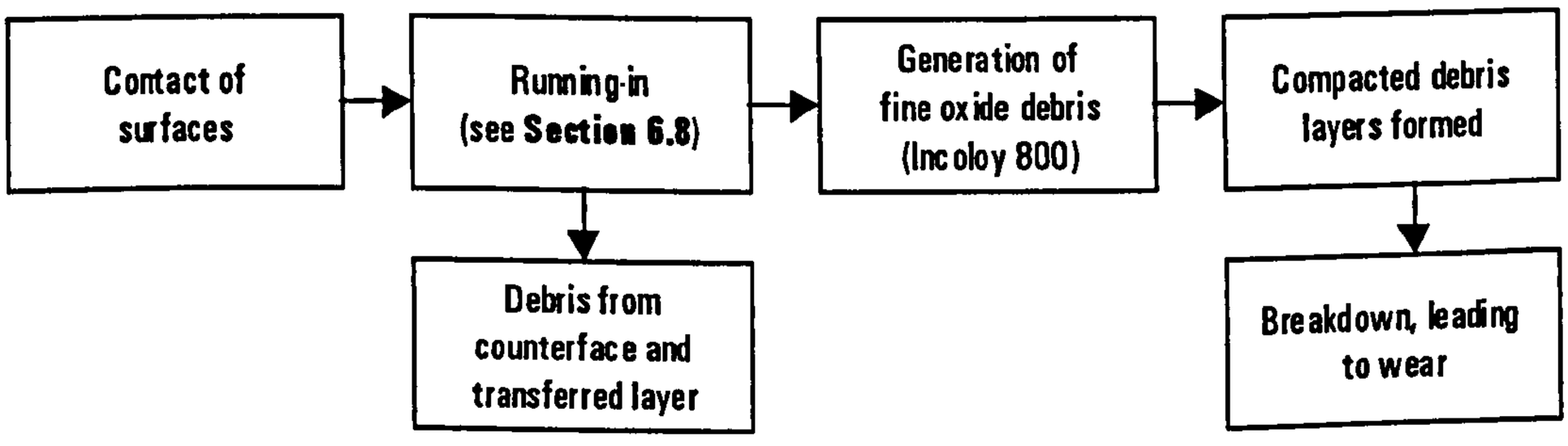

After the 'running-in' period (see **Section 6.8**), a similar mechanism to that occurring below 630°C, fine debris generated from Incoloy 800, which then forms the compacted debris layer. This layer formation leads to a marked decline in the coefficient of friction

Figure 6.13 Wear mechanism for Nimonic 80A worn with Incoloy 800 from ~25 to 750°C at 7N load

At higher temperatures >630°C, increased oxidation of the contacting surfaces led to the production of fine oxidational debris (confirmed by XRD and EDX analysis – **Figures 5.39** and **5.37**) which promoted the formation of wear resistant layers upon the surfaces. The rates of these processes increased with temperature, as shown by the fall in friction (**Figure 6.12**), which facilitated formation of a compacted oxide layer [62] (**Section 2.11.1**). At 630°C the transition from high-to-low friction occurred after 90 minutes – thus fell to 10

minutes at 750°C. The layer formed consisted of iron, chromium and nickel indicating that it had been generated from Incoloy 800 material (**Figure 5.64**). The sample itself underwent virtually no wear, it being protected by first the transferred then the oxide layer.

The counterfaces were also seen to undergo considerably less wear above the transition temperature (590 to 630°C). This mechanism is shown in **Figure 6.13 (b)**.

6.6.4 Sliding of Incoloy 800 samples with Nimonic 80A counterface at 750°C

Despite the apparent establishment of an oxidational-type mechanism after 25 to 30 minutes (**Figure 5.60**) of wear and the formation of a compacted layer of oxide debris, the weight loss recorded for this couple was relatively high (**Figure 5.54**).

With this couple the transfer of counterface material to the sample did not take place (**Table 5.9**), a mechanism which is often responsible for very low wear rates of the sample (at the expense of the counterface). The relatively thin layer formed (**Figure 5.65**) remained unstable and did not become wear-protective, undergoing a rapid rate of break-down and reformation. Two observations confirm this: (a) the wear debris recovered consisted of both finer particles, and larger fragments which resemble the removed sections of the compacted oxide layer (**Figure 5.63 (a)**); and (b) the presence on the wear scar of many fine debris particles (**Figure 5.36 (d)**), indicating that the rates of break-down and reformation of the surface layers were relatively rapid – so accounting for the high weight losses. This is outlined in **Figure 6.14**.

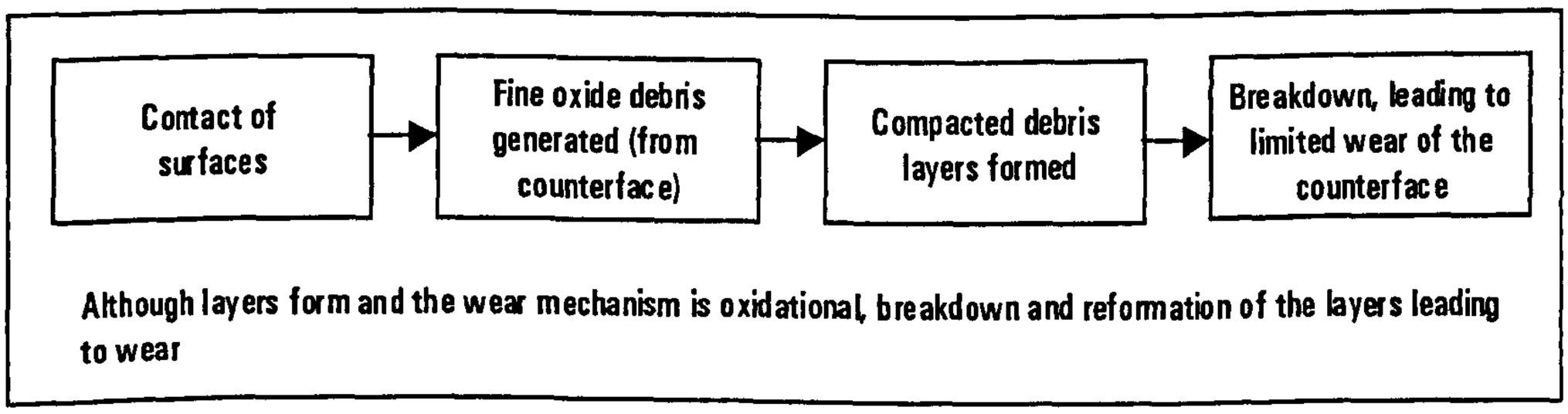

Figure 6.14 Wear mechanism for Incoloy 800 worn with Nimonic 80A counterfaces at 750°C at 7N load

6.7 Like-on-like sliding at 750°C of the four test alloys

6.7.1.a Like-on-like sliding of MA956 at 750°C

The like-on-like wear of MA956 at 750°C operated under the most severe conditions. Metal-to-metal contact dominated the mechanism, which resulted in adhesion and junction growth leading to high friction (as demonstrated by the failure of the test). Highly damaged surfaces (**Figure 5.72**) were produced.

The negligible oxidation of the contacting surfaces was unable to promote an oxidational mechanism [101-102]. The severity of the mechanism did not allow the production of suitable, fine oxide particles.

The general pattern of wear over a range of temperatures, in this investigation, showed a gradual increase in weight losses with temperature, dependent on material strength, until sufficient oxidation occurred allowing the formation of compacted debris layers (see sliding of MA956 with Incoloy 800 and Stellite 6 counterfaces, **Section 5.6.4**). Further loss in strength at 750°C together with the absence of sufficient oxidation led to the severe wear. This wear mechanism is shown in **Figure 6.15**.

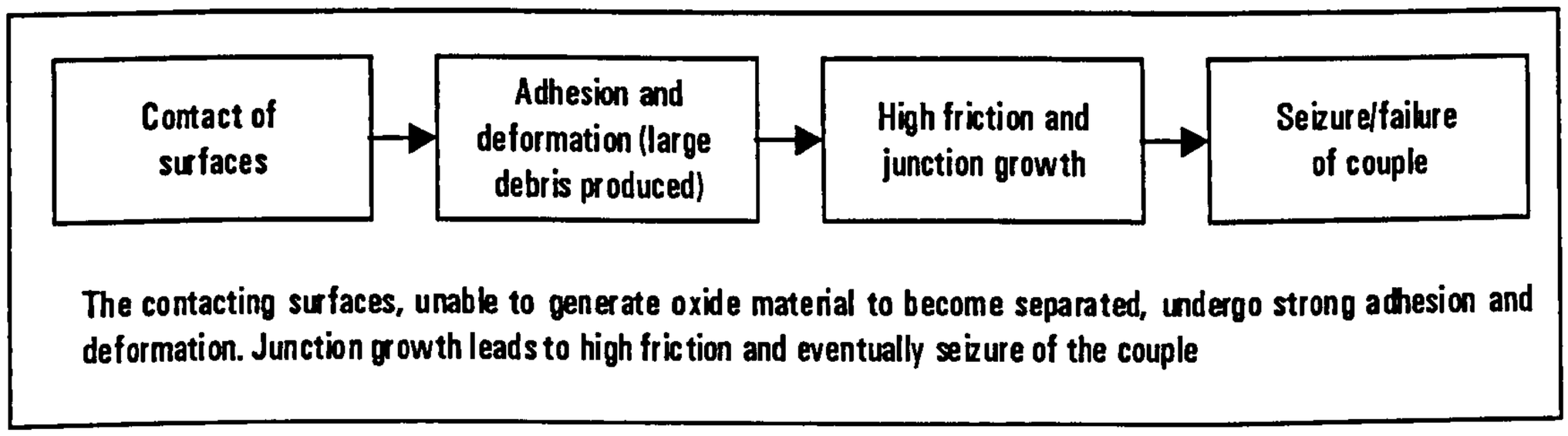

Figure 6.15 Wear mechanism for like-on-like sliding of MA956 at 750°C at 7N load

6.7.1.b Like-on-like sliding of Nimonic 80A at 750°C

In the initial stages of wear the surfaces of Nimonic 80A underwent metal-to-metal contact as indicated by the initial high coefficient of friction (falling from 0.85 at the start of the test to 0.35–0.45 after 40 minutes – **Figure 5.67**) and large debris produced (**Figure 5.76**). Oxidation of the damaged surfaces was responsible for the generation of finer oxide debris which accumulated between the surfaces, separating the contacting elements. This promoted the formation of a compacted debris layer. Hence a reduction in friction and smooth sliding were achieved. However this layer (**Figure 5.73**) did not thicken or become sufficiently stable to reduce the wear rates to the low levels recorded for other systems. Wear continued via the break-down and reformation of the surface layer – an oxidational-wear mechanism. It appeared that no net

transfer of material from the counterface occurred to allow the layer to thicken and protect the sample at the expense of the counterface. This process is presented in **Figure 6.16.**

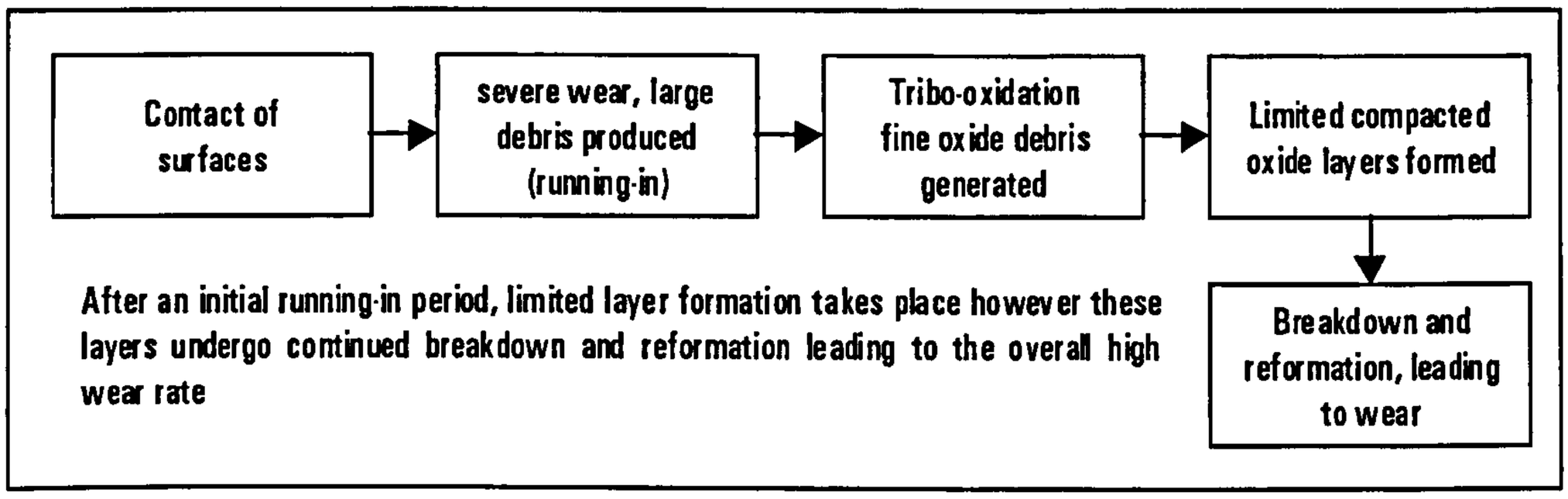

Figure 6.16 Wear mechanism for like-on-like sliding of Nimonic 80A at 750°C at 7N load

6.7.1.c Like-on-like sliding of Stellite 6 at 750°C

The like-on-like sliding of Stellite 6 formed wear resistant layers very quickly after the commencement of sliding – thus gave rise to the low friction **(Figure 5.67)** and negligible wear experienced by the couple **(Figure 5.66)** (Note: insufficient debris was produced to be collected for analysis).

The exceptionally low wear recorded for this couple was due to the high hardness – resistance to deformation – of the alloy combined with the rapid generation of suitable oxide material for the formation of wear resistant layers. Once generated the layer remained very stable and virtually no further wear occurred.

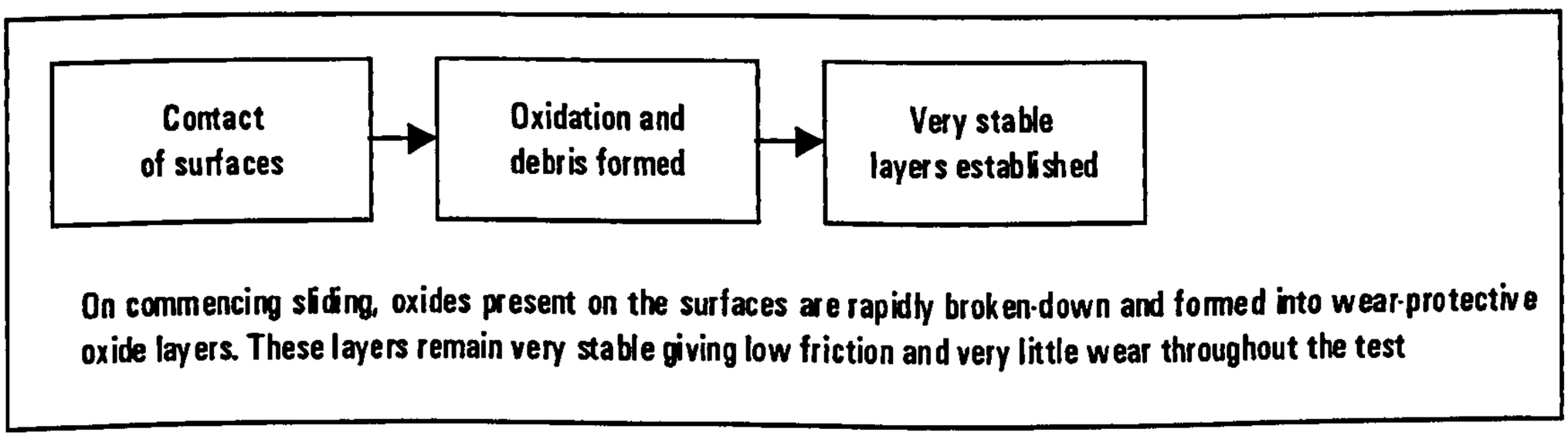

Figure 6.17 Wear mechanism for like-on-like sliding of Stellite 6 at 750°C at 7N load

Although the surface of the samples (and counterfaces) showed the distinctive 'glaze'-type surface **(Figure 5.72)**, the cross-sections revealed the surface layer to be very thin **(Figure 5.74)**. Once the first layers had appeared both surfaces were protected and no further wear took place allowing the layers to thicken as demonstrated by the low friction observed from the start of the test. This mechanism is presented in **Figure 6.17.**

6.7.1.d Like-on-like sliding of Incoloy 800 at 750°C

During a period of 'running-in' of ~40 minutes an oxidational-wear mechanism was established as demonstrated by the coefficient of friction achieving a stable level (**Figure 5.67**) in this time. This resulted in the formation of a limited compacted debris layer. The high weight loss can be accounted for by losses in the 'running-in' period and those accompanying continued formation and break-down of the layers. This was demonstrated by the debris recovered, which contained large fragments produced during the severe wear 'running-in' process and the fine oxidational-type particles and fragments of compacted oxide layer recovered (**Figure 5.76**). The low strength of the alloy at this temperature and damaged appearance of the surface oxide layers further supported this argument. These processes are summarised in **Figure 6.18.**

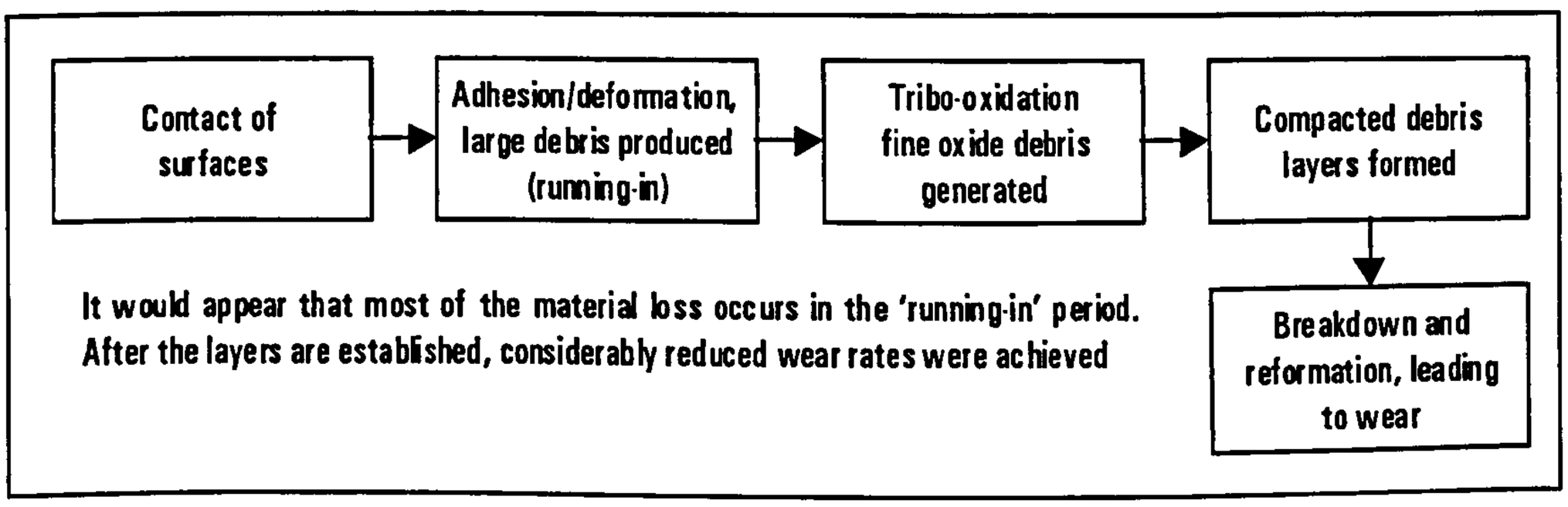

Figure 6.18 Wear mechanism for like-on-like sliding of Incoloy 800 at 750°C at 7N load

6.7.2 Comparison of the like-on-like sliding systems

The overall processes occurring in the like-on-like sliding of the four test alloys showed that wear was dependent upon: (a) the resistance to deformation; and (b) the oxidation of the surfaces under conditions of wear. The formation of wear resistant layers was able to take place when the two conditions are satisfied.

6.8 Formation of compacted oxide layers, MA956 worn with Incoloy 800 at 690°C

In the initial stage of wear (10 to 30 minutes) metal-to-metal contact gave rise to a severe wear mechanism. The large wear debris produced (**Figure 5.81**) were easily expelled and the surfaces were free of attached particles (**Figure 5.80 (a)** and **(b)**) thus preventing the formation of glazed layers at the initial stages – transfer of metallic materials did not occur. This was a similar

mechanism to that seen for MA956/Incoloy 800 counterface below 690°C (**Section 6.4.3**). These processes are presented in **Figure 6.19 (a)**

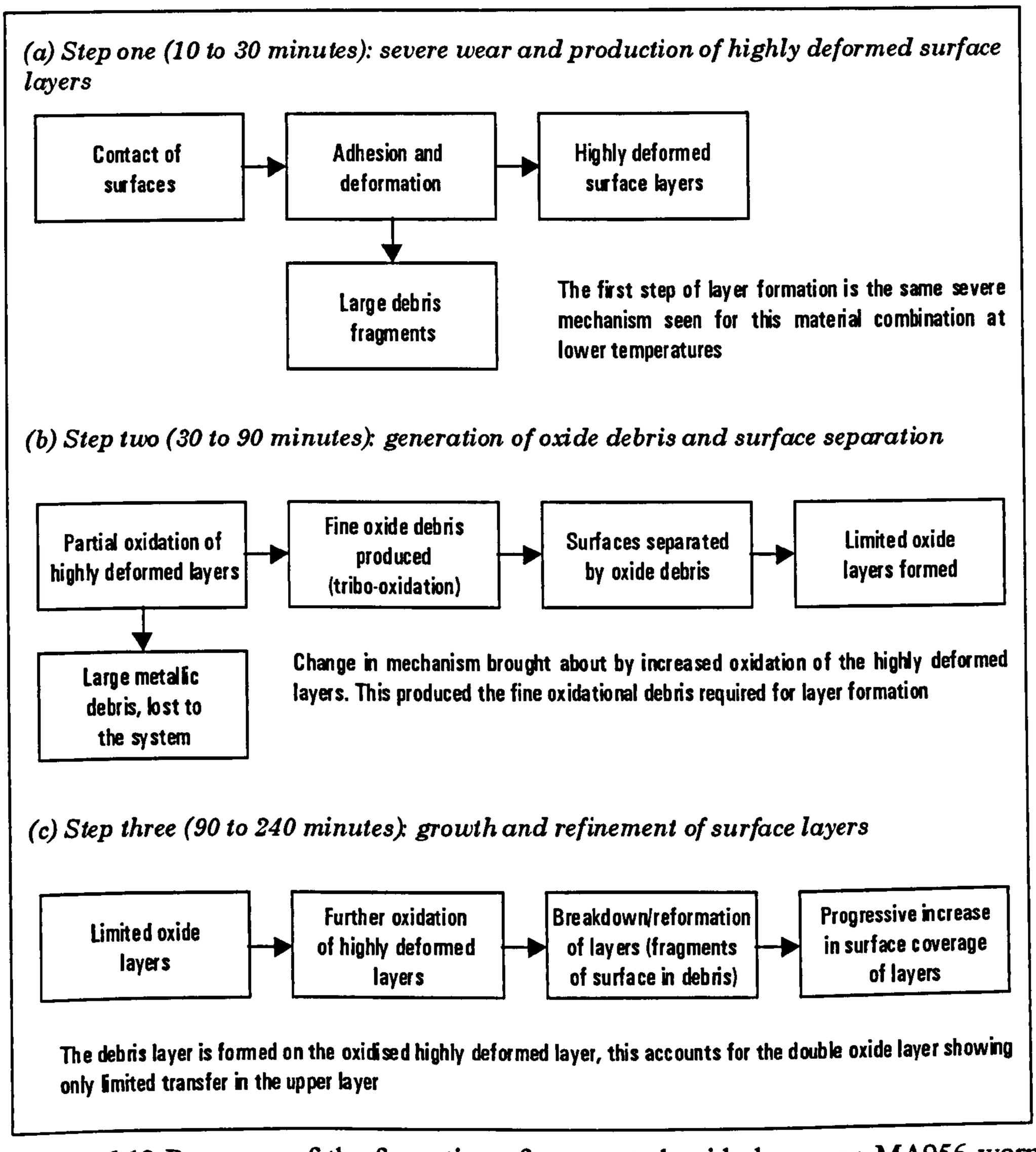

Figure 6.19 Processes of the formation of compacted oxide layers on MA956 worn with Incoloy 800 counterfaces at 690°C and 7N load

At approximately 30 minutes, the surfaces became increasingly deformed and these highly deformed surfaces underwent oxidation at enhanced rates [34, 35] forming (oxidational-type) wear-generated oxidised debris (confirmed by XRD **Table 5.11**) required for the formation of glazed layers.

Once areas of compacted oxide material began to appear on the wear scar and track the mechanism took on a more 'oxidational' character and the levels of metal-to-metal adhesion and deformation began to decrease. Further oxidation

and debris generation from the surfaces led to further layer formation. This is presented schematically in **Figure 6.19 (b)**.

By 90 minutes, discrete areas of compacted oxide layer had been established on the contacting surfaces (**Figure 5.80 (c)** and **(d)**), reducing weight losses to a markedly lower level. Further wear occurred by the breaking-down and reforming of the surface layers, a process which refined the layer gradually giving greater coverage of the wear scars' surfaces. Further oxidation of the highly deformed material led to the formation of a double layer, consisting of a compacted debris layer on top of an oxidised deformed layer. By this stage the oxide layer became load-bearing and the contact was wholly oxide-oxide. This was shown by the slight reduction in the coefficient of friction, the smooth sliding achieved and the reduced rate of material loss. This final stage of the wear process is summarised in **Figure 6.19 (c)**.

6.9 Formation of compacted oxide layers, Nimonic 80A worn with Incoloy 800 at 630°C

Here in the first 60 minutes, wear occurred by a severe mechanism similar to that seen for Nimonic 80A worn with Incoloy 800 counterface below 630°C (**Section 5.5.2**). The wear was of a severe type dominated by the transfer (in metallic form) of Incoloy 800 (**Table 5.10**) from the counterface to the sample, thus accounting for the small weight gains recorded up to 60 minutes (**Figure 5.82**). This type of transfer was not seen with the MA956/Incoloy 800 counterface system. Metal-to-metal contact dominated giving rise to the high coefficient of friction (**Figure 5.83**), and although some fine debris was on the contacting surfaces (**Figure 5.85**) these particles were not as yet affecting the dominant wear mechanism. These processes are displayed in **Figure 6.20 (a)**.

Beyond ~60 minutes the oxidation of the highly deformed surfaces – and the Incoloy 800 layer on the samples – led to the oxidational wear-generated fine oxide debris. The fine debris separated the surfaces and so prevented further transfer of the counterface material.

The oxidational-wear mechanism became established and the formation of compacted debris layers upon the surfaces followed, giving reduced weight losses. The friction fluctuated as the contact condition alternated between the two conditions until layers were firmly established by ~120 minutes of sliding. This transitional stage of the mechanism is displayed schematically in **Figure 6.20 (b)**.

From 120 minutes onwards the process of wear was accompanied by progressive refinement of the compacted debris layer by repeated compaction and sintering. Some degree of break-down of this compacted layer by fracture led to further material loss, and was responsible for progressively covering the whole of the scars' and tracks' surfaces with the highly smooth oxide layers, as shown in **Figure 6.20 (c)**.

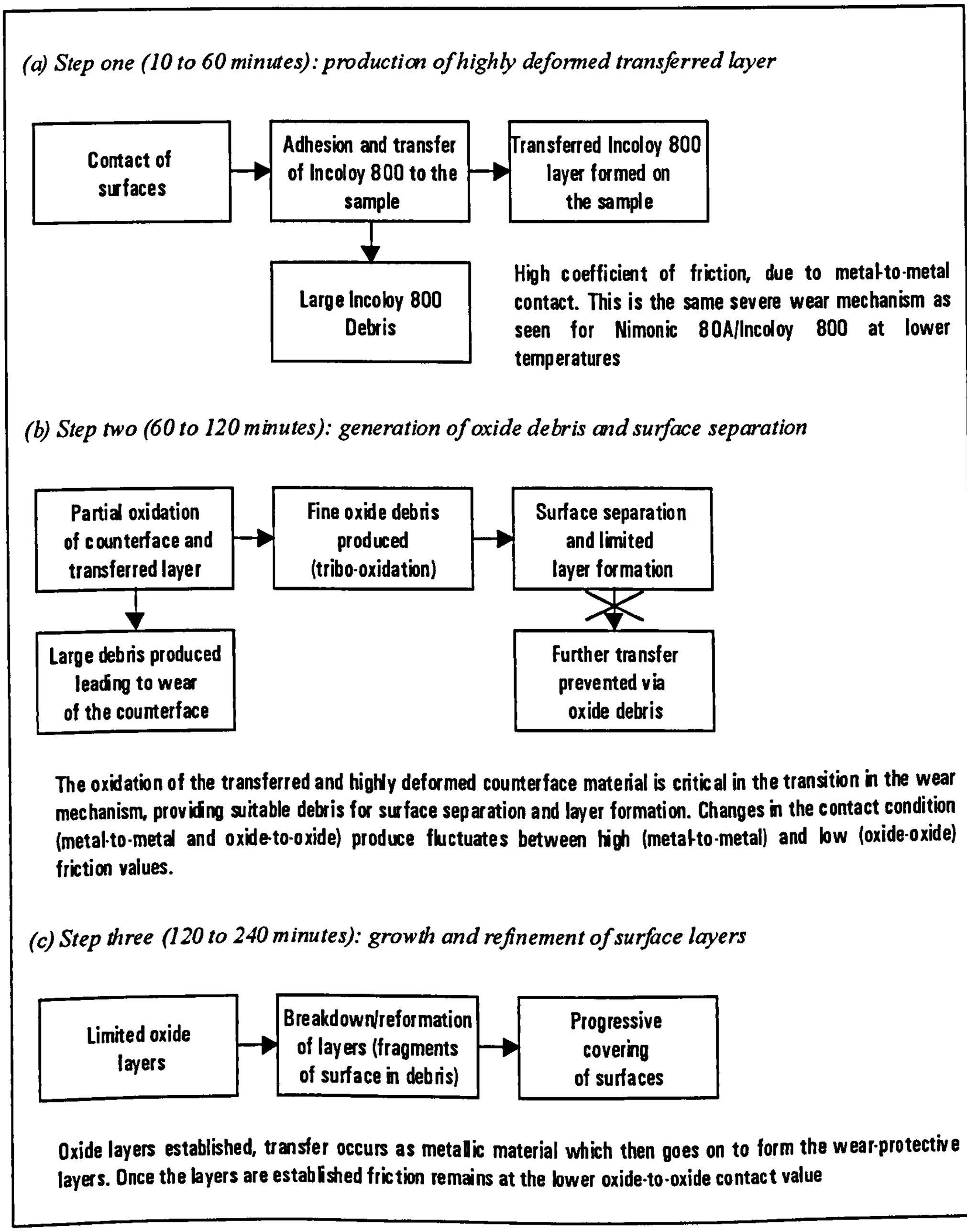

Figure 6.20 Processes of the formation of compacted oxide layers on Nimonic 80A worn with Incoloy 800 counterfaces at 630°C at 7N load

7. Conclusions

7.1 Wear of MA956 with two counterfaces – Stellite 6 and Incoloy 800 – at 750°C over a range of normal loads (7 to 25 N)

1) The formation of compacted oxide layers occurred in MA956 with both counterfaces over the range of loads tested (7 to 25N) at 750°C.
2) The compacted oxide layer formed with the Stellite 6 counterface was comprised predominantly of transferred material (cobalt/chromium oxides) from the counterface, giving low weight losses for the sample. The generation of large quantities of suitable fine oxide debris from the counterface facilitated the formation of the compacted layer.
3) For MA956 worn with Incoloy 800 counterfaces, the compacted oxide layers developed predominately from the material originating from the sample (iron/chromium oxides). This mode of formation of compacted layers was responsible for higher weight losses compared to that shown by MA956/Stellite 6 combinations.
4) MA956 samples worn with Incoloy 800 counterfaces underwent considerably more working to produce debris suitable for layer formation, compared to Stellite 6 counterfaces. This resulted in higher wear of the samples worn with Incoloy 800 counterfaces.
5) For MA956 worn with both counterfaces at 750°C, the weight losses increased linearly up to 20N load and above this load the weight losses showed much greater increases. Above 20N, the substrate was not able to provide the support for the compacted layers which was required for this compacted layer to be effective in reducing wear.

7.2 Wear of Nimonic 80A with two counterfaces – Stellite 6 and Incoloy 800 – at 750°C over a range of normal loads (7 to 25 N)

6) For Nimonic 80A worn with Stellite 6 counterfaces, the wear mechanism was predominantly oxidational with elements of abrasive wear. No compacted debris layers were formed across the range of loads examined (7 to 25N) at 750°C.
7) Layers were unable to form due to insufficient adhesion of the debris to the sample's surfaces, and lack of debris cohesion caused by the ploughing of the sample's surface by hard carbide particles present in the Stellite 6 counterface (origin of the abrasive element in the mechanism).

8) For Nimonic 80A worn with Incoloy 800 counterfaces, limited compacted oxide layers formed at 7 and 10N loads; at loads between 15 to 25N the wear was oxidational/abrasive and no layers were formed without the build-up of debris.
9) The presence of limited compacted debris layers at 7 and 10N loads significantly reduced the wear compared to that achieved with a Stellite 6 counterface.
10) For Nimonic 80A/Incoloy 800, compacted oxide layers were unable to develop above 10N load. Between 15 and 25N an oxidation mechanism operated in which an abrasive element was present.

7.3 Wear of MA956 with Stellite 6 counterfaces in the temperature range ~25 to 750°C

11) MA956 worn with Stellite 6 counterfaces between ~25 to 390°C gave low weight losses due to the separation of the surfaces by the fine cobalt-chromium wear debris originating from the counterface.
12) The presence of these particles prevented working of the surfaces and the production of large debris, i.e. severe wear. Here the wear mechanism was oxidational.
13) At 450°C the wear mechanism for MA956 worn with Stellite 6 counterfaces become severe. This led to considerably higher rates of material loss. At this temperature large debris particles were produced from both surfaces which remained non-adherent to the wear scars. The transition to this mechanism was due to the loss in strength of the materials with temperature, combined with insufficient rate of oxide production to establish an oxidational mechanism.
14) The extent of the severe mechanism for MA956 worn with Stellite 6 (compared to other couples studied, MA956/Incoloy 800 counterfaces for instance) at intermediate temperatures (between 390 and 510°C) was limited due to the incompatibility of structures in these two materials (MA956/Stellite 6) which gave comparatively low adhesion.
15) Between 450 and 510°C a second transition in the wear mechanism, marked by the formation of compacted layers, gave rise to the low wear recorded. The formation of compacted oxide layers upon the contacting surfaces, resulted from the increase in the oxidation rate of the wear-affected surfaces at this

temperature providing sufficient oxide particles required for the formation of compacted layers.

16) The layer on the sample was formed from cobalt/chromium oxides originating from the counterface. This layer became increasingly stable with increasing temperature and gave rise to lower wear.

17) The break-down of the layer led to further wear, as demonstrated by the wear debris recovered. Longer 'running-in' times also accounted for the higher wear rates at lower temperatures, although no direct evidence was available to support this, for this system.

18) The coefficient of friction remained unchanged across the range of temperatures investigated (~25 to 750°C).

7.4 Wear of Stellite 6 samples with MA956 counterfaces at 750°C

19) Oxidational wear became established after ~20 minutes; this led to the separation of the surfaces and the generation of compacted oxide layers.

20) Deformation of the MA956 counterface by the Stellite 6 sample promoted tribo-oxidation which facilitated the production of fine debris. This debris formed the transferred layer on the sample's surface. This layer was protective, and gave rise to the slight weight gain of the sample.

21) The layer formed was not as stable as others formed, as demonstrated by its susceptibility to spalling on cooling, indicating a lesser degree of compaction and sintering compared to the other cases of layer formation seen. This represented a similar mechanism to the Stellite 6/Nimonic 80A counterface system at 750°C.

7.5 Wear of MA956 samples with Incoloy 800 counterfaces in the temperature range ~25 to 750°C

22) From ~25 to 630°C MA956 worn with Incoloy 800 counterfaces exhibited a severe wear mechanism. Relatively large, flat angular debris was produced from highly deformed surface layers, probably via a delamination-type mechanism.

23) The rates of material loss in this temperature range (~25 to 630°C) were controlled by the material's ability to resist deformation. The presence of oxide films and debris was insignificant, the mechanism being dominated by metal-to-metal contact.

24) Between 630 to 690°C a transition occurred in the wear mechanism which led to the formation of compacted oxide layers. This transition was brought about by the production of fine oxide debris via the oxidation of the wear-affected surfaces, providing the material for layer formation.

25) The formation of the compacted debris layer upon the highly deformed wear-affected surfaces, which became oxidised (either before or after layer formation), so producing the 'double layer' appearance of the surface layers in cross-section.

26) No net transfer of material took place in the formation of the compacted oxide layer, although mixing of debris in the interface led to the inclusion of some counterface material in the compacted oxide layer.

7.6 Wear of Incoloy 800 samples with MA956 counterfaces at 750°C

27) Metal-to-metal contact dominated the wear of Incoloy 800 with MA956 counterfaces which led to the transfer of metallic material from the counterface to the sample. Highly damaged surfaces, production of large (>50μm) debris and rapidly rising friction were also the consequences of the strong adhesion between the surfaces.

28) Insufficient oxide particles were generated to affect an oxidational-type mechanism. This was due to the low oxidation rate of the counterface (as the counterface tended to supply more oxide to an interface) combined with the similar structures of the alloys which favoured strong adhesion leading to severe wear. This represented a similar mechanism to like-on-like sliding of MA956 at 750°C.

7.7 Wear of Nimonic 80A samples with Stellite 6 counterfaces in the temperature range ~25 to 750°C

29) From ~25 to 450°C the surfaces were separated by fine particles of cobalt-chromium debris which prevented metal-to-metal contact and led to low weight losses.

30) At ~25°C the wear regime fluctuated between metal-to-metal contact and oxide-to-oxide contact, due to insufficient production of oxide at this temperature. This was manifested by intermittent changes in coefficient of friction.

31) Between 540 and 510°C the wear mechanism underwent a transition to severe, giving rise to high rates of material loss. This mechanism transition

was brought about by the loss in strength of the materials with increasing temperature, combined with insufficient oxide material to separate the surfaces.

32) In this temperature range relatively large, flat angular debris was produced from the work-hardened surfaces, corresponding to a delamination-type wear mechanism. Fine oxide debris was not produced so the surfaces were unable to become separated.

33) Between 630 and 690°C a second wear mechanism transition occurred, causing some degree of reduction in the weight losses. However compacted oxide layers did not form and the weight losses remained relatively high.

34) The surfaces were separated by oxide debris 'smeared' across their surfaces. However insufficient cohesion combined with the ploughing/abrasive effect of hard particles in the counterface prevented the formation of a compacted debris layer.

7.8 Wear of Stellite 6 samples with Nimonic 80A counterfaces at 750°C

35) The working of the counterface against the sample produced oxide debris from the counterface surface which promoted generation of a transferred debris layer upon the sample's surface.

36) Although the layer formed was not a perfect compacted layer, it was responsible for protecting the sample from wear. This represented a similar mechanism to the Stellite 6/MA956 counterface system at 750°C.

7.9 Wear of Nimonic 80A samples with Incoloy 800 counterfaces in the temperature range ~25 to 750°C

37) From ~25 to 570°C the contacting surfaces were free of oxide material or oxide wear debris particles. Wear occurred via transfer of Incoloy 800 from counterface to sample where it formed a hardened layer which was subsequently removed as large angular fragments of Incoloy 800. Damage to the counterface increased with increasing temperature due to the loss in strength of the alloys (**Figure 6.1**).

38) Between 570 and 630°C a wear mechanism transition occurred which resulted in the formation of compacted oxide layers on the contacting surfaces. Layer formation was accompanied by a marked decrease in the coefficient of friction, due to the change in the contact condition from metal-metal to oxide-oxide. Further increases in temperature reduced the transition time.

39) The formation of the layer was promoted by the generation of fine debris from the wear-affected surfaces, once separation of the surfaces occurred further transfer was prevented and compacted layers dominated the mechanism.

7.10 Wear of Incoloy 800 samples with Nimonic 80A counterfaces at 750°C

40) The formation of a partly complete oxide layer after ~25 to 30 minutes took place, however this was insufficient to prevent relatively high weight losses.

41) It would appear that this 'limited' compacted layer formed was unable to thicken and become wear-protective due to the low strength of the substrate at temperature, combined with the lack of transfer from the counterface.

7.11 General conclusions for MA956 and Nimonic 80A samples with Stellite 6 and Incoloy 800 counterfaces tested between ~25 to 750°C

42) At low temperatures, from ~25 to between 400 to 500°C, all the couples exhibited low wear, either 'mild' or 'severe' mechanisms where the materials were sufficiently resistant to deformation to give low rates of material loss.

43) At intermediate temperatures, 400 to 600°C, the loss of strength of the materials combined with the low rate of oxidation favoured the operation of a severe wear mechanism.

44) Higher temperatures gave rise to sufficient oxidation for mild oxidational wear to operate, oxidation taking place via tribo-oxidation from the work hardened 'activated' surfaces.

45) Layers of compacted debris were only able to form from fine 'oxidational debris, as larger fragments were not retained in the system to be broken-down for layer formation (hence the higher transition temperatures compared to studies conducted with other rigs). This equates to layer formation via the oxidation-scrap-reoxidation and total-oxidation mechanisms only, not the metal debris mechanism [73] (**Section 2.11.4**).

46) Transfer of oxide material was able to take place when significantly more oxide was produced by the counterface (MA956/Stellite 6 counterfaces at 750°C for example) or when the samples were considerably harder than the counterface causing more surface damage and tribo-oxidation (Stellite 6/Nimonic 80A counterfaces at 750°C). The exception was the Nimonic 80A/Incoloy 800 counterfaces system where metallic particles were transferred from the counterface to the sample.

7.12 Like-on-like sliding of MA956, Nimonic 80A, Stellite 6 and Incoloy 800 at 750°C

47) Like-on-like sliding tests of MA956 were unsuccessful after ~20 minutes because of the strong adhesion produced by metal-to-metal contact. Sufficient fine debris to allow the formation of protective oxide layers was not present with the like-on-like wear of MA956. This resulted in continued metal-to-metal contact and eventual failure of the test. This represented a severe wear mechanism similar to the Incoloy 800/MA956 counterface system at 750°C.

48) Under like-on-like sliding conditions Nimonic 80A, Incoloy 800 and Stellite 6 all exhibited oxidational wear mechanisms, promoted by the formation of compacted oxide layers. The relative wear resistance of these materials showed dependence upon the high temperature strengths of the materials.

49) For the case of Nimonic 80A and Incoloy 800, the formation of compacted layers was non-uniform, showing a lack of stability as indicated by the ease of break-down of the layers. Higher weight losses occurred from such unstable layers.

50) The like-on-like sliding of Stellite 6 very quickly led to the formation of wear resistant surface layers after sliding commenced. The high resistance to deformation of the alloy combined with sufficient oxide particle generation led to the formation of compacted layers resulted in low wear.

51) In general, under like-on-like sliding no significant amounts of material were transferred from the counterfaces to the samples. Wear rates depended upon the resistance to deformation of the alloys combined with sufficient oxidation to establish mild wear conditions.

7.13 Comparison of the development of compacted oxide layers on MA956 and Nimonic 80A worn with Incoloy 800 counterfaces at 690 and 630°C respectively

52) For both cases development of compacted oxide layers took place via a 'running-in' step of severe wear of similar mechanism to that seen for the wearing couples at lower temperatures (MA956 ~25 to 630°C, Nimonic 80A ~25 to 570°C).

53) For the MA956 samples the 'running-in' step persisted for approximately 30 minutes and operated via metal-to-metal contact resulting in the loss of material from both the sample and the counterface.

54) The 'running-in' step for Nimonic 80A worn with Incoloy 800 involved the transfer of Incoloy 800 from the counterface to the sample and the formation of large (>50μm) metallic Incoloy 800 debris. This process persisted for ~60 minutes.

55) For both couples the transitions from severe to mild wear occurred when sufficient oxidation of the wear-affected surfaces took place which produced fine 'oxidational-type' debris. During this second stage of the process metal-to-metal contact was gradually eliminated in favour of oxide-to-oxide type contact. The fine debris generated adhered to the surfaces and began to form islands of connected debris material.

56) For MA956 samples a layer of compacted debris was present on the sample and counterface surfaces by 60 minutes. The compacted debris layer developed on top of the highly deformed surface layer, which became partially oxidised, so producing the 'double layer' discussed previously (**Section 7.5**) with this couple.

57) Layers were fully established on Nimonic 80A samples by 120 minutes; these layers were generated wholly from the Incoloy 800 material transferred from the counterface, giving exceptionally low wear of the sample.

8. Recommendations for future work

The mechanisms by which compacted debris layers are formed during high temperature wear under certain conditions are relatively well understood. However it is still not possible to predict precisely the conditions which are lightly to promote formation of 'glaze'-type layers. This work revealed many limitations of current models when dealing with unlike sliding systems and where debris is not well maintained in the interface.

The future of wear research lies in the development of predictive models(s) which explain wear under a wide range of conditions and the development of wear maps. Clearly the current work needs to be further extended to achieve these aims. In order to pursue these goals the following suggestions are made for further investigation of wear at elevated temperatures:

1) In further investigations with the current experimental set-up the use of contact resistance [103] would be beneficial to determine the state of the surfaces and the contact condition during wear testing.
2) Investigation of the influence of sliding speed on the formation of compacted debris layers. Studies of the sliding speeds which promote layer break-down may provide an estimation of the cohesive strength of the compacted layers formed and of the layers/substrates adhesion.
3) Testing over a range of speed would require greater assessment of the frictionally generated heat [33] and so it may be necessary to calculate the temperature at the interface via a thermocouple fitted to the back of the sample and calculation of the heat flow.
4) Studies using other experimental arrangements (for example cup-on-flat or pin-on-disc) may be employed to facilitate controlled retention and removal of wear debris and hence encourage and discourage layer formation.
5) Studies to investigate a greater range of materials including intermetallics and ceramics to further improve the understanding of the influence of material properties in layer formation.
6) Studies of the oxidation behaviour of the test alloys to include 'tribo-oxidation' – oxidation of the wear deformed surfaces, and pre-worn samples (in an inert atmosphere).
7) Studies into the sintering behaviour of the oxides involved in layer formation and the adhesion of fine particles to surfaces at elevated temperature (possibly via elevated temperature atomic force microscopy).

Such information would be invaluable in modelling of the layer-forming process.

From such future work the development of predictive models for the wear processes may be attempted. The further characterisation of the wear processes should allow the production of wear maps [104-106] to aid the design and materials selection for high temperature applications.

References

[1] I. M. Hutchings, "Tribology", Publ. By Arnold, London (1992).

[2] "Superalloys II" Ed C. T. Sims *et al.* Wiley, New York (1987).

[3] F. H. Stott, C. W. Stevenson and G. C. Wood, "Friction and wear properties of Stellite 31 at temperatures from 293 to 1074K" *Metals Tech.*, **4** (1977) 66-74.

[4] J. Jiang, F. H. Stott and M. M. Stack, "Some frictional features associated with the sliding wear of the nickel-base alloy N80A at temperatures to 250°C", *Wear* **176** (1994) 185-194.

[5] F. H. Stott and G. C. Wood, "The influence of oxides on the friction and wear of alloys", *Tribo. Int.*, **11** (1978) 211-218.

[6] J. Jiang *et al.*, "Characterisation of wear scar surfaces using combined three dimensional topographic analysis and contact resistance measurements" *Tribo. Int.*, **30** (1997) 517-526.

[7] P. D. Wood, "The effect of the counterfaces on the wear resistance of certain alloys at room temperature and 750°C" Ph.D. thesis, SERG, University of Northumbria at Newcastle (1997).

[8] P. D. Wood, P. K. Datta, J. S. Burnell-Gray and N. Wood, "Investigation into the high temperature wear properties of alloys contacting against different counterfaces" *Mat. Sci. Forum*, **251-254** (1997) 467-474.

[9] F. P. Bowden and D. Tabor, "Friction, an introduction to tribology" Publ. Heinemann, London (1973).

[10] J. A. Greenwood and J. B. P. Williamson, "Contact of nominally flat surfaces", *Proc. R. Soc. Lond.*, **295A** (1966) 300-319.

[11] J. I. Mc. Cool, "Comparison of models for the contact of rough surfaces" *Wear* **107** (1986) 37-60.

[12] K. L. Johnson, K. Kendall and A. D. Roberts, "Surface energy and the contact of elastic solids" *Proc. R. Soc. Lond.*, **A 324** (1971) 301-313.

[13] A. R. Savkoor and G. A. D. Briggs, "The effect of tangential force on the contact of elastic solids in adhesion" *Proc. R. Soc. Lond.*, **356A** (1977) 103-114.

[14] R. B. Waterhouse and D. E. Taylor, "High temperature fretting wear of like metallic contacts" *Reviews on High Temperature Materials*, **4** (1980) 299-346.

[15] D. Tabor, "Wear – a critical synoptic view" *Proc. Int.* Conference on Wear of Materials, St. Louis, Missouri, in April 1977 ASME.

[16] E. C. Rabinowicz, "Friction and wear of materials" Publ. New York Wiley (1965).

[17] J. F. Archard and W. Hirst, "The wear of metals under unlubricated conditions" *Proc. R. Soc. Lond.*, **236A** (1956) 397-410.

[18] T. F. J Quinn, "Review of Oxidational Wear. Part 1: The Origins of Oxidational Wear" *Tribo. Int.*, **16** (1983) 257-270.

[19] N. C. Welsh, "The dry wear of steels 1, The general pattern of behaviour" *Phil. Trans.*, **257A** (1965) 31-50.

[20] N. C. Welsh, "The dry wear of steels 2. Interpretation and special features" *Phil. Trans.*, **257A** (1965) 51-70.

[21] T. S. Eyre and D. Maynard "Surface aspects of unlubricated metal-to-metal wear" *Wear*, **18** (1971) 301-310.

[22] J. K. Lancaster, "The formation of surface films at the transition between mild and severe metallic wear" *Proc. R. Soc. Lond.*, **273A** (1963) 466-483.

[23] D. H. Buckley, "Surface effects in adhesion, friction, wear and lubrication" Tribology series, 5 Publ. by Elsevier (1981).

[24] C. Subramanian, "Effects of sliding speed on the unlubricated wear behaviour of Al-12.3 wt.% Si alloy" *Wear*, **151** (1991) 97-110.

[25] C. Subramanian, "Wear of Al-12.3 wt.% Si alloy slid against various counterfaces materials" *Scripta Metallurgica* **25** (1991) 1369-1374.

[26] C. Subramanin, "On mechanical mixing during dry sliding of aluminium - 12.3wt.% silicon alloy against copper" *Wear* **161** (1993) 53-60.

[27] Ed J Halling 'Principles of Tribology' Publ Macmillan Press.

[28] N. P. Suh, "The delamination theory of wear" *Wear* **25** (1973) 111-124.

[29] D. A. Rigney and W. A. Glaeser, "The significance of near surface microstructure in the wear process" *Wear*, **46** (1978) 241-250.

[30] S. Fayeulle, A. B. Vannes and L. Vincent, "First body behaviour before debris formation" 'Wear particles: from the cradle to the grave', Proceedings of the 18th Leeds-Lyon Symposium on Tribology, 3-6th September 1991, Lyon, France, Ed. D. Dowson, Publ. Elsevier, 229-235.

[31] H.-C. Sim and N. P. Suh, "Subsurface crack propagation due to surface traction in sliding wear" *J. App. Mech. Trans.* ASME **51** (1984) 317-323.

[32] T. F. J. Quinn, "Oxidational wear", *Wear* **18** (1971) 413-419.

[33] J. F. Archard, "The temperature of rubbing surfaces" *Wear* **2** (1958/59) 438-455.

[34] T. F. J Quinn, "Review of oxidational wear. Part 2: Recent developments and future trends in oxidational wear research" *Tribo. Int.*, **16** (1983) 305-314.

[35] J. Molgaard and V. K. Srivastava, "The activation energy of oxidation in wear" *Wear* **41** (1977) 263-270.

[36] J. Molgaard, "A discussion of oxidation, oxide thickness and oxide transfer in wear" *Wear* **40** (1976) 277-291.

[37] J. Molgaard and V. K. Srivastava, "Apparatus for the study of oxidative wear of unlubricated surfaces" *Wear* **33** (1975) 179-188.

[38] T. F. J. Quinn, "Oxidational wear modelling: Part 1" *Wear* **153** (1992) 179-200.

[39] T. F. J. Quinn, "Oxidational wear modelling: Part 2 The general theory of oxidational wear" *Wear* **175** (1994) 199-208.

[40] T. F. J. Quinn, "Computational methods applied to oxidational wear" *Wear*, **199** (1996) 169-180.

[41] N. Soda and T. Sasada, "Mechanism of lubrication by surrounding gas molecules in adhesive wear" ASME *Trans., J. Lubr. Technol.*, **100, 4** (1978) 492-499.

[42] W-Z Wu, J-D Xing and J-Y Su, "An investigation on three-body abrasive wear test at elevated temperature" *Wear*, **210** (1997) 299-303.

[43] P. J. Blau, "Mechanisms for transitional friction and wear behaviour of sliding metals" *Wear*, **72** (1981) 55-66.

[44] A. Iwabuchi, "The role of oxide particles in the fretting wear of mild steel" *Wear*, **151** (1990) 301-311.

[45] E. R. Leheup and R. E. Pendleburg, "Unlubricated reciprocating wear of stainless steel with an interfacial air flow" *Wear*, **142** (1991) 351-372

[46] A. Iwabuchi, H. Kubosawa and K. Hori, "The effect of oxide particles supplied at the interface before sliding on the severe – mild wear transition", *Wear*, **128** (1988) 123-137.

[47] A. Iwabuchi, H. Kubosawa and K. Hori, "The dependence of the transition from severe to mild wear on load and surface roughness when the oxide particles are supplied before sliding" *Wear*, **139** (1990) 319-333.

[48] K. Hiratsuka, T. Sasada and S. Norose, "The magnetic effect on the wear of metals" *Wear*, **110** (1986) 251-261.

[49] J. Jiang, F. H. Stott and M. M. Stack, "The role of triboparticles in dry sliding wear" *Tribo. Int.*, **31** (1998) 245-256.

[50] J. Jiang, F. H. Stott and M. M. Stack, "The effect of partial pressure of oxygen on the tribological behaviour of a nickel-based alloy N80A, at elevated temperature" *Wear*, **203-204** (1997) 615-625.

[51] Ch. Colombie *et al.*, "Fretting: load carrying capacity of wear debris" *Trans.* ASME **106F** (1984) 194-201.

[52] H. M. Hawthorne, "On the role of interfacial debris morphology in a conforming contact tribosystem" *Proc. Wear of Materials Conf.* ASME, Orlando (1991) 277-288.

[53] H. Heshmat, "The rheology and hydrodynamics of dry powder lubrication" *Tribology Trans.* **34, 3** (1991) 433-439.

[54] K. C. Ludema, "Third bodies in wear models" 'Wear particles: from the cradle to the grave', Proceedings of the 18th Leeds-Lyon Symposium on Tribology, 3-6th September 1991, Lyon, France, Ed. D. Dowson, Publ. Elsevier, 155-160.

[55] S. L. Rice *et al.* "The role of wear particles in modifying coefficients of friction" 'Wear particles: from the cradle to the grave', Proceedings of the 18th Leeds-Lyon Symposium on Tribology, 3-6th September 1991, Lyon, France, Ed. D. Dowson, Publ. Elsevier, 463-467.

[56] J. S. Halliday and W. Hirst, "The fretting corrosion of mild steel" *Proc. R. Soc. Lond,* A 236 (1956) 411-425.

[57] N. P. Suh and H.-C. Sin, "The genesis of friction" *Wear* **69** (1981) 91-114.

[58] M. Yamamoto and K. Nakajima, "A study of the physical adhesive state between solids" *Wear,* **70** (1981) 321-327.

[59] D. J. Shaw, "Colloid and surface chemistry" Fourth Edition, Publ Butterworth Heinemann (1992).

[60] Y-H Zhou, M. Harmelin and J. Bigot, "Sintering behaviour of ultra-fine Fe, Ni and Fe-25wt%Ni powders" *Script. Metall* **23** (1989) 1391-1396.

[61] F. H. Stott, "The role of oxidation in the wear of alloys" *Tribo. Int.,* **31** (1988) 61-71.

[62] F. H. Stott, D. S. Lin and G. C. Wood, "The structure and mechanism of formation of the 'glaze' oxide layer produced on nickel based alloys during wear at high temperature" *Corr. Sci.,* **13** (1973) 449-469.

[63] F. H. Stott, D. S. Lin and G. C. Wood, "The wear and friction of nickel-base alloys under oxidising conditions" Proc. 5th Eur. Congr. On Corrosion (1973) 452-455.

[64] D. S. Lin, F. H. Stott and G. C. Wood, "The effects of friction and wear behaviour of some commercial nickel base alloys" *Trans* ASLE **17, 4** (1973) 251-262.

[65] F. H. Stott, D. S. Lin and G. C. Wood, "'Glazes' produced on nickel-based alloys during high temperature wear", *Nature Physical Science* 242 April **2** (1973) 75-77.

[66] D. S. Lin, F. H. Stott, G. C. Wood, K. W. Wright and J. H. Allen, "The friction and wear behaviour of nickel-base alloys in air at room temperature", *Wear,* **24** (1973) 261-278.

[67] F. H. Stott, D. S. Lin, G. C. Wood and C. W. Stevenson, "The tribological behaviour of nickel and nickel-chromium alloys at temperatures from 20° to 800°C", *Wear,* **36** (1976) 147-174.

[68] B. Chattopadhyay and G. C. Wood, "The transient oxidation of alloys" *Oxidat. Metals*, **2** (1970) 373-399.

[69] D. J. Barnes, F. H. Stott and G. C Wood, "The frictional behaviour of iron and iron chromium alloys at elevated temperatures", *Wear*, **45** (1977) 199-209.

[70] D. J. Barnes, J. E. Wilson, F. H. Stott and G. C. Wood, "The influence of oxide films on the friction and wear of Fe-5%Cr alloy in controlled environments", *Wear*, **45** (1977) 161-176.

[71] D. J. Barnes, J. E. Wilson, F. H. Stott and G. C. Wood, "The influence of specimen geometry and sliding mode on the friction and wear of iron-chromium alloys in controlled environments", *Wear* **45** (1977) 97-111.

[72] D. H. Burckley "Adhesion, friction and wear of cobalt and cobalt-base alloys" *Cobalt* **38** (1968) 20-28.

[73] F. H. Stott, J. Glascott and G. C. Wood, "Models for the generation of oxides during sliding wear", *Proc. R. Soc. Lond.*, **402A** (1985) 167-186.

[74] F. H. Stott, J. Glascott and G. C. Wood, "The sliding wear of commercial Fe-12%Cr alloys at high temperature" *Wear* **101** (1985) 311-324.

[75] J. Glascott, F. H. Stott and G. C. Wood, "The transition from severe to mild sliding for Fe-12%Cr base alloy at low temperatures", *Wear* **97**, (1984) 155-178.

[76] F. H. Stott, J. Glascott and G. C. Wood, "The sliding wear of in-situ formed oxides on iron and nickel-base alloys", Corrosion-Erosion-Wear of Materials at Elevated Temperatures, ed. A. V. Levey, (1987), 263, National Association of Corrosion Engineers, Houston, Texas.

[77] J. Glascott, G. C. Wood and F. H. Stott, "The influence of experimental variables on the development and maintenance of wear-protective oxides during sliding of high temperature iron-base alloys", *Proc. Instn. Mech. Engrs.*, **99C** (1985) 35-41.

[78] F. H. Stott, J. Glascott and G. C. Wood, "Factors affecting the progressive development of wear-protective oxides on iron-base alloys during sliding at elevated temperatures", *Wear*, **97** (1984) 93-106.

[79] R. C. Bill, "Fretting wear of iron, nickel and titanium under varied environmental conditions" *Wear of Materials* ASME New York (1979) 356-370.

[80] J. L. Sullivan and N. W. Granville, " Reciprocating sliding wear of 9%Cr steel in carbon dioxide at elevated temperatures", *Tribo. Int.*, **17** (1984) 63-71.

[81] A. F. Smith, "The unlubricated reciprocating sliding wear of 316 stainless steel in CO_2 at 20 – 600°C", *Tribo. Int.*, **19** (1986) 65-71.

[82] A. Iwabuchi, K. Hori and H. Hudo, "The effects of temperature, preoxidation and presliding on the transition from severe wear to mild wear

for S25C carbon steel and SUS304 stainless steel" Proc. Int. Conf. On Wear of Materials 1987, ASME, New York (1987), 211-220.

[83] F. H. Stott and D. R. G. Mitchell, "The influence of coating on wear at elevated temperatures" Surface Engineering, Volume I Fundamentals of coatings, Ed. P. K. Datta and J. S. Gray (1993), 141-150.

[84] K. langguth, A. Kluge and H. Ryssel, "Wear of steels after implantation of oxygen ions or oxidation at 670K", *Wear*, **155** (1992) 343-351.

[85] J. Jiang, F. H. Stott, M. M. Stack, "A mathematical model for sliding wear of metals at elevated temperatures", *Wear*, **181-182** (1995) 20-31.

[86] D. Play, "Mutual overlap coefficient and wear debris motion in dry oscillating friction and wear tests", *Trans* ASLM, **28**, **4** (1985) 527-535.

[87] F. P. Bowden and T. H. C. Childs, "The friction and deformation of clean metals at very low temperatures", *Proc. Roy. Soc.* **312A** (1966) 451-466.

[88] J. K. Lancaster, "Accelerated wear testing of PTFE composite bearing materials", *Tribo. Int.*, **12** (1979) 65-75.

[89] M. P. Johnson, P. Moorhouse and J. R. Nicholls, "Hot wear tests on candidate materials", Publ. DTI, 1990.

[90] J. F. Archard, "The temperature of rubbing surfaces", *Wear*, **2** (1958-1959) 438-455.

[91] M. Gee, "Problems of wear testing at high temperatures", spoken presentation, Workshop on High Temperature Wear, 23ed June 1998, The Institute of Materials, 1 Carlton House Terrace, London, SW1Y 5DB.

[92] M.-O. Gellue, personal correspondence, University of Exeter (1998).

[93] J. J. Fischer, I. Astley and J. P. Morse, "The structure and properties of a dispersion-strengthened Fe-Cr-Al alloy, Incoloy alloy MA956E" Superalloys Metallurgy and Manufacture, Proceedings of the 3rd International Symposium on Superalloys at Seven Springs, USA, September 1976, 361-371.

[94] "Incoloy Alloy MA956" Special Metals Corporation, Publ. No. SMC-008.

[95] W. Betteridge, "The Nimonic Alloys" (1961) Publ. Edward Arnold, London.

[96] Y. L. George, "High temperature corrosion of engineering alloys" (1990) ASM International, Materials Park OH 44073 USA.

[97] "Incoloy Alloys 800, 800H and 800HT" Inco Alloys International Inc. Publ. No. IAI-172.

[98] G. Fisher, Unpublished work, University of Northumbria at Newcastle (1998).

[99] "Inco Alloys Product Handbook", Publ. No. IAI 38, 1998.

[100] M. J. Bibby and J. Gorden Parr, "The α→ε transformation in polycrystalline cobalt" *Cobalt* **20** (1963) 111-113.

[101] T. A. Ramanarayanan *et al.*, "The influence of yttrium on oxide scale growth and adherence", *Oxid. Met.*, **Vol 29** No 5/6 (1988) 445-471.

[102] M. J. Bennett *et al.*, "The oxidation behaviour of alumina forming ferritic oxide dispersion strengthened alloys" Materials for Advanced Power Engineering Part II (1994) Publ. Kluwer Academic 1553-1562.

[103] F. H. Stott, J. Glascott and G. C. Wood, "The use of contact resistance measurements to study oxide film developed during high-temperature sliding" *J. Phys. D: Appl. Phys.*, **18** (1985) 541-556.

[104] C. Subramanian, "Methodology of wear testing" Surface Engineering Case Book, ed. J. S. Burnell-Gray and P. K. Datta (1996), 224-245.

[105] S. C. Lim, "Recent developments in wear mechanism maps" Tribo. Int., **31** (1988) 87-97.

[106] Y. Saito and K. Mino, "Elevated temperature wear maps of X40 and Mar-M247 alloys" *Trans.* ASME **117** (1995) 524-528.